NOAA Technical Memorandum ERL PMEL-82

BEAUFORT SEA MESOSCALE CIRCULATION STUDY - PRELIMINARY RESULTS

K. Aagaard
C. H. Pease
S. A. Salo

Pacific Marine Environmental Laboratory
Seattle, Washington
July 1988

UNITED STATES DEPARTMENT OF COMMERCE

C.William Verity
Secretary

NATIONAL OCEANIC AND ATMOSPHERIC ADMINISTRATION

Environmental Research Laboratories

Vernon E. Derr,
Director

NOTICE

Mention of a commercial company or product does not constitute an endorsement by NOAA/ERL. Use of information from this publication concerning proprietary products or the tests of such products for publicity or advertising purposes is not authorized.

Contribution No. 1040 from NOAA/Pacific Marine Environmental Laboratory

For sale by the National Technical Information Service, 5285 Port Royal Road
Springfield, VA 22161

CONTENTS

TABLES

FIGURES

Frontispiece. Ice conditions along the Beaufort shelf during April 1987.

Beaufort Sea Mesoscale Circulation Study - Preliminary Results

K. Aagaard, C.H. Pease, and S.A. Salo

ABSTRACT. The Beaufort Sea Mesoscale Circulation Study was initiated in the autumn of 1986 and included measurements of currents, winds, and ice velocities, as well as observations of state variables and nutirent distributions in the ocean and state variables in the polar atmosphere, principally between Barrow and Demarcation Point along the American Beaufort Sea shelf. This report describes the preliminary results from observations made during the first year of the project, including current velocity results from meters recovered through the ice in April 1987, hydrographic and nutrient sections completed in October 1986 and April 1987, wind velocity, air pressure and temperature records recovered continuously through the end of 1987, ARGOS buoy tracks through 1987, and a representative sample of analyzed weather maps during the first year. Data collection continued through April 1988. The total data set is extraordinary in the temporal and spatial extent of its synoptic coverage, and in the variety of its constituent measurements. The data set is also extremely large, and its full reduction and analysis will provide an exceptional opportunity for improving our understanding of the shelf circulation and its forcing, as well as conditions important to the marine ecology of the area.

1. INTRODUCTION

The purpose of this study is to gain a quantitative and dynamically founded understanding of the circulation over the Beaufort Sea shelf and its atmospheric and oceanic forcing. The study is within the overall context of a regional environmental assessment related to petroleum exploration and development.

Earlier work under OCSEAP was either concentrated within restricted nearshore areas, or did not provide sufficiently broad spatial and temporal coverage to define the shelf circulation on appropriately large scales. A further serious limitation on earlier work was the grossly inadequate determination of the wind field, so that relatively little could be said about the atmospheric forcing of the ocean. Finally, hydrographic sampling on the shelf including nutrients and dissolved oxygen had earlier been restricted to a brief period during the summer, giving no idea of conditions during other times. To substantially remedy this situation, the present study was designed to provide spatially broad coverage of the circulation and hydrography over the shelf, together with the synoptic wind field; and to do so over a sufficiently long period that the important longer time scales could be defined.

We began by setting up the coastal meteorological stations along the north slope by aircraft, and then proceeded with an October 1986 ice breaker cruise on board the USCGC POLAR STAR during the summer-winter transition. On this cruise we occupied six closely-spaced sections which provided full hydrographic coverage over the entire shelf from Barrow to the U.S.-Canadian border, including five-channel nutrients. The section locations are shown in Figure 1. These data have been published by Aagaard *et al.* (1987). Moored instrument arrays

were deployed on four of the six sections, including current meters and a prototype new instrument, the SeaCat, which is a very stable conductivity/temperature recorder.

The majority of the instruments were recovered during March-April 1987, using helicopter logistics, while three more current meters were picked up in September 1987 from the Canadian research vessel J.P. TULLY (cf. Figure 1 for mooring locations). During April 1987 we also ran four hydrographic sections across the shelf from Barrow to Barter Island. Section locations are shown in Figure 2. These are the first full hydrographic sections done during winter. The data have been published by Aagaard *et al.* (1988).

Additionally, during 1986-87 two moored arrays with a total of 16 instruments were deployed in Barrow Canyon for the purpose of determining the outflow from the shelf of dense winter water and the fluid mechanical structure of the outflow plume. These matters are of major importance in understanding the structure of the Arctic Ocean. The project is sponsored by the National Science Foundation and will provide information complementary to that of the Beaufort Sea study.

Extensive meteorological and ice drift data were obtained throughout this period, using a combination of drifting and land based stations transmitting through the ARGOS and GOES satellite telemetry systems (Figure 3). Three GOES stations were installed to fill gaps in the primary National Weather Service (NWS) coastal observing network. Stations were established at Resolution Island in Prudhoe Bay, at the Lonely Dewline site near Pitt Point east of Barrow, and at Icy Cape southwest of Barrow. Each station in the GOES network transmited hourly meteorological observations every three hours to the GOES-West satellite. These data are then rebroadcast to the GOES-West receiving station in Wallops Island, VA, which maintains a computer database which our laboratory computer interrogated daily. The GOES stations at Lonely and Resolution were recovered in April 1988. Further data were obtained from the primary NWS stations at Barter Island, Barrow, Kotzebue, and Nome. A fourth GOES station funded by the Office of Naval Research was placed at the Cape Prince of Wales navigation daymarker along Bering Strait. The data from this station will be available for September 1987 through April 1988.

Additional meteorological coverage was provided by deployments of ARGOS buoys and stations by helicopter onto sea ice floes along the Beaufort and Chukchi coasts. Eleven ARGOS buoys and three ARGOS stations were deployed over 18 months in support of this study. ARGOS buoys transmit to the NOAA polar orbiting satellites which rebroadcast to the Service ARGOS receiving station in Toulouse, France or in Suitland, MD. Positions are calculated from the doppler shift of the transmissions, and the calculated positions and the sensor data are then available in preliminary form for daily computer interrogation and through fortnightly distribution by magnetic tape. Buoys and stations were not recovered from the ice, but were left to drift until failure.

While not included in this interim report, a further set of moored oceanographic instruments and meteorlogical stations were deployed in April and September 1987, and these were retrieved in March and April 1988. In addition, three ARGOS buoys were deployed in cooperation with the Polar Science Center of the University of Washington and three were deployed for the ONR FREEZE program. These data will be included in the final analysis, together with pertinent supporting data from the Chukchi Sea.

2. OCEANOGRAPHIC TIME SERIES

Table 1 lists the maximum speed and the vector mean velocity observed at moorings MA1 (in water 1216 m deep), MA2 (168 m), MB1 (1008 m), MB2 (170 m), and MD1 (165 m); and Figures 4-6 show the 35-hr low-passed time series from both the current meters and the SeaCats at these moorings. All the mooring locations are shown in Figure 1. The time series depictions of Figures 4-6 are 12-hr realizations of the low-passed data. Each time tick is 3 days, and the vertical axis units are cm s^{-1}, °C, and psu, respectively, for velocity, temperature, and salinity. In the figures, each current meter record is identified by the mooring designation, the depth, and in parentheses the direction of the principal axis (the axis of greatest variance). The latter is in degrees true, and in practice it is normally nearly parallel with the vector mean direction of the flow, as can be seen by comparison with Table 1. Note that the SeaCats on MA2 and MB2 were located within 2 m of the bottom.

Consider first Table 1. In the mean, the flow above about 60-90 m, depending on location, is westward; but below this the flow is eastward and generally increases with depth. (Note, however, that the upper westward flow is sufficiently variable that the rms error exceeds the mean.) The subsurface easterly flow apparent in Table 1 is the Beaufort Undercurrent described by Aagaard (1984). While maximum speeds in this current normally appear to be in the range 30-70 cm s^{-1} (compare our Table 1 with Table 2 in Aagaard, 1984), long-term mean flows are much less, typically below 10 cm s^{-1}. Note, however, the extremely high maximum speed recorded at 143 m at MA2, well over twice as great as any ever observed. Figure 4 shows that this represents a single event, albeit of over a week's duration, and we speculate that the event may represent an intense baroclinic eddy passing the mooring site. Less extreme examples of such eddies, centered on about the same depth, were first found in the Beaufort Sea in 1972 (Newton *et al.*, 1974). The sequential orientation of the current vectors in Figure 4 suggests that the hypothesized eddy would have had a CW rotation (cf. Foldvik *et al.*, 1988).

Further comparison of our Table 1 with Table 2 of Aagaard (1984) suggests that at least near the shelf break, the Beaufort Undercurrent did not extend as close to the surface during 1986-87 as it did during the earlier observations. Specifically, Table 1 suggests that the zero in the mean velocity profile was at least 60 m deep (MB2) and possibly as deep as 90 m (MA2). In contrast, mean easterly flows of 3.8 cm s^{-1} and 6.4 cm s^{-1} were observed during 1978 at about

Table 1. Maximum 35-hour low-passed speed and vector mean velocity, 1986-87. The rms velocity error is given in parentheses.

Mooring	Instrument depth, m	Maximum speed cm s^{-1}	Mean Velocity cm s^{-1}	°T
MA1	1188	7.1	0.6(+/-0.2)	353
MA2	60	73.5	3.5(+/-4.1)[1]	291
	93	71.1	0.1(+/-0.5)[1]	219
	143	166.0	7.8(+/-4.7)	119
MB1	83	72.8	1.5(+/-1.4)	168
	148	58.1	6.9(+/-3.0)	097
	980	0.6	0.0(+/-0.0)	
MB2	62	34.4	0.3(+/-0.5)[1]	181
	95	44.2	5.0(+/-2.0)	112
	145	55.3	8.0(+/-1.8)	103
MD1	57	70.3	2.6(+/-2.7)[1]	292
	90	59.5	4.1(+/-2.6)	095
	140	52.0	4.2(+/-2.2)	100

[1] rms error exceeds mean, so that mean not statistically distinguishable from zero.

65 m depth in water respectively near 100 m and 200 m deep. While the data base at this point is certainly not sufficient to sustain firm conclusions in this regard, it does point to possible interannual differences in the velocity structure of the upper ocean.

We turn next to Figure 4, which portrays conditions at the three mooring sites along the 165-170 m isobath, distributed over essentially the entire length of the Alaskan Beaufort Sea. The mooring separation between MA2 and MB2 is ~240 km, and ~210 km between MB2 and MD1. The records point to very large low-frequency variability over a broad range of time scales. It is also clear from an inspection of Figure 4 that not only are there vertically coherent events, but that a large number of events are horizontally coherent over the entire length of the shelf. Table 2 lists selected vertical and horizontal correlations for lags between 0-24 hours. The letter T, M, or B by each mooring designates the top, middle, or bottom instrument at that mooring. For example, A2/T is the instrument at 60 m depth at mooring MA2, A2/M the instrument at 93 m at the same mooring, etc. (cf. Table 1 for instrument depths). The number in parentheses beneath each correlation is the lag, in multiples of six hours, for which the correlation was a maximum. The sense of the lag is such that the row instrument leads the column instrument. For example, A2/M leads D1/M by 24 hours. Several points are noteworthy. First,

Table 2. Selected correlations for 35-hr low-passed current meter data, 1986-87. Lags are given in parentheses.

A. Vertical correlations.

	A2/M	A2/B	B2/M	B2/B	D1/M	D1/B
A2/T	0.95 (0)	0.62 (0)				
A2/M	1.00	0.60 (0)				
B2/T			0.50 (1)	0.41 (1)		
B2/M			1.00	0.84 (0)		
D1/T					0.73 (0)	0.31 (0)
D1/M					1.00	0.53 (0)

B. Horizontal correlations.

	B2/T	B2/M	B2/B	D1/T	D1/M	D1/B
A2/T	0.35 (4)	0.65 (4)	0.59 (4)	0.32 (4)	0.52 (4)	0.49 (4)
A2/M	0.36 (4)	0.65 (3)	0.60 (4)	0.40 (4)	0.55 (4)	0.47 (4)
A2/B	0.51 (4)	0.61 (4)	0.56 (4)	0.27 (4)	0.38 (4)	0.24 (4)
B2/T	1.00			0.34 (2)	0.40 (2)	ns
B2/M		1.00		0.44 (2)	0.50 (1)	0.38 (4)
B2/B			1.00	0.30 (1)	0.40 (0)	0.41 (4)

ns means not significant at 95% level.

the vertical structure is different at the three moorings, despite their being sited on the same isobath. At MA1, the correlation between the top and middle instruments is very high, but degrades considerably between the middle and bottom instruments. In contrast, at MB2, the primary vertical correlation degradation occurs between the top and middle instruments, with the correlation between the middle and bottom being high. At MD1, the correlation pattern is qualitatively like that at MA1, but overall considerably weaker. The vertical correlations are essentially in phase. The second noteworthy point is that the maximum horizontal correlations occur for the middle instruments; are as high as 0.65, representing 42% of the variance; and that the western moorings lead the eastern ones, progressively more as the distance increases. Much of the low-frequency energy is therefore propagating coherently eastward over long distances along the shelf margin, with suggested phase speeds of order 5 m s^{-1}.

Figure 5 shows currents at the two deeper moorings, each sited in water over 1000 m deep. The flow at MB1 resembles that at MB2 in that in the mean it increases downward from near zero at about 80 m to marked easterly flow deeper. The depth at which the mean easterly flow achieves a maximum cannot be determined from the present data, but near bottom it is effectively zero again. In fact, at that depth the flow is essentially negligible throughout the nearly six months of record. Superimposed on the mean flow at the upper instruments is a large low-frequency variability similar to that farther inshore. The top and middle instruments at MB1 are well correlated (0.89), and the onshore correlation with MB2 is moderate, with slightly less than one-half the variance being accounted for by the correlation between the middle instruments. The impression is of a Beaufort Undercurrent which extends out over the slope well beyond the 1000-m isobath, with a mean eastward velocity maximum over the slope at a depth of probably at least 200 m. There appears to be offshore modal structure in this flow. The near-bottom current at MA1 is quite different from that at MB1, in that measurable speeds are found nearly all the time, with a maximum 35-hr low-passed value of over 7 cm s^{-1}. The flow alternates between approximately northerly and southerly, but with a significant net northerly set. The MA1 series is incoherent with that from any other instrument.

The SeaCat records are particularly interesting (Figure 6). They are marked by continual large low-frequency oscillations (~2° and ~2 psu, respectively in temperature and salinity) in which warm saline and cold fresher water alternately moves past the sensors. Considering typical ambient gradients, these oscillations must represent large vertical excursions (upwelling and downwelling) of perhaps 100-150 m. Furthermore, Figure 6 shows the oscillations to be reasonably coherent with the current record. The correlations vary considerably with the instruments being compared, but at MA2 over one-half the variance in the current records at the upper and middle instruments is linearly related to the variance of the bottom temperature records. The current leads the temperature by 12-24 hr. Furthermore, the SeaCat records themselves are quite coherent laterally, as can be seen in Figure 6. The correlation proves to be 0.78 between the

SeaCat temperatures for a lag of 24 hours, accounting for 61% of the variance, with the western mooring leading. This again suggests eastward propagation, with a phase speed of the same order as we calculated earlier. The overall impression from these records is therefore of a low-frequency current regime in which flow reversals to the west are followed within a day by geostrophic adjustment, with warm and saline water upwelling along the continental margin as the adjusting isopycnals tilt upward toward the south. The perturbations propagate eastward with the coast on their right-hand flank. Such a conceptualization of the upwelling is consonant with that proposed by Aagaard (1981), but differs from the directly wind-driven coastal upwelling proposed by Hufford (1974).

3. HYDROGRAPHIC MEASUREMENTS

Figures 7-60 show the fall distributions of hydrographic properties for sections W, A, E, B, C, and D, and Figures 61-96 the winter distributions for sections W, A, B, and C (locations of all sections shown in Figures 1 and 2). Several features are of immediate importance and interest.

First, consider Figures 16-24 and 70-78, showing Section A during fall and winter, respectively. During October, the shelf is still substantially occupied by the warm summer water which has moved in from the Chukchi Sea, and in fact water warmer than 3R extends seaward beyond the section as a subsurface layer. However, seaward of the shelf break the warm layer is capped by a cold low-salinity layer of ice melt. A prominent front over the shelf break points to an intensified eastward current there at the time of the section (with a shear reversal near 30 m). The oxygen distribution significantly reflects the temperature distribution, with the highest values in the ice melt water. Nutrients are variably reduced in the upper ocean, with nitrate in particular being nearly absent, consonant with a nitrogen-limited system. Note, however, that ammonia has rather large values on the shelf, whereas nitrite concentrations are very low, suggesting that nutrient regeneration has begun to replace the nitrate depleted during the summer, but that the process is still at a relatively early stage. The maxima in phosphate, nitrate, and silicate near 120-150 m represent the general Arctic Ocean nutrient maximum, which has been attributed to shelf sources (Moore *et al.*, 1983; Jones and Anderson, 1986).

During winter (Figures 70-78) Section A still shows a residue of the summer temperature maximum between 30-60 m, while above about 30 m the water is near freezing. The upper thermocline is notably sharp. In the upper layer, salinity gradients have all but disappeared due to convective mixing during freezing. Oxygen concentrations in the upper ocean have increased from the same process. Silicate has not changed significantly from fall, and phosphate has increased only moderately, since neither was apparently seriously depleted the previous October. However, the nitrogen distributions are substantially different, with a large increase in nitrate and significantly high values of nitrite as well. On the other hand, ammonia concentrations are near zero. It is apparent, therefore, that nitrogen regeneration has been substantial, but not complete

by the beginning of the spring production cycle in April. The very high concentrations of nitrate and silicate near the bottom on the middle shelf, with a maximum at station A4, are probably the residue of an earlier upwelling event from below 100 m.

Examples of both active upwelling and downwelling are in fact apparent in the sections themselves. For example, Section C from April (Figures 88-96) shows both the elevated density-related isopleths (temperature, salinity, and sigma-t) which we would expect to follow a current reversal toward the west (cf. the discussion in II. above), and the flooding of the shelf with nutrient-rich waters. Conversely, Section B from October (Figures 34-42) shows a pronounced down-turning toward the shelf of the isopleths of every parameter measured, as we would expect during eastward motion.

A very important matter is illustrated in Section W from October (Figures 7-15). The section runs southwest across the continental slope to its shallowest point on the shelf at station W8 (indicated by the vertical arrow) and then turns more southerly and crosses Barrow Canyon. Note the warm and relatively fresh water flowing eastward through Barrow Canyon and out of the Chukchi Sea onto the Beaufort shelf, and note also that this water is relatively nutrient-depleted, especially in nitrogen. This is the Alaskan coastal water which has moved northward through eastern Bering Strait (cf. Coachman *et al.*, 1974). The critical point, however, is that warm water is also seen over the slope seaward of station W8. It is the origin of this water which is of paramount interest. The most revealing parameter proves to be ammonia (Figure 14), which shows a remarkably strong core centered between about 50-150 m at station W3. An examination of all the nutrients, together with their corresponding density ranges, and a comparison of these values with recent work in the Chukchi and northern Bering seas under the ISHTAR program (Tripp, 1987), points to the relatively warm nutrient-rich water seen over the slope in Section W as having come through western Bering Strait, and then northward through the central Chukchi Sea. This is the Bering Sea water described by Coachman *et al.*, (1974), which the ISHTAR program has identified as being involved in the enormously high production of the northwestern Bering Sea, and more recently has also implicated in similarly high production rates in the central Chukchi Sea. The important point for present purposes is that a major source of water for the Beaufort Undercurrent lies farther west along the northern Chukchi margin than the Barrow Canyon input which has been the focus in earlier work (e.g., contrast Mountain, 1974, or Aagaard, 1981). Most likely, the principal point of exit from the Chukchi for this water is Hope Sea Valley and Herald Canyon, although the depression between Hanna and Herald shoals may also contribute.

Another point of interest in the fall sections is the contrast between conditions on the western and eastern portions of the Beaufort shelf. The transition appears to be located near Section B, which is near where Barnes and Toimil (1979) suggested that there is a change in the direction of the nearshore flow from westerly to easterly, possibly associated with a change in the

mean wind regime. In the fall the eastern shelf is marked by lower upper-layer salinities and considerably greater stratification, i.e., it has more of the Arctic Ocean character than the shelf farther west, where the Chukchi influence is strong. For example, contrast Section A (Figures 16-18) with sections C (Figures 43-45) or D (Figures 52-54). There are also differences in the nutrient distributions, with distinctly lower values of both ammonia and silicate on the eastern shelf, possibly reflecting the reduced connection with the Chukchi, although the relatively small data base doesn't allow firm conclusions in this regard. The following April, the upper-ocean salinities are again lower in the east and the density stratification greater (contrast Figures 71-72, Section A, with Figures 89-90, Section C). At the same time, the nutrients over the shelf show a marked decrease in going eastward from Section A (contrast Figures 75 with 84 or 93, and Figures 78 with 87 or 96). In this case the difference is most obviously a consequence of the recent upwelling at the western site discussed earlier, and it is conceivable that such events are more common there than on the eastern shelf and may therefore be responsible for the fall situation also. In this connection, note in Figure 6 that the temperature and salinity oscillations recorded at the western SeaCat (MA2) were considerably larger than at the eastern one (MB2). The point is that there appear to be significant large-scale longshore differences in the hydrography, reflecting differences in the governing processes.

4. METEOROLOGICAL TIME SERIES AND ICE DRIFT

We turn next to the meteorology. Table 3 summarizes the deployment positions, times, and data completeness for the ARGOS buoys and stations, and Table 4 summarizes the deployment information for the GOES coastal stations and the data acquisition periods for the NWS coastal stations. All ARGOS buoys were fitted with Y.S.I. thermistors in a gilled vane housing for a fully ventilated air temperature, typically 30 to 50 cm above the floe surface, with a resolution of 0.1°C and zero-point calibration to within 0.3°C. Also, each buoy measured air pressure with an A.I.R. digital barometer with a resolution of 0.1 mb and calibrated to within 0.4 mb. The ARGOS stations had similar temperature and pressure instrumentation; however, the pressure ports and thermistors were 2 m above the floe surface. The stations also had an R.M. Young aerovane-type anemometer at 3 m and an InterOcean S4 current meter at 6 m below the estimated floe bottom. The computer interfaces and tower assemblies were manufactured by Coastal Climate Co. The ESI and PMEL manufactured buoys used Synergetics ARGOS transmitters, while the Coastal Climate buoys and stations used Telonics transmitters. A typical station configuration is given in Figure 97.

Because the GOES satellite is so near the horizon in northern Alaska, slight variations in the geostationary orbit cause the stations to drop below the horizon. In addition, the satellite itself occasionally has transmission failures, resulting in additional data drops. To combat this problem without giving up the immediate knowledge of the condition of the station and

Table 3. ARGOS buoy deployment information. All ARGOS buoys had ventilated air temperature and surface air pressure sensors. In addition, stations 7420a, 7420b, and 7429 had 3-m vector-averaged anemometers and 6-m vector-averaged current meters.

BUOY IDENT	START TIME	DATE	START POSITION		END TIME	DATE	END POSITION		TOTAL HOURS	BUOY TYPE[1]
7424	[3]1855	9Oct 1986	71.528	145.239	0213	18Dec 1986	71.034	164.889	1662	EB
7420a	1707	14Oct 1986	70.660	141.282	0252	26Oct 1986	70.526	144.314	268	CS
7428	1730	17Oct 1986	71.919	152.146	0314	4Nov 1986	72.136	154.557	416	EB
7421	[2]0214	2Mar 1987	65.899	168.469	0719	20Mar 1987	66.886	167.909	436	PB
7422	[4,2]2121	1Mar 1987	64.737	167.570	1545	12Jun 1987	63.312	165.720	2464	PB
7423	[2]0500	8Mar 1987	71.843	151.910	1958	12Apr 1987	71.078	160.621	854	EB
7425	[2]1105	8Mar 1987	72.018	154.984	2232	16Mar 1987	72.025	154.860	205	EB
7426	[2]0313	13Mar 1987	71.338	149.020	1731	2Jun 1987	71.961	160.118	1956	EB
7427	[2]2017	13Mar 1987	71.041	145.915	0709	30Mar 1987	71.236	147.738	394	EB
7420b	1332	29Apr 1987	71.336	144.554	0253	14Jun 1987	71.644	159.344	1092	CS
7013	[2,6]2218	3Sep 1987	71.936	158.086		[5]	72.948	176.917	2855	CT
7429	[2,6]2213	5Sep 1987	72.001	160.765	0849	21Sep 1987	71.637	156.134	369	CS
7014	[2,6]0653	8Sep 1987	72.359	164.810		[5]	71.558	181.724	2729	CT
7015	[2,6]2308	9Sep 1987	72.810	168.930	0236	7Dec 1987	71.694	177.297	2114	CT
7430	1900	17Nov 1987	71.662	148.643		[5]	71.198	163.387	1032	CT
7431	0000	18Nov 1987	71.893	151.744		[5]	70.152	165.829	1029	CT
7432	2100	18Nov 1987	71.454	145.466		[5]	71.686	155.048	1018	CT

1 Buoy type codes: EB = ESI box, CS = Coastal Climate Company station, PB = PMEL/Synergetics box, CT = Coastal Climate Company short tube.

2 Buoy start time listed is time of first ARGOS transmission.

3 Buoy 7424 had low quality transmissions and stable positions were infreqent.

4 Buoy 7422 had a four-day data gap between 21 and 25 May 1987.

5 Buoy was still transmitting as of 31 December 1987; last transmission processed was 0000 31 December 1987.

6 ONR funded deployment.

Table 4. Coastal meteorological station summary information.

	Type	Start Time		End Time		Position	
Barter	NWS-10	0000	1Sep86	2300	31Dec87	70.125N	143.667W
Resolution [1]	GOES-6	1800	26Sep86	2200	31Dec87	70.370N	148.047W
Lonely [2]	GOES-6	2300	25Sep86	2300	31Dec87	70.917N	153.253W
Barrow	NWS-10	0000	1Sep86	2300	31Dec87	71.300N	156.733W
Icy Cape [3]	GOES-3	2100	22Mar87	2200	31Dec87	70.325N	161.867W
Kotzebue	NWS-10	0000	1Sep86	2300	31Dec87	66.883N	162.625W
Wales [4]	GOES-10	1300	14Sep87	2100	31Dec87	65.633N	168.117W
Nome	NWS-10	0000	1Sep86	2300	31Dec87	64.517N	165.433W

[1] Resolution GOES station did not record temperature from 1200 6Oct87 to 1600 18Nov87, and recorded no data from 1100 3Mar87 to 0000 12Mar87, from 1700 to 1900 18Nov87, and from 0200 to 0400 27Dec87. Missing data were linearly filled. The latter two breaks may be filled with data from internally recorded tapes before the final analysis.

[2] Lonely GOES station did not record from 0800 to 1000 28Sep86, sporadically and without wind speed from 2300 31Oct86 to 2200 12Mar87, 0300 to 1000 4Nov87, 1400 to 1600 12Nov87, 0800 to 1000 2Dec87, 0500 to 0700 4Dec87, 1700 9Dec87 to 0700 20Dec87, and from 1100 to 1300 20Dec87. Missing data were linearly filled. The latter five breaks may be filled from internally recorded tapes before the final analysis.

[3] Icy GOES station was first deployed in September 1986 but didn't function. A replacement was installed 22 March 1987. This is an older style station and doesn't record internally, so recovery from GOES transmission drops are not possible. The station did not transmit from 0200 to 0700 28Mar87, 2000 to 2200 31Mar87, 0200 to 0400 4Apr87, 0500 to 0700 7Apr87, 2000 to 2200 30Apr87, 0500 to 0700 17May87, 0200 to 0700 21May87, 0500 to 0700 11Jun87, 0800 to 1300 14Jun87, 0800 to 1000 19Jun87, 2300 29Jun87 to 0100 30Jun87, 2000 to 2200 30Jun87, 1400 to 1600 10Jul87, 2000 to 2200 11Jul87, 0800 14Jul87 to 0700 15Jul87, 0500 20Jul87 to 0400 21Jul87, 0500 22Jul87 to 0100 23Jul87, 2000 to 2200 25Jul87, 0500 29Jul87 to 0700 30Jul87, 0800 22Aug87 to 0400 23Aug87, 1700 to 1900 25Aug87, 2000 31Aug87 to 1600 2Sep87, 1700 to 1900 20Sep87, 0800 to 1000 24Sep87, 1700 26Sep87 to 0400 28Sep87, 1100 to 1300 28Sep87, 1700 28Sep87 to 0100 30 Sep87, 0200 to 0400 2Oct87, 1400 to 1600 3Oct87, 2000 3Oct87 to 0700 4Oct87, 1100 to 2200 5Oct87, 1400 6Oct87 to 1300 7Oct87, 0800 to 1000 8Oct87, 2000 to 2200 31Oct87, 0500 to 0700 and 1100 to 1300 4Nov87, 0200 to 0400 and 0800 to 1000 2Dec87, 1700 to 1900 3Dec87, 0200 to 0400 15Dec87, 0200 to 0400 27Dec87.

[4] Cape Prince of Wales GOES station was deployed as part of ONR-funded FREEZE experiment, but is included here because it contributes to understanding the spatial variability of the region. The station transmitted intermittently from 1300 15Sep87 to 1200 24Sep 87, and did not transmit from 1600 26Sep87 to 0300 28Sep87, 1300 28Sep87 to 0000 1Oct87, 0400 to 0600 2Oct87, 1000 3Oct87 to 0600 4Oct87, 1000 to 2100 5Oct87, 1300 6Oct87 to 1200 7Oct87, 0700 to 1200 8Oct87, 0100 to 0300 25Oct87, 0100 to 1200 4Nov87, 0400 to 1200 2Dec87, 0100 to 0300 15Dec87, and 0100 to 0300 27Dec87. All the breaks may be filled later. Missing data were linearly filled for this analysis.

providing protection against station loss from bears or humans, the Lonely and Resolution stations were also set to internally record. Overall data recovery was therefore quite good. The detailed list of missing and filled data in Table 4 mainly reflects transmission drops from non-recording stations and data missing since the March 1987 servicing visit. Additional problems were encountered with an unreliable batch of ARGOS buoys manufactured by ESI Company, designated as EB in Table 3. As a result, early failures with the first group of buoys deployed on the ice created an offshore data gap of three months. However, after the first week in March 1987, data coverage over the shelf is generally good, including the buoy data presented in this report, as well as those from buoys belonging to the Polar Science Center from which data will be available for our final analysis. Fleet Naval Oceanographic Center surface analyses will be used to interpolate missing station data.

The GOES station plots are presented in Figures 98-125 for Resolution Island, Lonely, Icy Cape and Cape Prince of Wales (Bering Strait) through the end of December 1987. ARGOS drift tracks are plotted in Figures 126-142 through the end of December 1987. Examples of weather affecting the region are presented in Figures 143-150.

The air temperatures over the coastal Beaufort and Chukchi seas did not cool off until the third week in November in 1986, nearly a month later than the climatological average. The September/October cruise of the Coast Guard icebreaker POLAR STAR encountered the least ice in the coastal Beaufort in thirty years this late in the fall. Low pressure centers passed through the area with frequencies and intensities typical of mid-latitude early autumn, and one storm immediately before the cruise caused extensive storm-surge damage in the Barrow area, including road damage, beach erosion, and destruction of archeological sites. This pattern was generally repeated in the autumn of 1987. The August/October 1987 cruise of the NOAA ship SURVEYOR also encountered nearly minimum ice extents. During light-ice summers, the open ocean plays a major role in affecting air temperatures but not necessarily sea-level pressure (Rogers, 1978).

During late winter and spring of 1987, the wind persisted from the east, the climatologically average direction. Approximately by the spring equinox, the solar radiation through relatively clear skies induced strong diurnal variations in air temperature, and the temperatures across the slope increased from -30°C at the end of the first week in April to around 0°C by the end of May 1987. At that time the temperature stabilized and the diurnal variations were diminished by the onset of persistent Arctic stratus.

Table 5 shows correlations of the unfiltered 1-hr coastal station data for calendar year 1987. This table shows that North Slope stations are substantially more like each other than like Kotzebue or Nome in temperature, pressure, and wind speed. Except for Resolution, the pressure lags are consistent with a picture that, during late summer and autumn, low pressure systems tend to propagate from the northeastern Bering Sea, northward along the Chukchi coast, and eastward

Table 5. Maximum correlations/at lag n at or above 95% confidence level for unfiltered, 1-hr data from six coastal meteorological stations (column lags row). Common time interval is from 0100 1Jan87 to 2200 31Dec87 with 8758 points. Number of lags is 30 (30 hours).

A. Sea-level pressure (SLP in mb).

	Barter	Resolution	Lonely	Barrow	Kotzebue	Nome
Barter	1.00/ 0	0.90/ 0	0.91/ 8	0.96/ 0	0.82/ 0	0.68/ 0
Resolutn	0.91/ 5	1.00/ 0	0.85/15	0.89/ 5	0.77/ 0	0.65/ 0
Lonely	0.88/ 0	0.81/ 0	1.00/ 0	0.89/ 0	0.65/ 0	0.53/ 0
Barrow	0.96/ 1	0.89/ 0	0.92/ 9	1.00/ 0	0.75/ 0	0.61/ 0
Kotzebue	0.85/ 8	0.78/ 5	0.74/17	0.78/ 8	1.00/ 0	0.96/ 0
Nome	0.74/12	0.67/ 9	0.64/21	0.66/13	0.96/ 4	1.00/ 0
Mean SLP	1014.87	1013.57	1013.13	1015.62	1009.43	1007.11

B. Surface air temperature (SAT in C).

	Barter	Resolution	Lonely	Barrow	Kotzebue	Nome
Barter	1.00/ 0	0.96/ 8	0.96/ 9	0.95/ 0	0.89/ 0	0.82/ 1
Resolutn	0.96/13	1.00/ 0	0.96/ 0	0.94/ 0	0.87/ 0	0.81/16
Lonely	0.95/ 0	0.96/ 0	1.00/ 0	0.95/ 0	0.88/ 0	0.83/16
Barrow	0.96/21	0.95/ 9	0.97/ 9	1.00/ 0	0.90/ 0	0.84/ 0
Kotzebue	0.89/22	0.88/ 8	0.89/ 9	0.90/ 0	1.00/ 0	0.94/ 0
Nome	0.83/23	0.82/ 9	0.83/30	0.84/ 0	0.94/ 1	1.00/ 0
Mean SAT	-11.47	-11.76	-12.26	-12.07	-5.12	-2.15

C. Station wind speed (SPD in m/s).

	Barter	Resolution	Lonely	Barrow	Kotzebue	Nome
Barter	1.00/ 0	0.52/ 0	0.41/ 8	0.49/ 0	0.04/30	-0.07/10
Resolutn	0.59/15	1.00/ 0	0.60/24	0.56/13	0.11/10	-0.08/28
Lonely	0.37/ 0	0.40/ 0	1.00/ 0	0.54/ 0	-0.02/30	-0.13/28
Barrow	0.50/ 2	0.50/ 0	0.62/ 8	1.00/ 0	0.12/ 0	-0.05/12
Kotzebue	0.10/20	0.13/16	0.08/30	0.21/24	1.00/ 0	0.42/ 0
Nome	-0.08/ 5	-0.05/ 0	-0.10/ 0	0.07/25	0.43/ 4	1.00/ 0
Mean SPD	6.13	5.40	3.58	5.90	5.68	4.68

along the Beaufort coast (Overland, 1981; Pease, 1987). For example, Barter lags Resolution by five hours, Lonely lags Barrow by nine hours, Barrow lags Kotzebue by eight hours, and Kotzebue lags Nome by four hours. This conclusion is further supported by the observation that all the North Slope stations lag Kotzebue by four hours less than they do Nome.

In a separate correlation (not shown) for a six-month interval including the spring and summer of 1987, a period of sustained easterly winds, pressure at Resolution strongly led all other stations, suggesting the westward propagation of high pressure anomalies. Also, the Brooks Range foots near Resolution, and there are interactions with the topography during winter and spring because of the strong capping inversions (Kozo, 1980; Overland, 1985). In the summer, sea breezes asymmetrically modify the surface wind along the north slope, as well (Kozo, 1982a,b; Kozo, 1984).

Considering the surface air temperature correlations in Table 5, we see that Resolution and Lonely lag both Barter and Barrow by 8-9 hours, which supports the idea that warm low pressure systems from the southwest and cold high pressure systems from the northeast pass over the area. All the stations have very high temperature correlations at low lags, because the solar diurnal cycle (especially during the spring months before the summer stratus develops) and the annual cycle account for a large portion of the variance of the air temperature in the polar and polar-marine climatic zone (Overland, 1981; Pease, 1987). Due to the prevalence of summer clouds, short wave radiation peaks in early June (Maykut and Church, 1973).

The wind speeds at Nome are essentially uncorrelated with the wind speeds along the North Slope, related to the orientation of the topography relative to the station and to the fact that many low pressure systems felt in the northeastern Bering Sea do not propagate northward into the Chukchi/Beaufort (Overland and Pease, 1982). Kotzebue wind speeds lag Nome by about four hours, but the correlation is modest and accounts for less than 20% of the variance at Kotzebue. Wind speed variance at Kotzebue leads that at all the North Slope stations by 16-30 hours, but only accounts for 4% of the variance at Barrow. In contrast, wind speed variance at Resolution leads variance at all North Slope stations by 13-24 hours and accounts for about 36% of the variance at the other stations. In general, however, the wind speed correlations are relatively low among all the stations because topographical and other local effects reduce the correlations (Kozo, 1980) compared to pressure correlations.

In order to evaluate the quality of the FNOC surface analyses for use in filling missing data and to aid in spatial interpolations, we compared FNOC data with two independent GOES stations and two non-independent NWS stations along the north slope. Table 6 shows the correlations for pressure, wind speed, and temperature for the four coastal meteorological stations compared with point data stripped from the FNOC gridded fields by METLIB and interpolated to each site. Table 7 correlates pressure measured at two of the ARGOS buoys with FNOC pressure. Since FNOC analyses are generated every six hours (twelve hours for

Table 6. Maximum correlations/at lag n at or above 95% confidence level for 6-hr data from four coastal meteorological stations and the equivalent FNOC data for the same sites (column lags row). N stands for NWS station, G stands for GOES station, and F stands for FNOC equivalent. Common time interval is from 0100 26Sep86 to 2200 31Aug87. Number of lags is 5 (30 hours).

A. Sea-level pressure (SLP in mb) for 6-hr data.

	BarterN	BarterF	ResoluG	ResoluF	LonelyG	LonelyF	BarrowN	BarrowF
BarterN	1.00/0	0.99/2	0.93/1	0.99/1	0.98/1	0.98/1	0.96/0	0.96/1
BarterF	0.94/0	1.00/0	0.91/0	1.00/0	0.97/0	0.98/0	0.90/0	0.96/0
ResoluG	0.93/0	0.93/1	1.00/0	0.93/1	0.92/1	0.93/1	0.90/0	0.91/1
ResoluF	0.95/0	1.00/0	0.92/0	1.00/0	0.99/0	0.99/0	0.92/0	0.97/0
LonelyG	0.95/0	0.97/0	0.92/0	0.99/0	1.00/0	1.00/0	0.95/0	0.99/0
LonelyF	0.95/0	0.93/0	0.92/0	0.99/0	1.00/0	1.00/0	0.95/0	0.99/0
BarrowN	0.96/0	0.96/2	0.91/1	0.97/2	0.99/2	0.99/2	1.00/0	1.00/2
BarrowF	0.94/0	0.96/0	0.90/0	0.97/0	0.99/0	0.99/0	0.96/0	1.00/0

B. Station wind speed (SPD in m/s) for 6-hr data.

	BarterN	BarterF	ResoluG	ResoluF	LonelyG	LonelyF	BarrowN	BarrowF
BarterN	1.00/0	0.35/2	0.52/1	0.28/1	0.25/1	0.27/1	0.42/0	0.28/1
BarterF	0.26/0	1.00/0	0.33/0	0.93/0	0.23/0	0.77/0	0.33/0	0.67/0
ResoluG	0.45/0	0.35/1	1.00/0	0.31/1	0.41/4	0.30/1	0.40/0	0.28/1
ResoluF	0.23/0	0.93/0	0.31/0	1.00/0	0.15/0	0.92/0	0.35/0	0.81/0
LonelyG	0.21/0	0.23/1	0.35/0	0.15/0	1.00/0	0.14/0	0.36/0	0.13/0
LonelyF	0.22/0	0.77/0	0.30/0	0.92/0	0.14/0	1.00/0	0.39/0	0.97/0
BarrowN	0.42/0	0.43/2	0.44/1	0.43/2	0.44/1	0.47/2	1.00/0	0.48/2
BarrowF	0.24/0	0.67/0	0.28/0	0.81/0	0.13/0	0.97/0	0.41/0	1.00/0

C. Surface air temperature (SAT in C) for 12-hr data.

	ResoluG	ResoluF	LonelyG	LonelyF
ResoluG	1.00/0	0.97/2	0.96/0	0.96/2
ResoluF	0.37/0	1.00/0	0.35/0	1.00/0
LonelyG	0.96/0	0.95/0	1.00/0	0.96/2
LonelyF	0.36/0	1.00/0	0.36/0	1.00/0

Table 7. Correlation between pressure measured at two of the ARGOS buoys and pressure from the FNOC fields at the position of the buoys. The analysis was carried out for the lifetime of the buoy: from 1 March to 12 June 1987 for buoy 7422 and from 7 March to 11 April, 1987 for buoy 7423.

	7422A	7422M		7423A	7423M
7422A	----	.99(0)	7423A	----	1.0(0)
7422M	.99(0)	----	7423M	1.0(0)	----

temperature fields), we subsampled the hourly station data at the appropriate intervals. In general, temperatures and pressures were well modeled by the FNOC analyses with one caveat: the FNOC analyses were lagged six to twelve hours from the stations data, although they were in phase with the ARGOS data. For example, both Barter and Barrow pressure and wind speed led the FNOC data by 12 hours.

5. SUMMARY

During the period from October 1986 to April 1987, near-surface currents over the Beaufort Sea continental shelf and margin were westward, although the vector mean magnitude at many moorings was smaller than the RMS error. The depth at which the mean flow became easterly, i.e., the depth at which the Beaufort Undercurrent began, was between 60-90 m. This depth varied spatially and also appears to change from year to year. Flow reversals in the undercurrent to westerly motion occurred frequently, and these reversals may have driven upwelling of warm, saline water onto the shelf. Vertical excursions were in the range of 100-150 m. Such upwelling events were evident both in the time-series records and in the hydrographic sections.

An important point is evident from the October occupation of section W, viz. that a major source of water for the Beaufort Undercurrent must lie farther west than had previously been considered. Most likely, this other injection occurs in the vicinity of Herald Canyon.

Many low-frequency flow events were coherent vertically and over large horizontal distances. Maximum horizontal correlations over the outer shelf were measured at depths of 90-100 m. Variance at the western moorings led that at the eastern ones, and the phase difference suggests an eastward propagation rate of about 5 m s^{-1}.

The hydrographic data provide extensive coverage of both fall and winter conditions. A possibly important feature in the data is the longshore variability in the hydrography of the Beaufort Sea shelf, including possible major hydrographic differences between the western and eastern Beaufort. The latter transition appears to occur in the vicinity of Prudhoe Bay.

With respect to the meteorology, both the autumns of 1986 and 1987 were abnormally warm, and an unusual number of low-pressure centers passed through the Beaufort Sea. The

autumn ice extents were well below average. The late winter and spring of 1987 were more climatically normal.

Pressure and air temperature measured at the GOES stations were generally better spatially correlated than was wind speed, because of topographic and other effects. Pressure and temperature fields were well modeled by the FNOC analyses, which can therefore be used to fill in missing data. Correlation coefficients and lags suggest that warm low-pressure systems propagate up the Chukchi Sea coast and then eastward along the Beaufort Sea coast, while cold high-pressure systems originate farther east and propagate towards the west.

The total data set is extraordinary in the temporal and spatial extent of its synoptic coverage, and in the variety of its constituent measurements. The data set is also extremely large, and its full reduction and analysis will provide an exceptional opportunity for improving our understanding of the shelf circulation and its forcing, as well as conditions important to the marine ecology of the area.

At the same time, the size of the data set provides a genuine challenge in processing and analysis. Major processing tasks remain. For example, the numerous long current and pressure records for April 1987-April 1988, and just now recovered, have not yet been processed and reduced. Likewise, the ARGOS data from 1988 have not been analyzed, and in fact some of the ARGOS buoys are still transmitting. As the various meteorological and oceanographic components of the composite data set become available in a fully processed form, their synthesis promises new insights into the processes governing conditions over the Beaufort Sea shelf.

6. ACKNOWLEDGMENTS

The Beaufort Mesoscale Circulation Study is a contribution to the Marine Services Project of the Pacific Marine Environmental Laboratory. It was financed in part by the Minerals Management Service through an interagency agreement with the National Oceanic and Atmospheric Administration (NOAA) under a multiyear program, responding to the needs of petroleum development of the Alaskan continental shelf and managed by the Outer Continental Shelf Environmental Assessment Program Office. A portion of the ARGOS buoy deployments were funded by the Office of Naval Research-Arctic Programs.

C.H. Darnall was chief engineer for the project. K. Krogslund completed the oceanic chemical analyses. Lt(jg) G.A. Galasso was the engineer for the meteorological stations. V.L. Long and N. Jenkins contributed to the data analyses. We also acknowledge the numerous other NOAA, Coast Guard, and civilian personnel who contributed to the successful completion of the experiment in a hostile physical environment.

7. REFERENCES

Aagaard, K., 1981. Current measurements in possible dispersal regions of the Beaufort Sea. In *Final Reports of Principal Investigators*, Volume 3, Physical Science Studies. National Oceanic and Atmospheric Administration, Boulder, CO, 1-74.

Aagaard, K., 1984. The Beaufort Undercurrent. In *The Alaskan Beaufort Sea: Ecosystems and Environment* (ed. by D. Schell, P. Barnes, and E. Reimnitz), Academic Press, New York, 47-71.

Aagaard, K., S. Salo, and K. Krogslund, 1987. Beaufort Sea Mesoscale Circulation Study: Hydrography USCGC Polar Star Cruise, October 1986. NOAA Data Report ERL PMEL-19, Seattle, WA, 83 pp.

Aagaard, K., S. Salo, and K. Krogslund, 1988. Beaufort Sea Mesoscale Circulation Study: Hydrography Helicopter Operations, April 1987. NOAA Data Report ERL PMEL-22, Seattle, WA, 25 pp.

Barnes, P.W., and L.J. Toimil, 1979. Inner shelf circulation patterns Beaufort Sea, Alaska. U.S.G.S. Miscellaneous Field Studies Map MF-1125, Menlo Park, CA, 1 plate.

Coachman, L.K., K. Aagaard, and R.B. Tripp, 1974. Bering Strait: The Regional Physical Oceanography. University of Washington Press, Seattle, WA, 172 pp.

Foldvik, A., K. Aagaard, and T. Torresen, 1988. On the velocity field of the East Greenland Current. *Deep-Sea Research, 35*, in press.

Hufford, G.L., 1974. On apparent upwelling in the southern Beaufort Sea. *Journal of Geophysical Research, 79*, 1305-1306.

Jones, E.P., and L.G. Anderson, 1986. On the origin of the chemical properties of the Arctic Ocean halocline. *Journal of Geophysical Research, 91*, 759-10, 767.

Kozo, T.L., 1980. Mountain barrier baroclinicity effects on surface winds along the Alaskan Arctic coast. *Geophysical Research Letters, 7*, 377-380.

Kozo, T.L., 1982a. An observational study of sea breezes along the Alaskan Beaufort Sea Coast: Part I. *Journal of Applied Meteorology, 21*, 891-905.

Kozo, T.L., 1982b. An observational study of sea breezes along the Alaskan Beaufort Sea Coast: Part II. *Journal of Applied Meteorology, 21*, 906-924.

Kozo, T.L., 1984. Mesoscale wind phenomena along the Alaskan Beaufort Sea coast. In *The Alaskan Beaufort Sea: Ecosystem and Environment* (ed. by P. Barnes, D. Schell, and E. Reimnitz), Academic Press, Orlando, FL, 23-45.

Kozo, T.L. and R.Q. Robe, 1986. Modeling winds and open-water buoy drift along the eastern Beaufort Sea coast, including the effects of the Brooks Range. *Journal of Geophysical Research, 91*, 13011-13032.

Maykut, G.A., and P.E. Church, 1973. Radiation climate of Barrow, Alaska, 1962-1966. *Journal of Applied Meteorology, 12*, 620-628.

Moore, R.M., M.G. Lowings, and F.C. Tan, 1983. Geochemical profiles in the central Arctic Ocean: Their relation to freezing and shallow circulation. *Journal of Geophysical Research, 88*, 2667-2674.

Mountain, D.G., 1974. Bering Sea Water on the North Alaskan Shelf. Ph.D. dissertation, University of Washington, Seattle, 154 pp.

Newton, J.L., K. Aagaard, and L.K. Coachman, 1974. Baroclinic eddies in the Arctic Ocean. *Deep-Sea Research, 21*, 707-719.

Overland, J.E., 1981. Marine climatology of the Bering Sea. In *The Eastern Bering Sea Shelf: Oceanography and Resources*, Volume 1 (ed. by D.W. Hood and J.A. Calder), University of Washington Press, Seattle, WA, 15-22.

Overland, J.E., 1985. Atmospheric boundary layer structure and drag coefficients over sea ice. *Journal of Geophysical Research, 90*, 9029-9049.

Overland, J.E. and C.H. Pease, 1982. Cyclone climatology of the Bering Sea and its relation to sea ice extent. *Monthly Weather Review, 110*, 5-13.

Pease, C.H., 1987. Meteorology of the Chukchi Sea: an overview. In *Chukchi Sea Information Update* (ed. by D.A. Hale), NOAA/NOS Ocean Assessments Division – Alaska Office, Anchorage, AK, 11-19.

Rogers, J.C., 1978. Meteorological factors affecting interannual variability of summertime ice extent in the Beaufort Sea. *Monthly Weather Review, 106*, 890-897.

Tripp, R.B., 1987. ISHTAR Cruise Report, R/V *Thomas G. Thompson* Cruise TT-212, 29 June-19 July 1987. University of Washington, School of Oceanography, informal report, 149 pp.

FIGURES

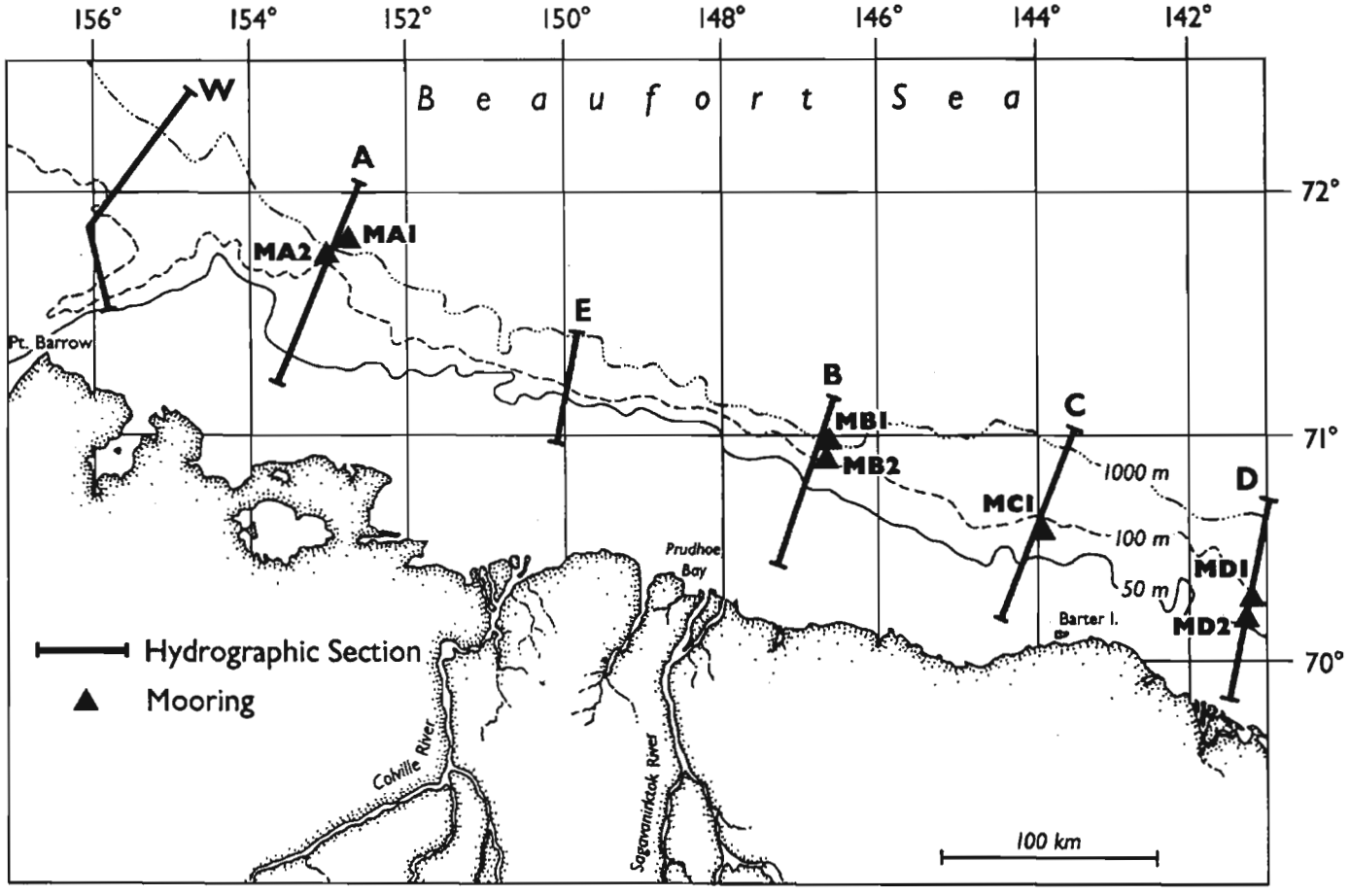

Figure 1. Locations of hydrographic sections occupied in October 1986 and moorings recovered in 1987.

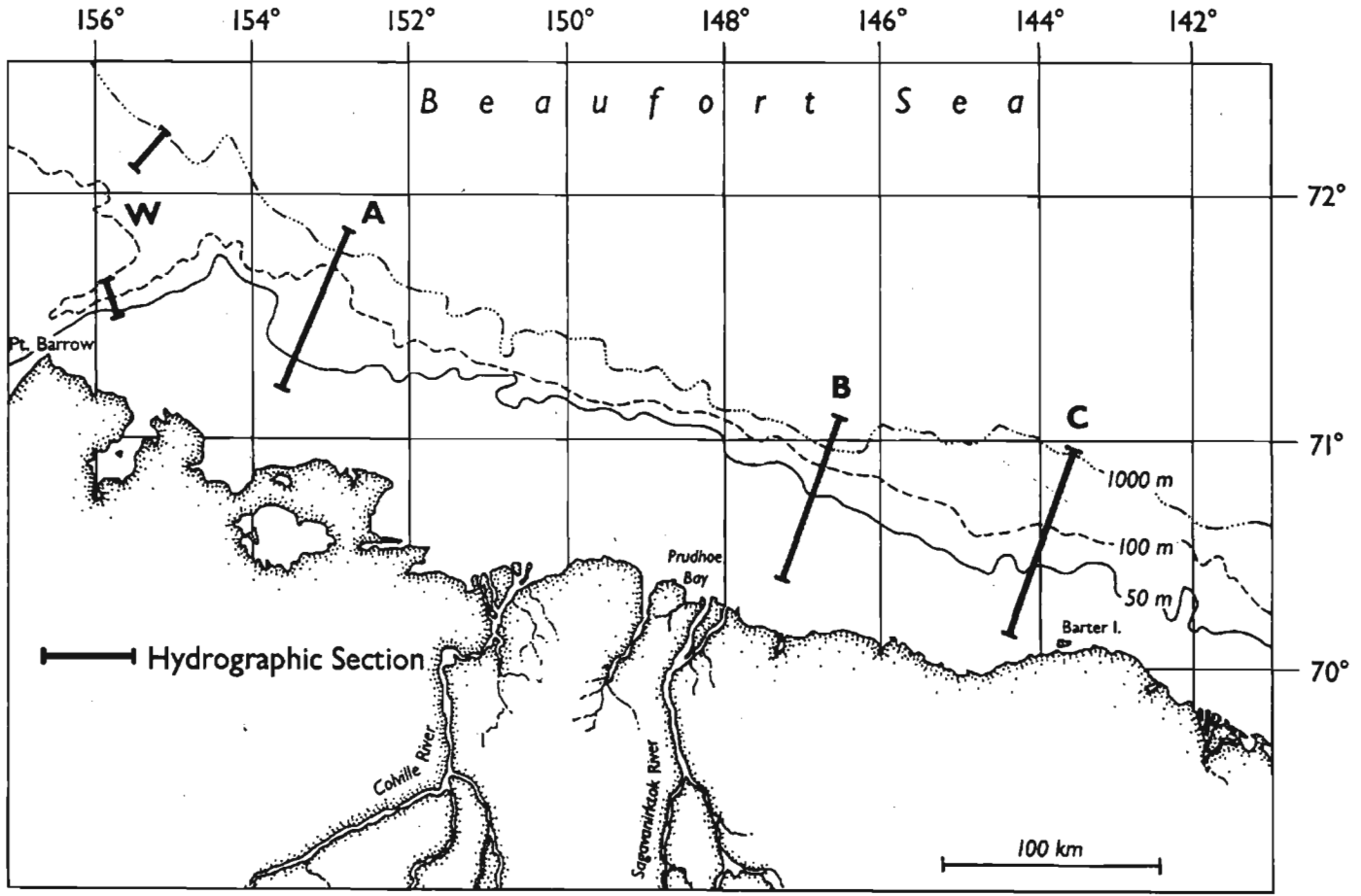

Figure 2. Locations of hydrographic sections occupied in April 1987.

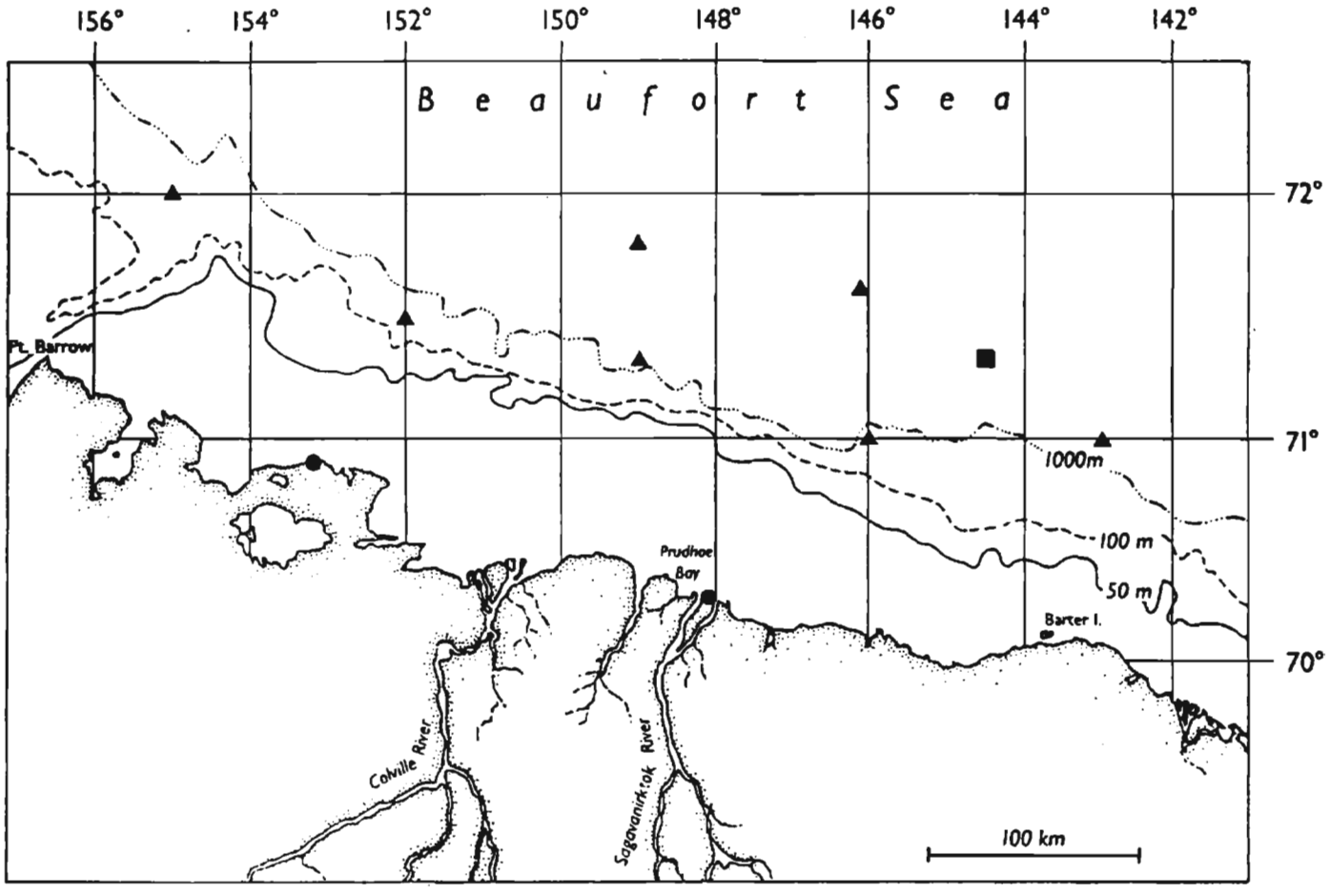

Figure 3. Positions at which ARGOS buoys (▲) and stations (■), and GOES meteorological stations (●) were deployed in 1986-87. Buoys and stations deployed south or west of Barrow are not shown.

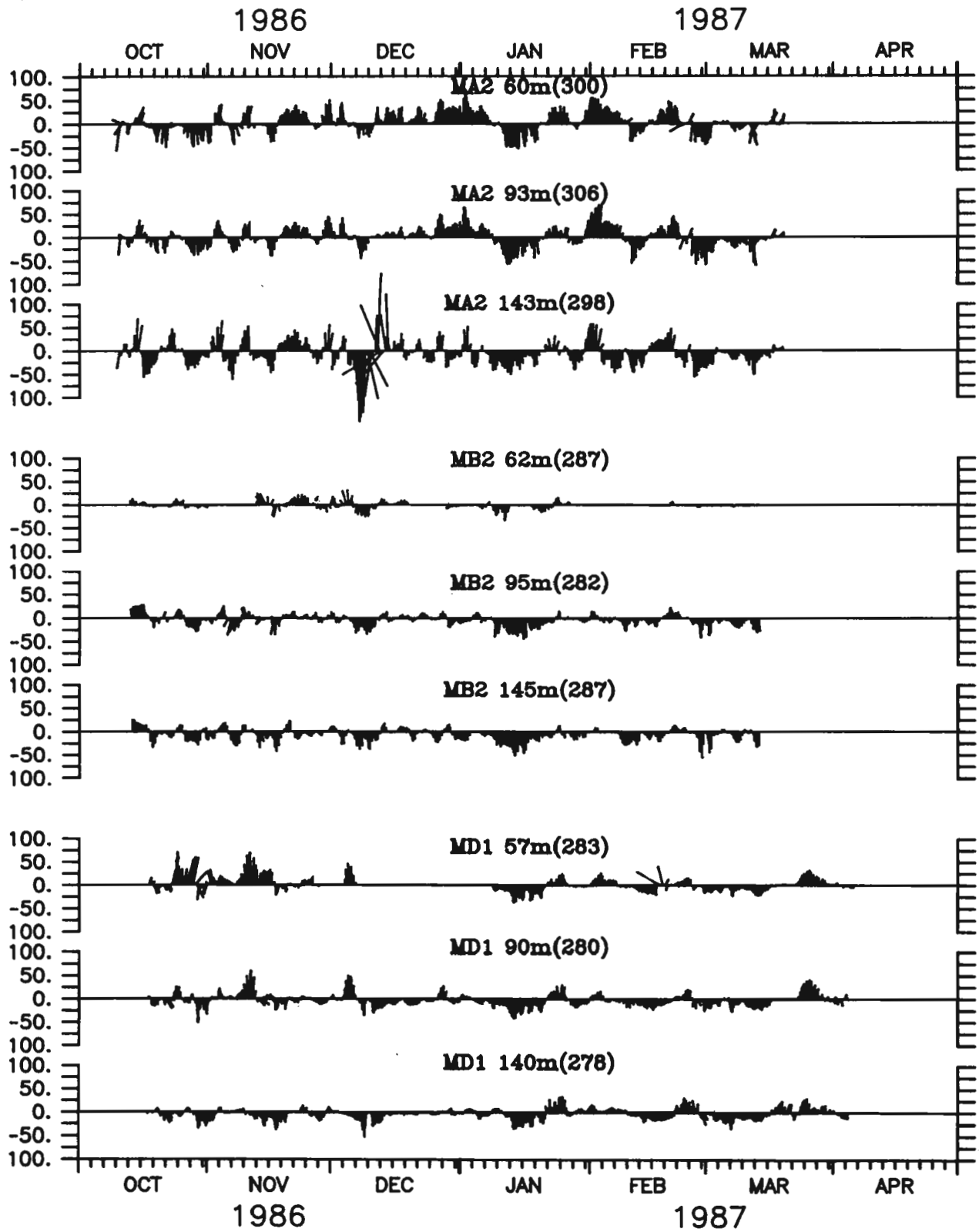

Figure 4. Current vectors from the instruments deployed in October 1986 at the moorings in water 165-170 m deep. Currents were 35-hour filtered.

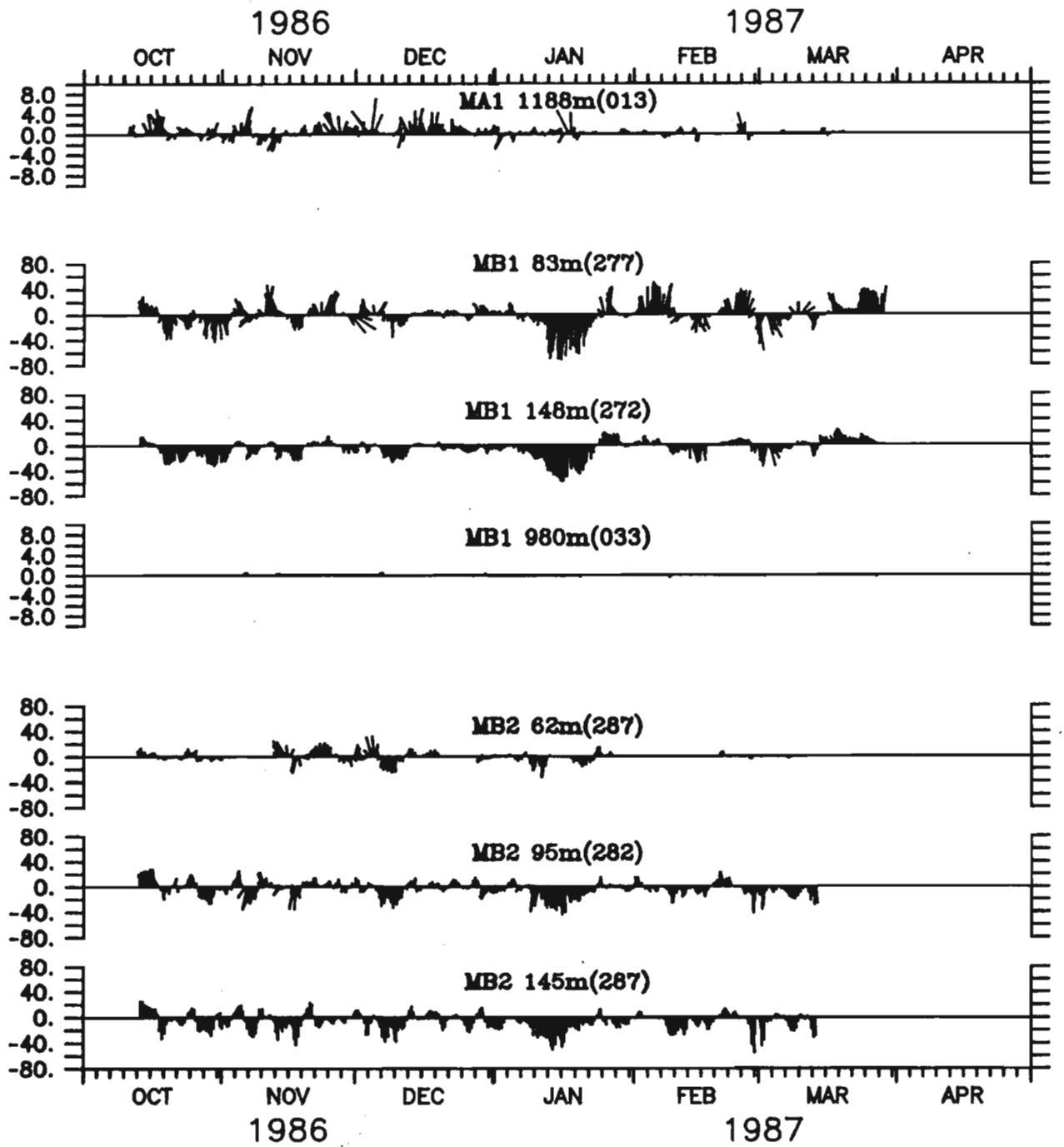

Figure 5. Current vectors at the deeper moorings deployed in October 1986. Mooring MB2 is repeated from Figure 4 for comparison.

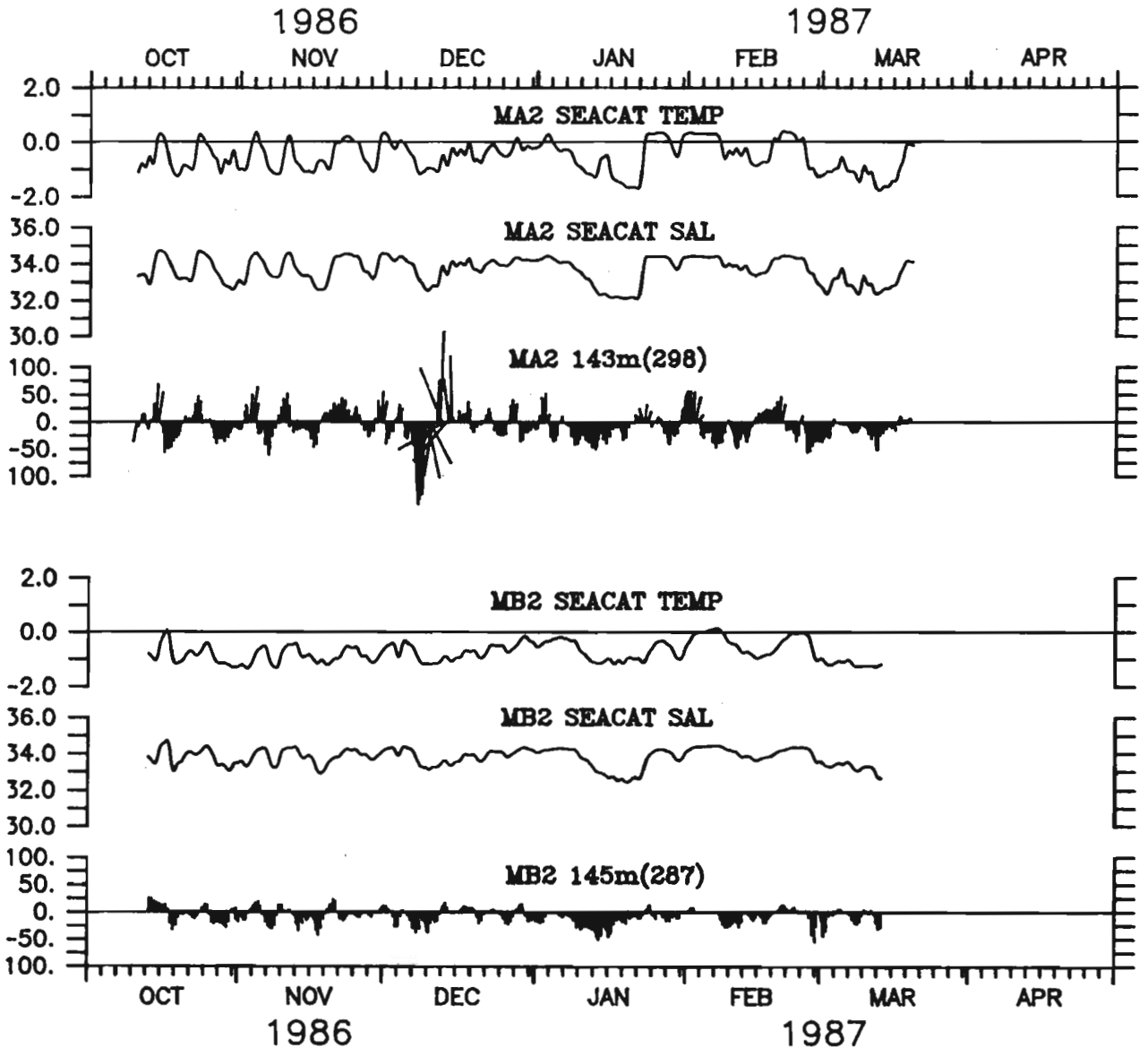

Figure 6. SeaCat temperature and salinity at MA2 and MB2, and current vectors at the deepest meter from these moorings. Data were 35-hour filtered.

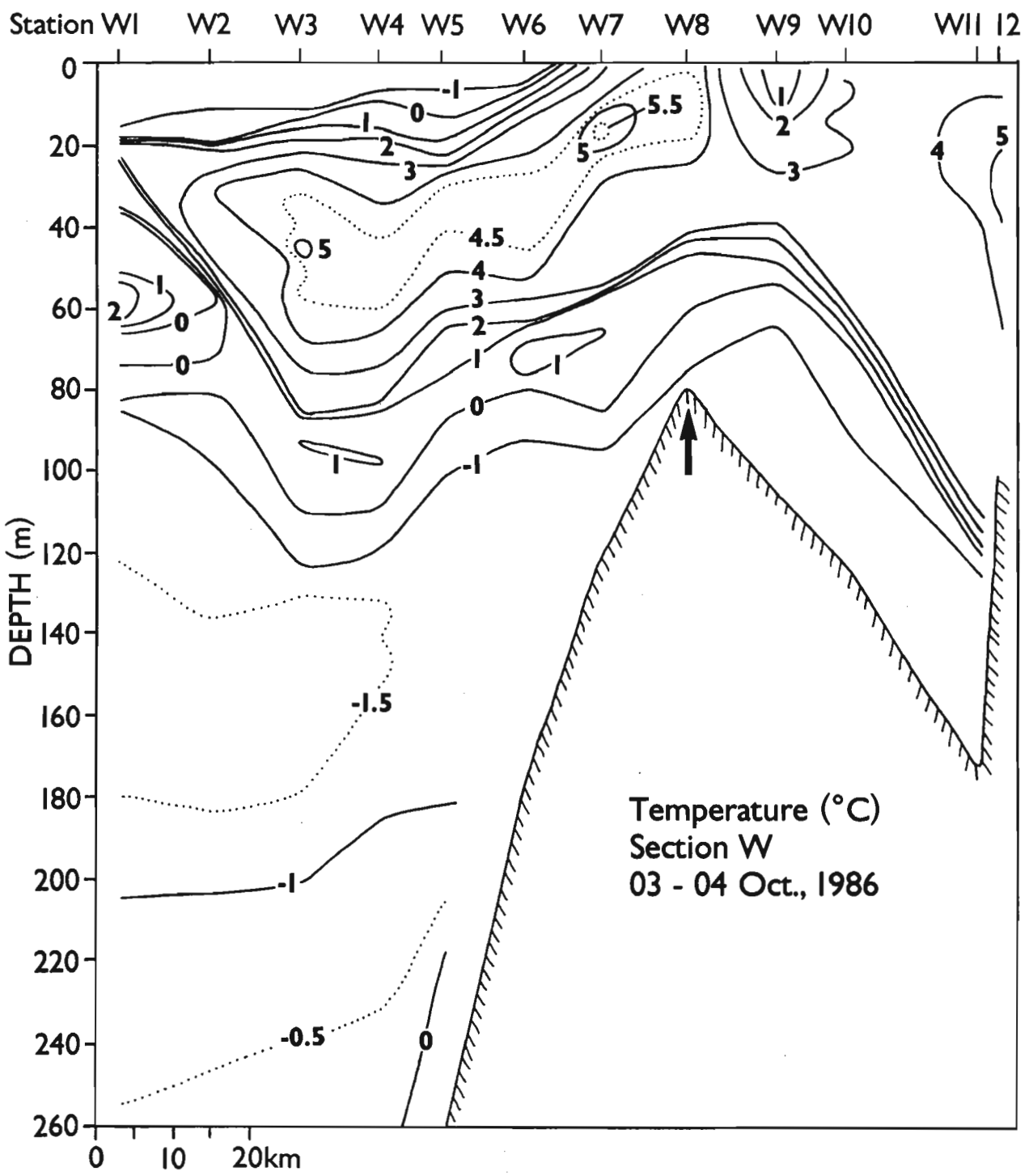

Figure 7. Temperature at section W in October 1986.

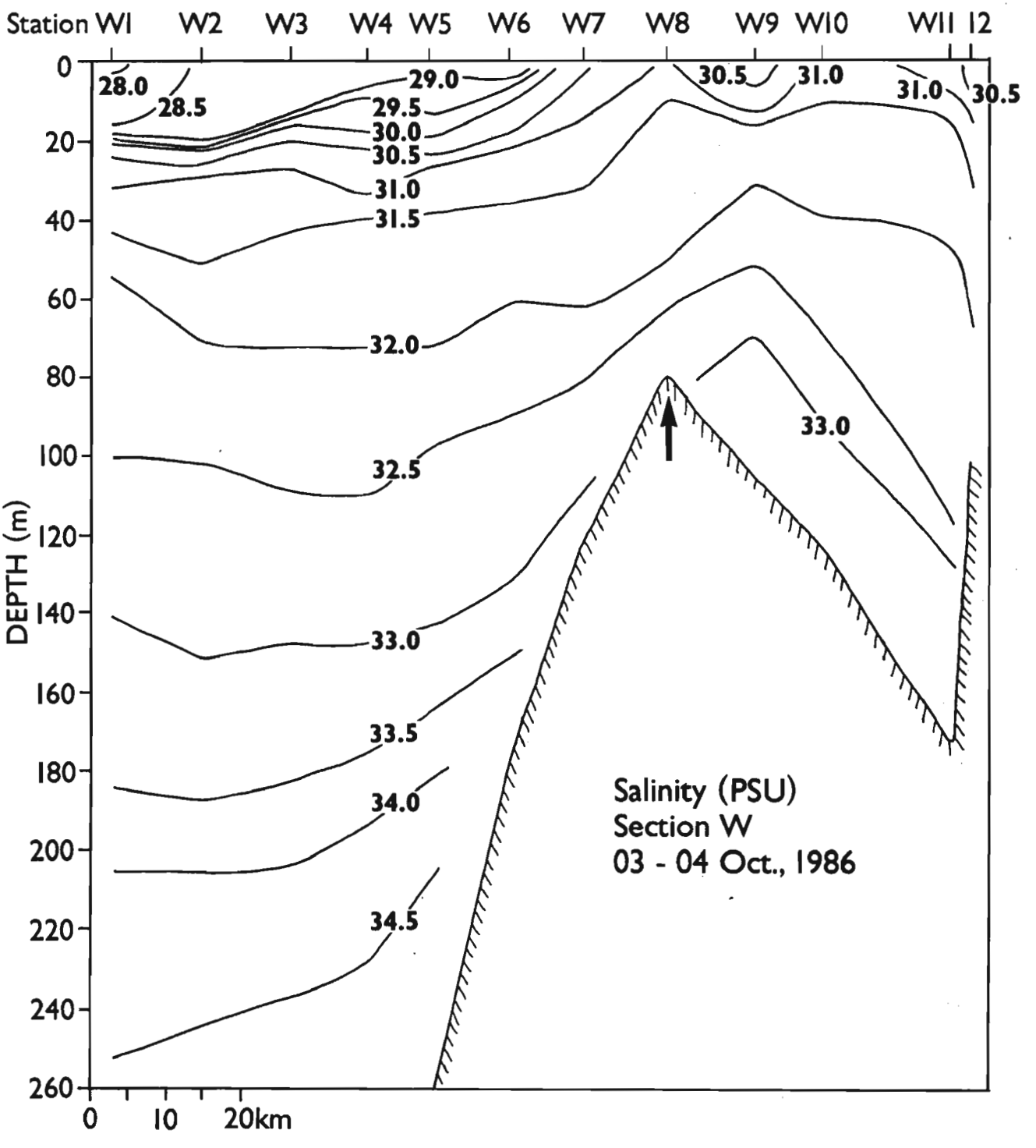

Figure 8. Salinity at section W in October 1986.

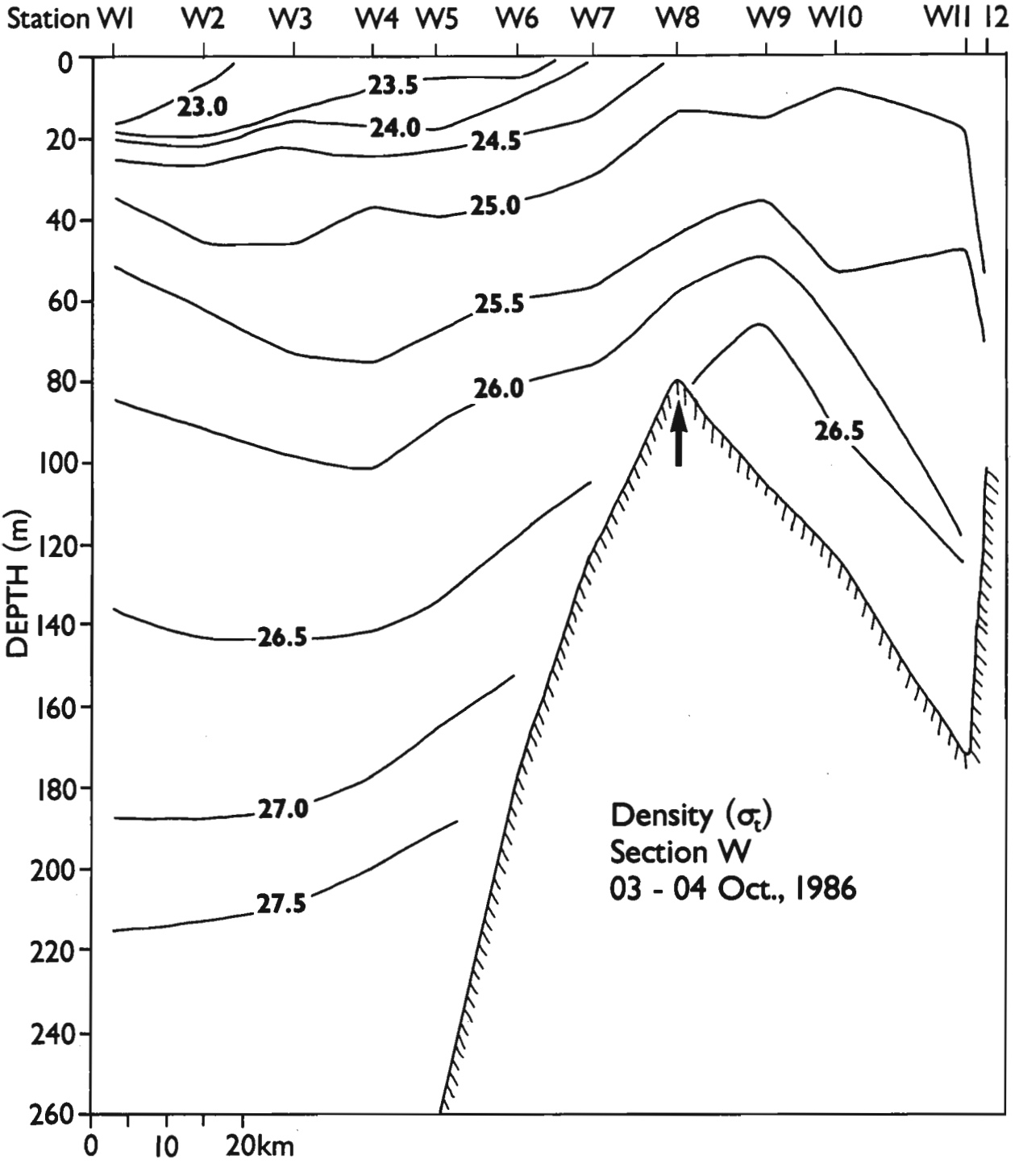

Figure 9. Density at section W in October 1986.

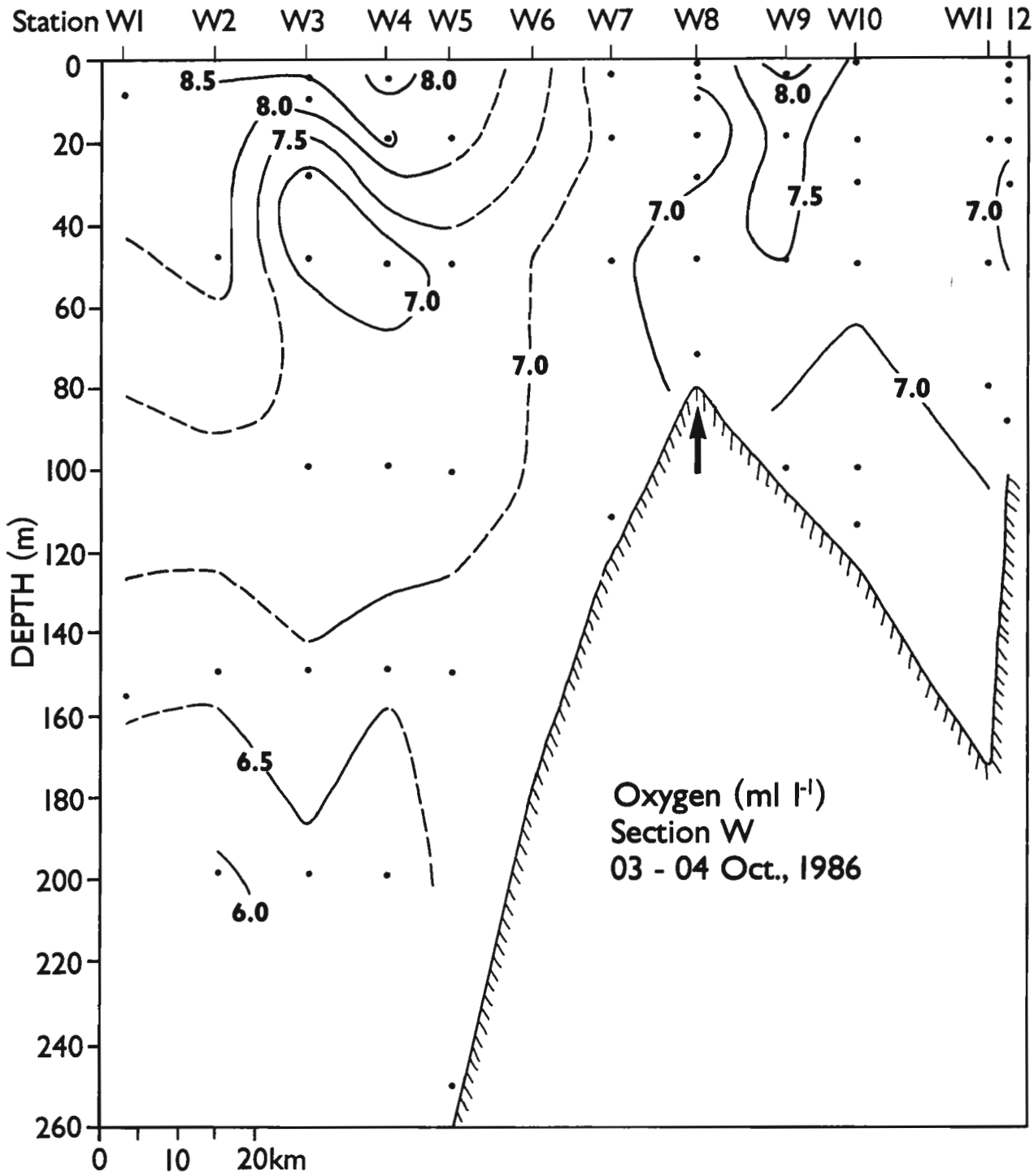

Figure 10. Dissolved oxygen at section W in October 1986.

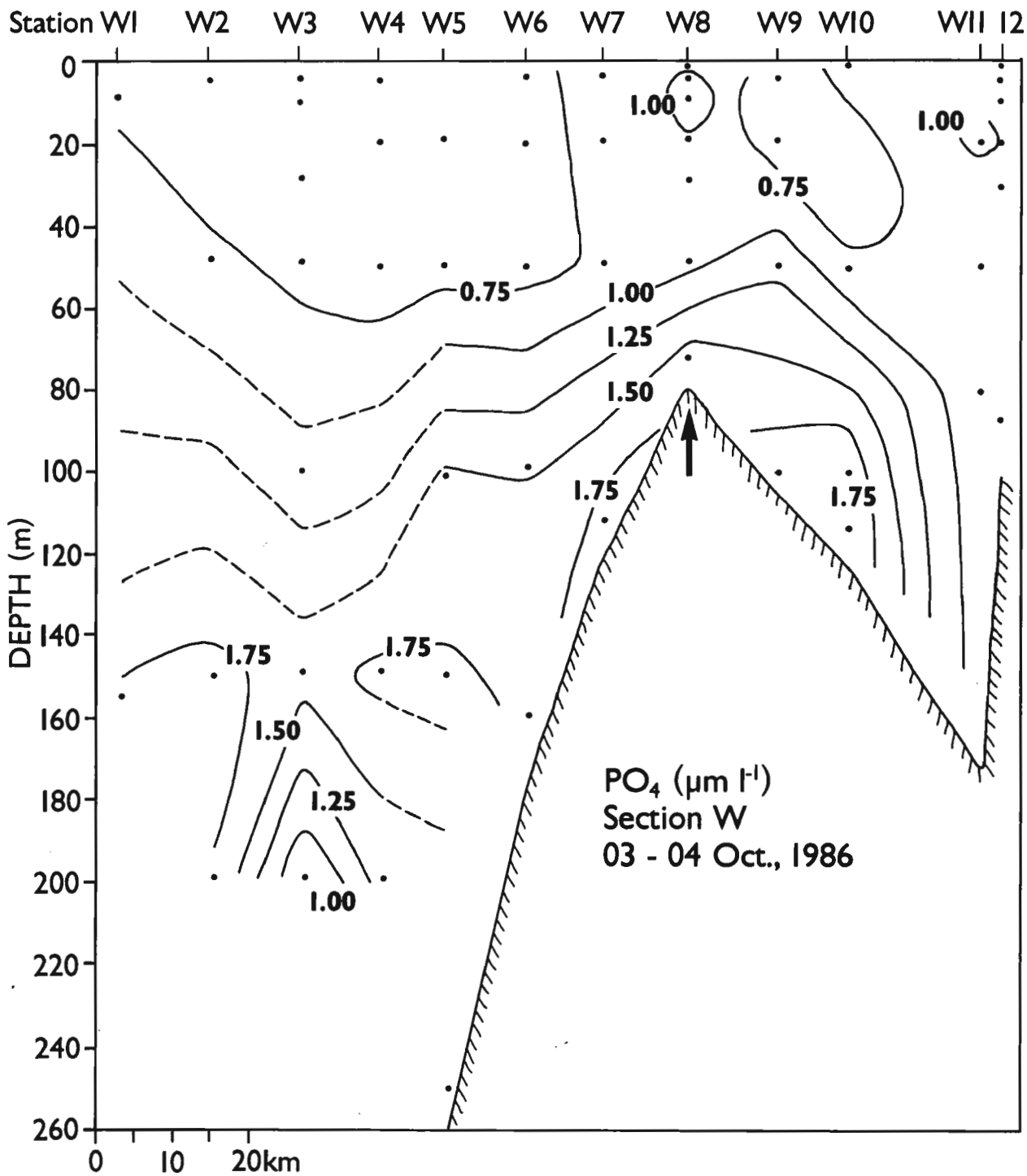

Figure 11. Phosphate at section W in October 1986.

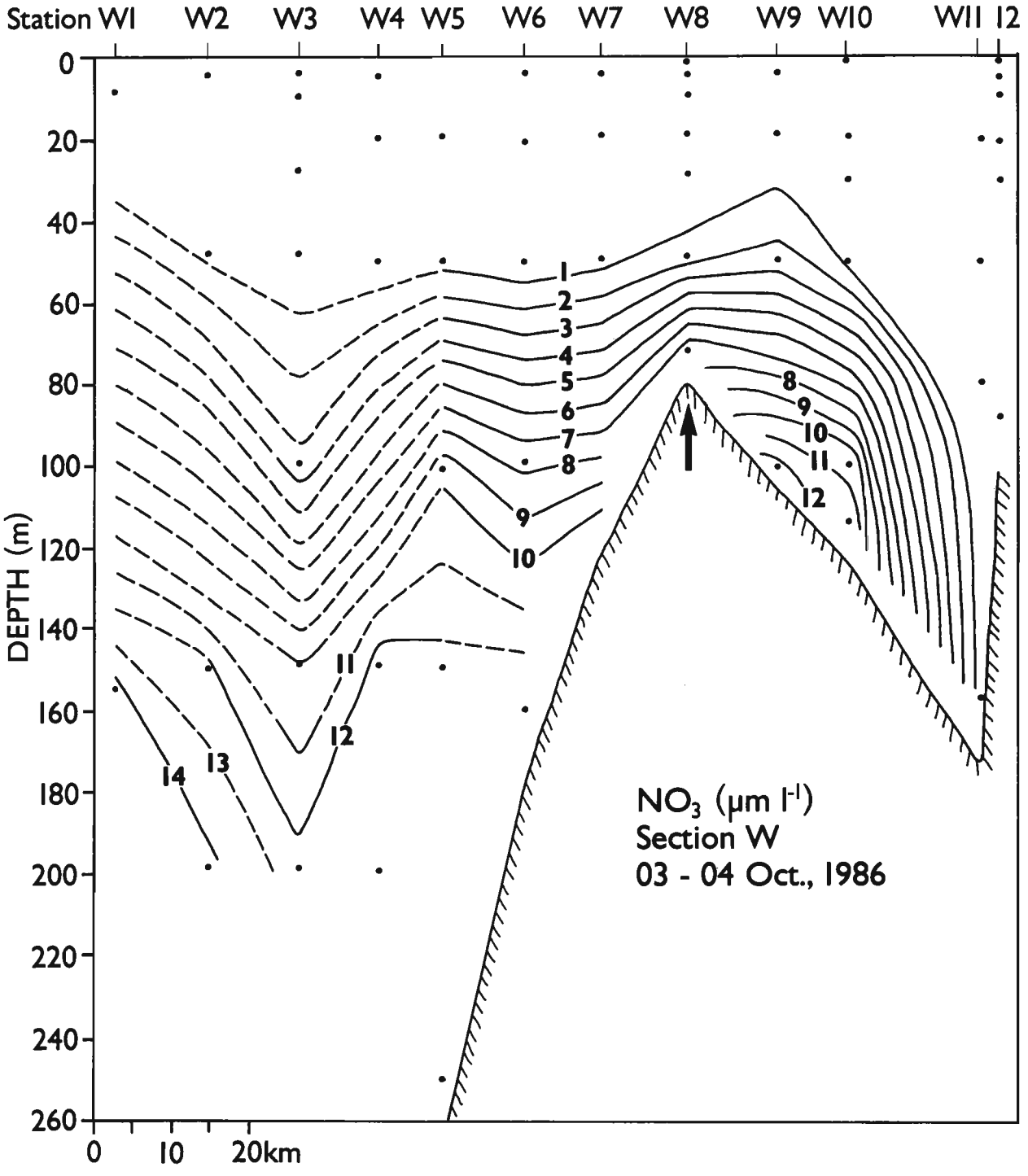

Figure 12. Nitrate at section W in October 1986.

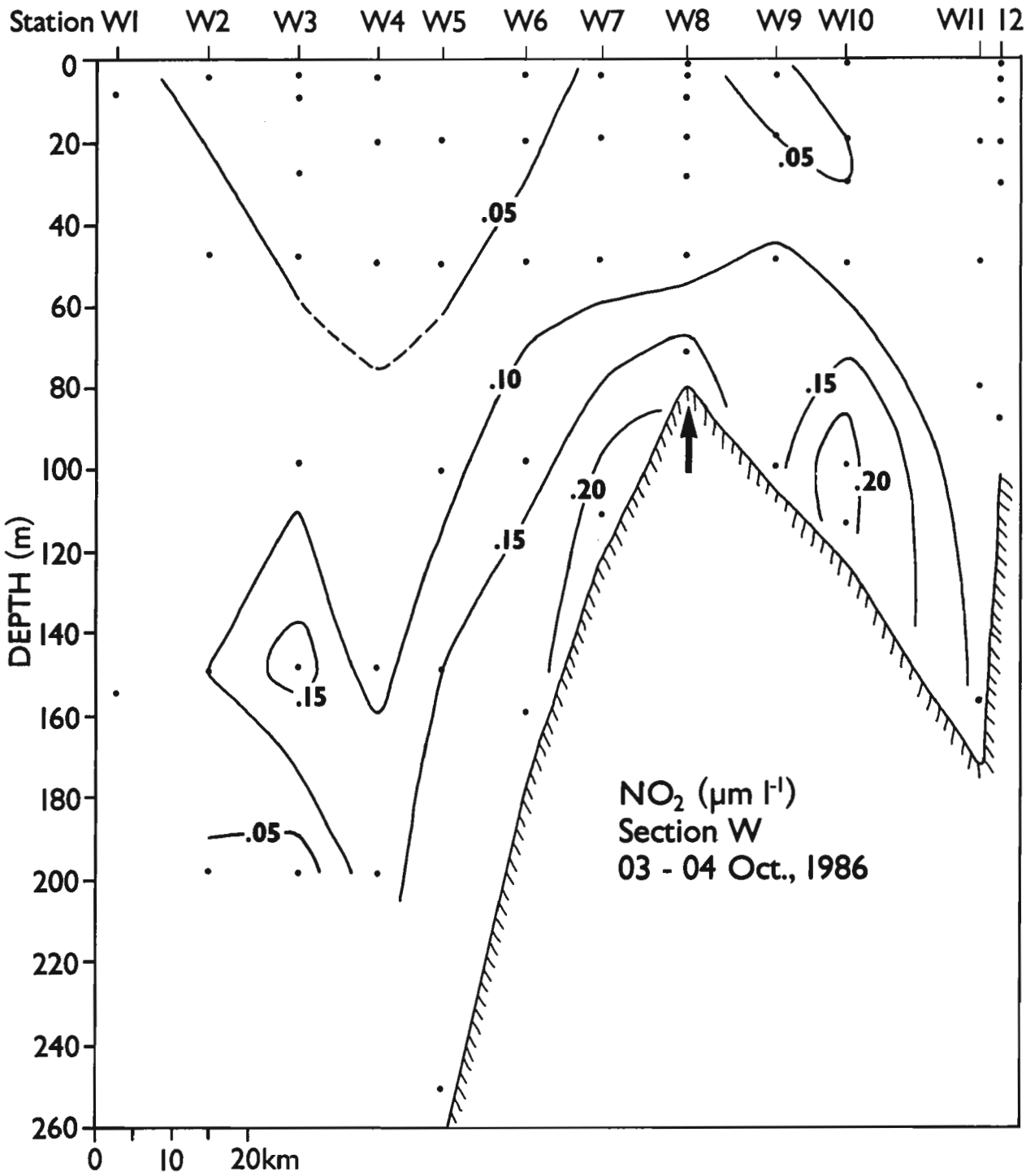

Figure 13. Nitrite at section W in October 1986.

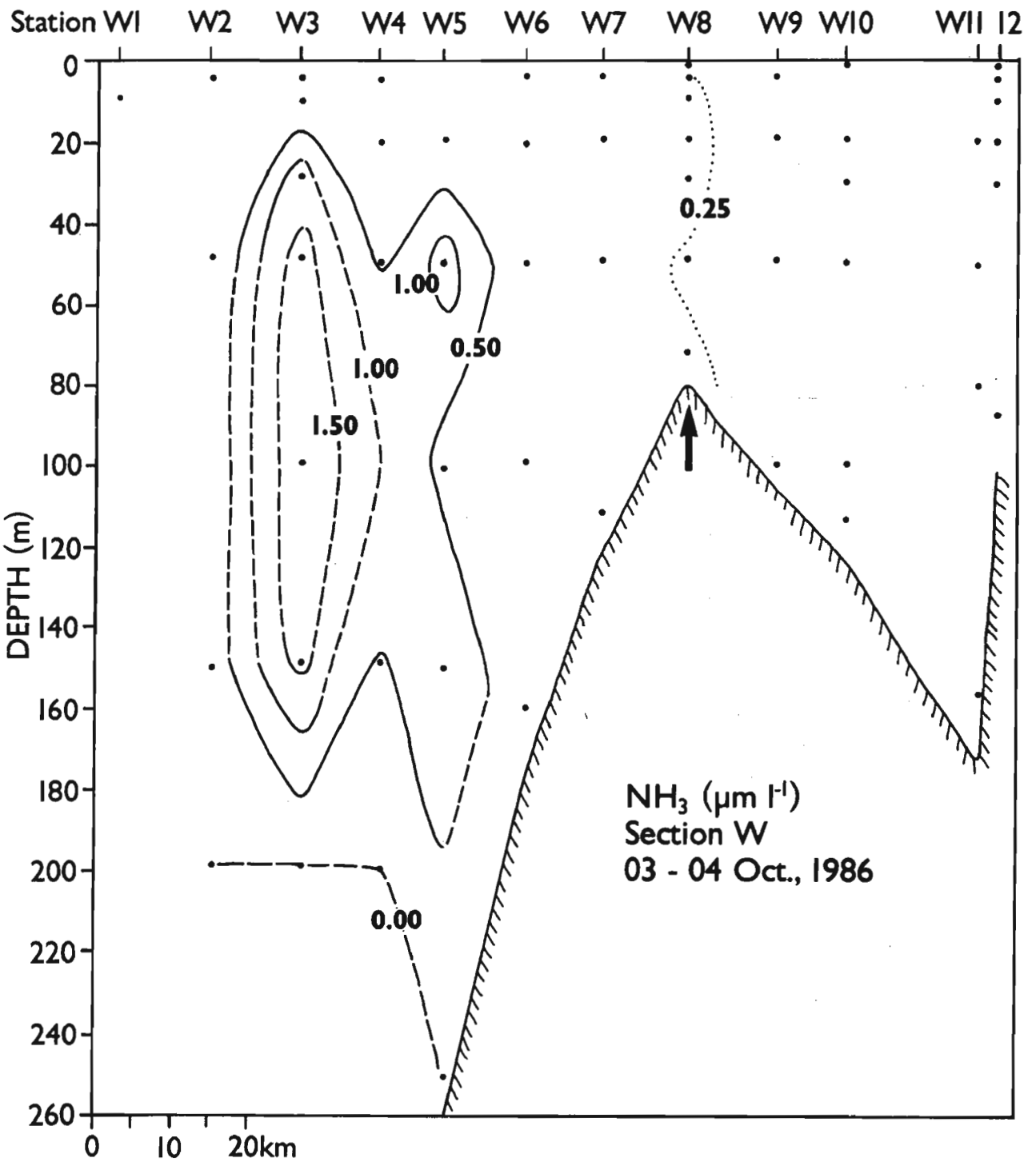

Figure 14. Ammonia at section W in October 1986.

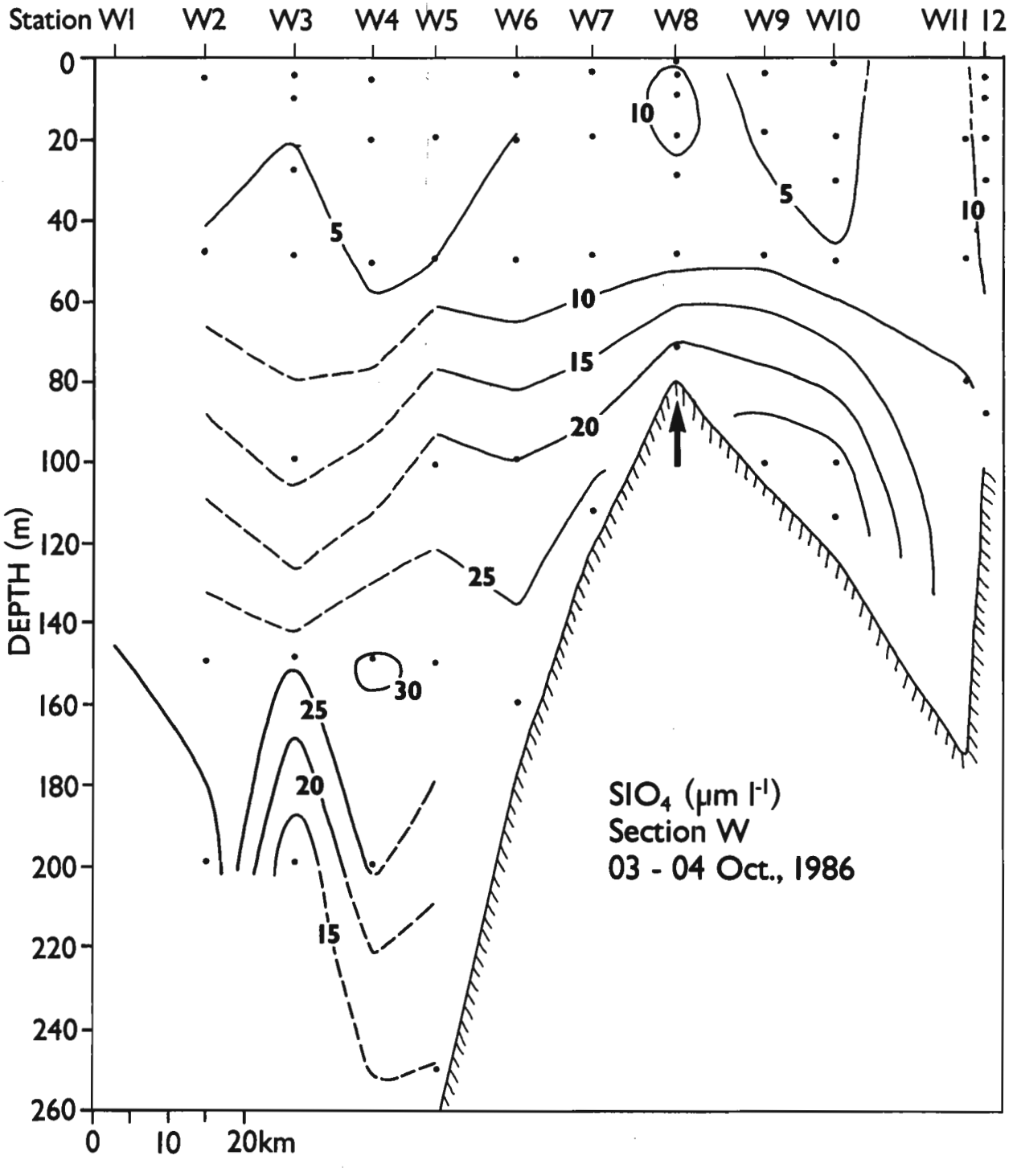

Figure 15. Silicate at section W in October 1986.

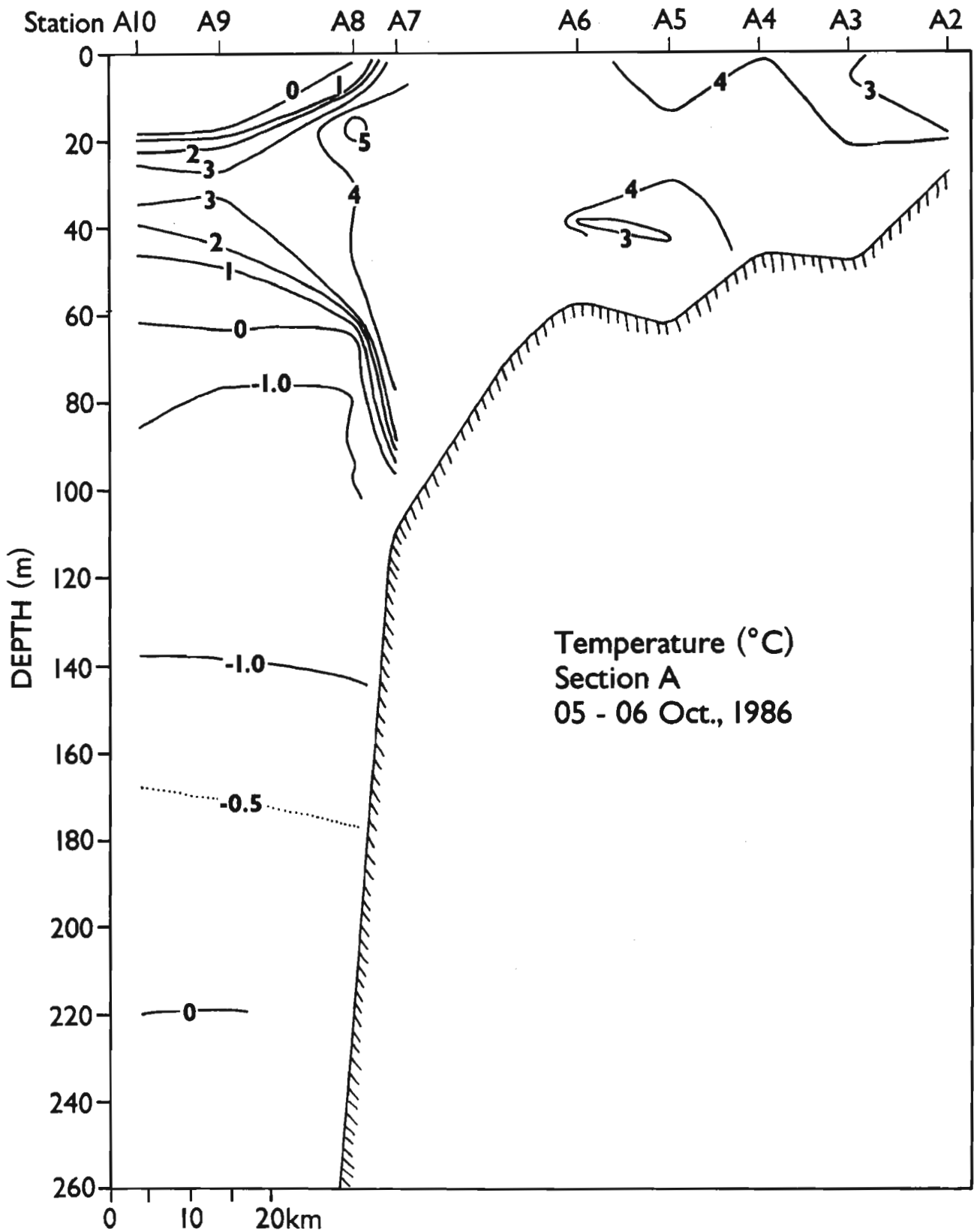

Figure 16. Temperature at section A in October 1986.

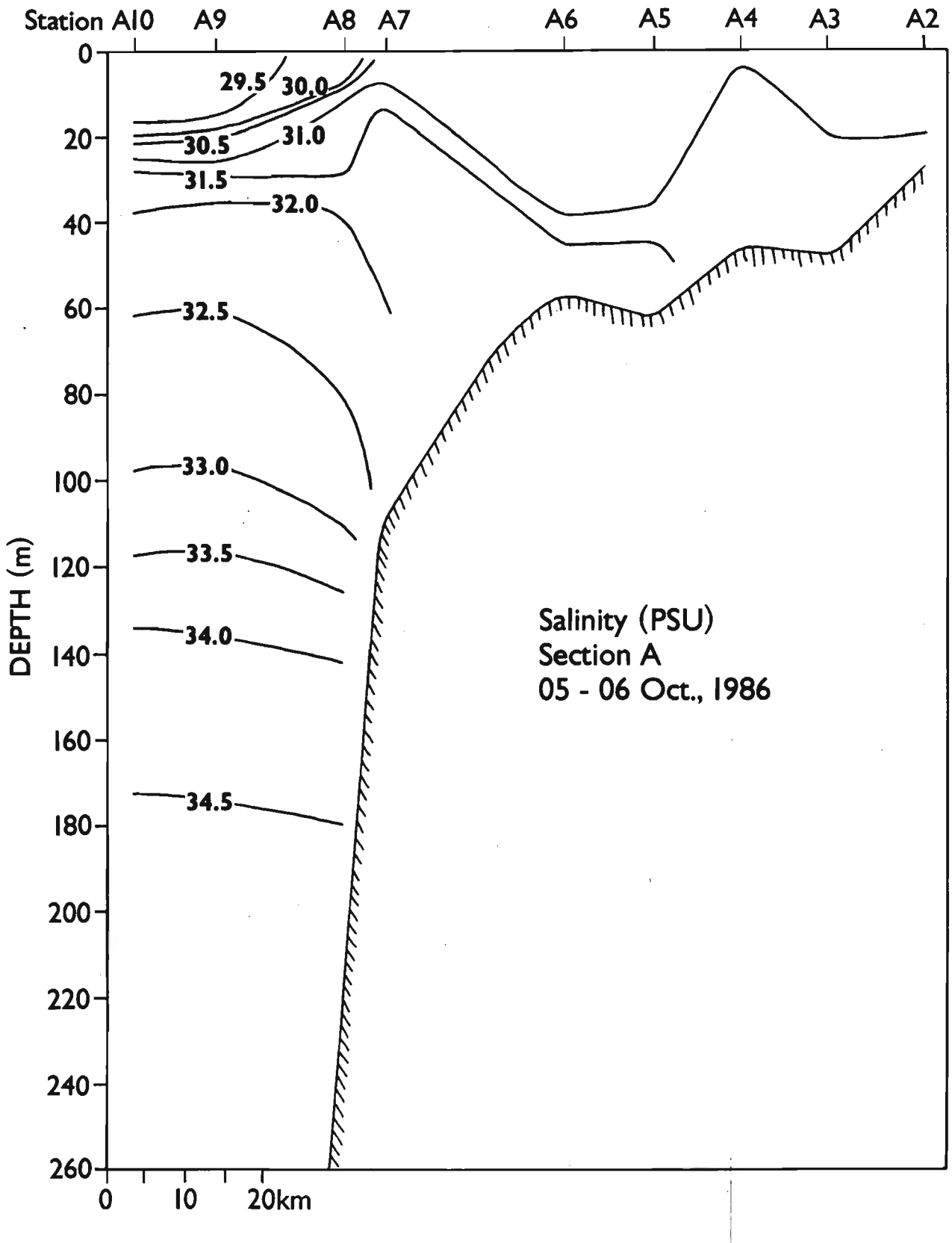

Figure 17. Salinity at section A in October 1986.

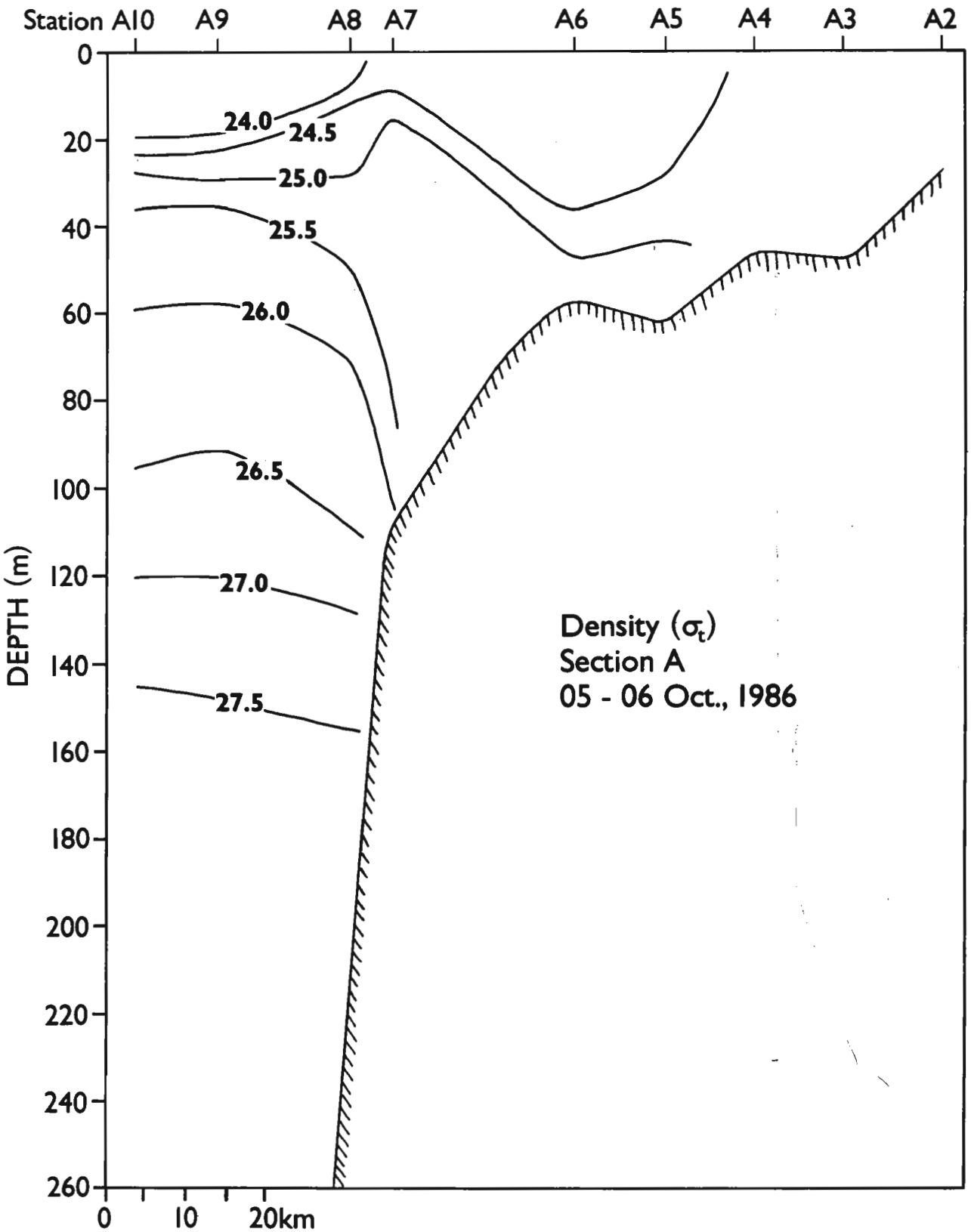

Figure 18. Density at section A in October 1986.

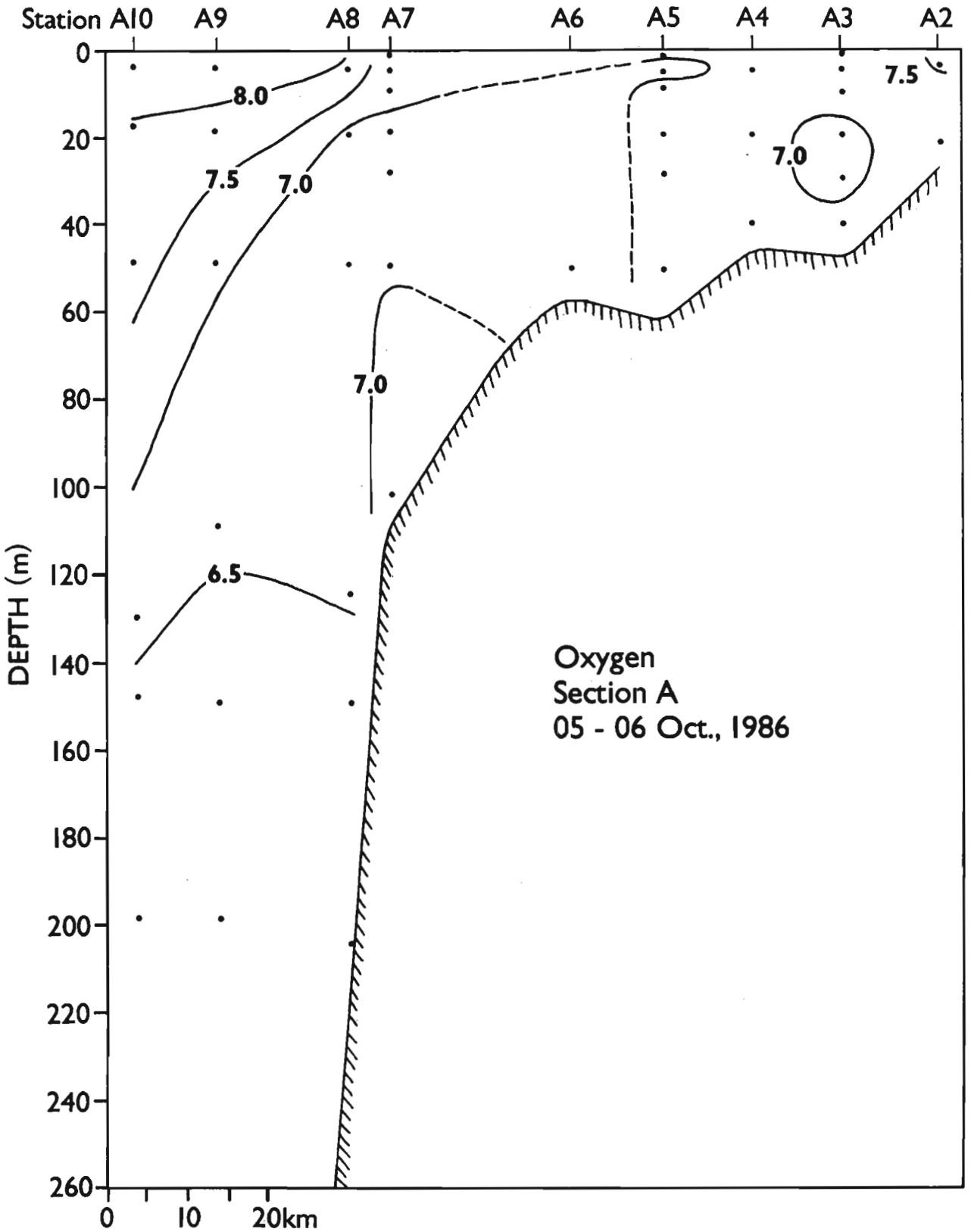

Figure 19. Dissolved oxygen at section A in October 1986.

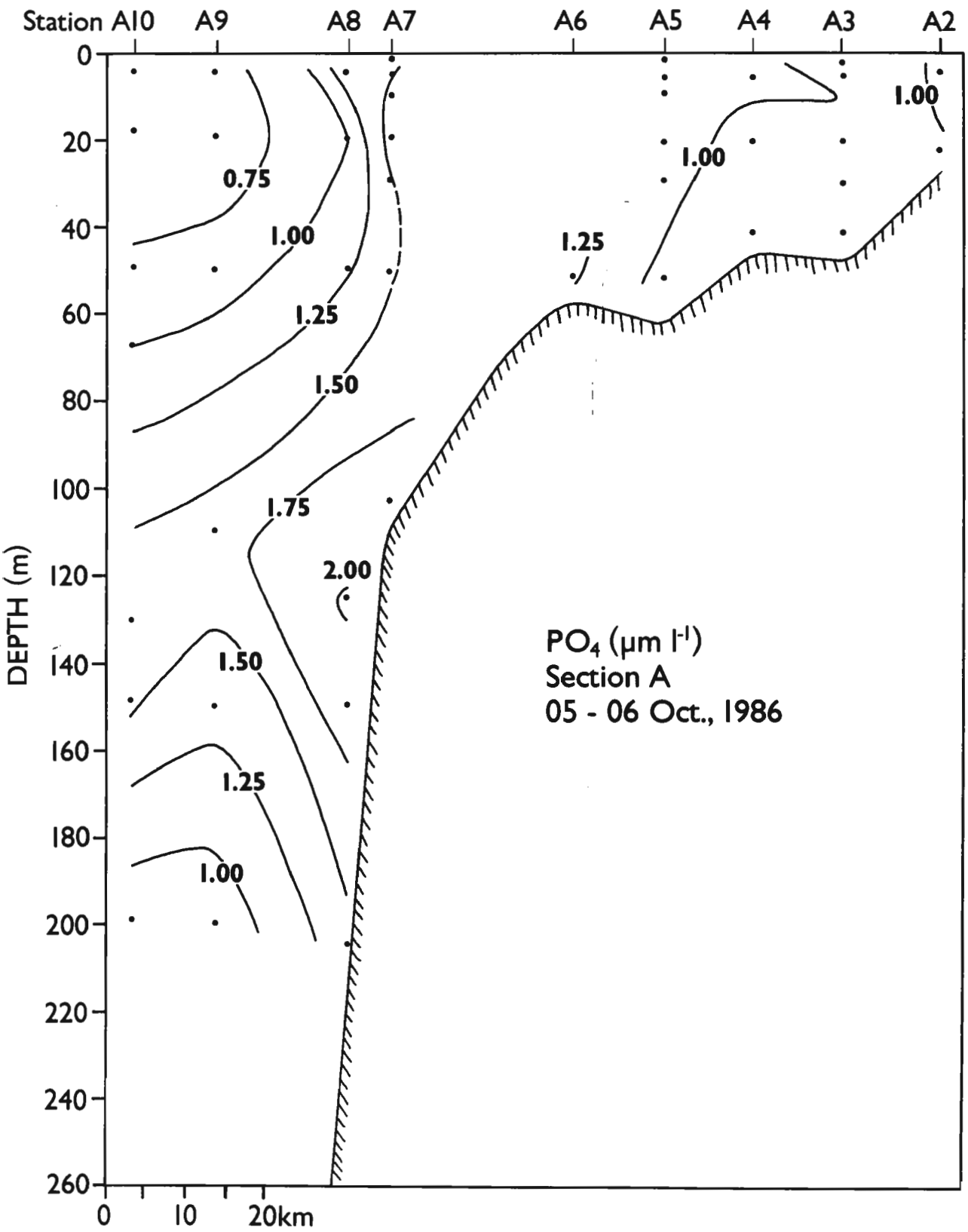

Figure 20. Phosphate at section A in October 1986.

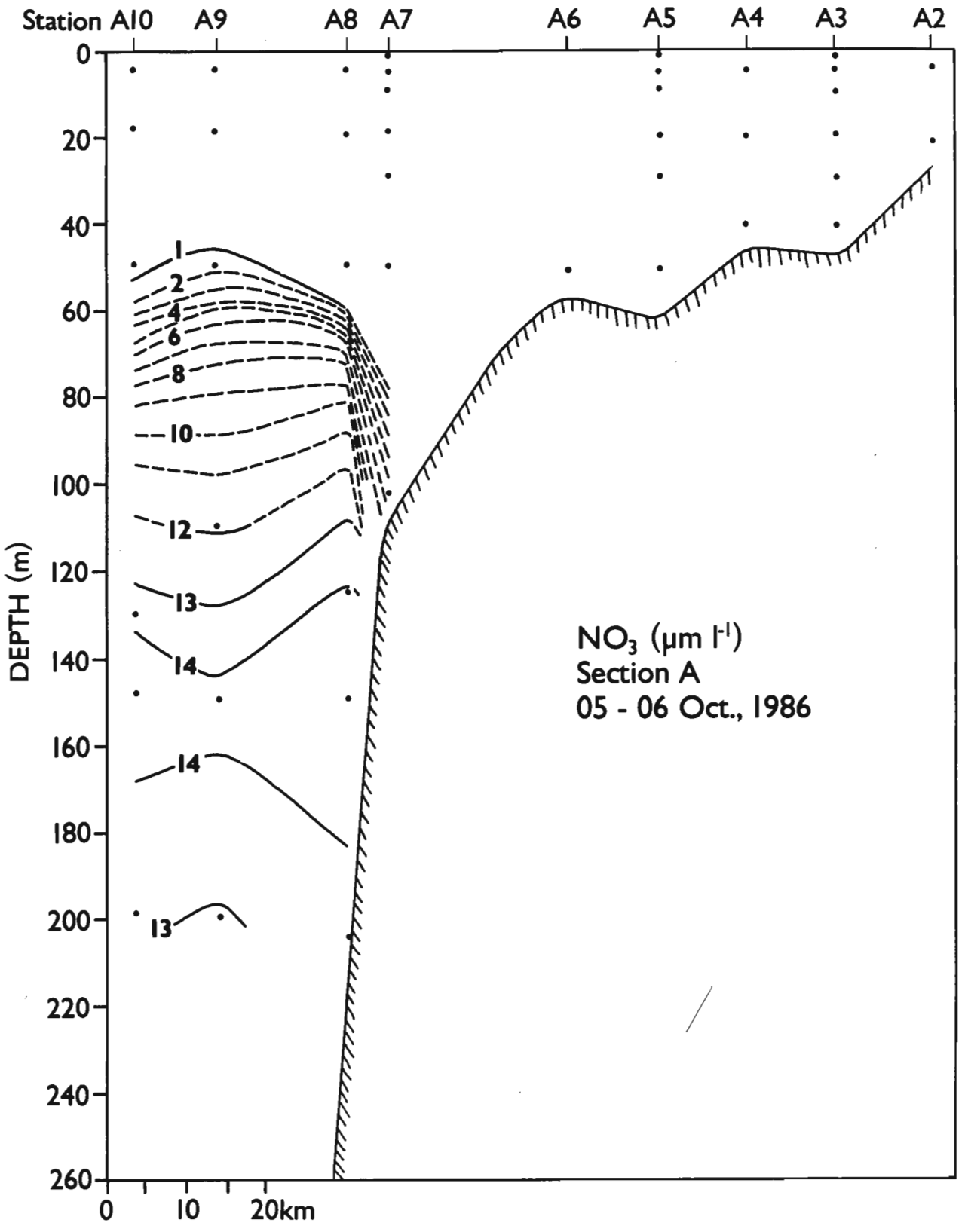

Figure 21. Nitrate at section A in October 1986.

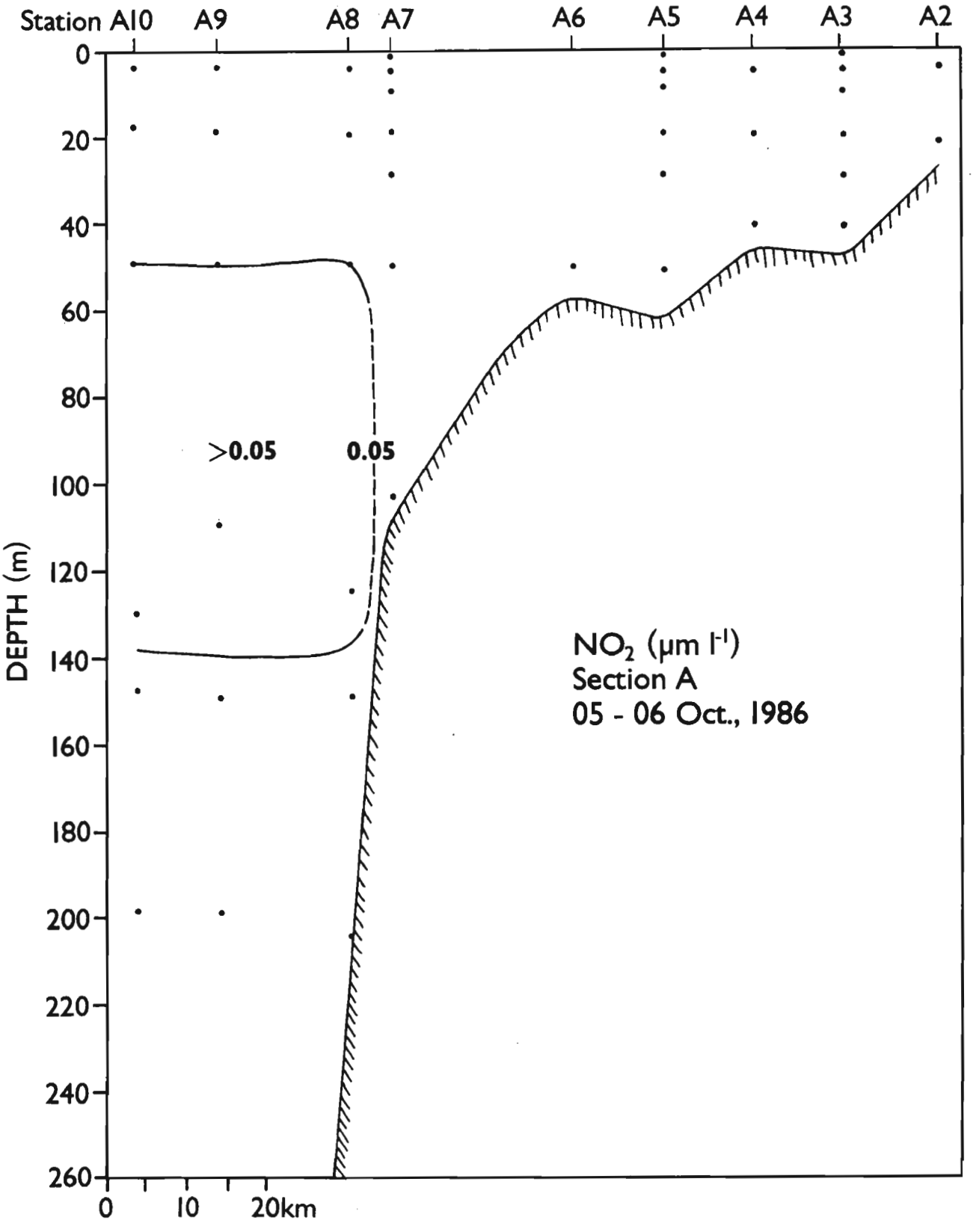

Figure 22. Nitrite at section A in October 1986.

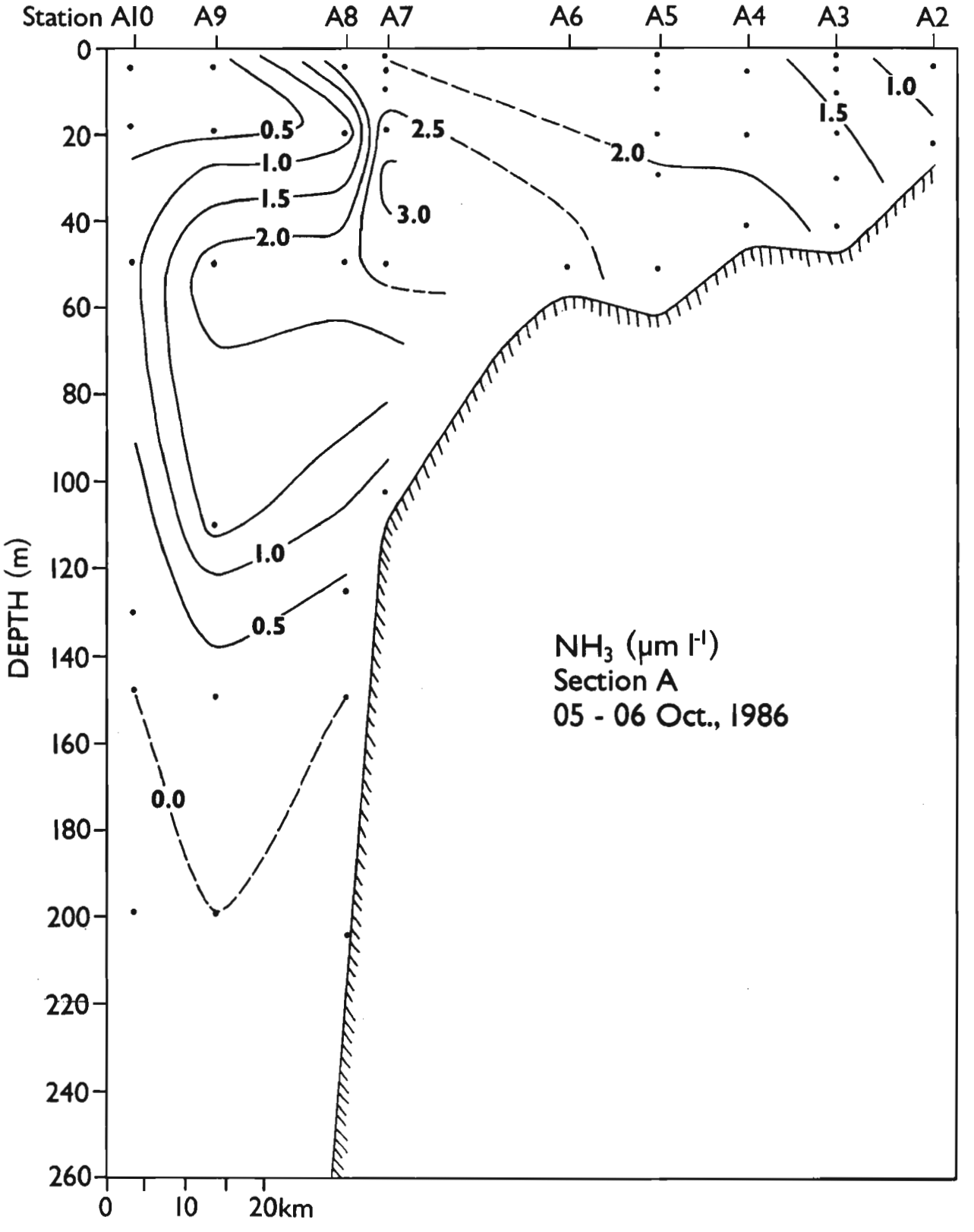

Figure 23. Ammonia at section A in October 1986.

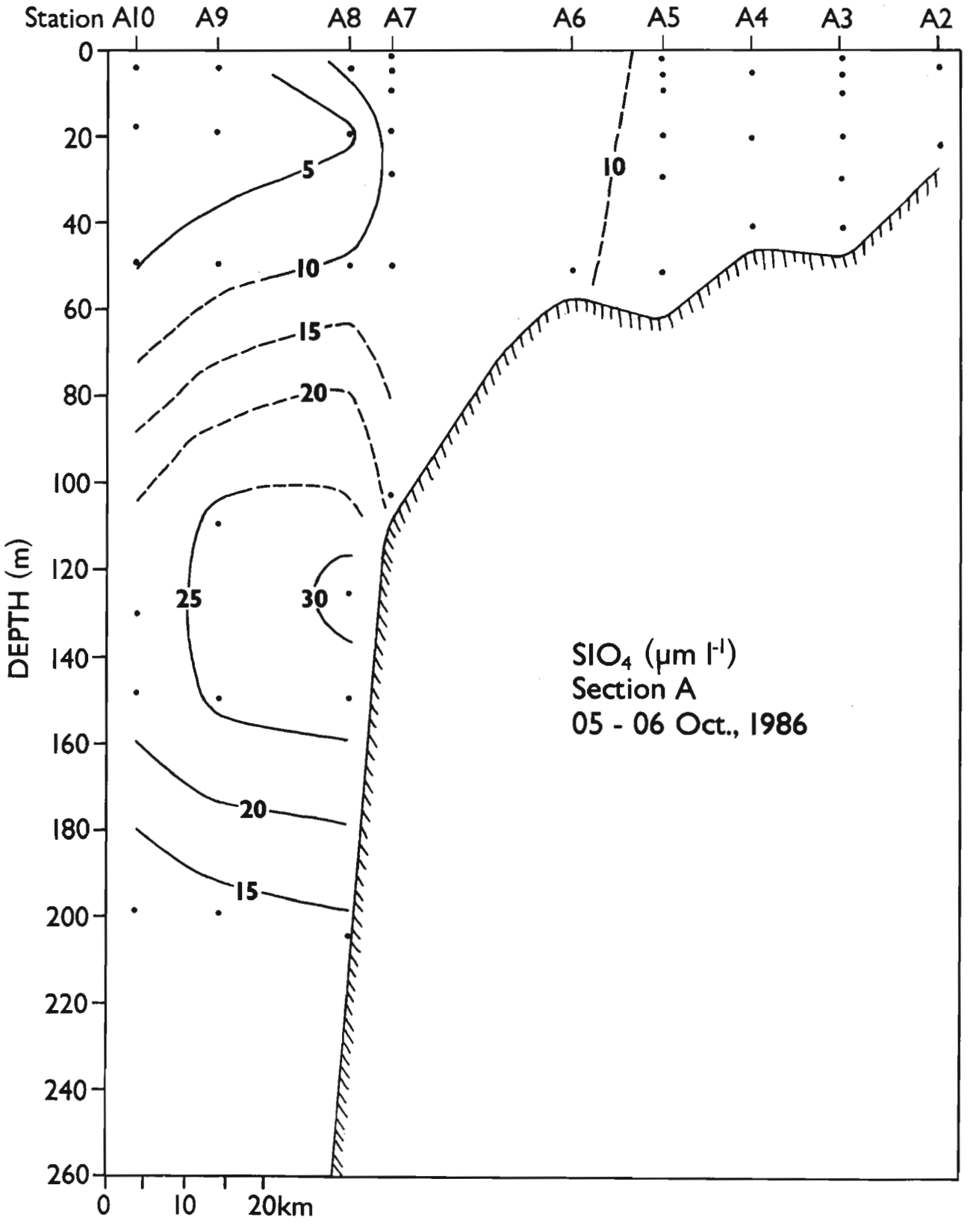

Figure 24. Silicate at section A in October 1986.

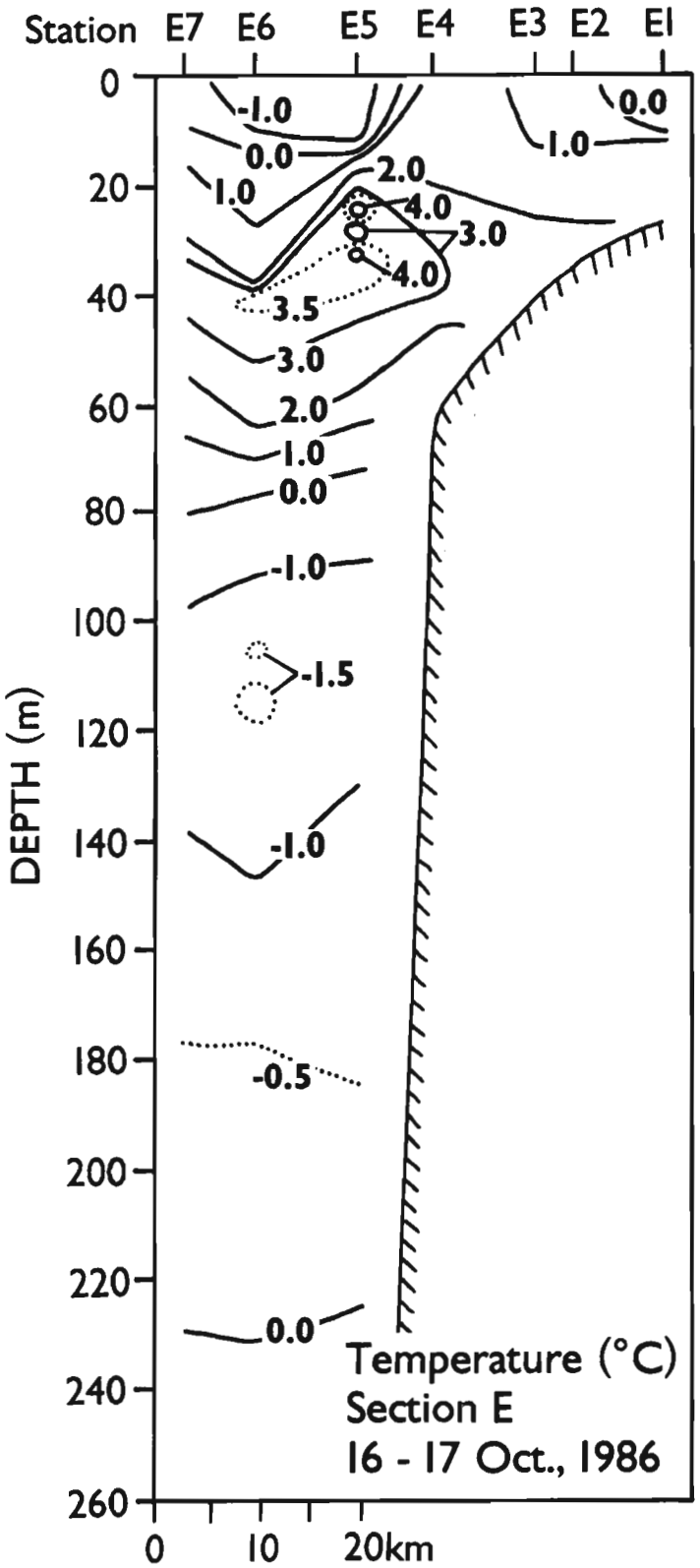

Figure 25. Temperature at section E in October 1986.

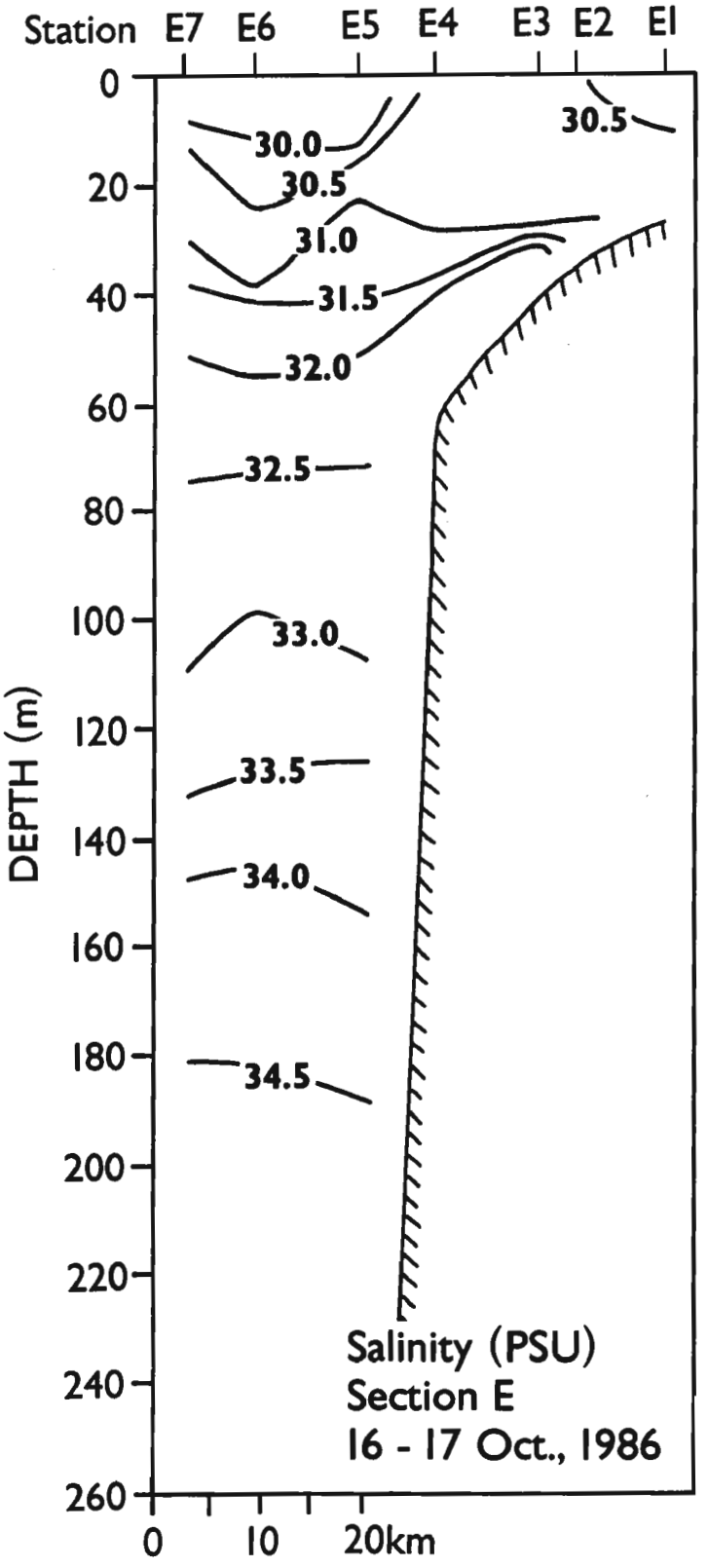

Figure 26. Salinity at section E in October 1986.

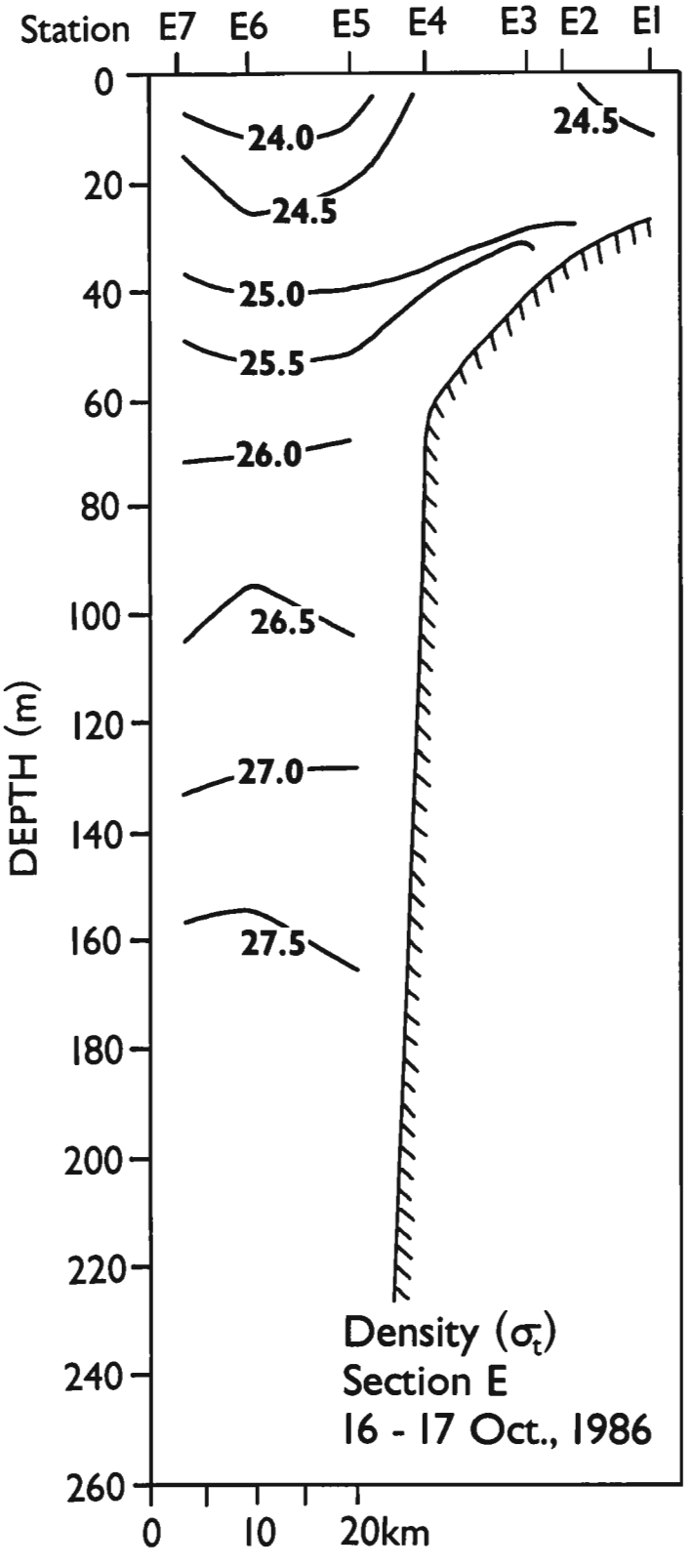

Figure 27. Density at section E in October 1986.

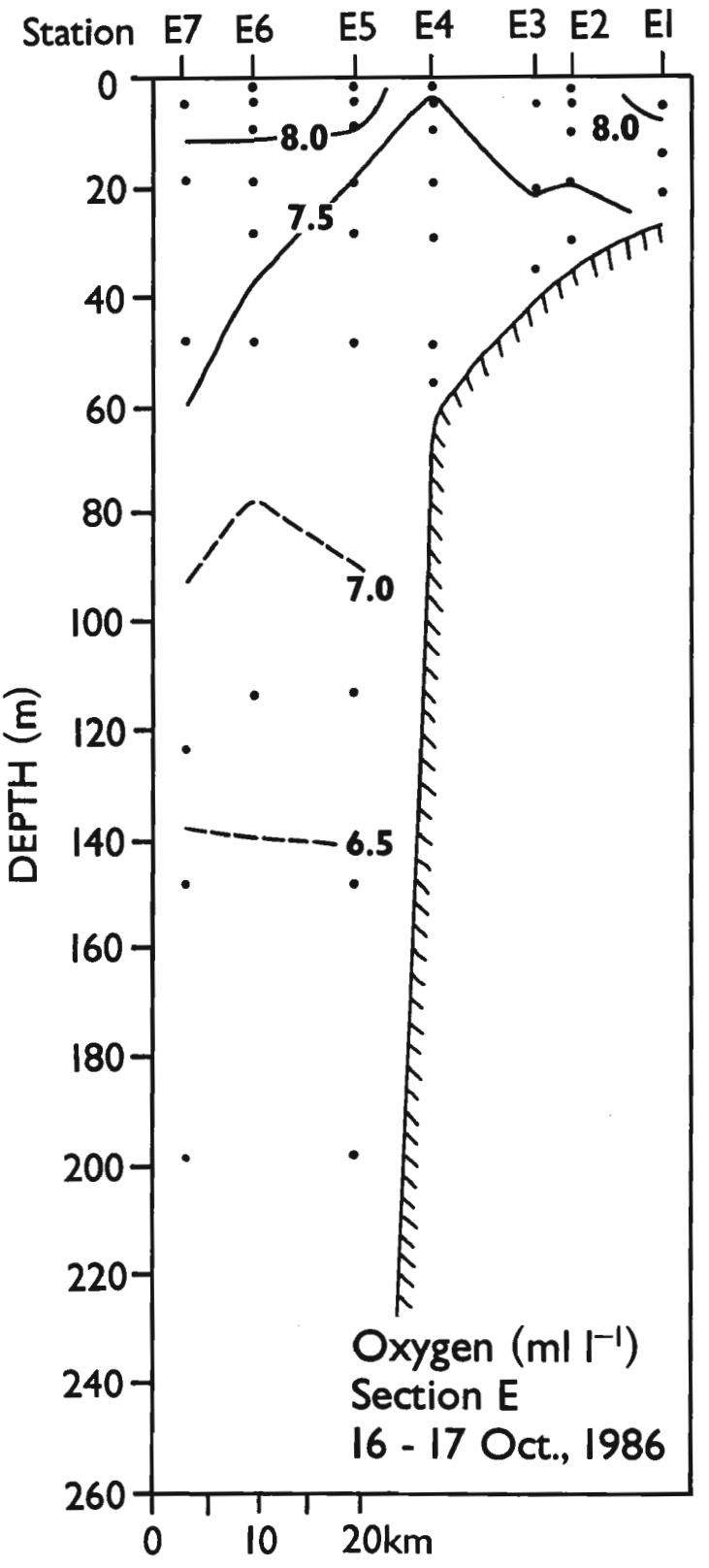

Figure 28. Dissolved oxygen at section E in October 1986.

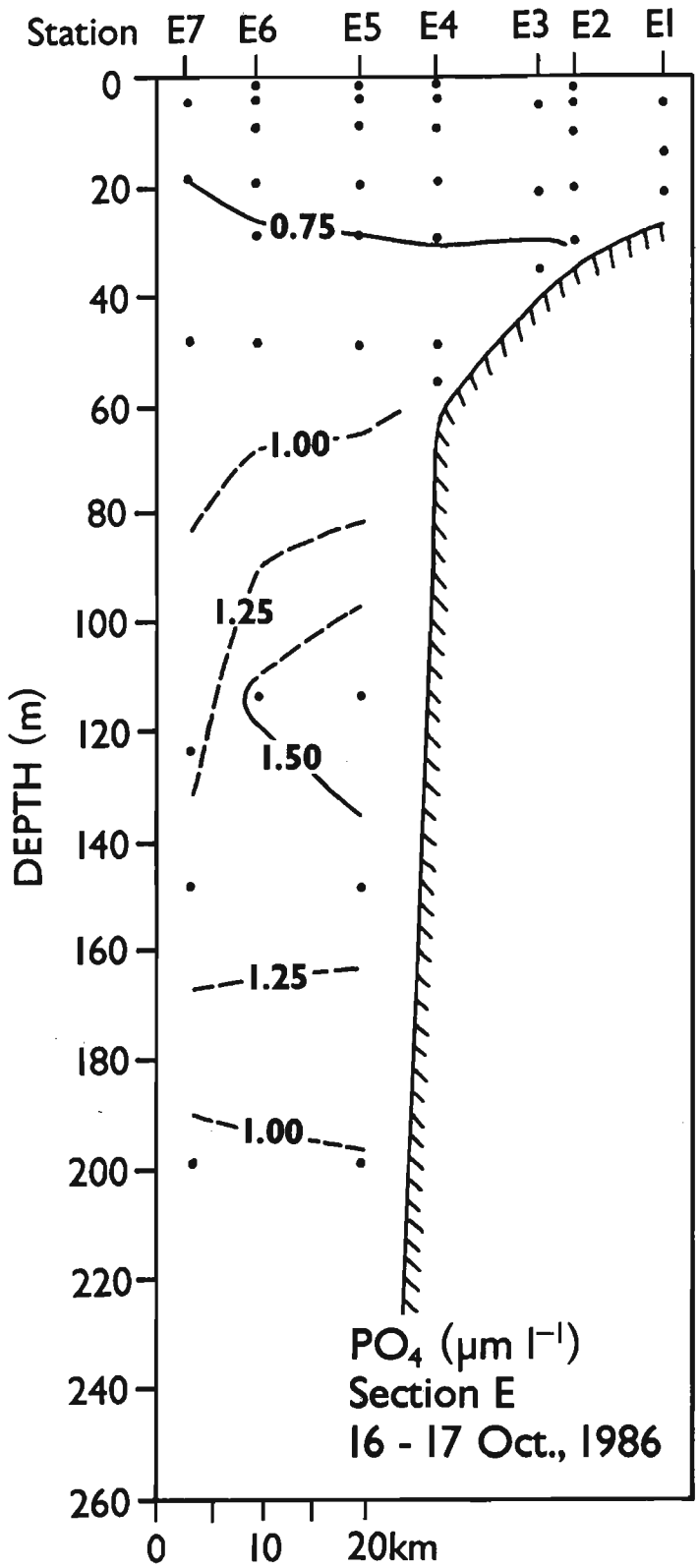

Figure 29. Phosphate at section E in October 1986.

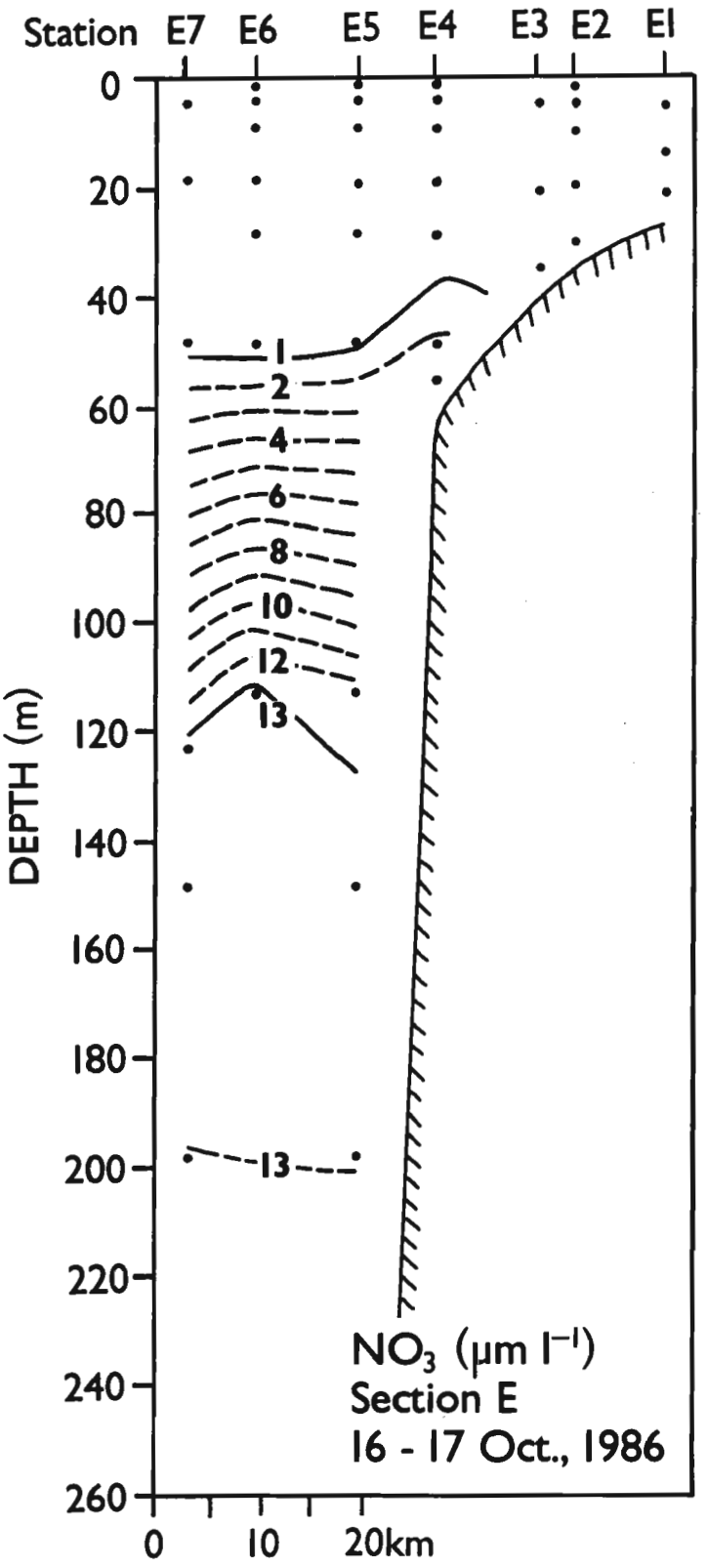

Figure 30. Nitrate at section E in October 1986.

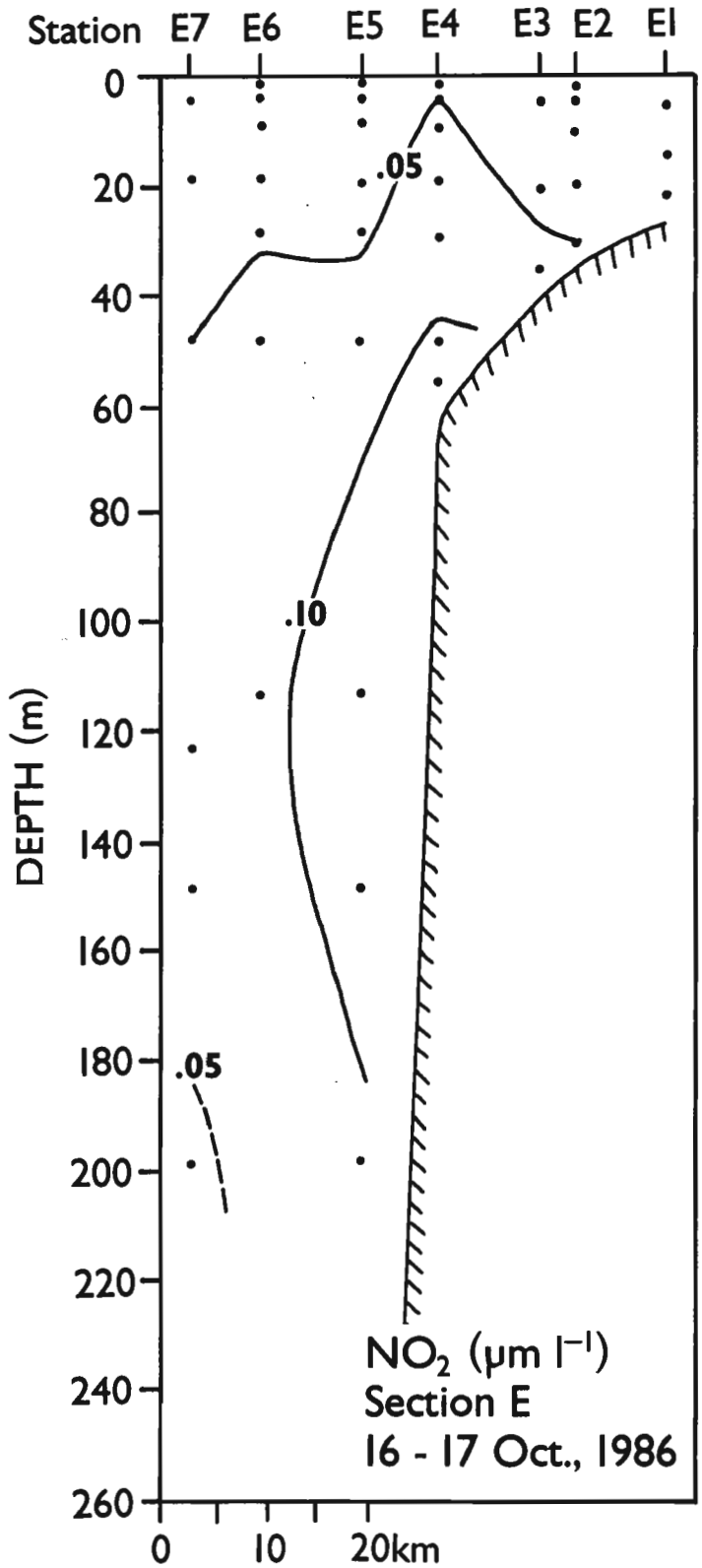

Figure 31. Nitrite at section E in October 1986.

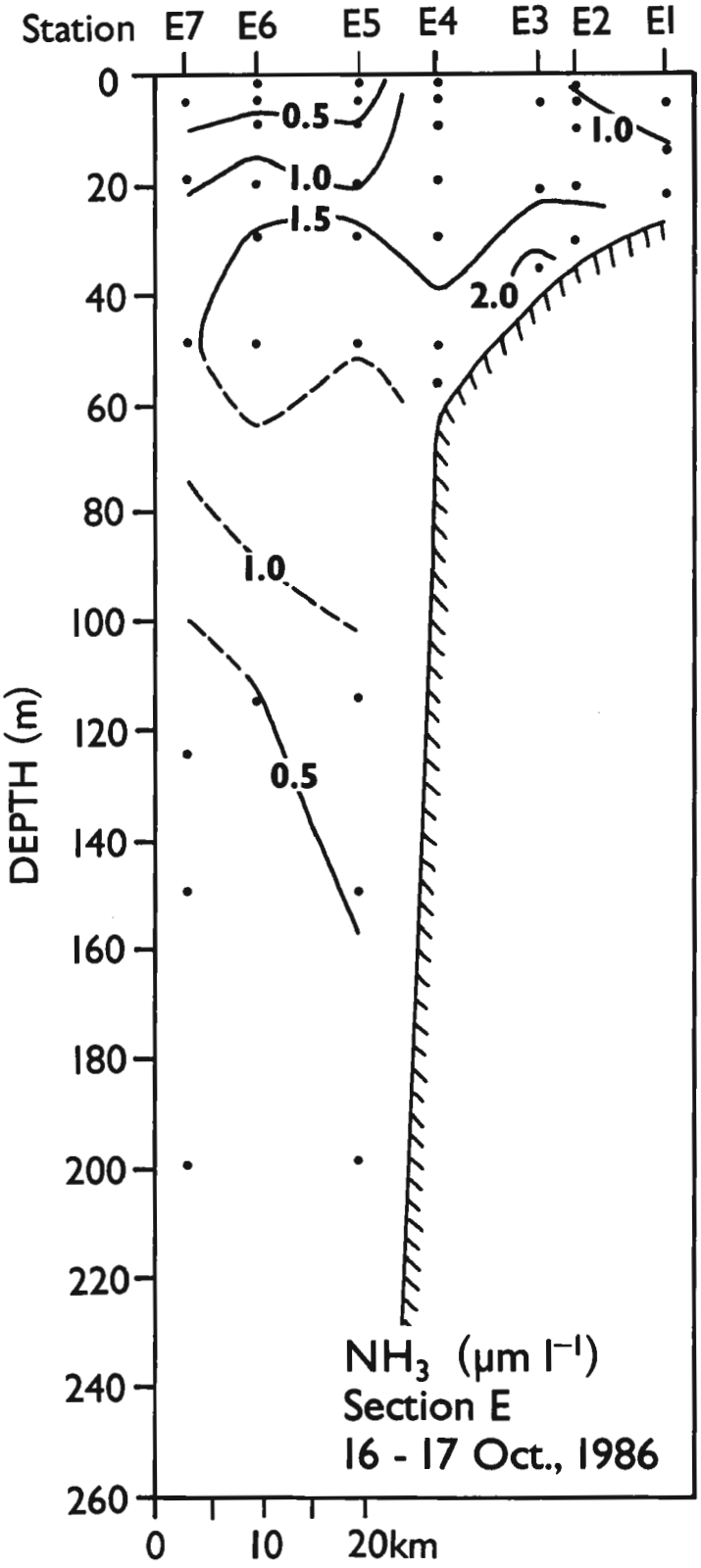

Figure 32. Ammonia at section E in October 1986.

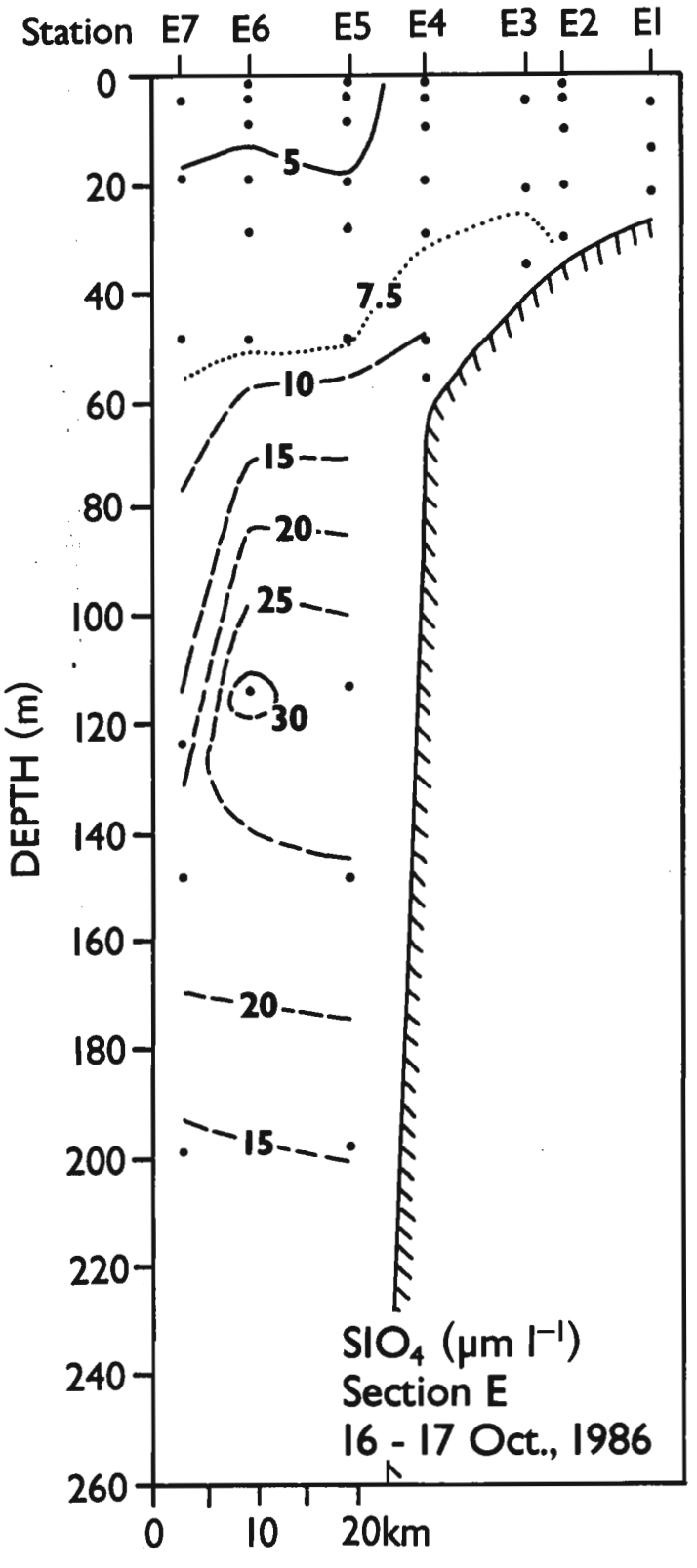

Figure 33. Silicate at section E in October 1986.

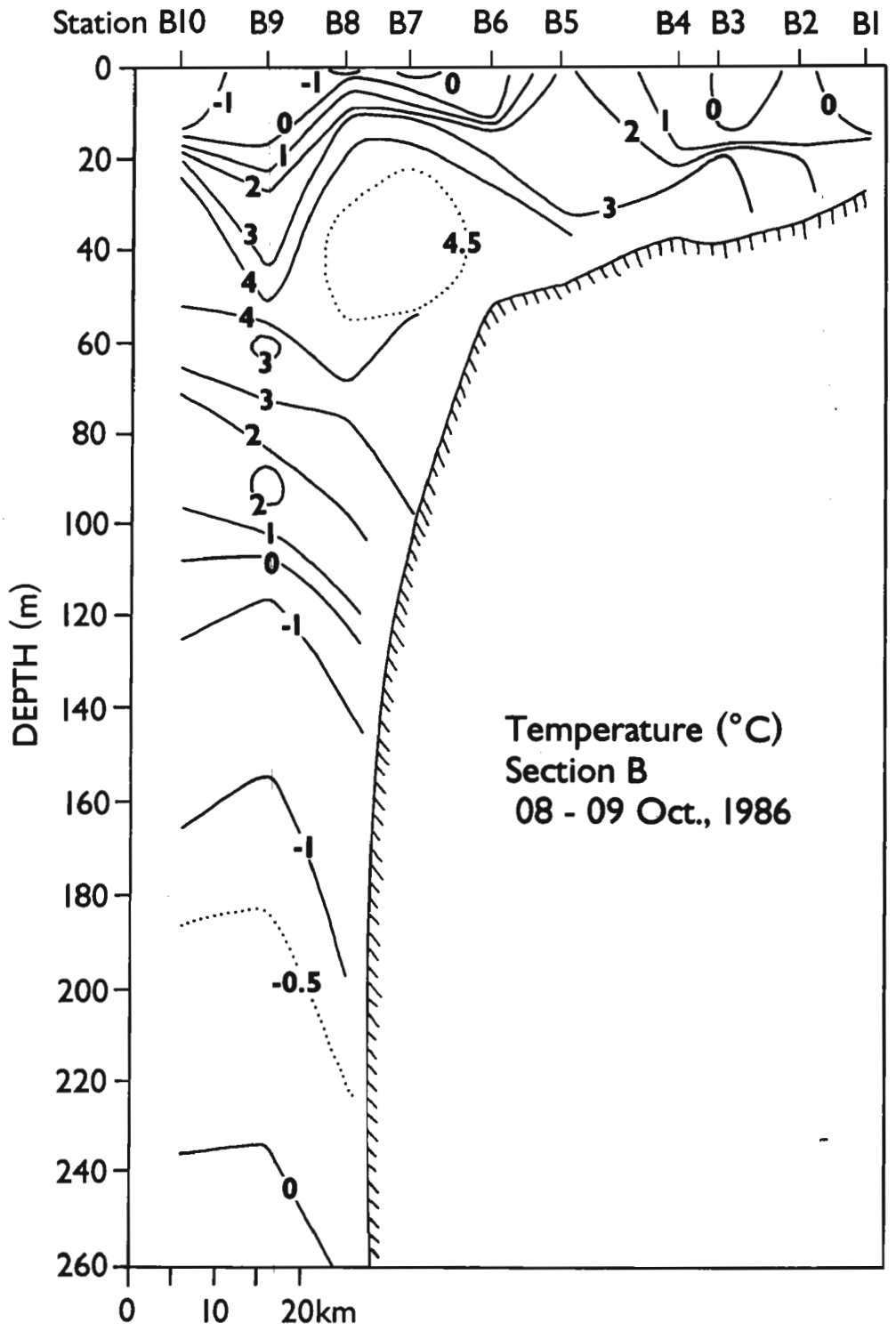

Figure 34. Temperature at section B in October 1986.

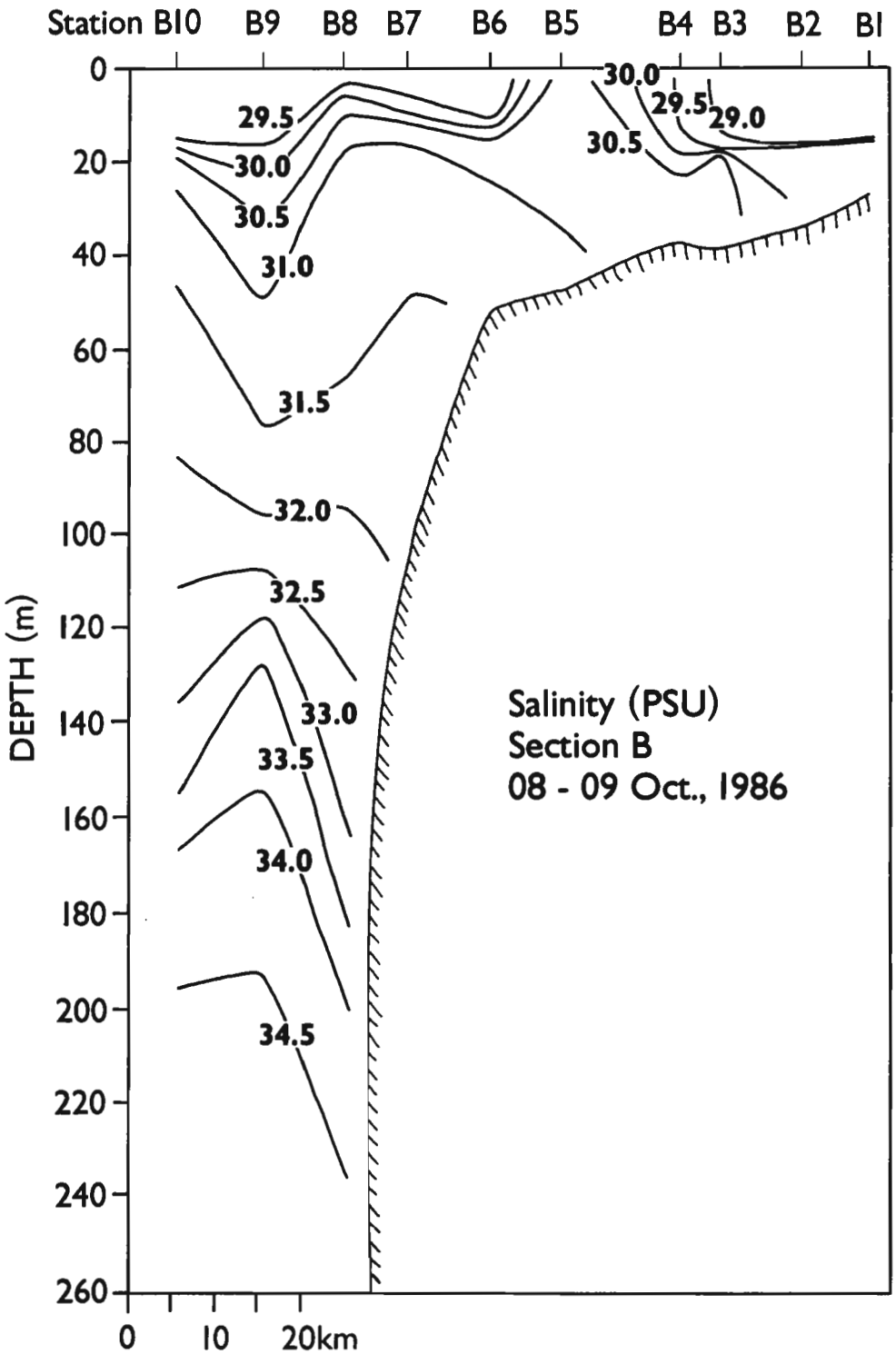

Figure 35. Salinity at section B in October 1986.

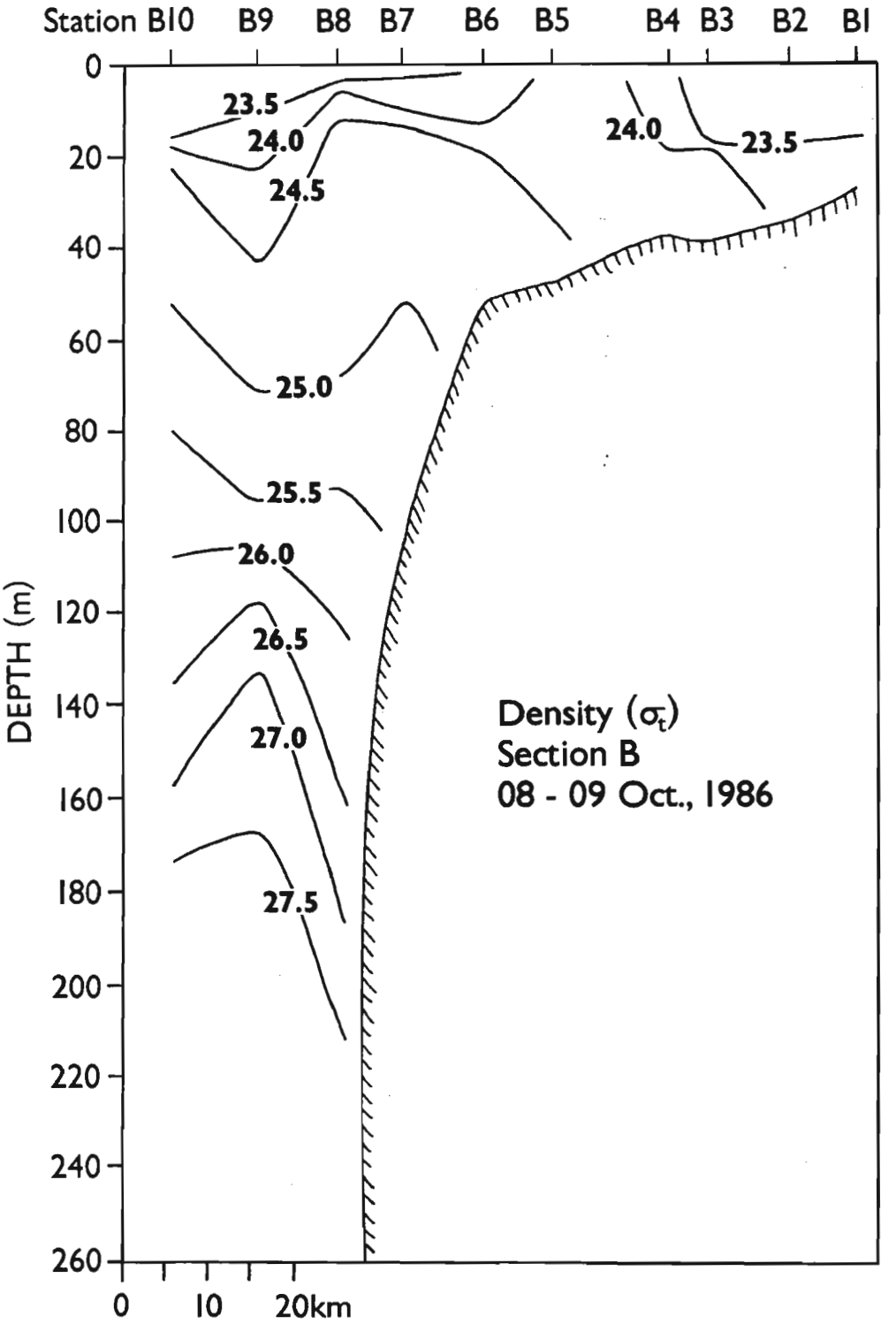

Figure 36. Density at section B in October 1986.

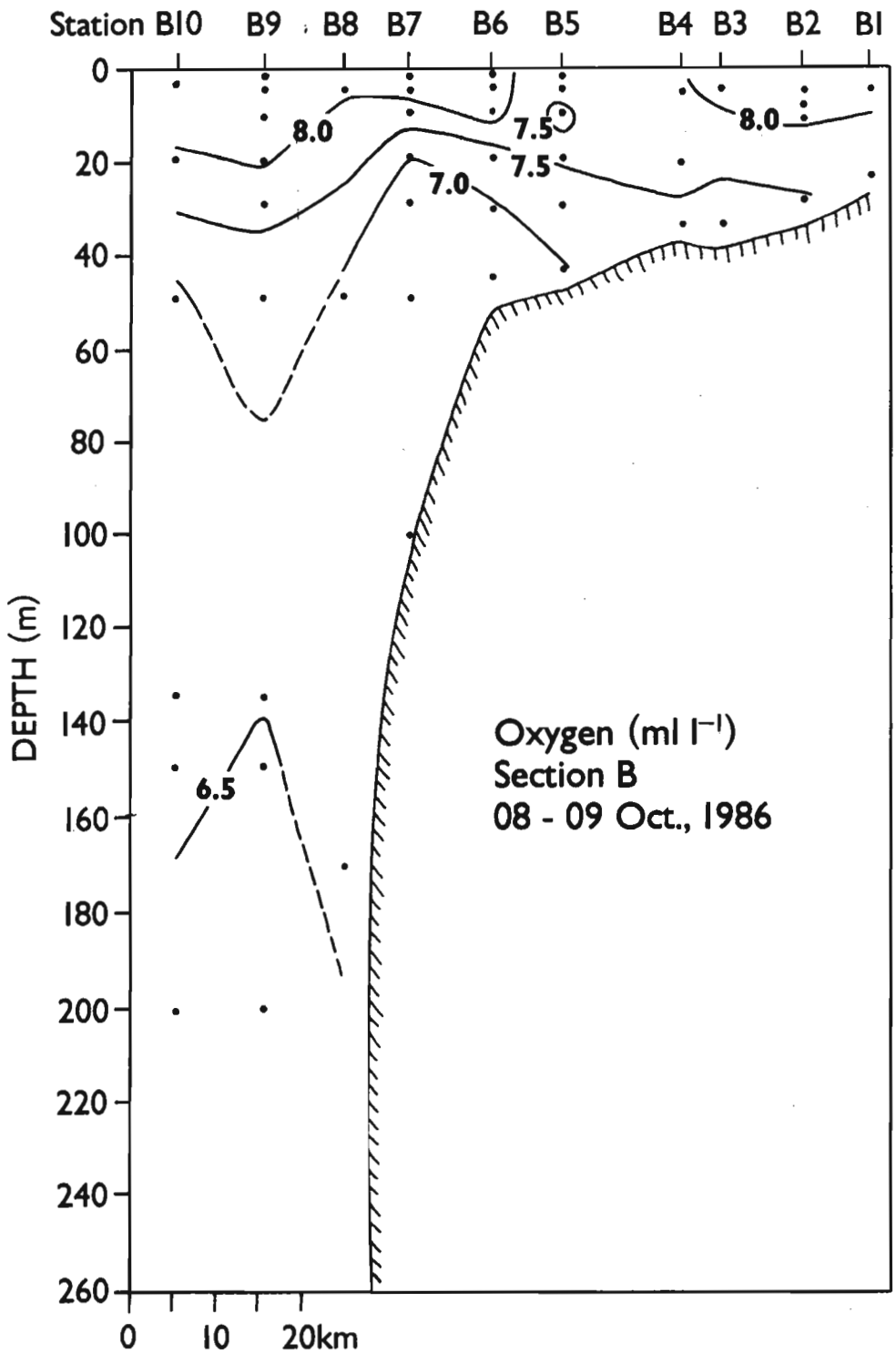

Figure 37. Dissolved oxygen at section B in October 1986.

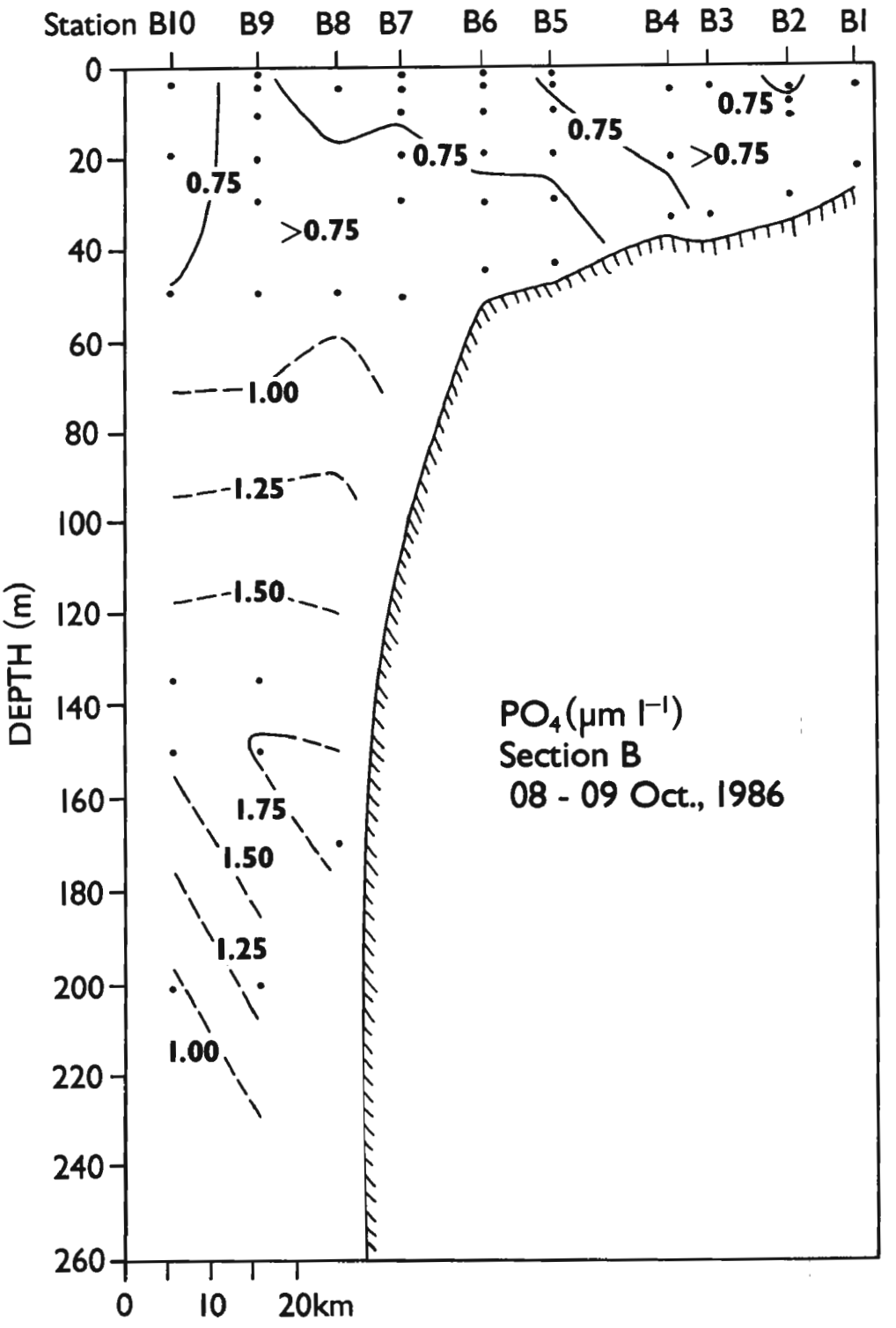

Figure 38. Phosphate at section B in October 1986.

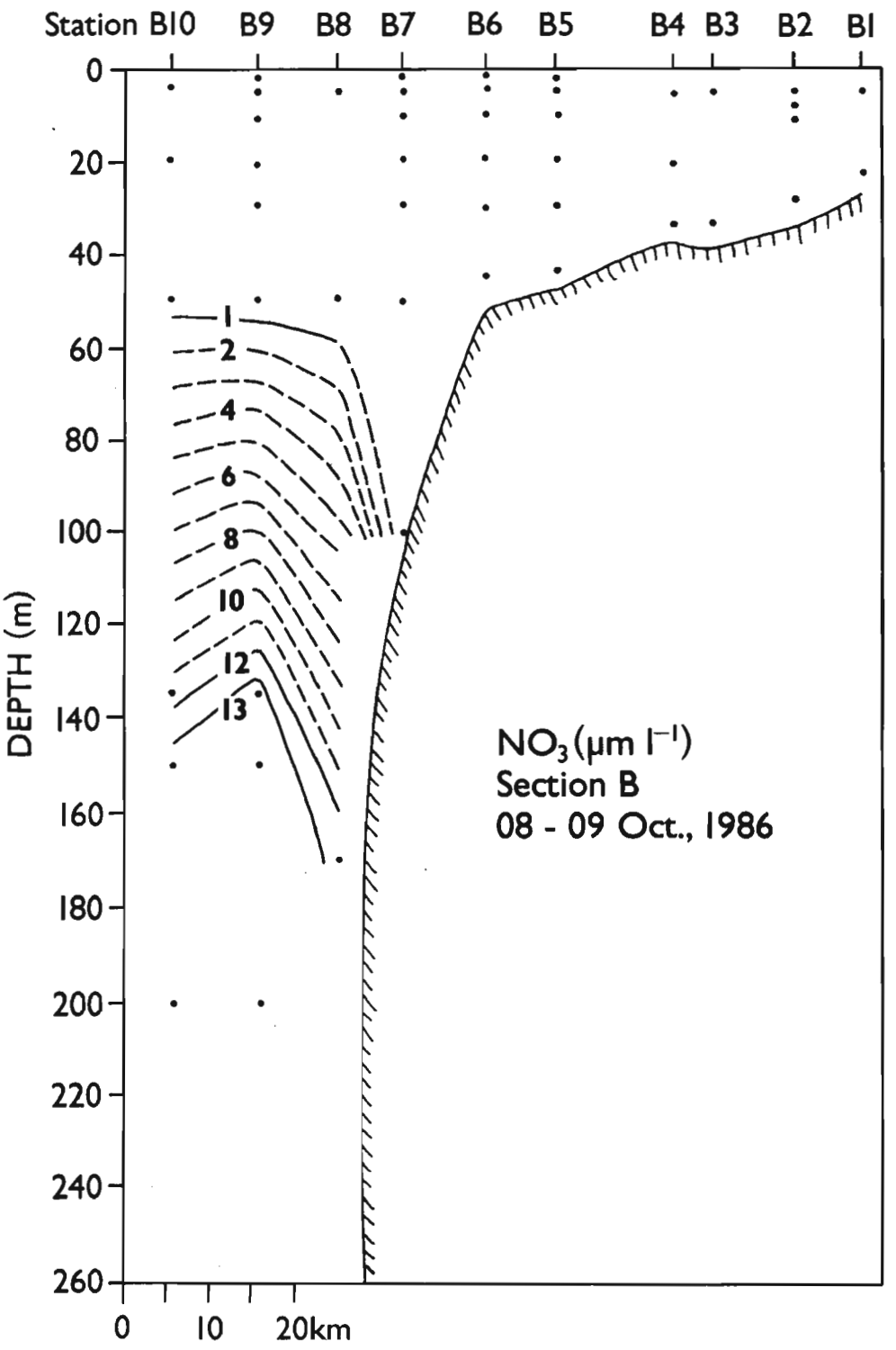

Figure 39. Nitrate at section B in October 1986.

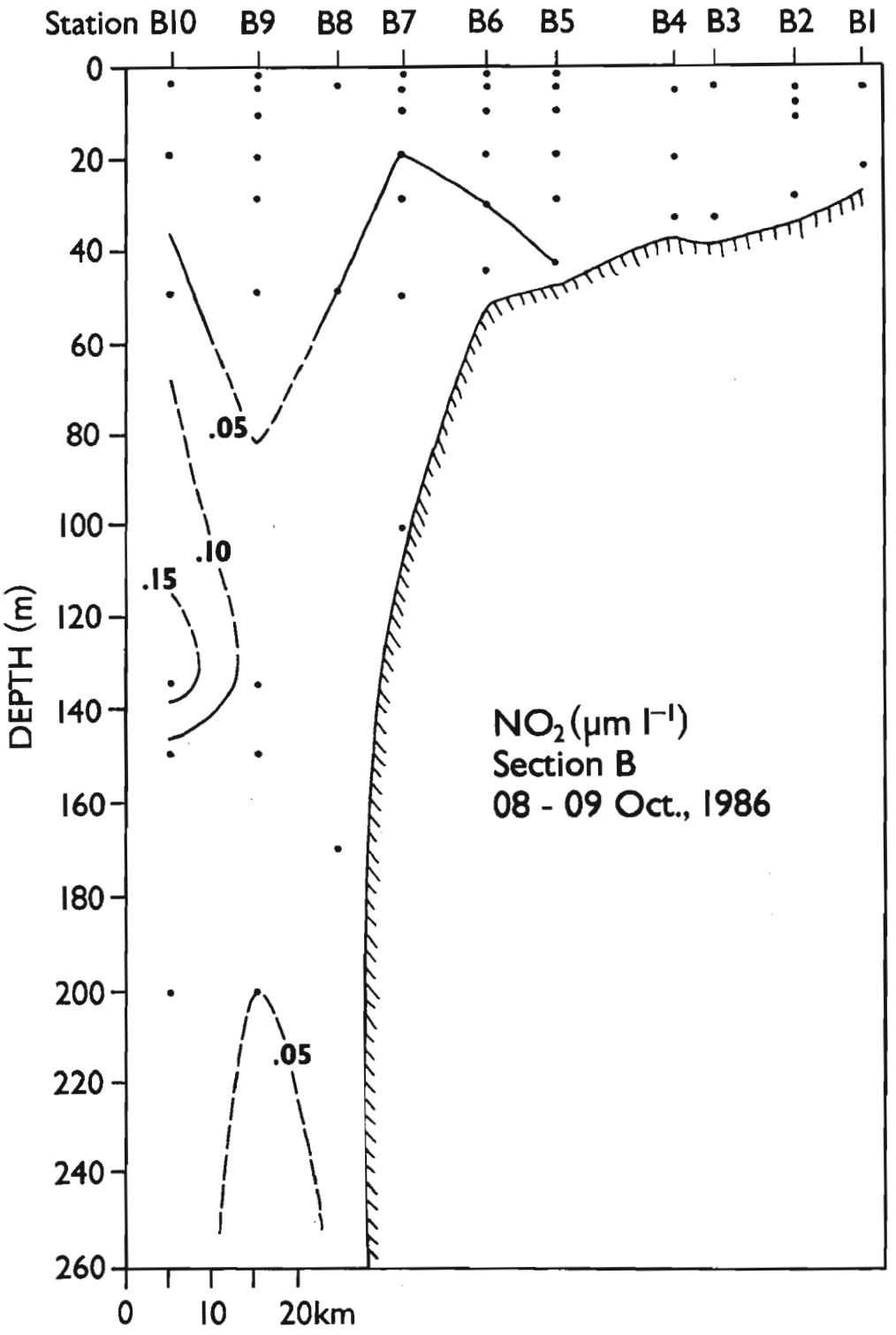

Figure 40. Nitrite at section B in October 1986.

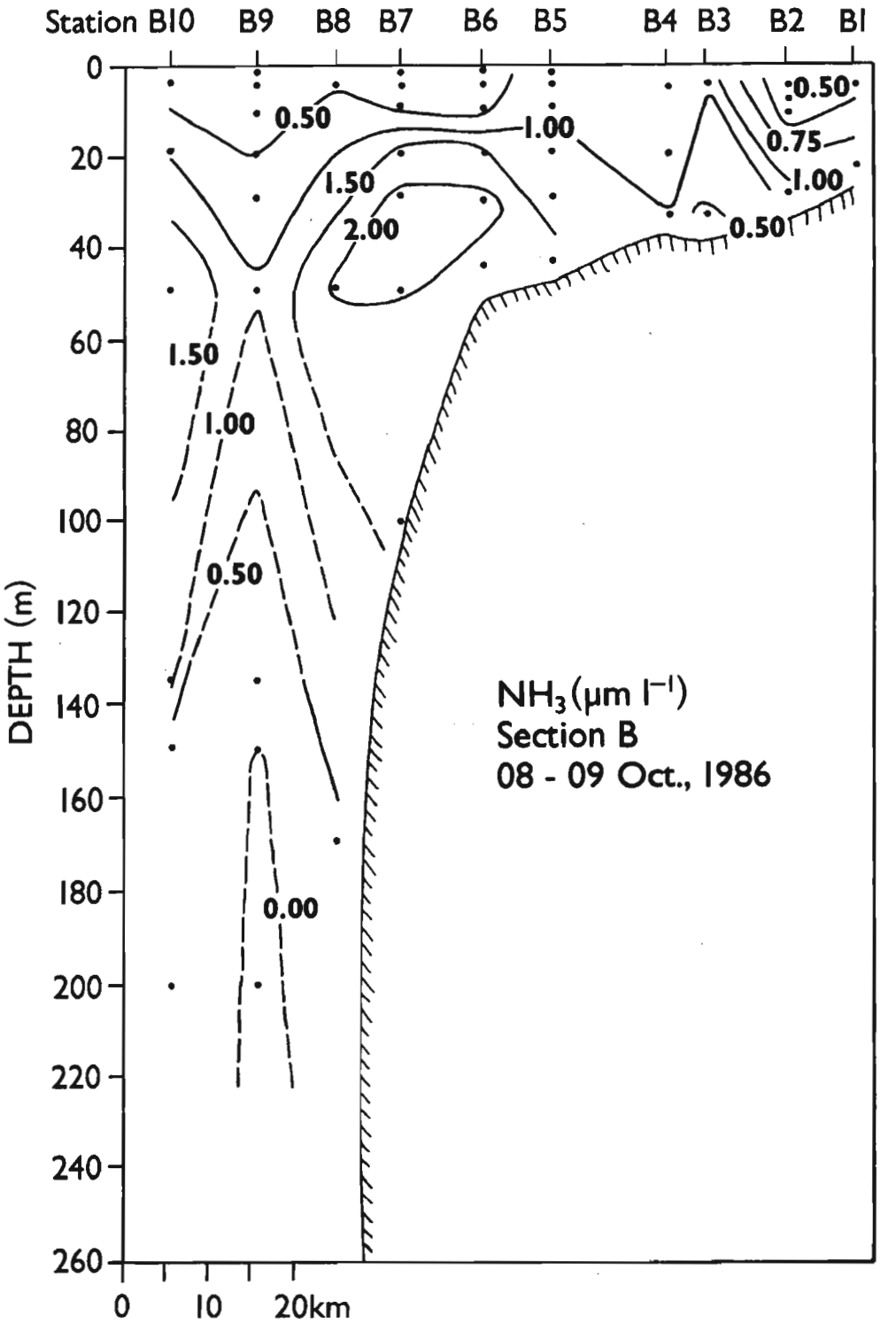

Figure 41. Ammonia at section B in October 1986.

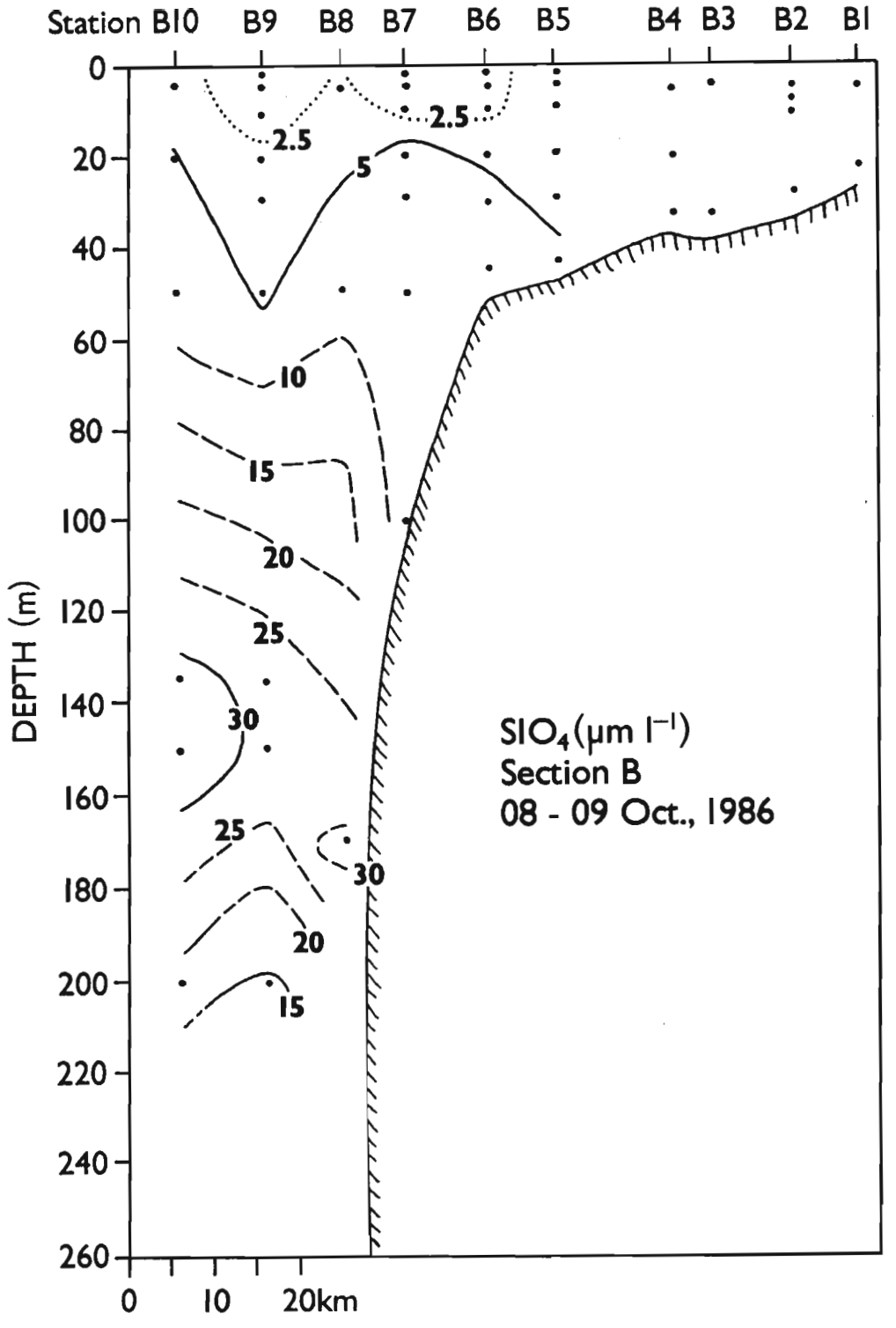

Figure 42. Silicate at section B in October 1986.

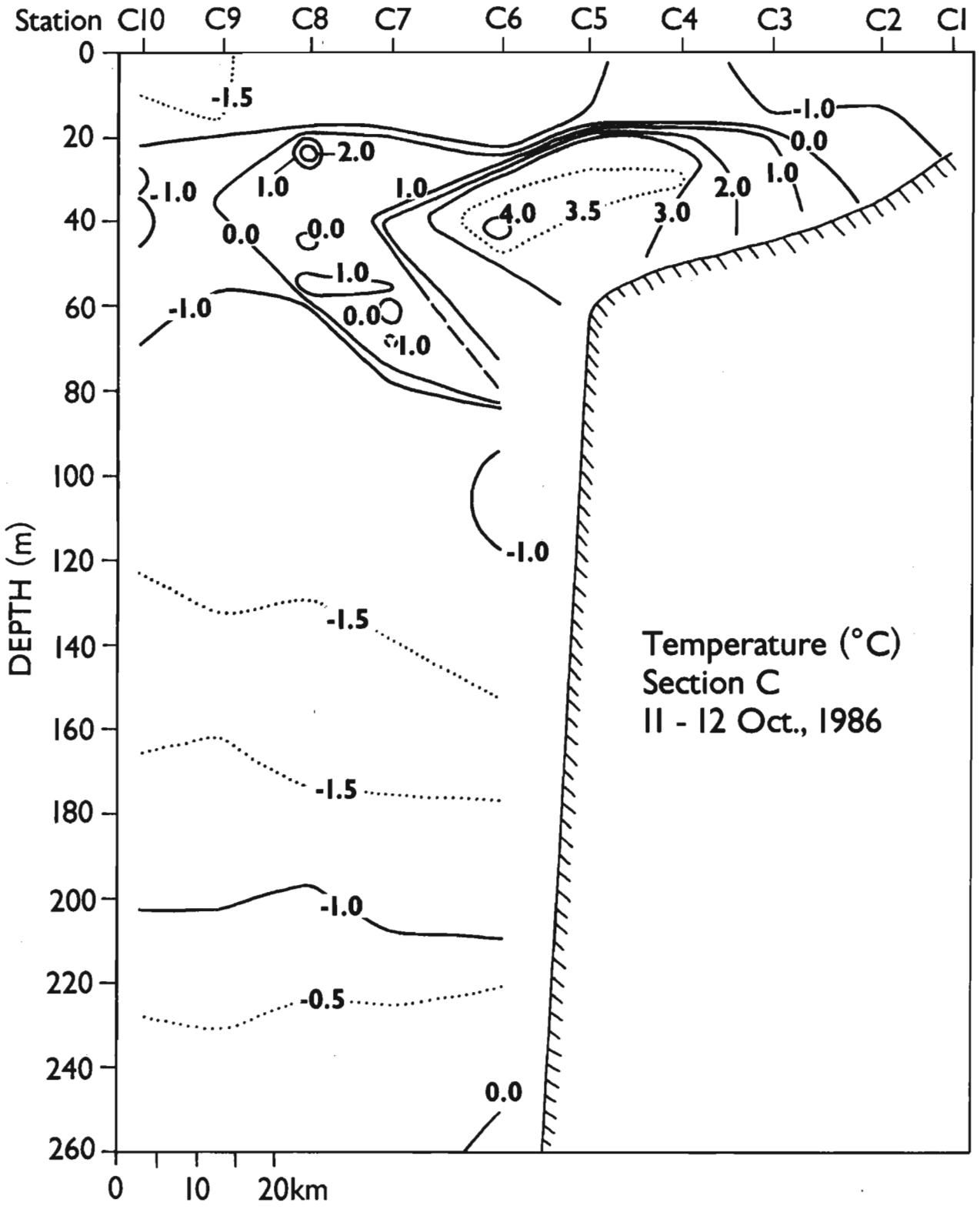

Figure 43. Temperature at section C in October 1986.

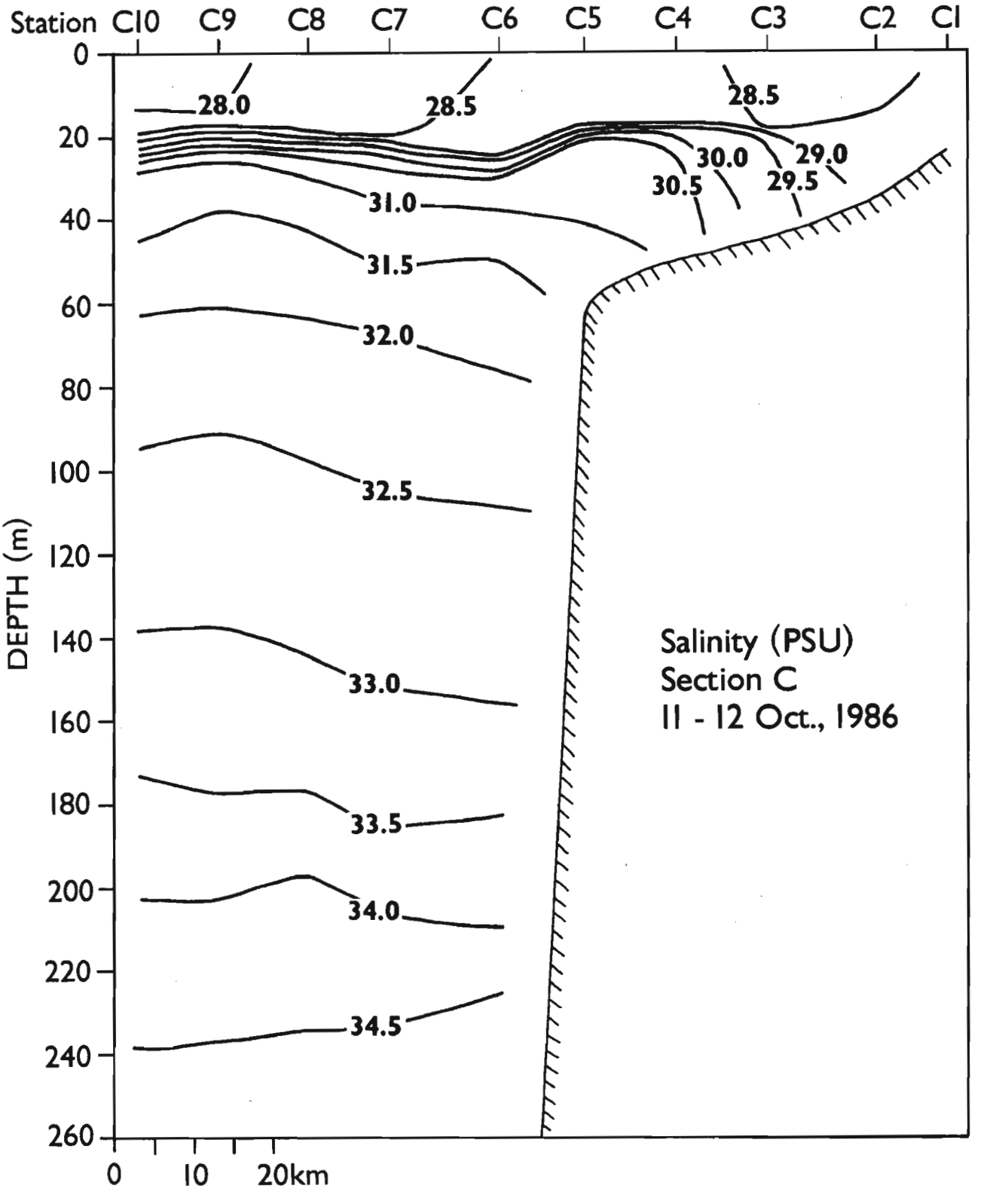

Figure 44. Salinity at section C in October 1986.

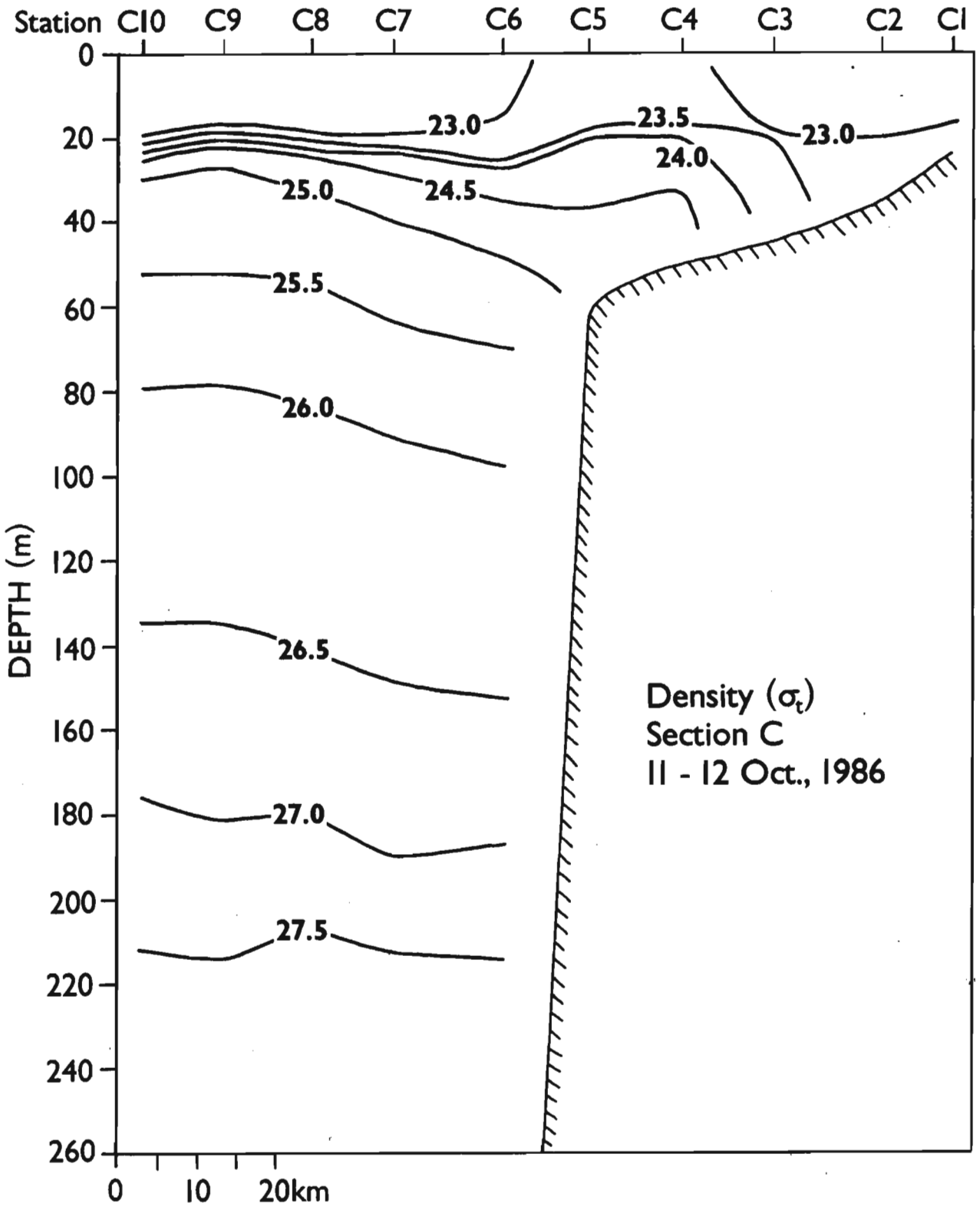

Figure 45. Density at section C in October 1986.

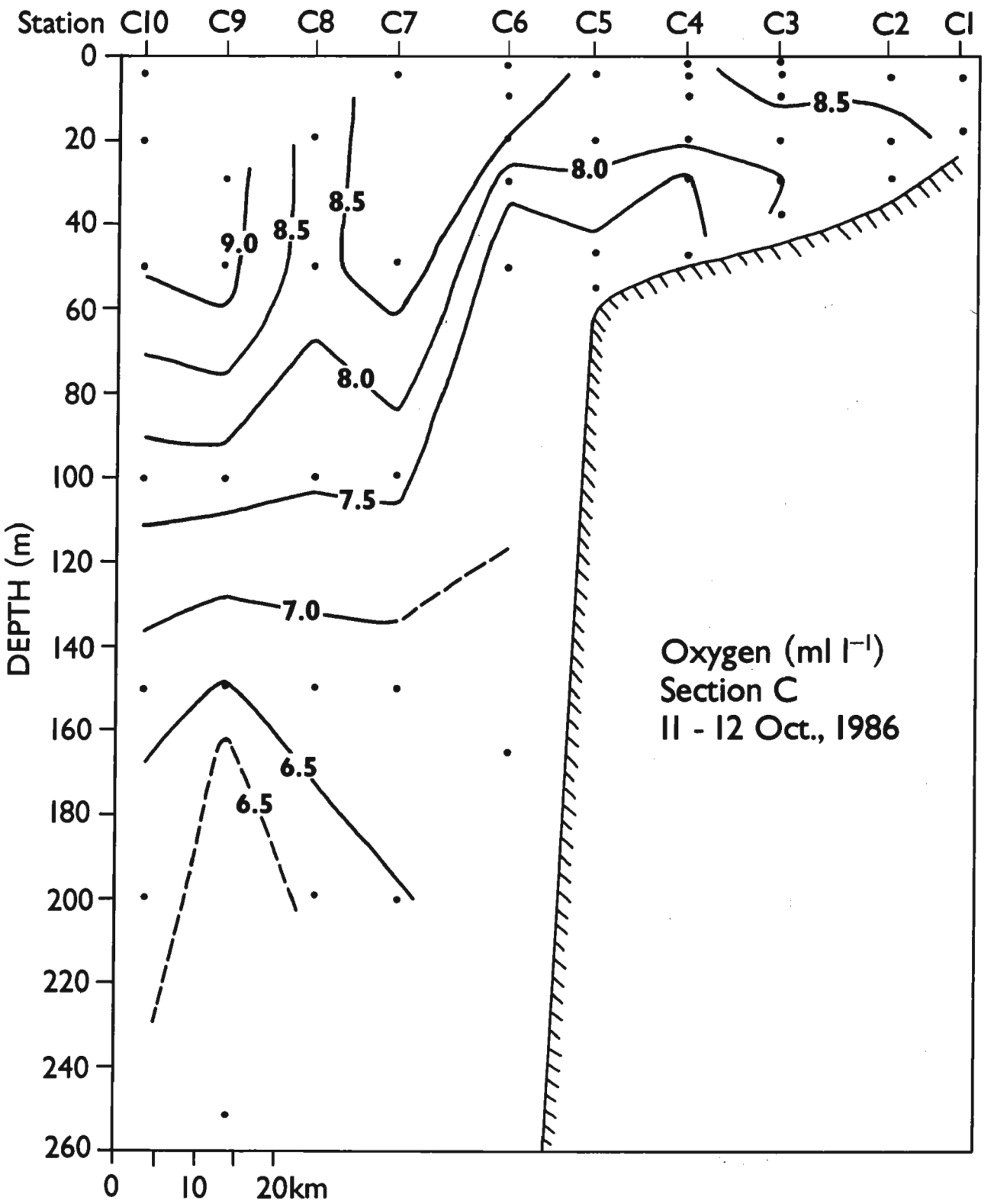

Figure 46. Dissolved oxygen at section C in October 1986.

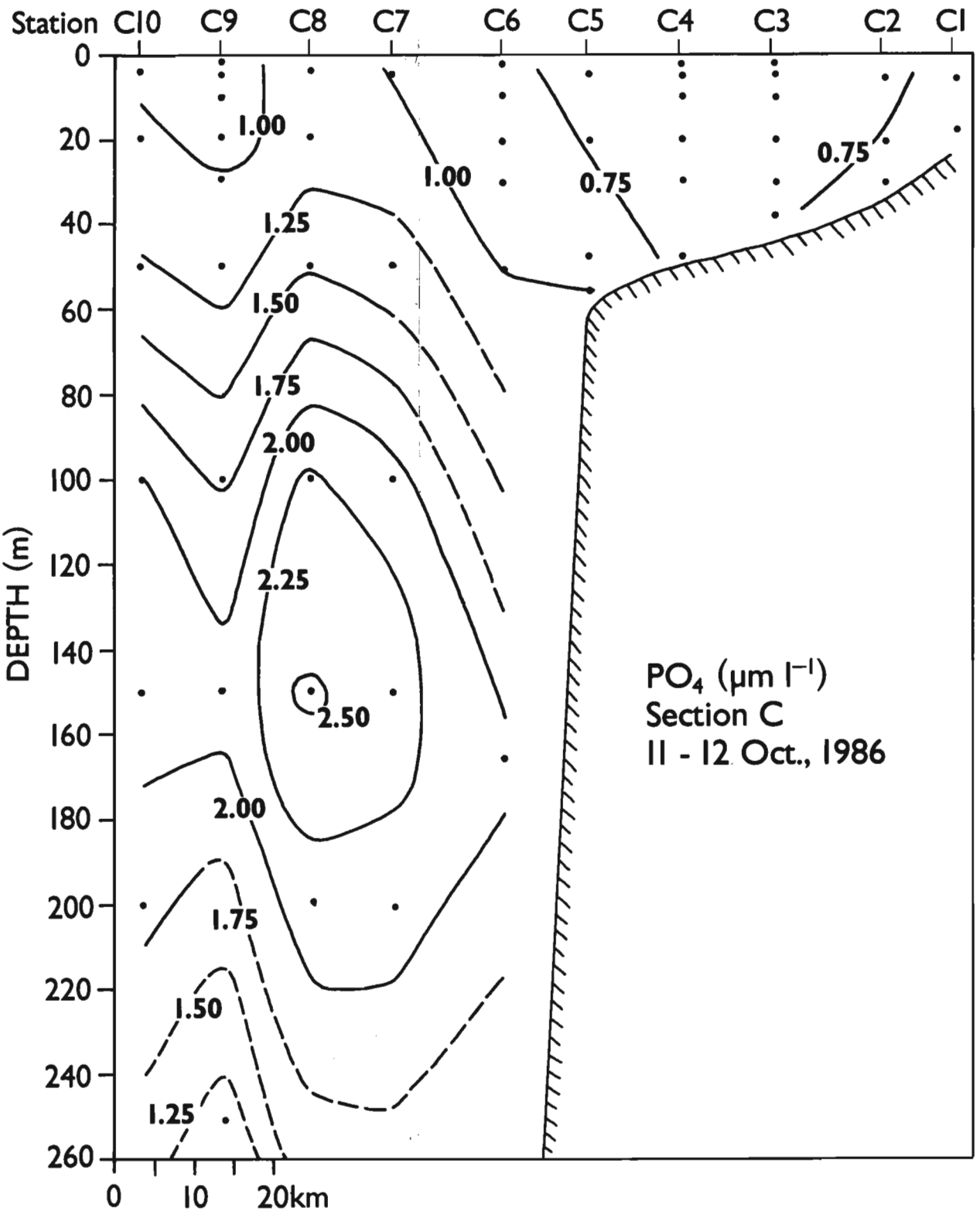

Figure 47. Phosphate at section C in October 1986.

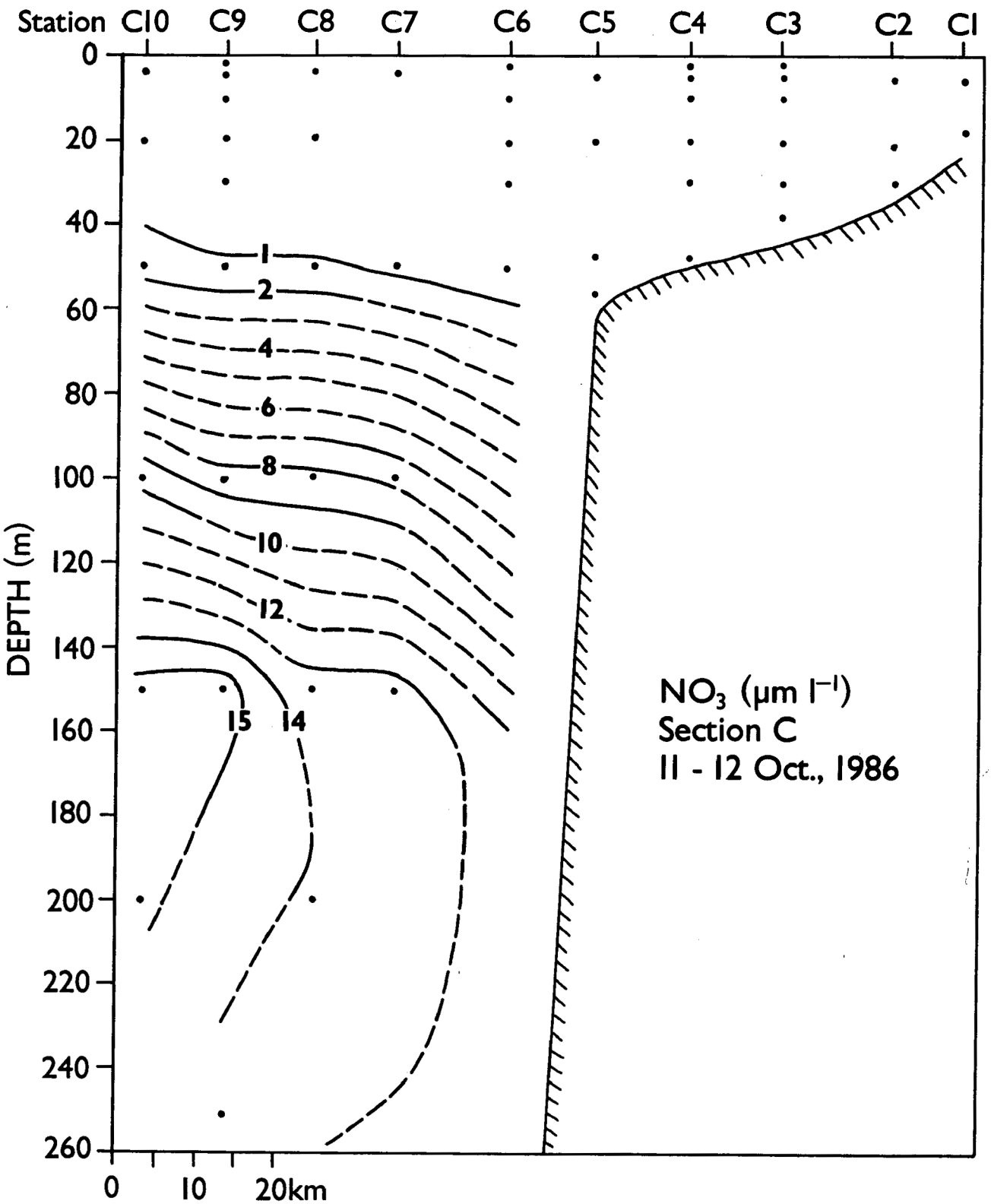

Figure 48. Nitrate at section C in October 1986.

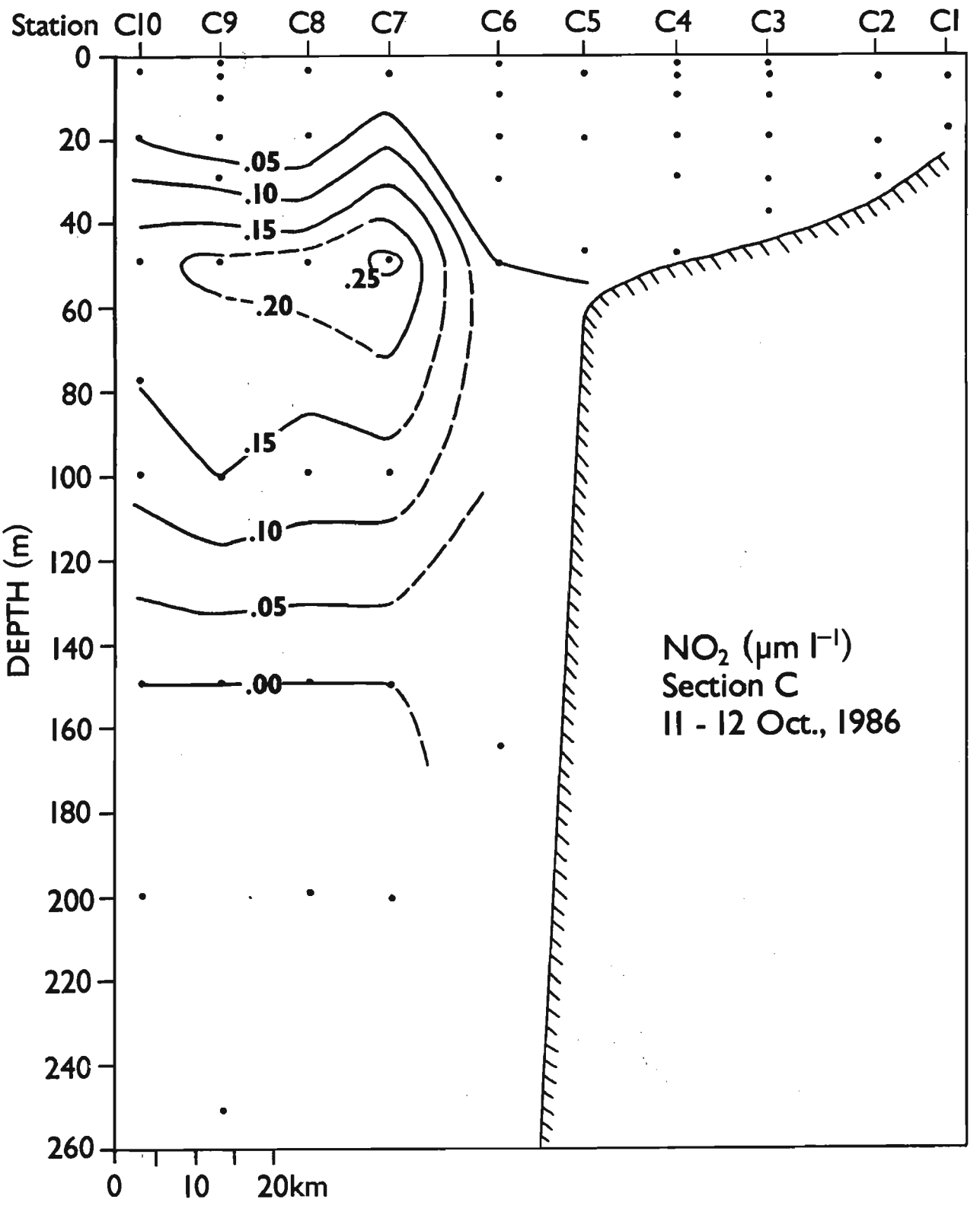

Figure 49. Nitrite at section C in October 1986.

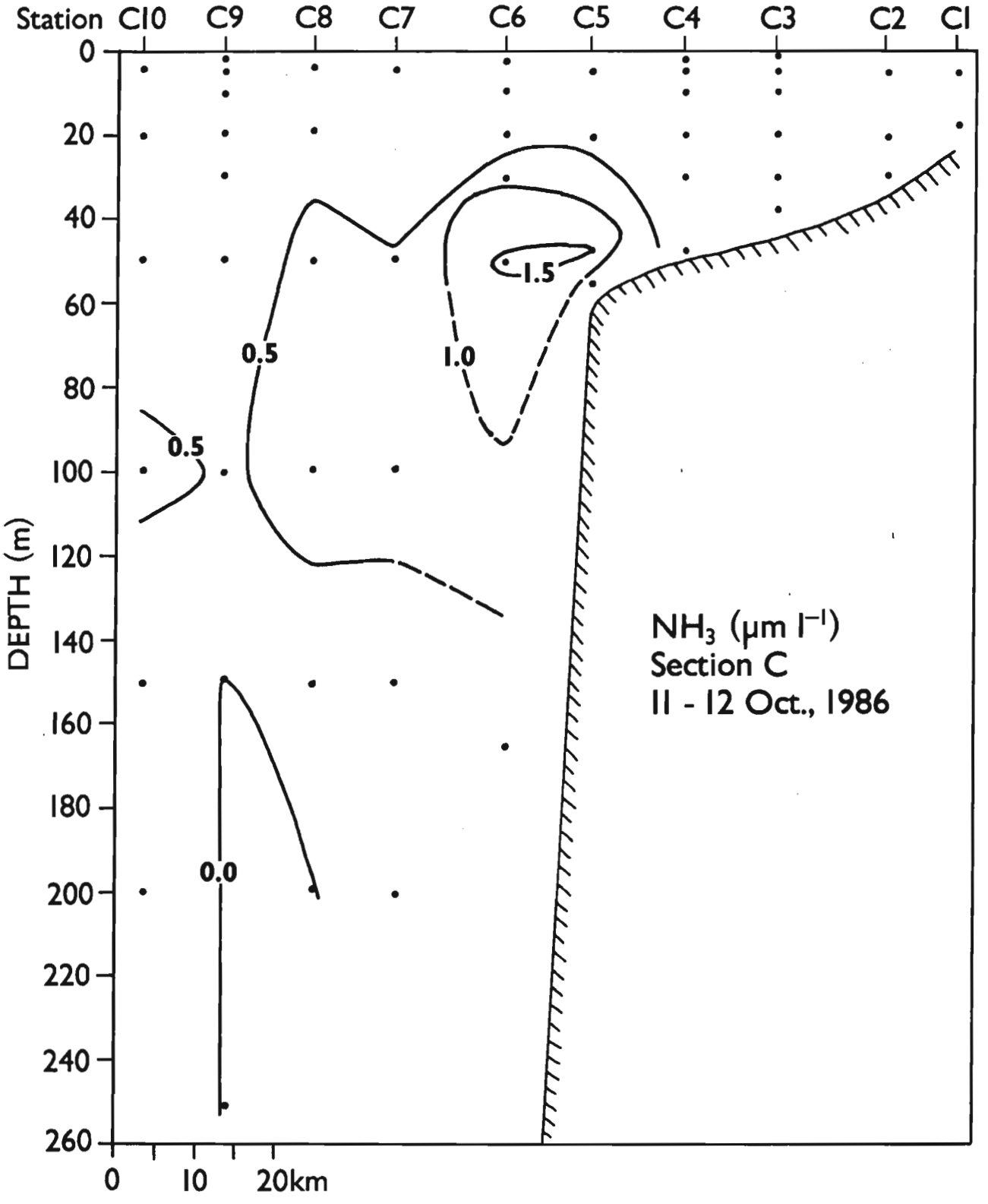

Figure 50. Ammonia at section C in October 1986.

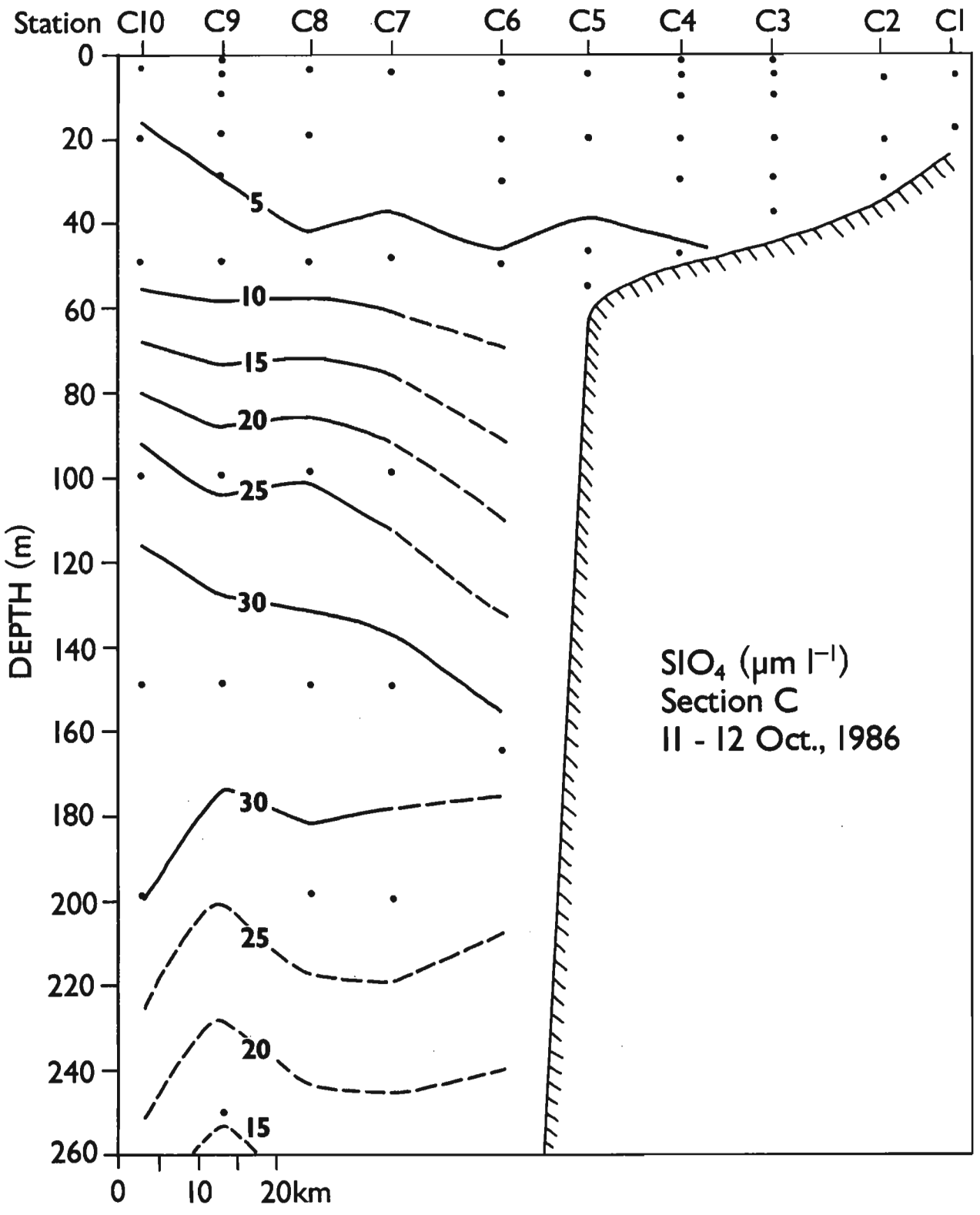

Figure 51. Silicate at section C in October 1986.

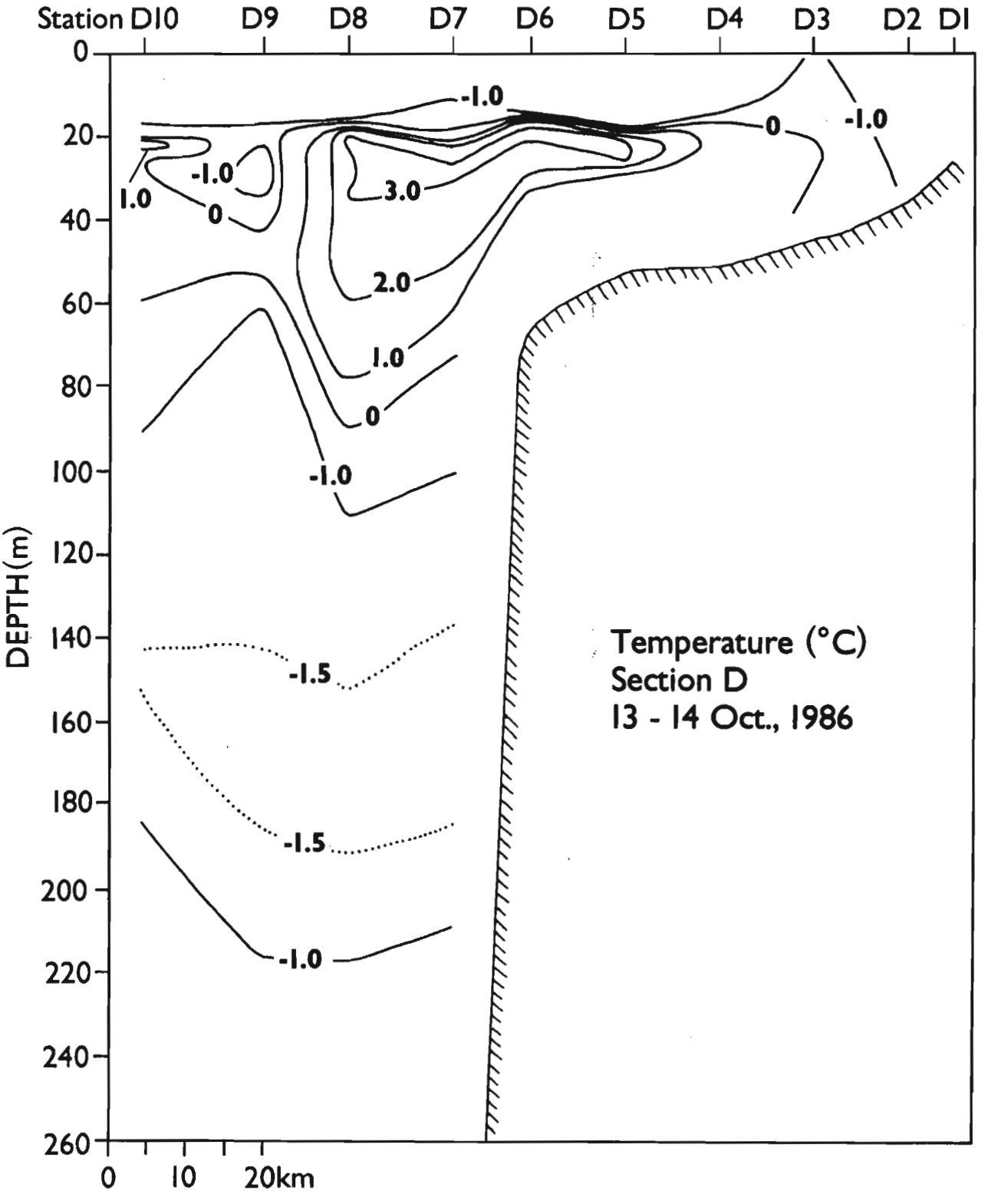

Figure 52. Temperature at section D in October 1986.

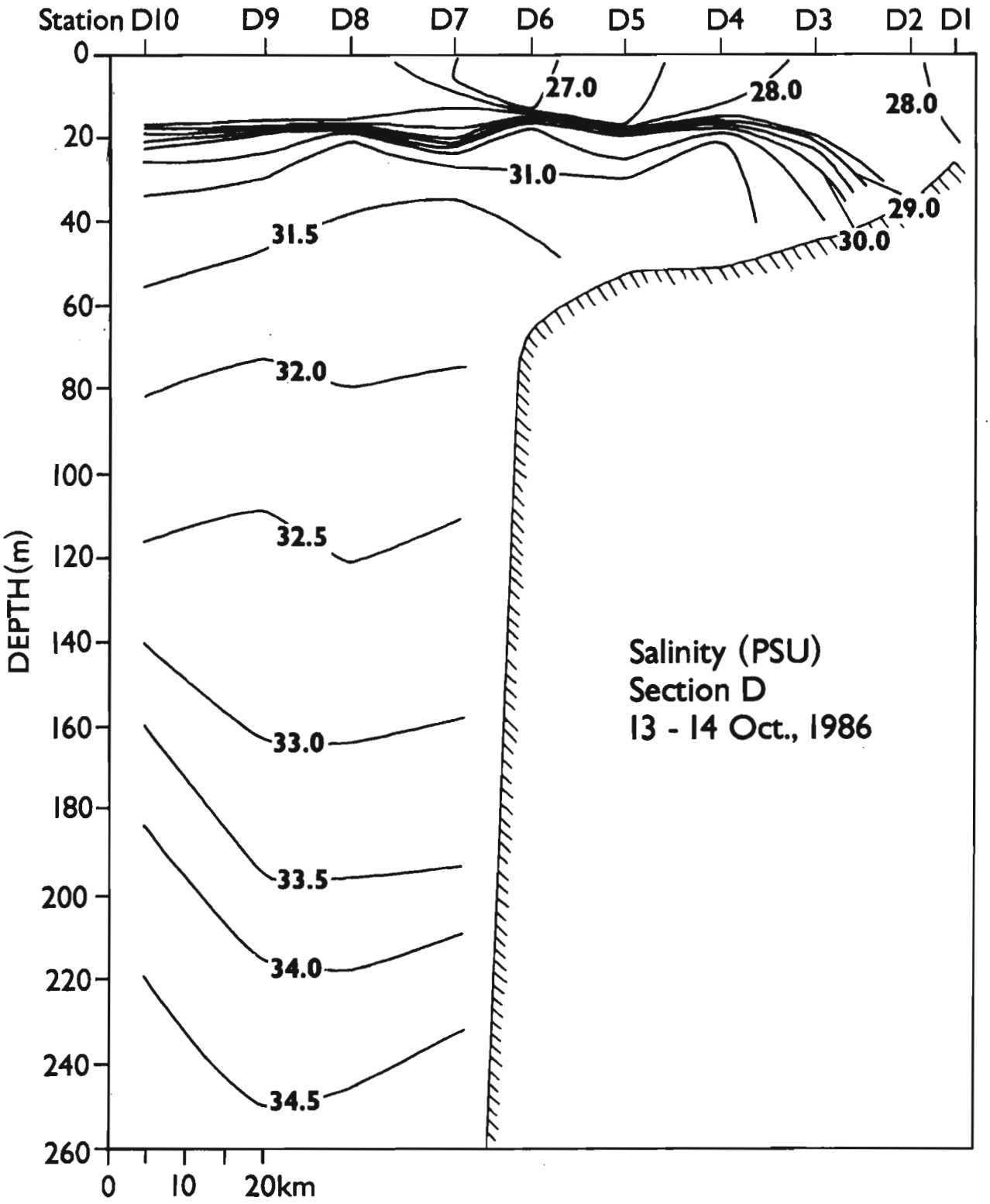

Figure 53. Salinity at section D in October 1986.

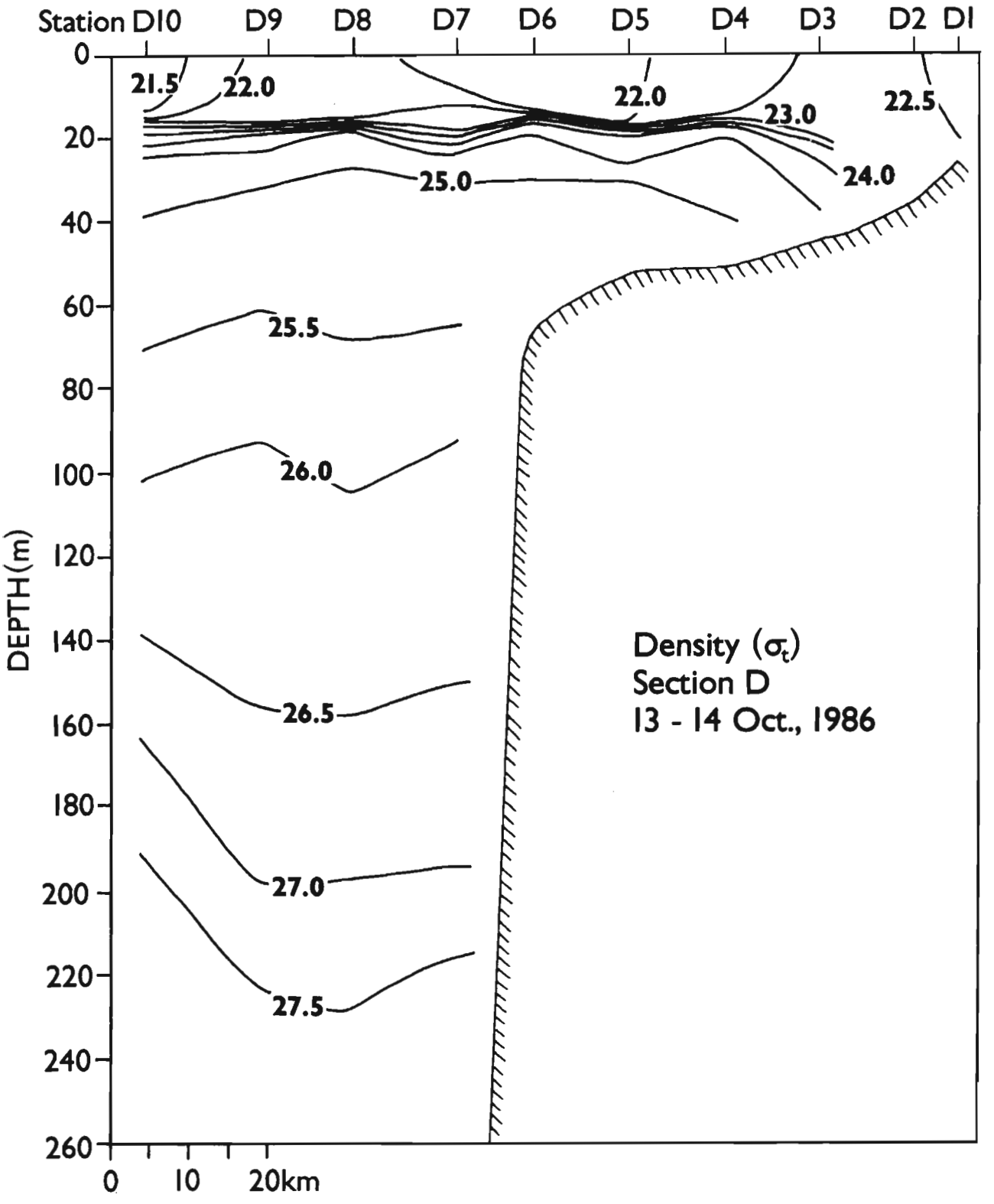

Figure 54. Density at section D in October 1986.

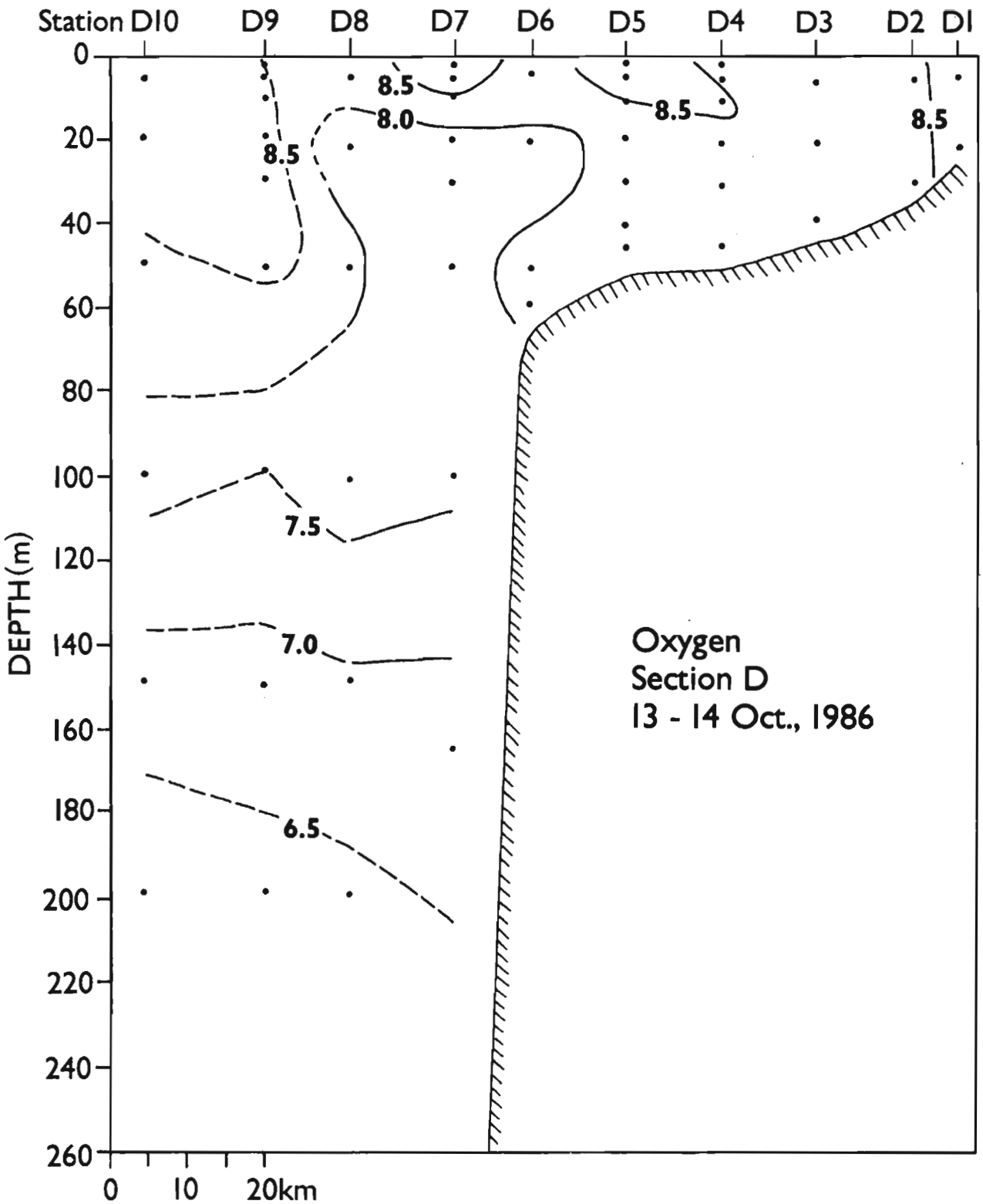

Figure 55. Dissolved oxygen at section D in October 1986.

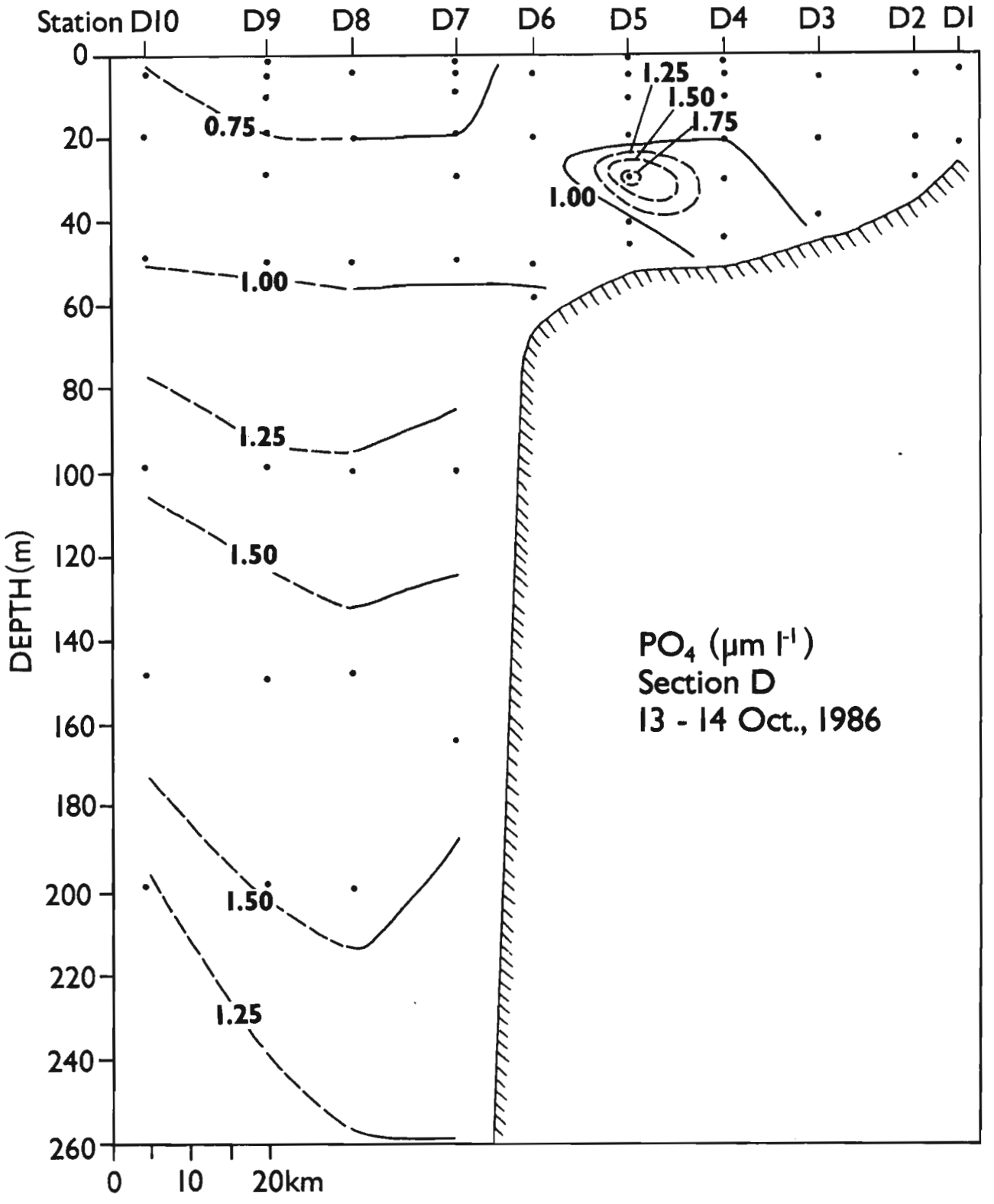

Figure 56. Phosphate at section D in October 1986.

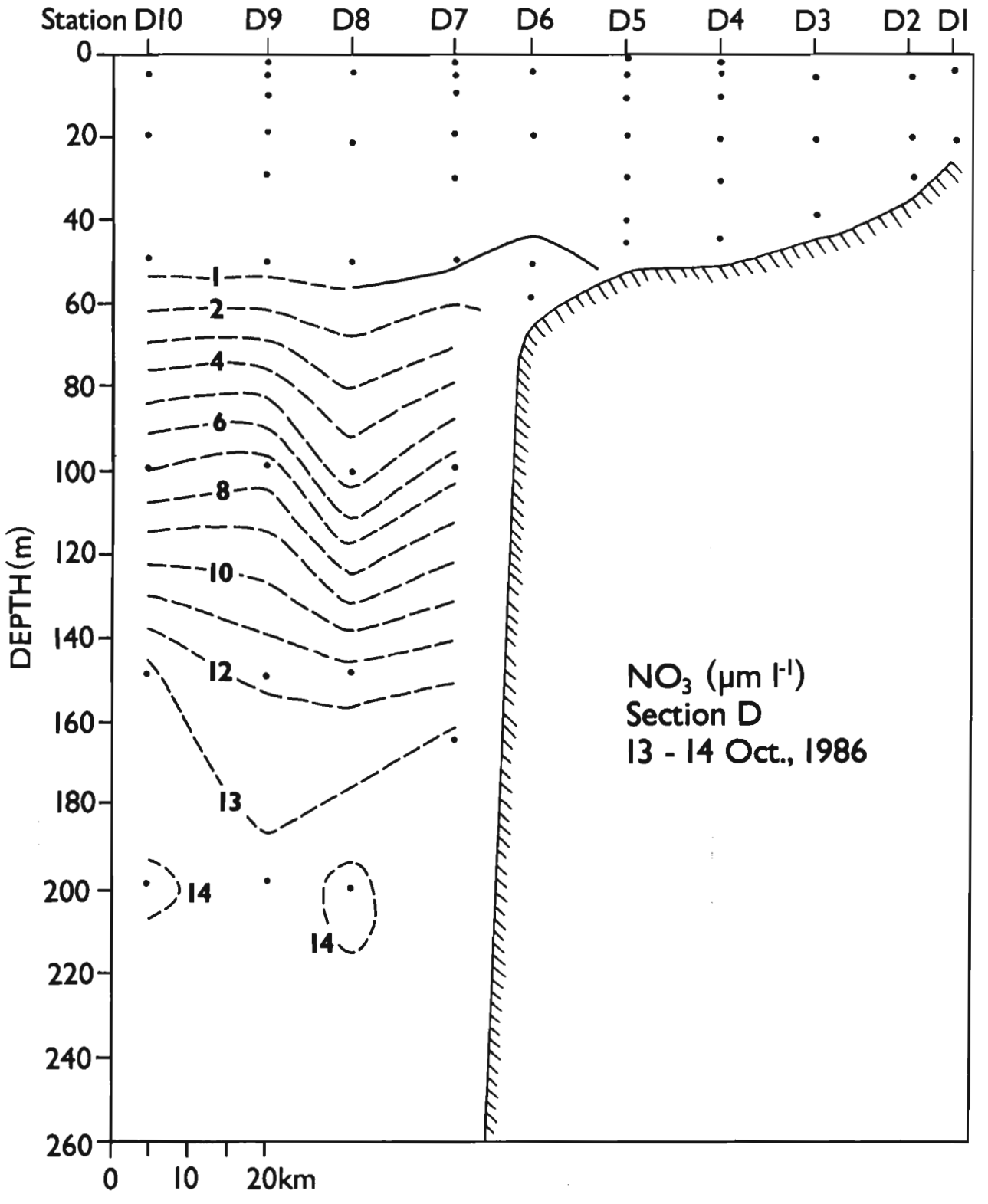

Figure 57. Nitrate at section D in October 1986.

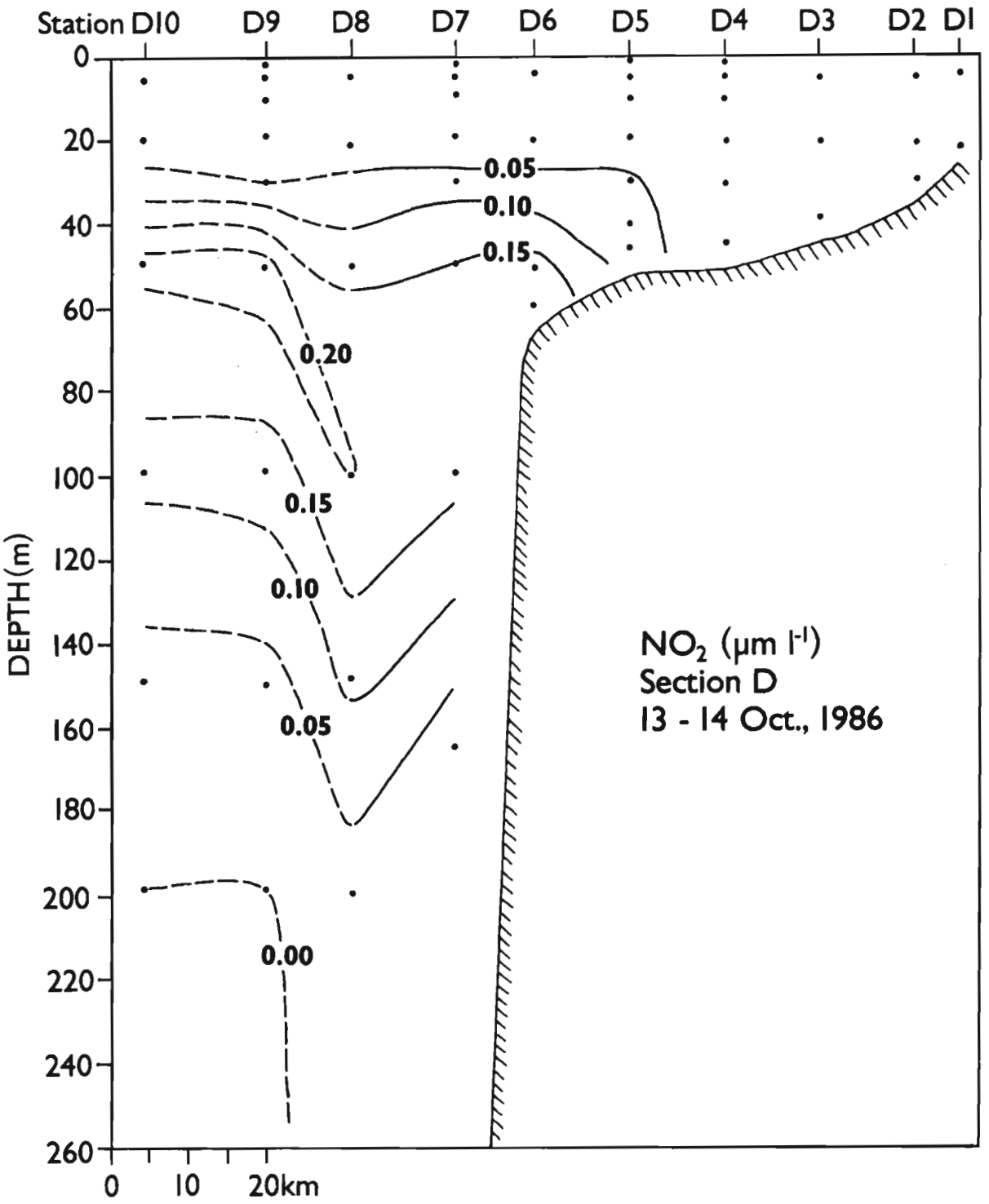

Figure 58. Nitrite at section D in October 1986.

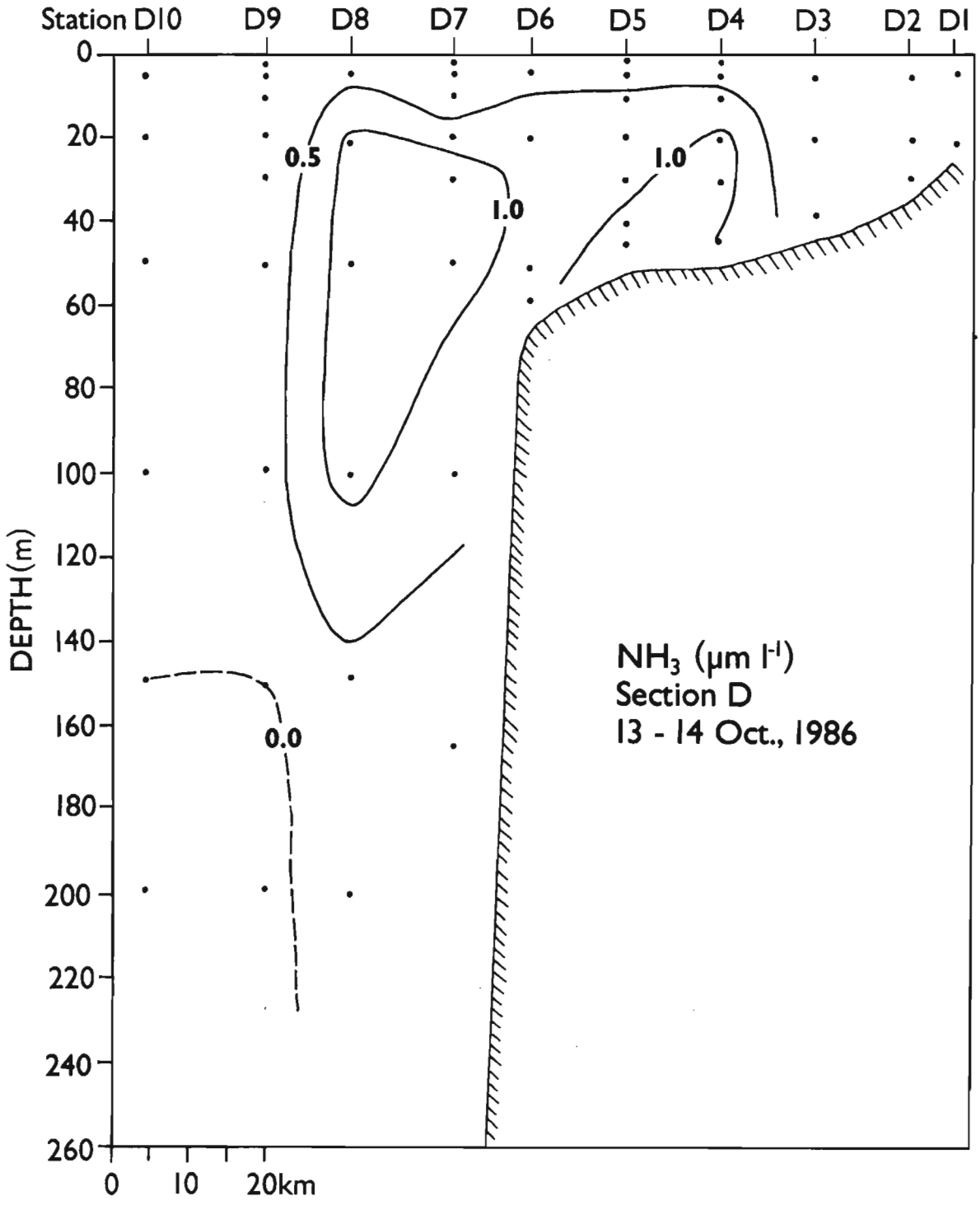

Figure 59. Ammonia at section D in October 1986.

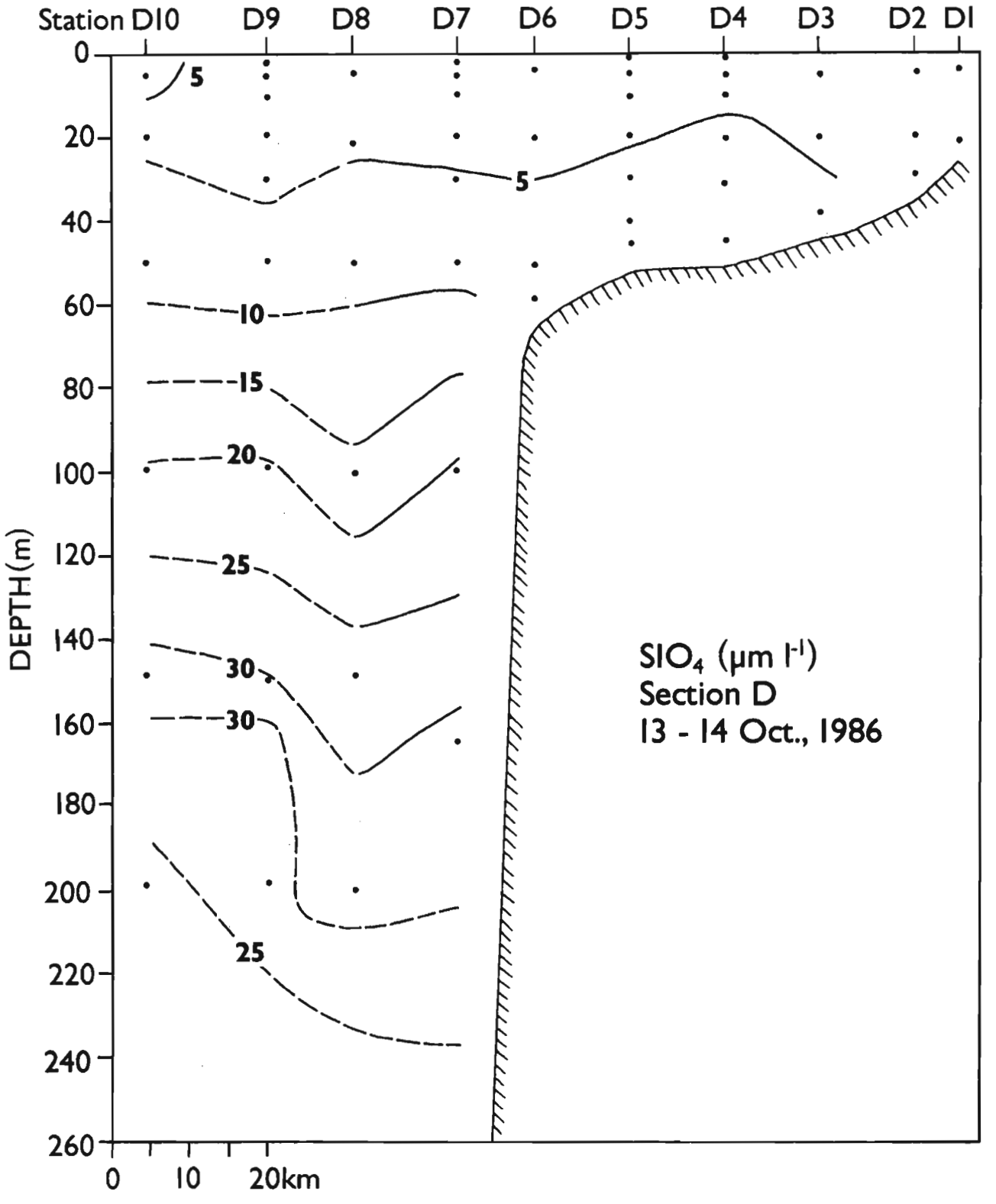

Figure 60. Silicate at section D in October 1986.

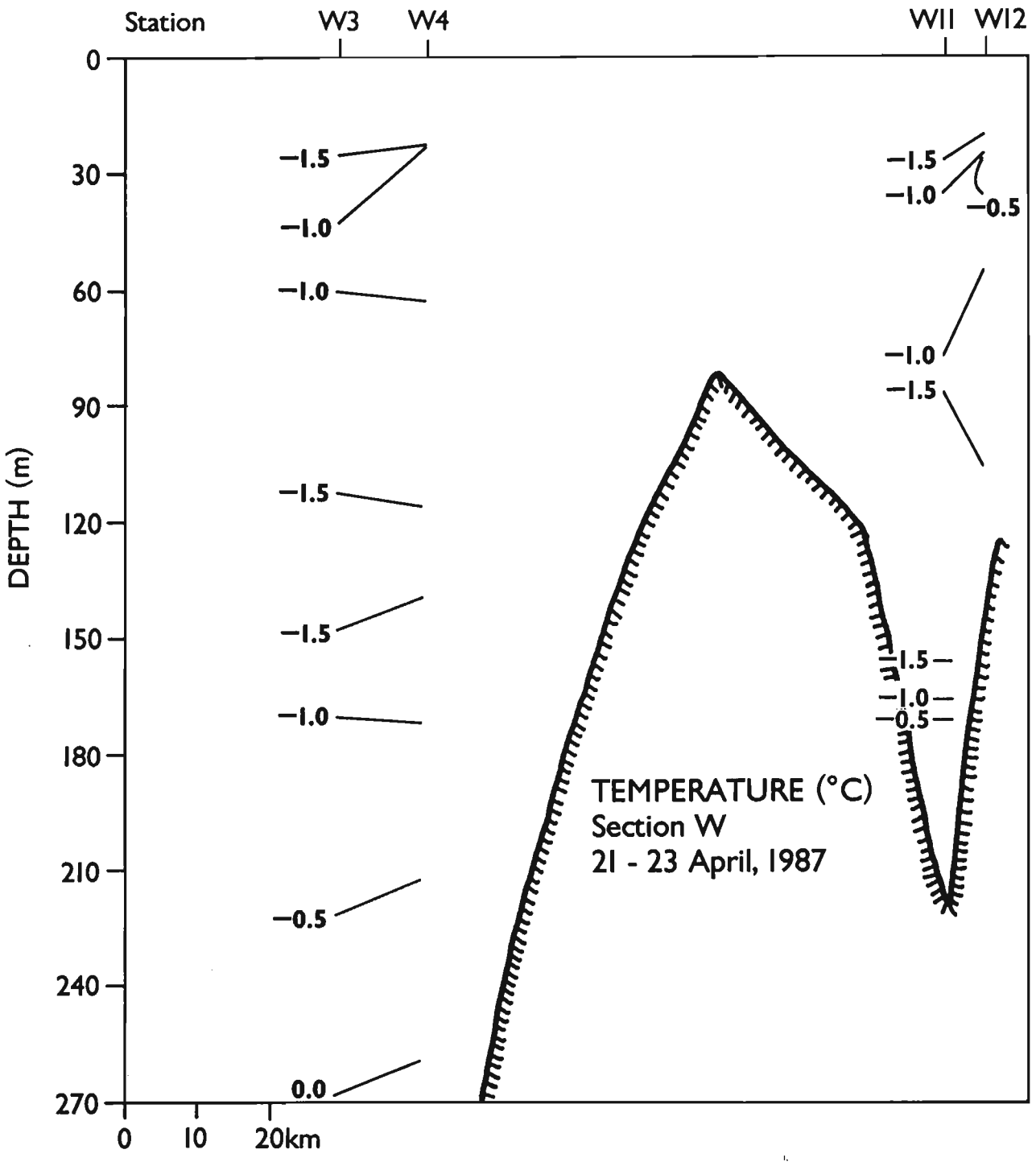

Figure 61. Temperature at section W in April 1987.

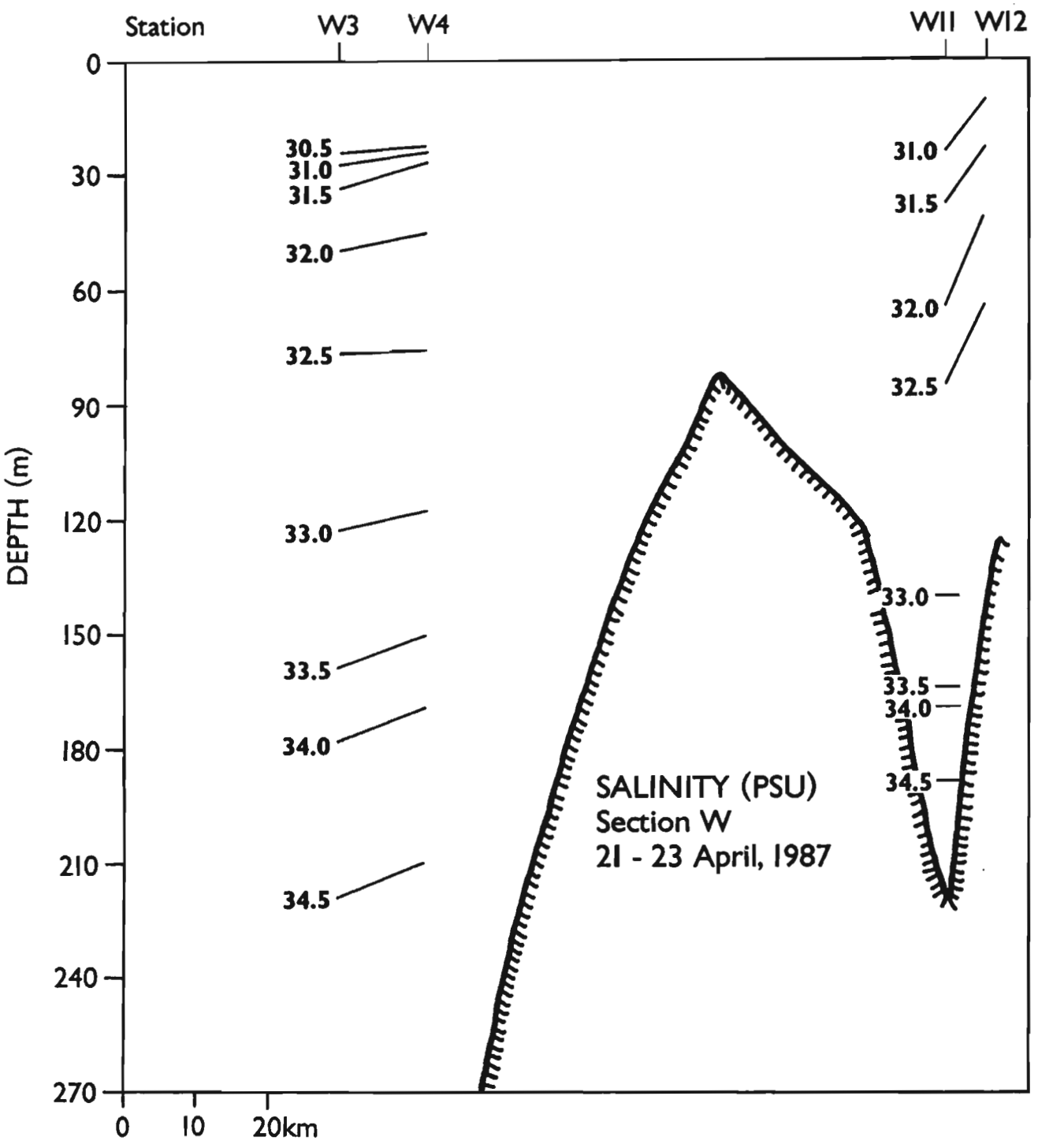

Figure 62. Salinity at section W in April 1987.

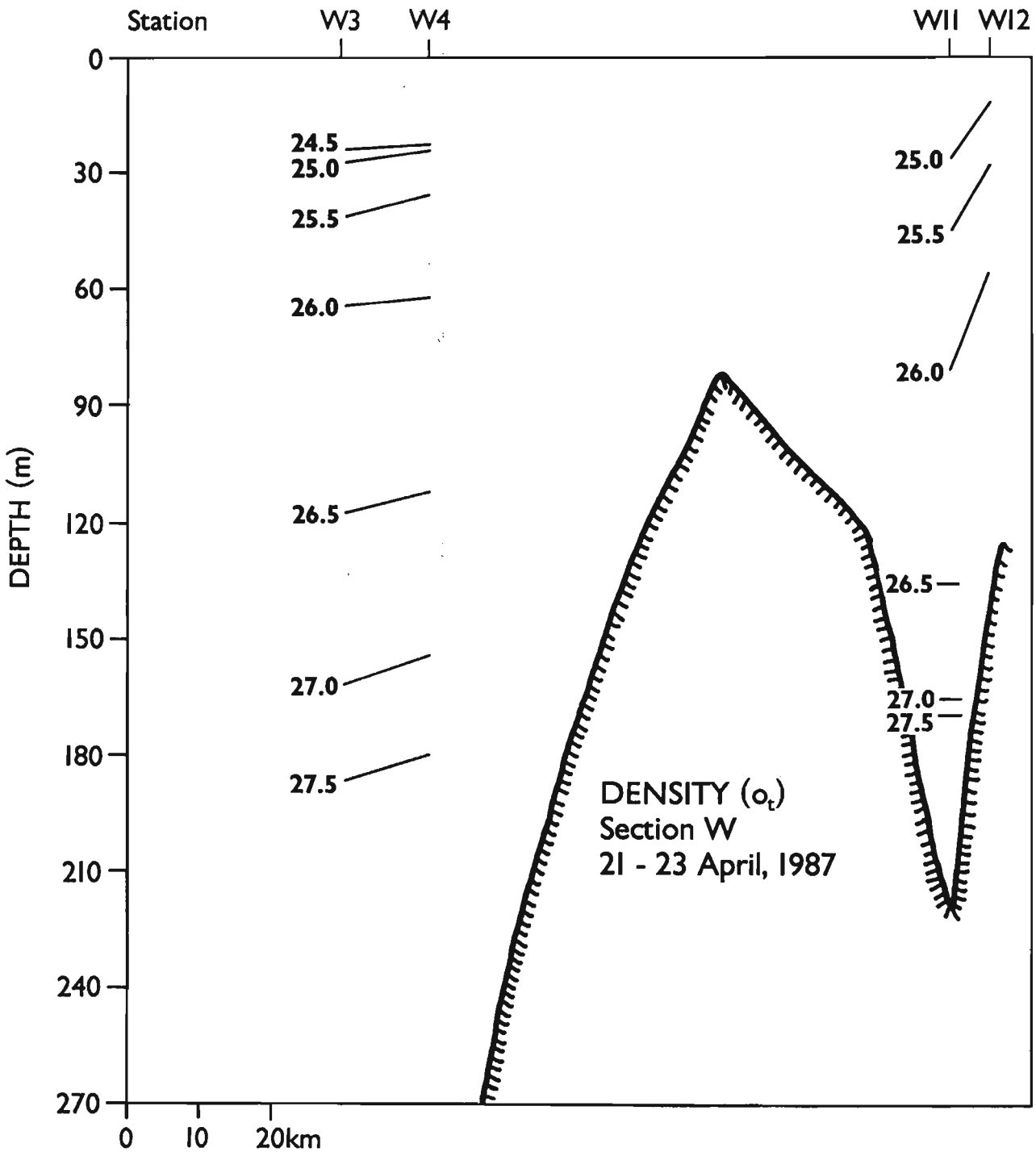

Figure 63. Density at section W in April 1987.

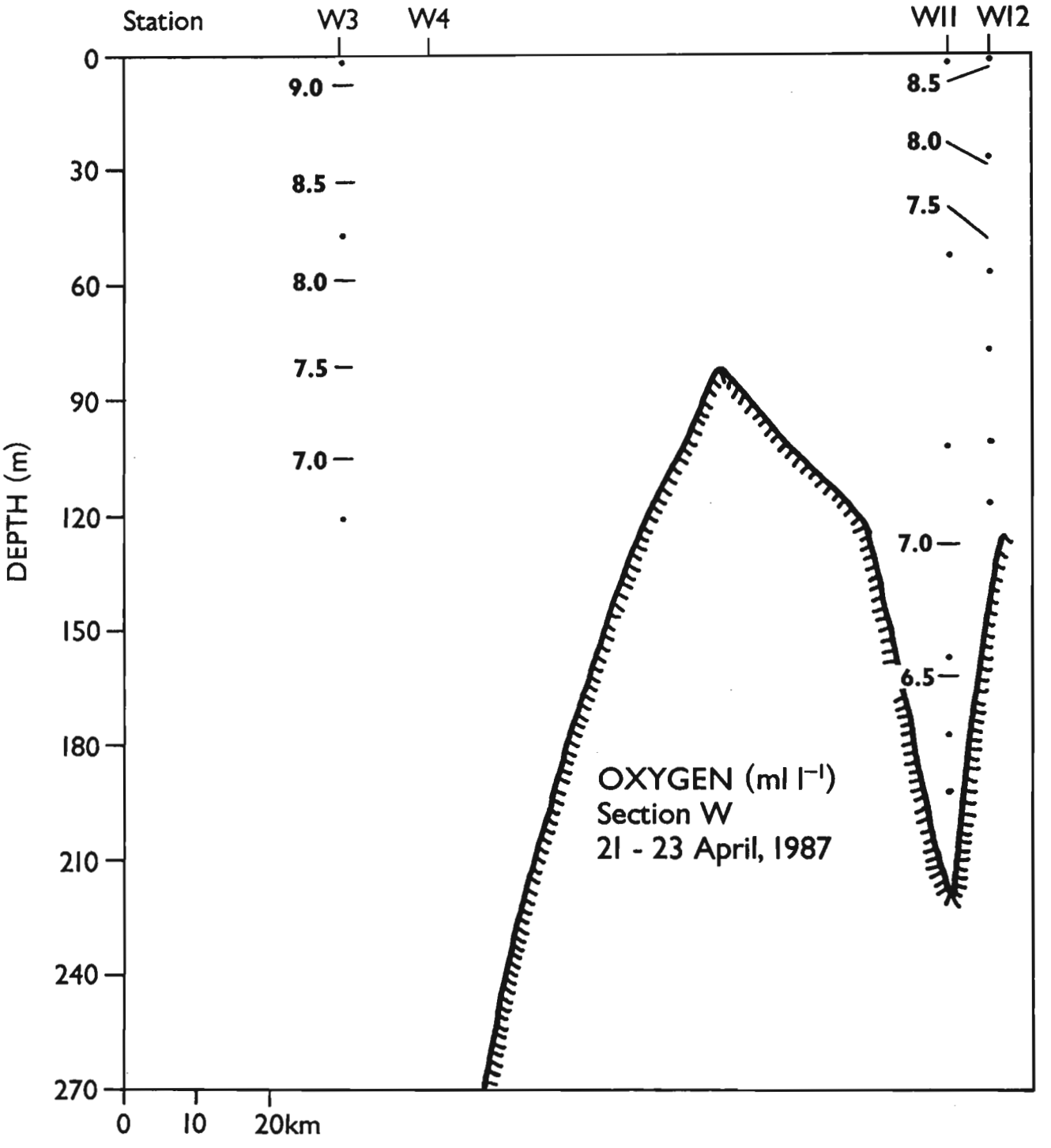

Figure 64. Dissolved oxygen at section W in April 1987.

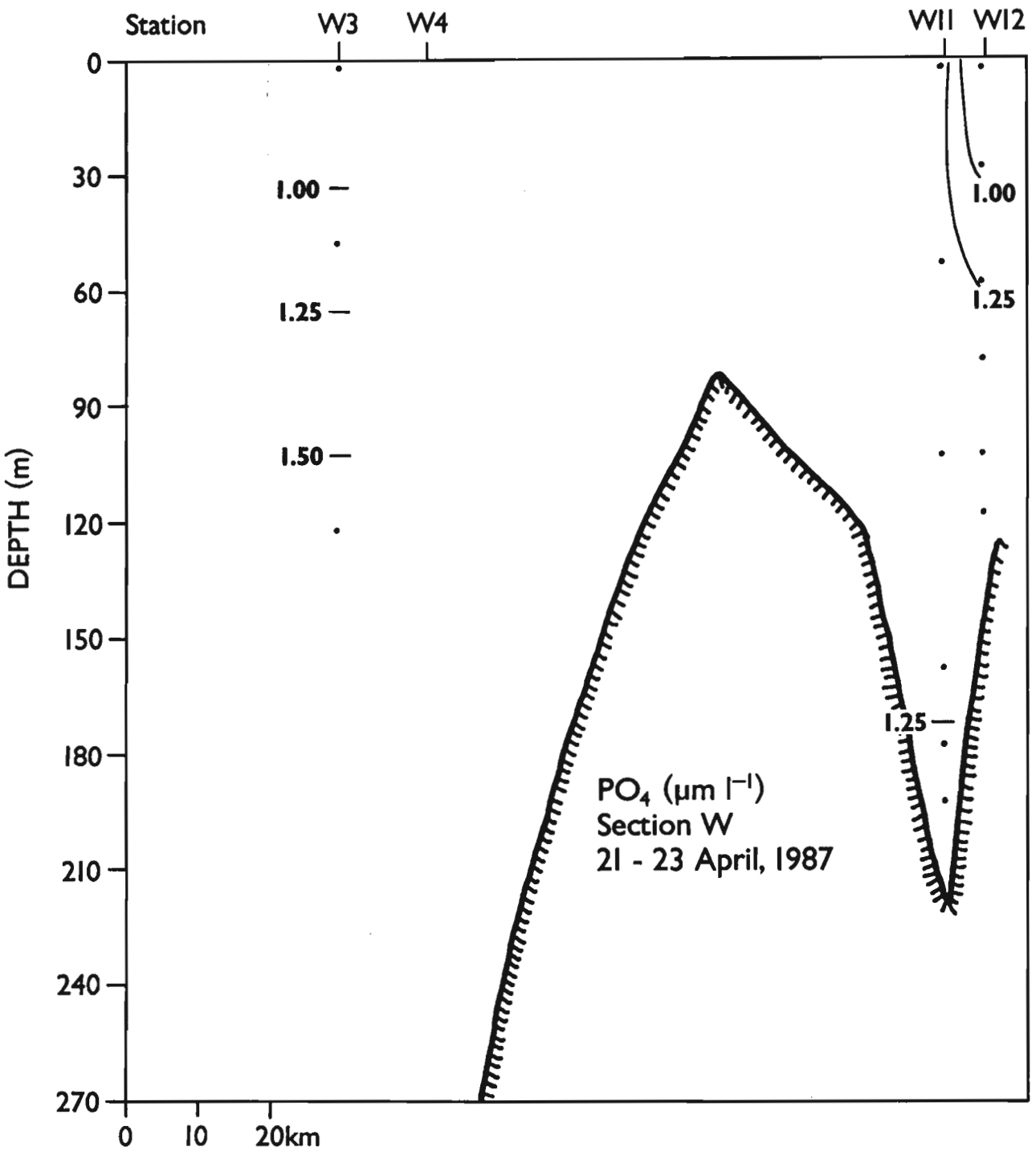

Figure 65. Phosphate at section W in April 1987.

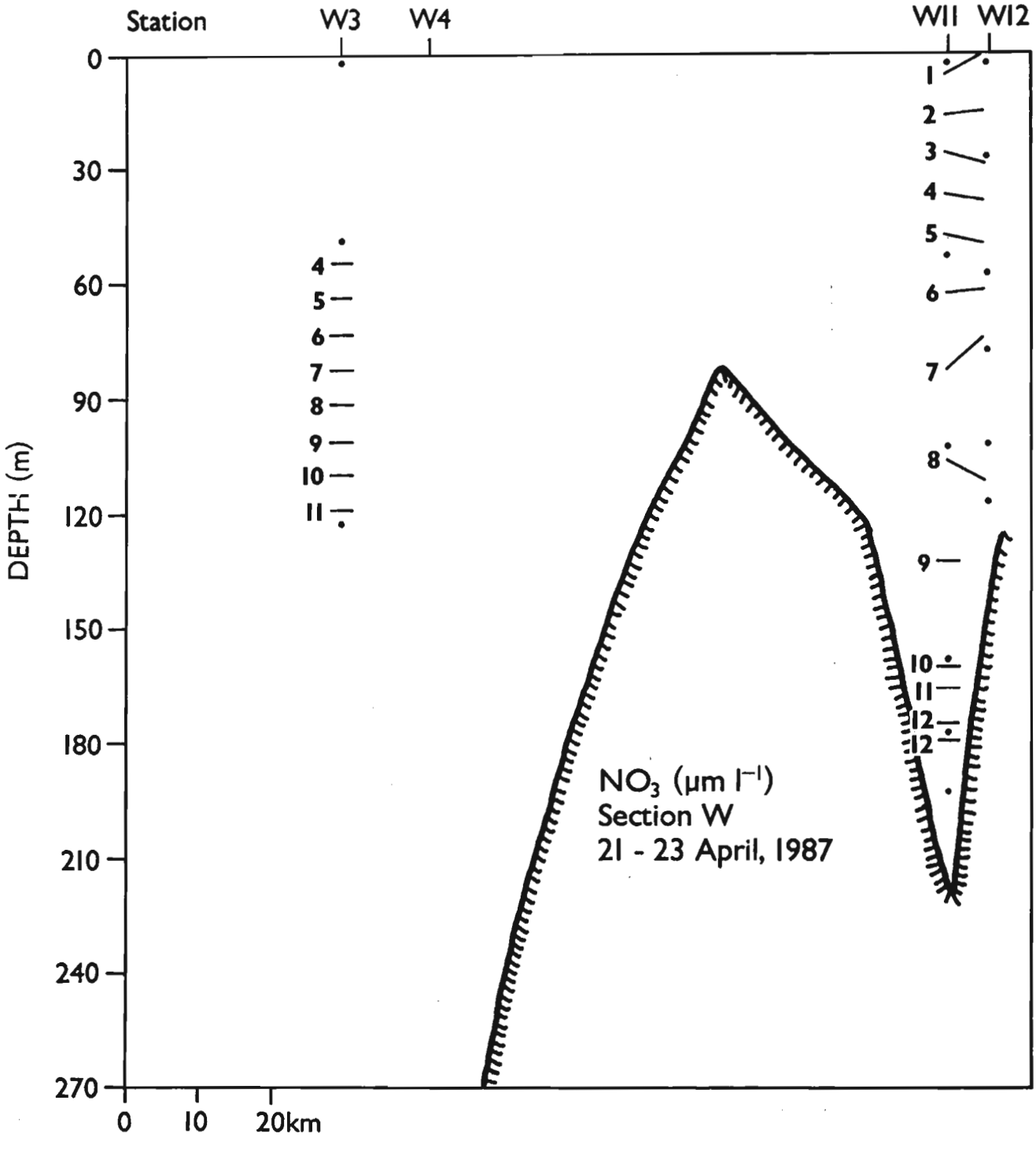

Figure 66. Nitrate at section W in April 1987.

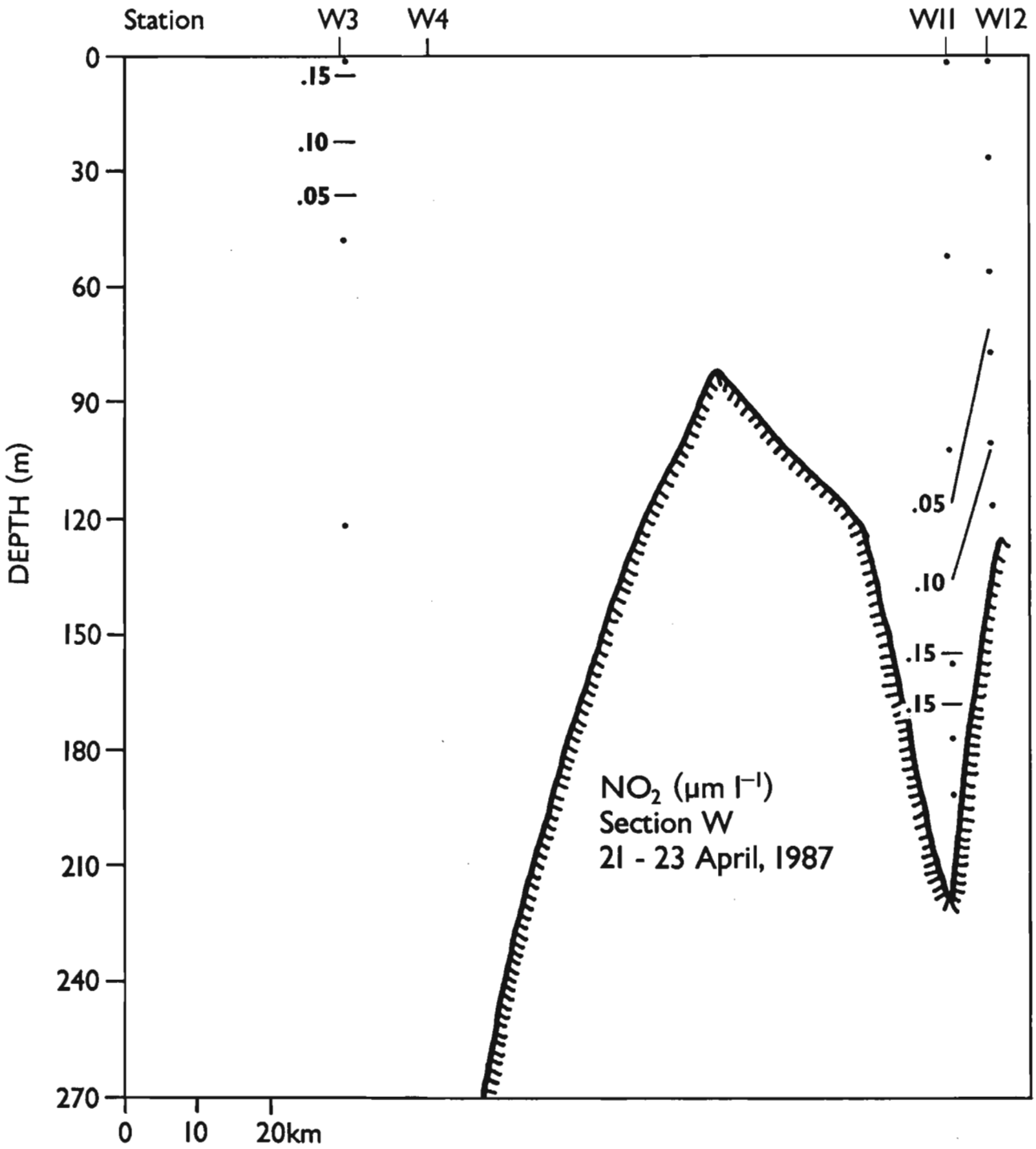

Figure 67. Nitrite at section W in April 1987.

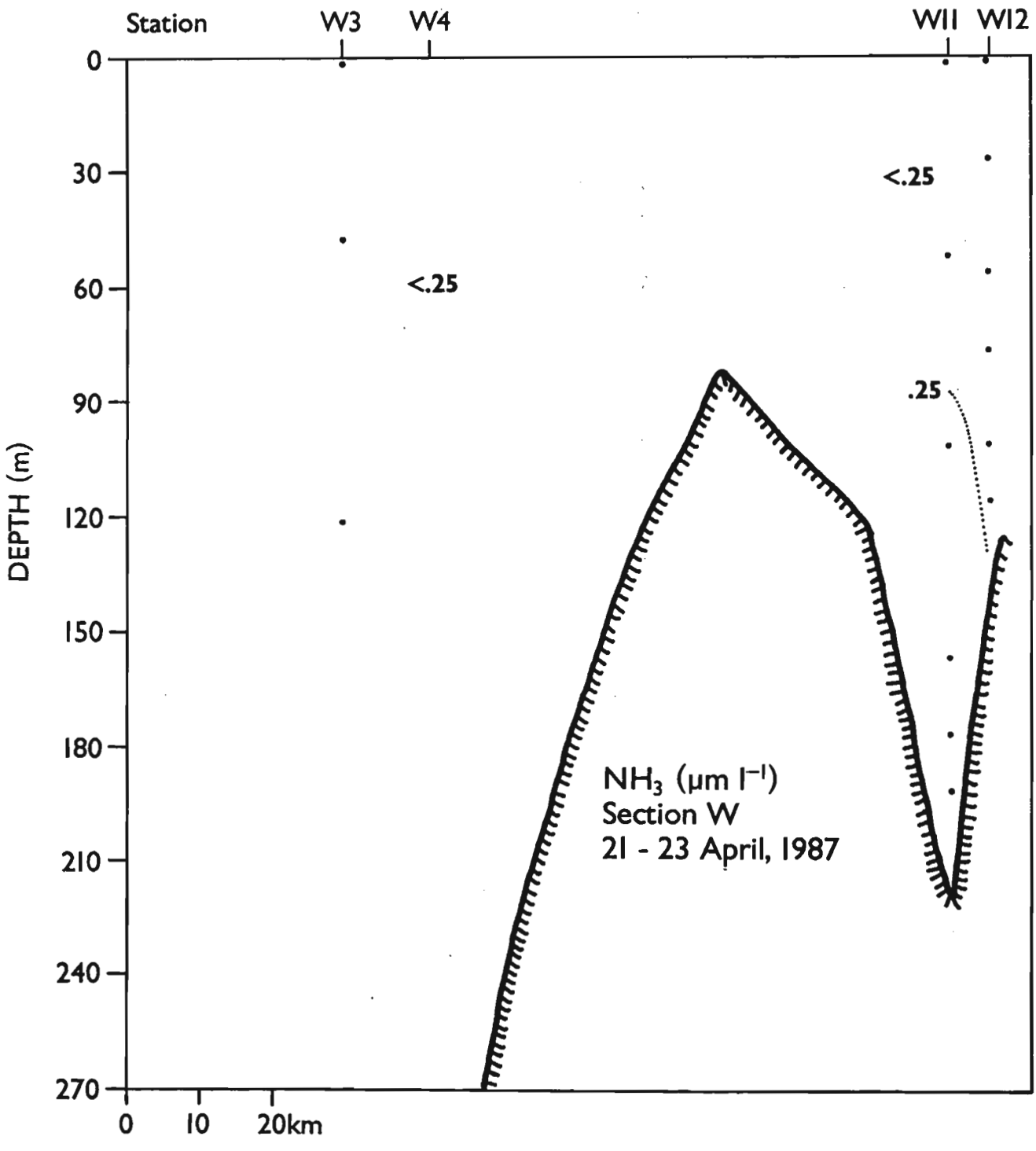

Figure 68. Ammonia at section W in April 1987.

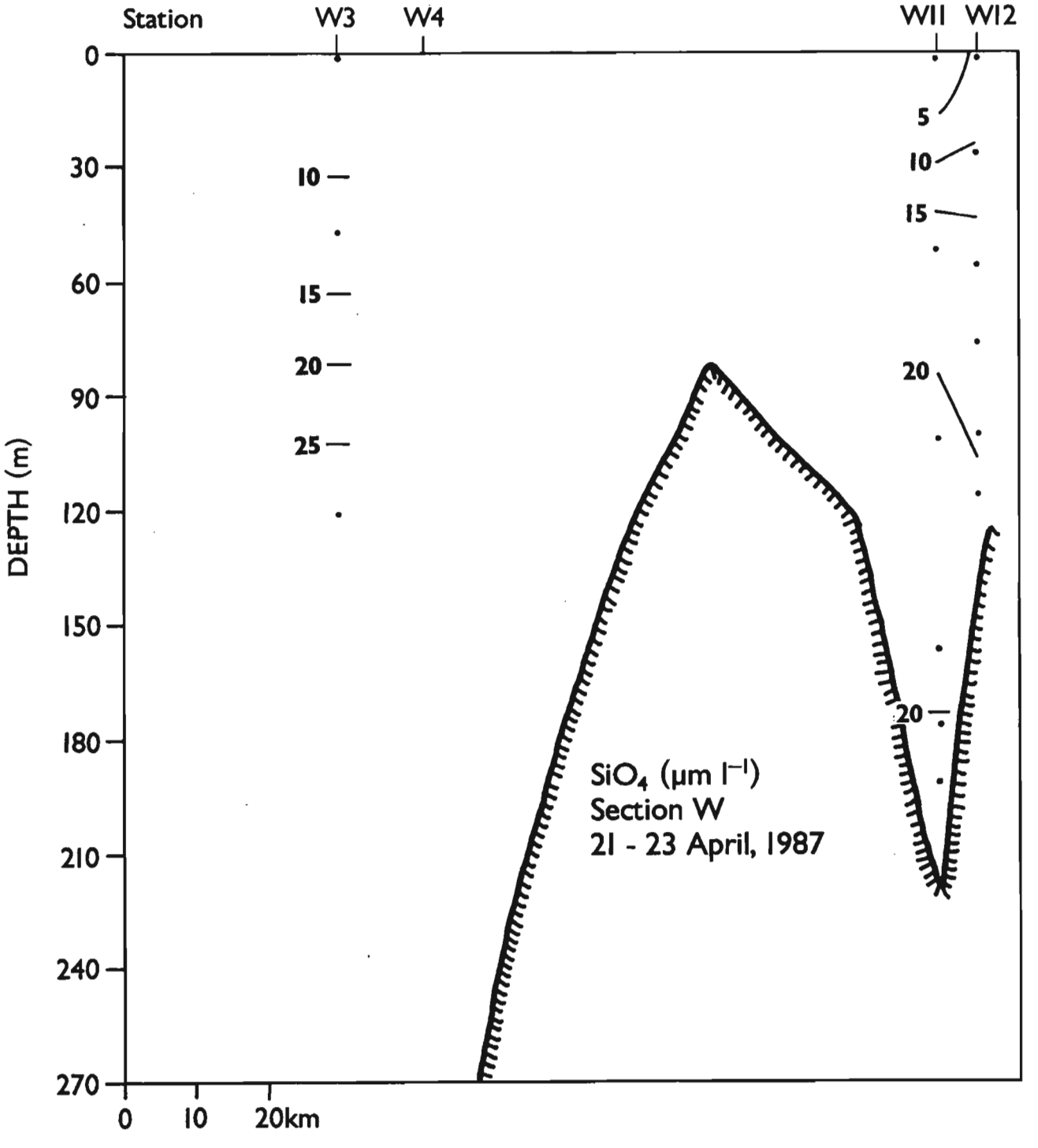

Figure 69. Silicate at section W in April 1987.

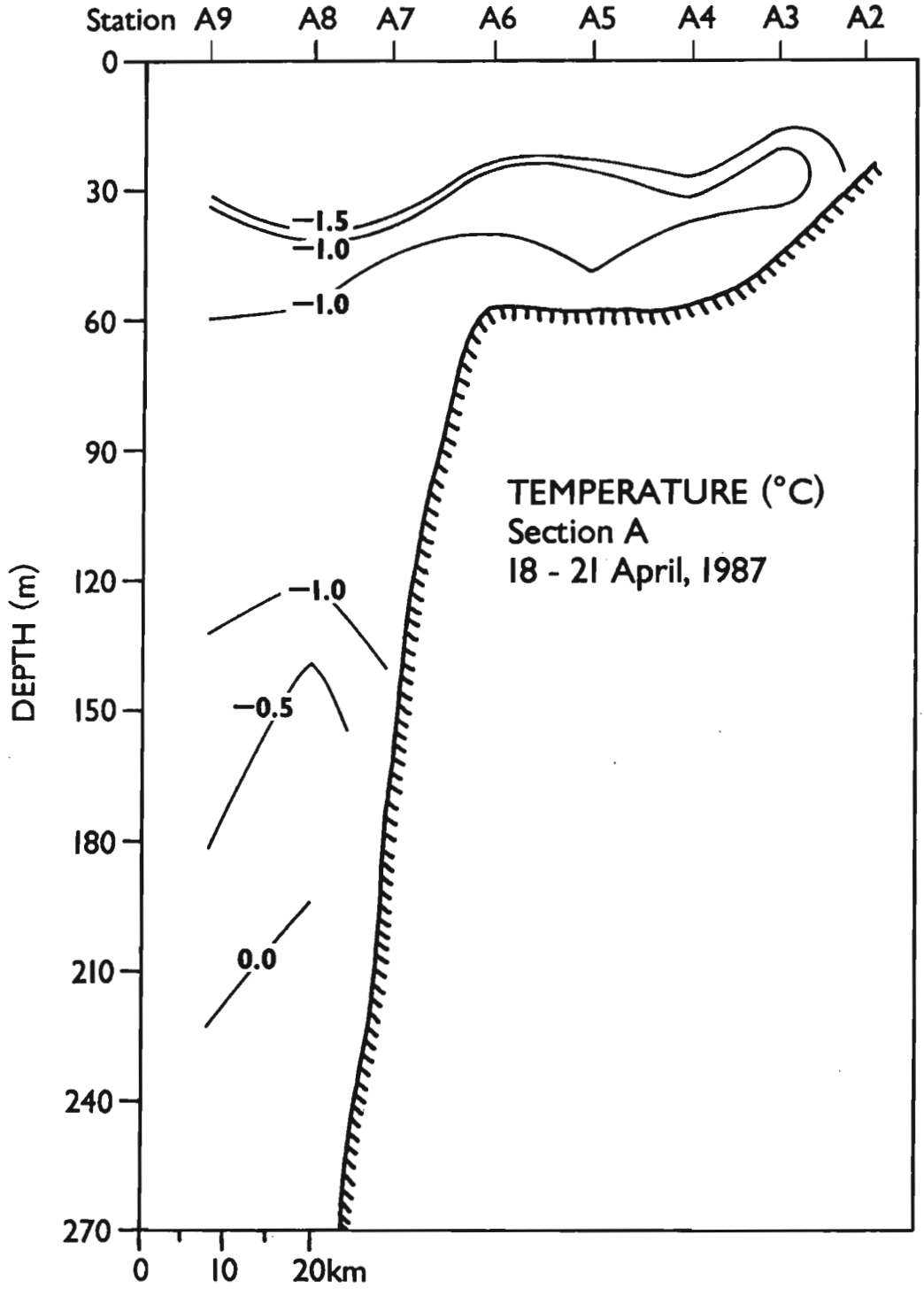

Figure 70. Temperature at section A in April 1987.

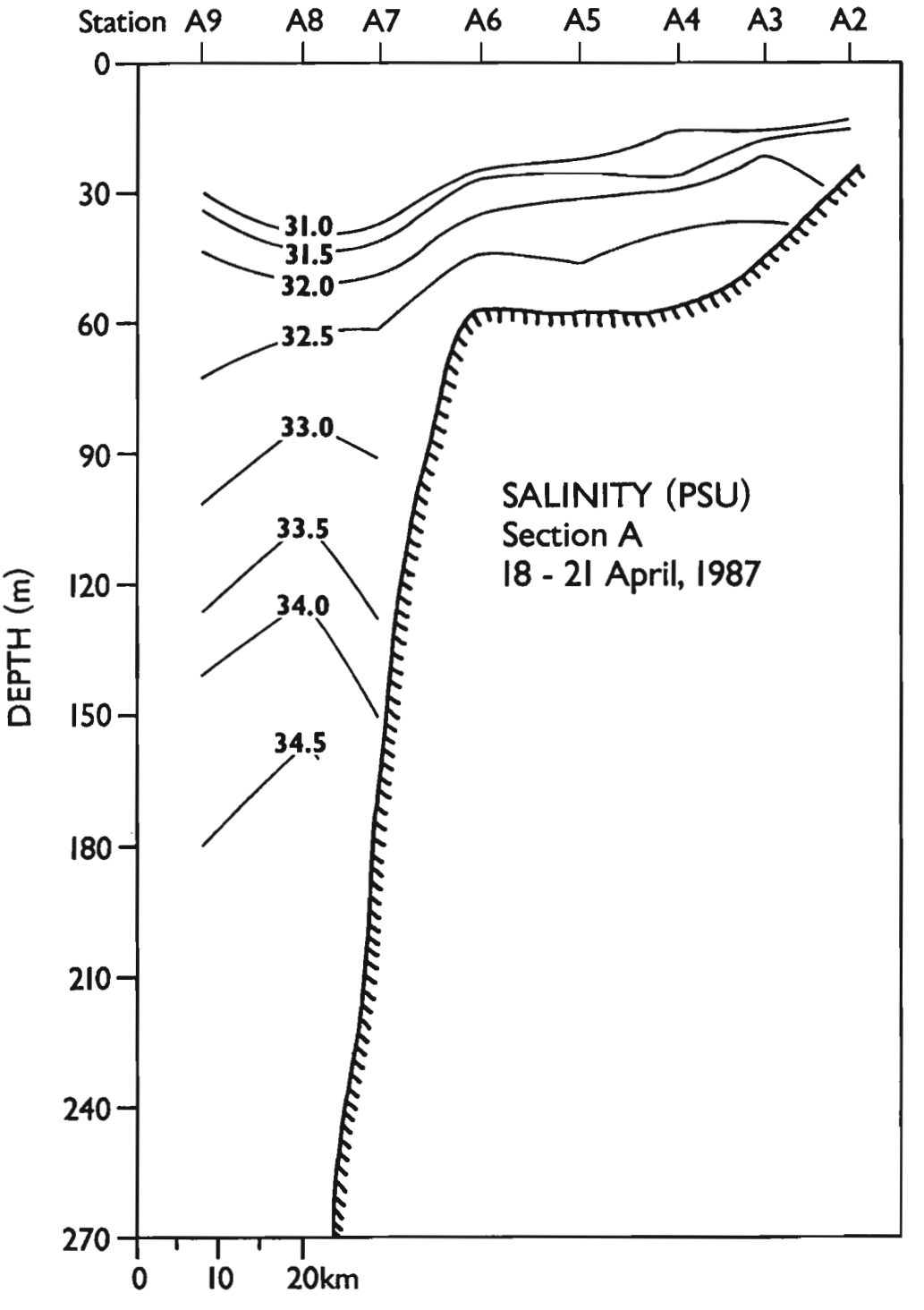

Figure 71. Salinity at section A in April 1987.

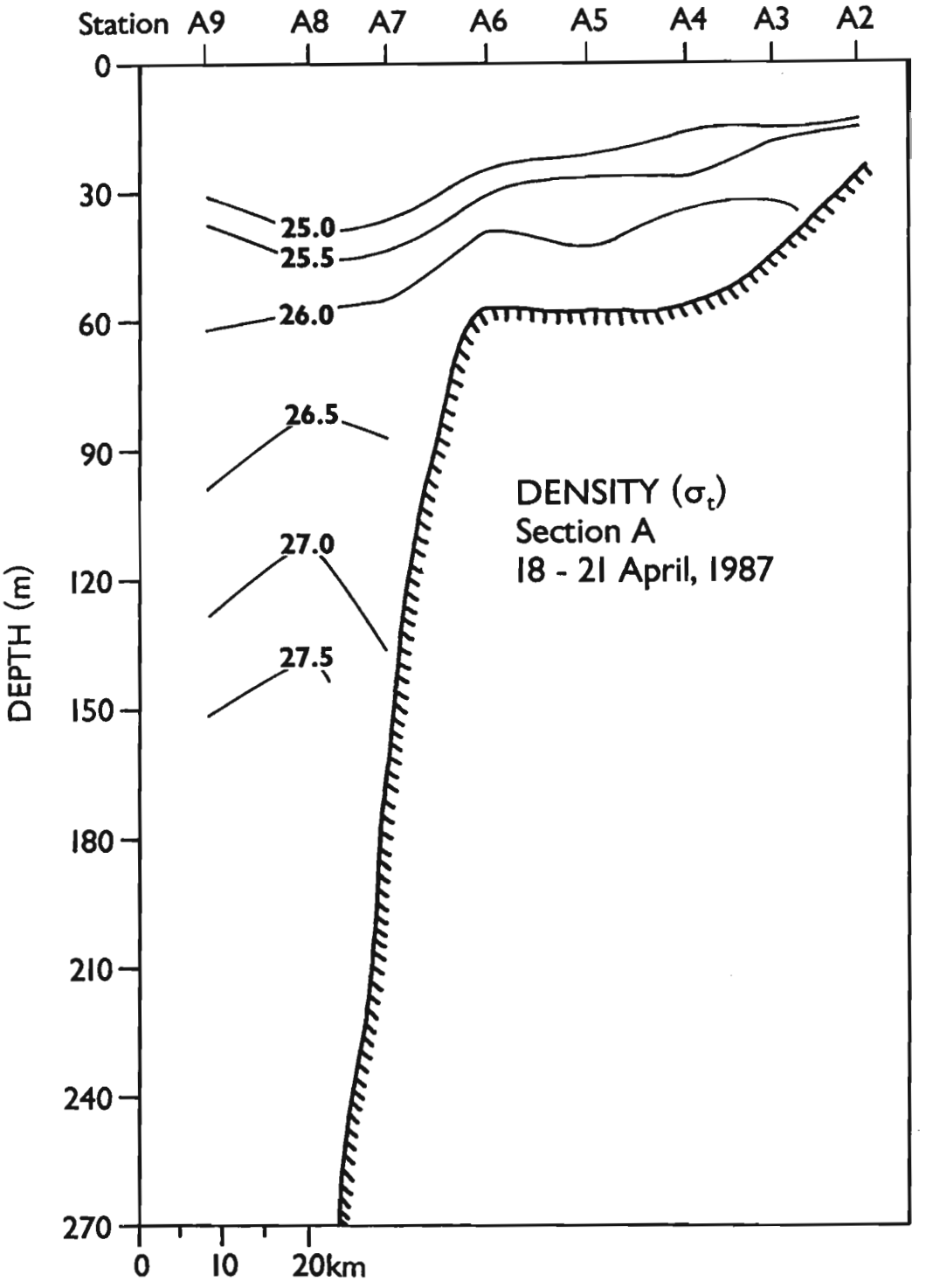

Figure 72. Density at section A in April 1987.

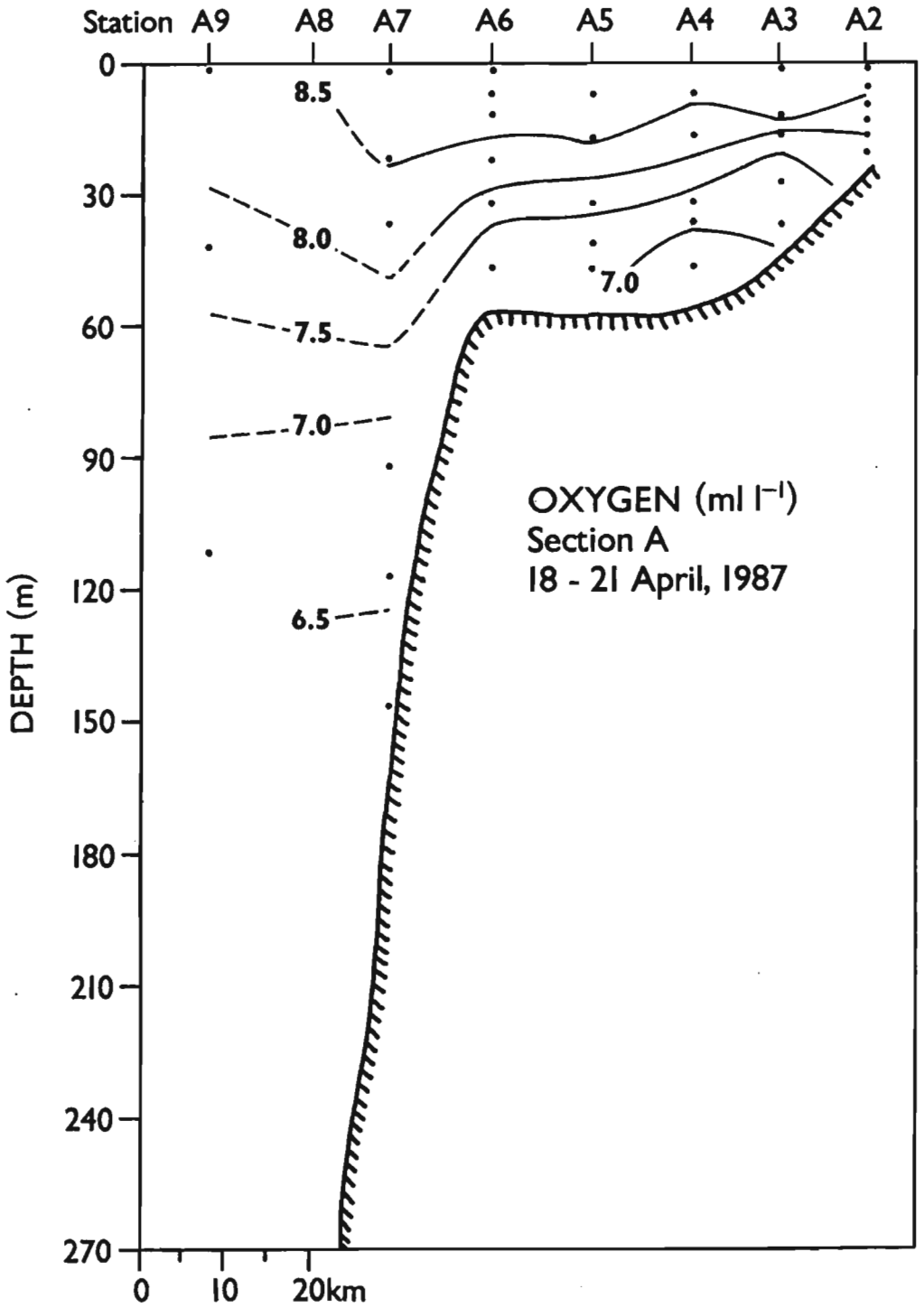

Figure 73. Dissolved oxygen at section A in April 1987.

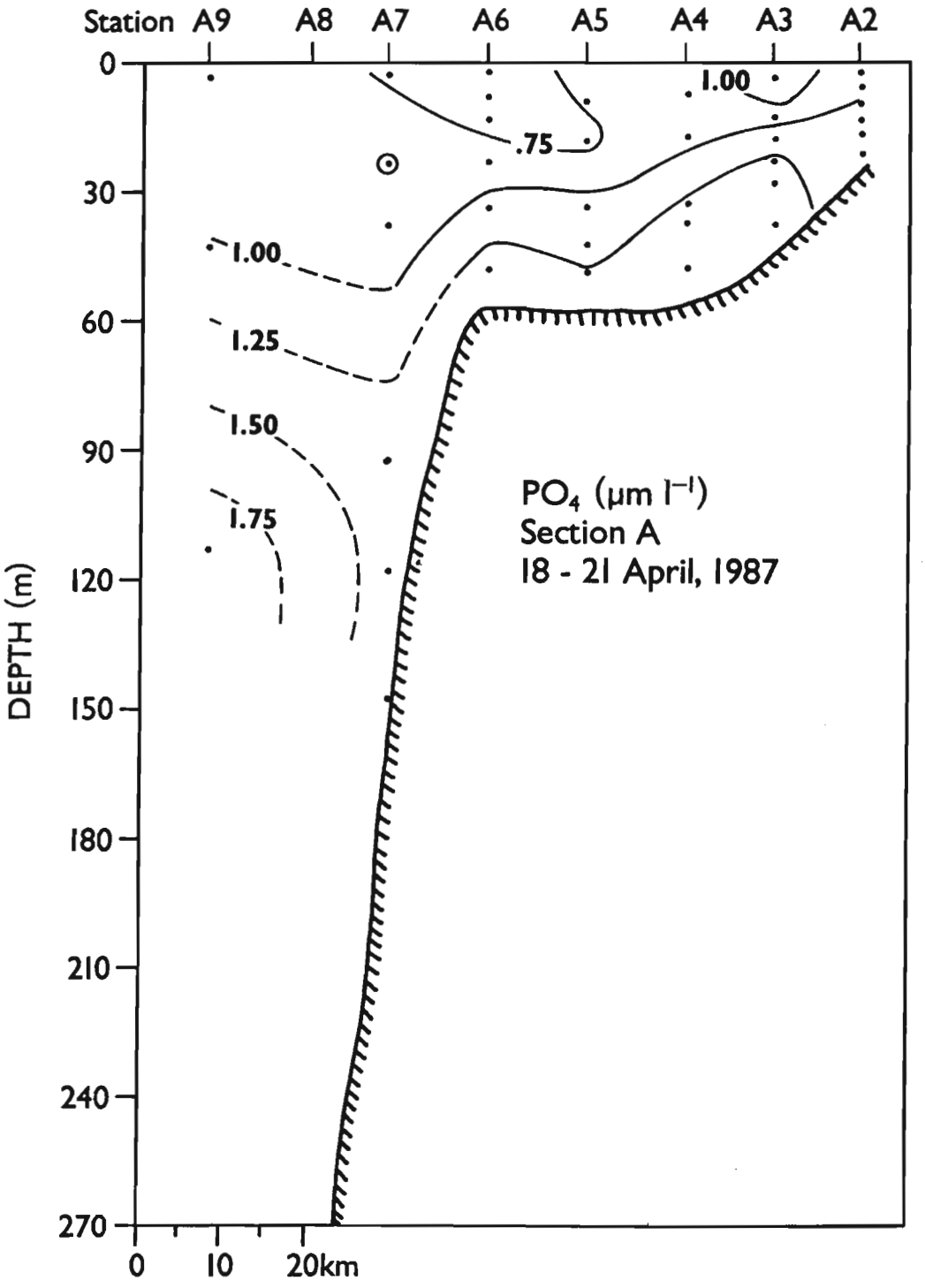

Figure 74. Phosphate at section A in April 1987.

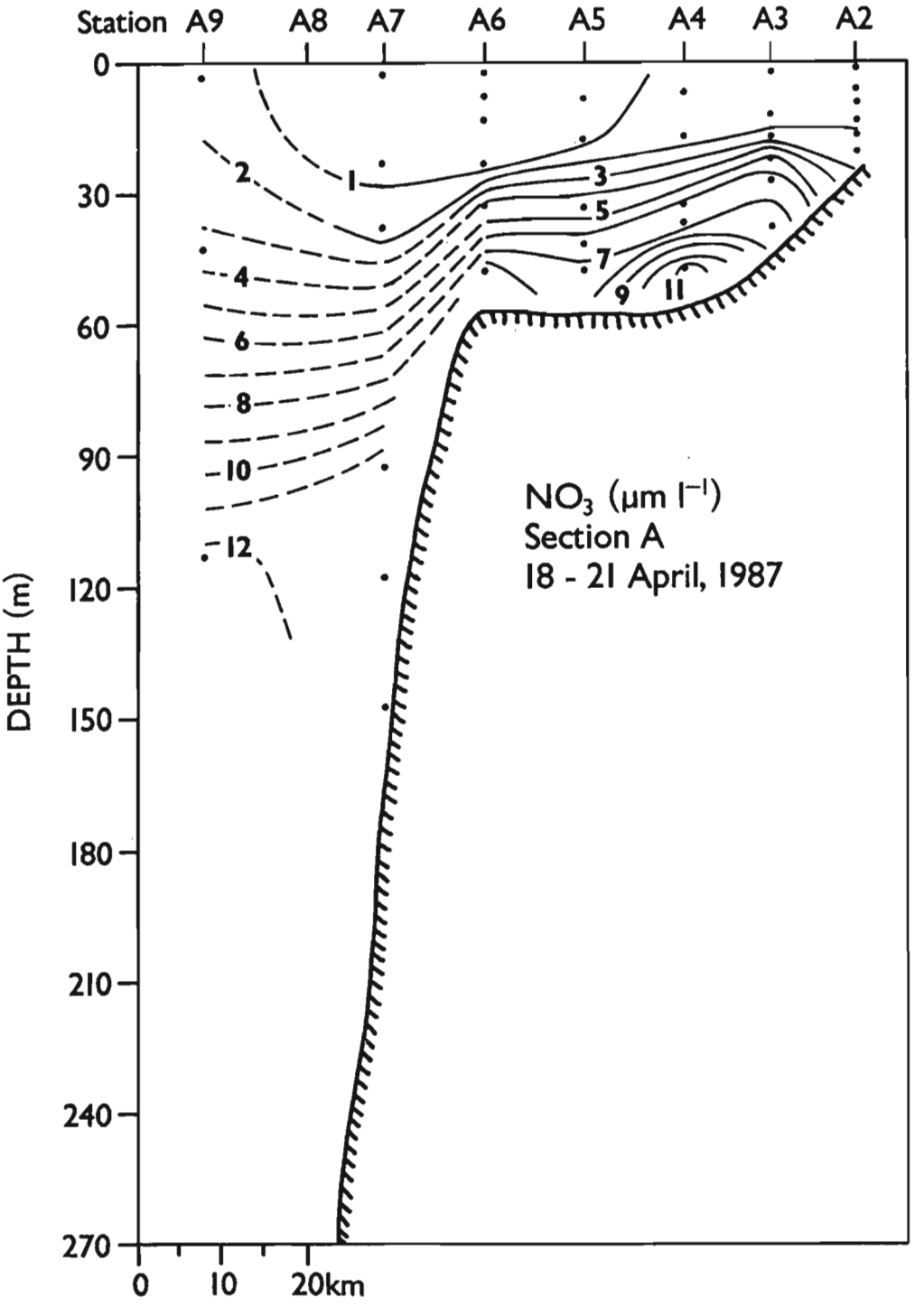

Figure 75. Nitrate at section A in April 1987.

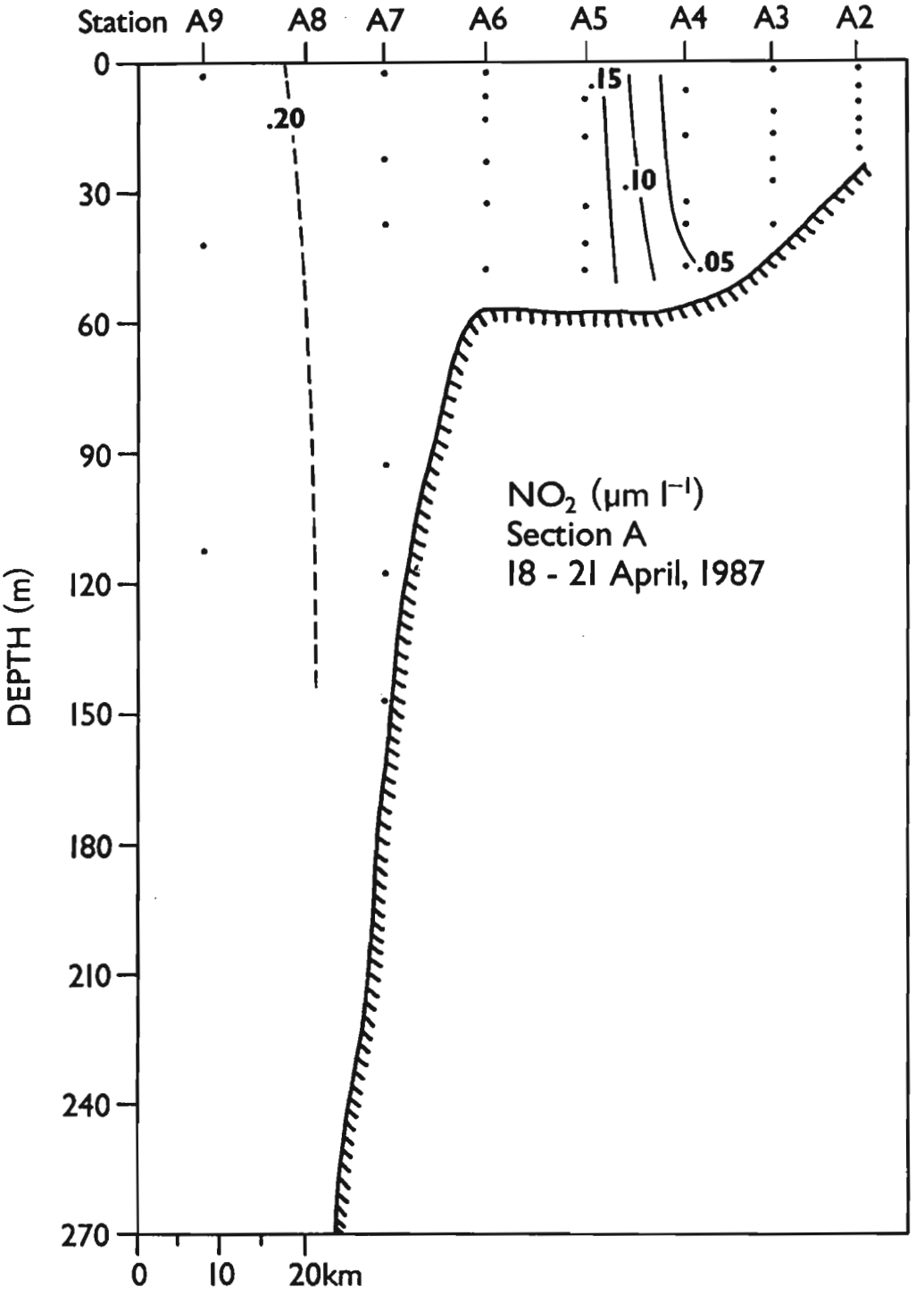

Figure 76. Nitrite at section A in April 1987.

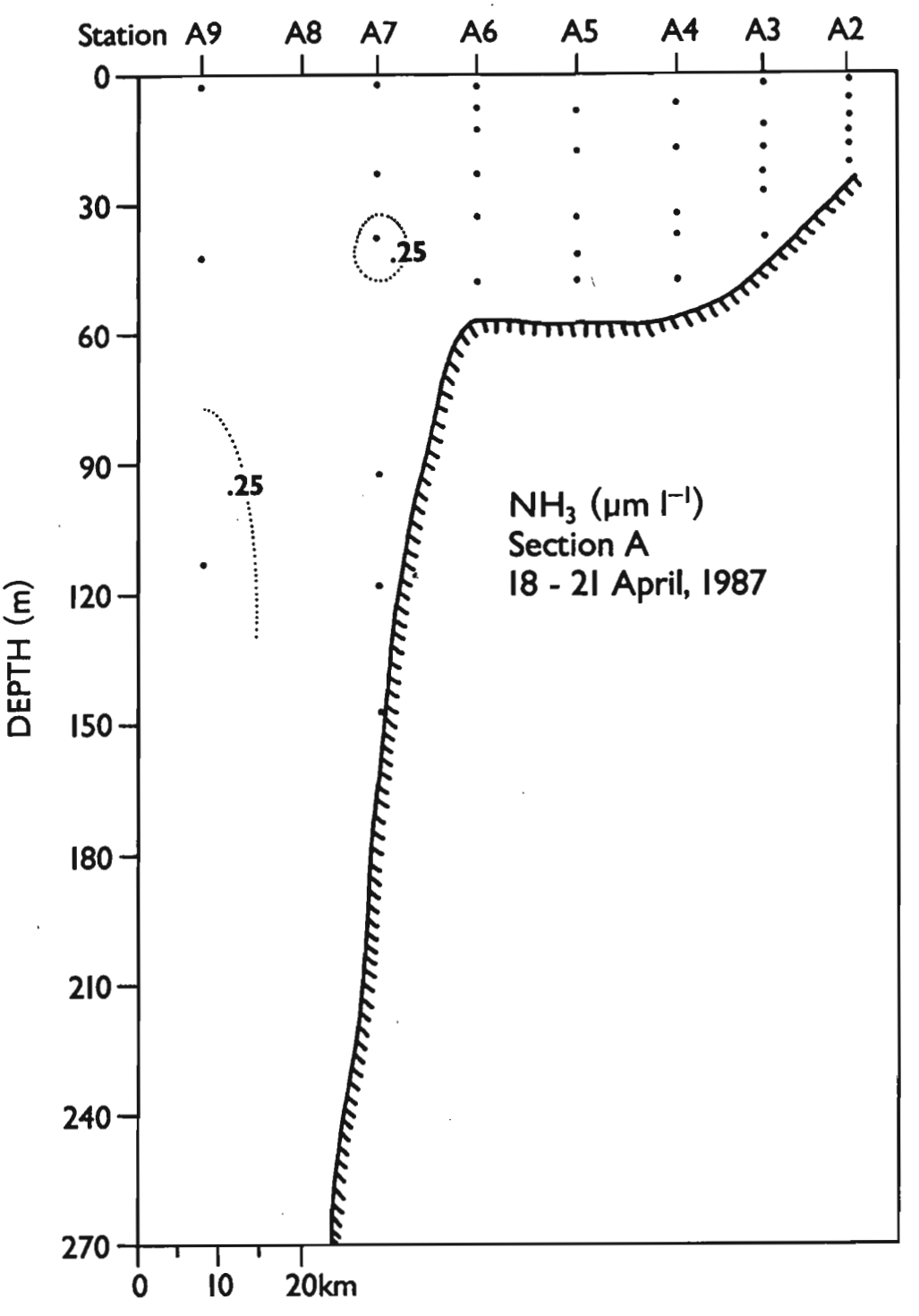

Figure 77. Ammonia at section A in April 1987.

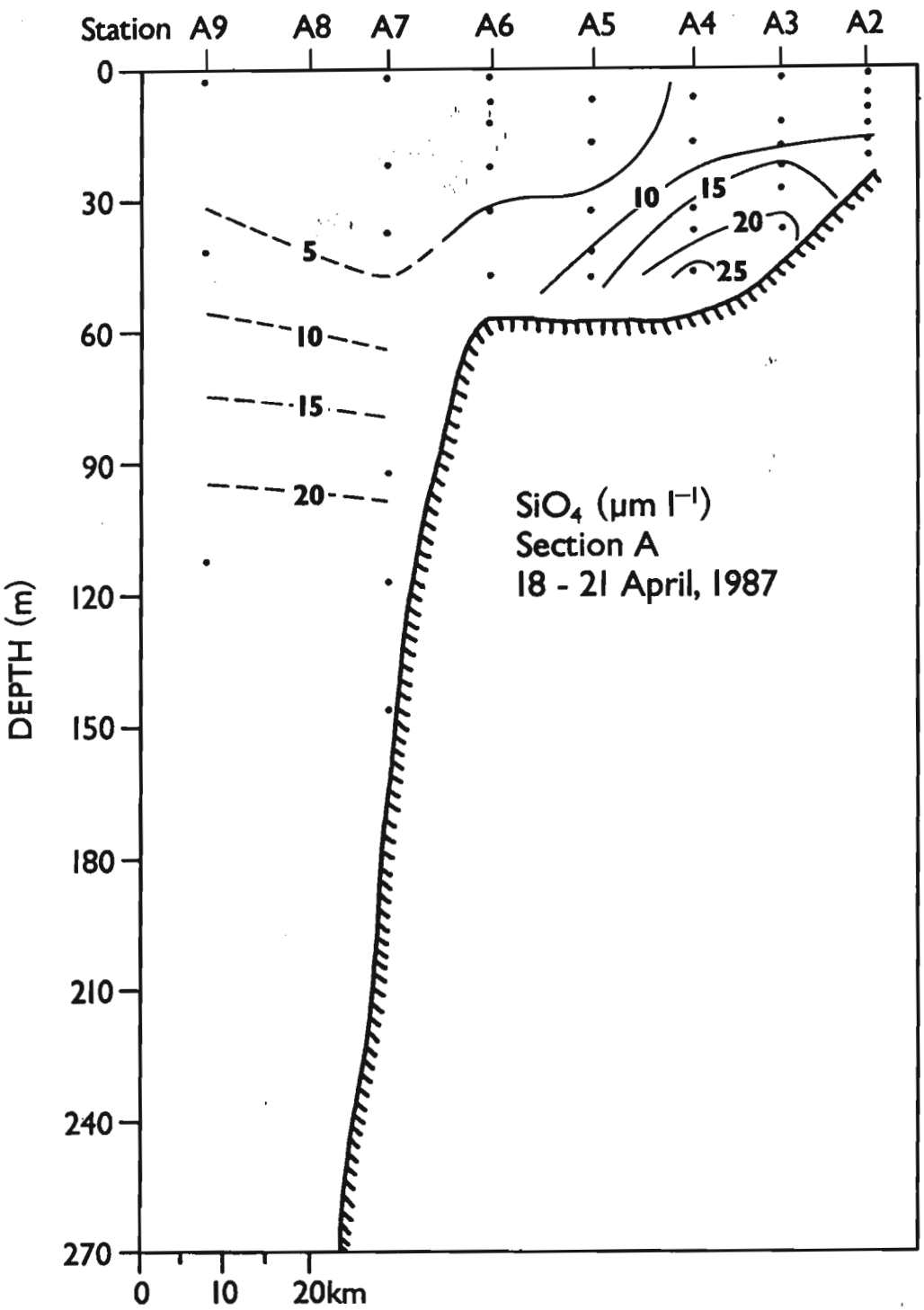

Figure 78. Silicate at section A in April 1987.

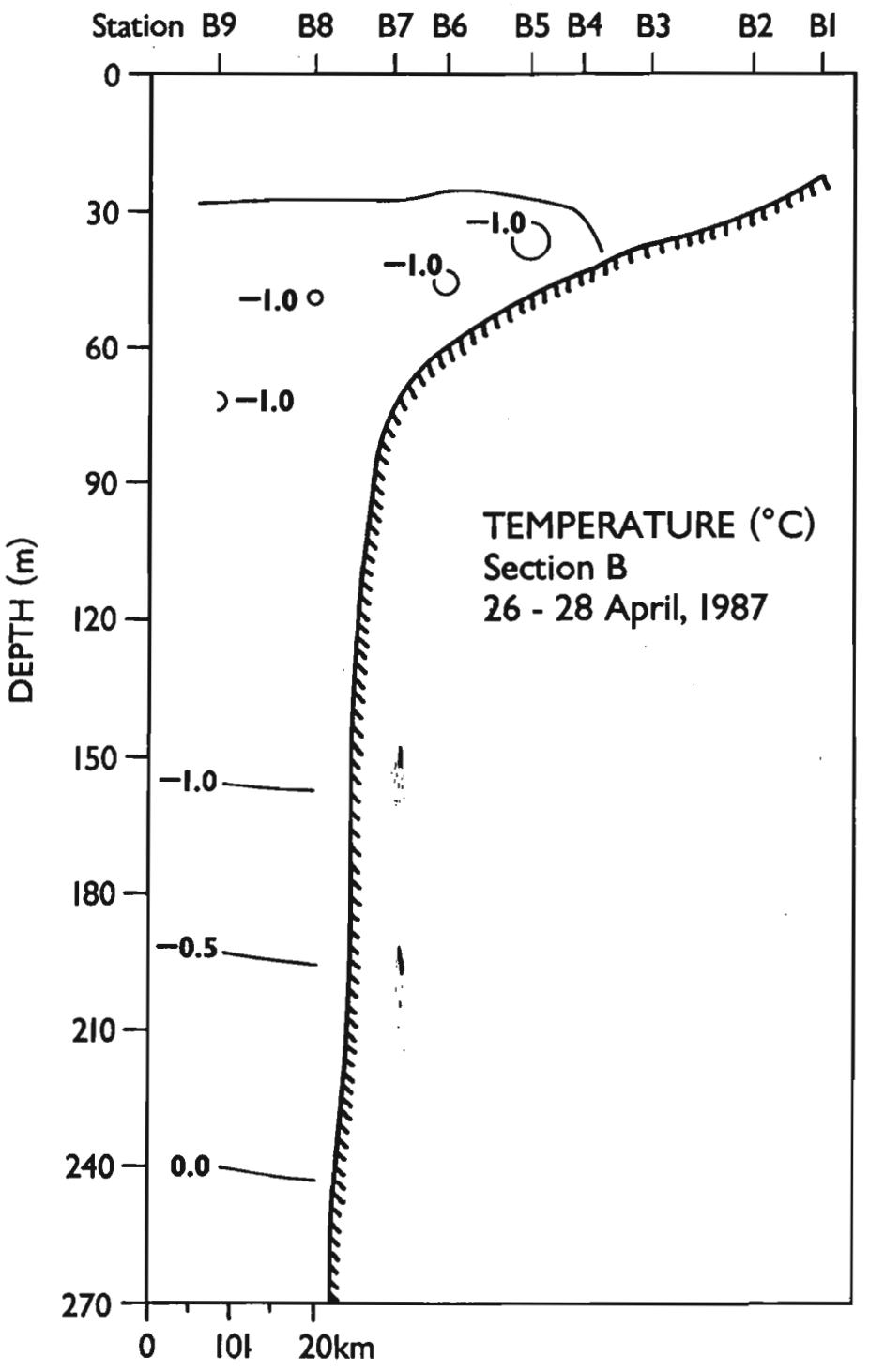

Figure 79. Temperature at section B in April 1987.

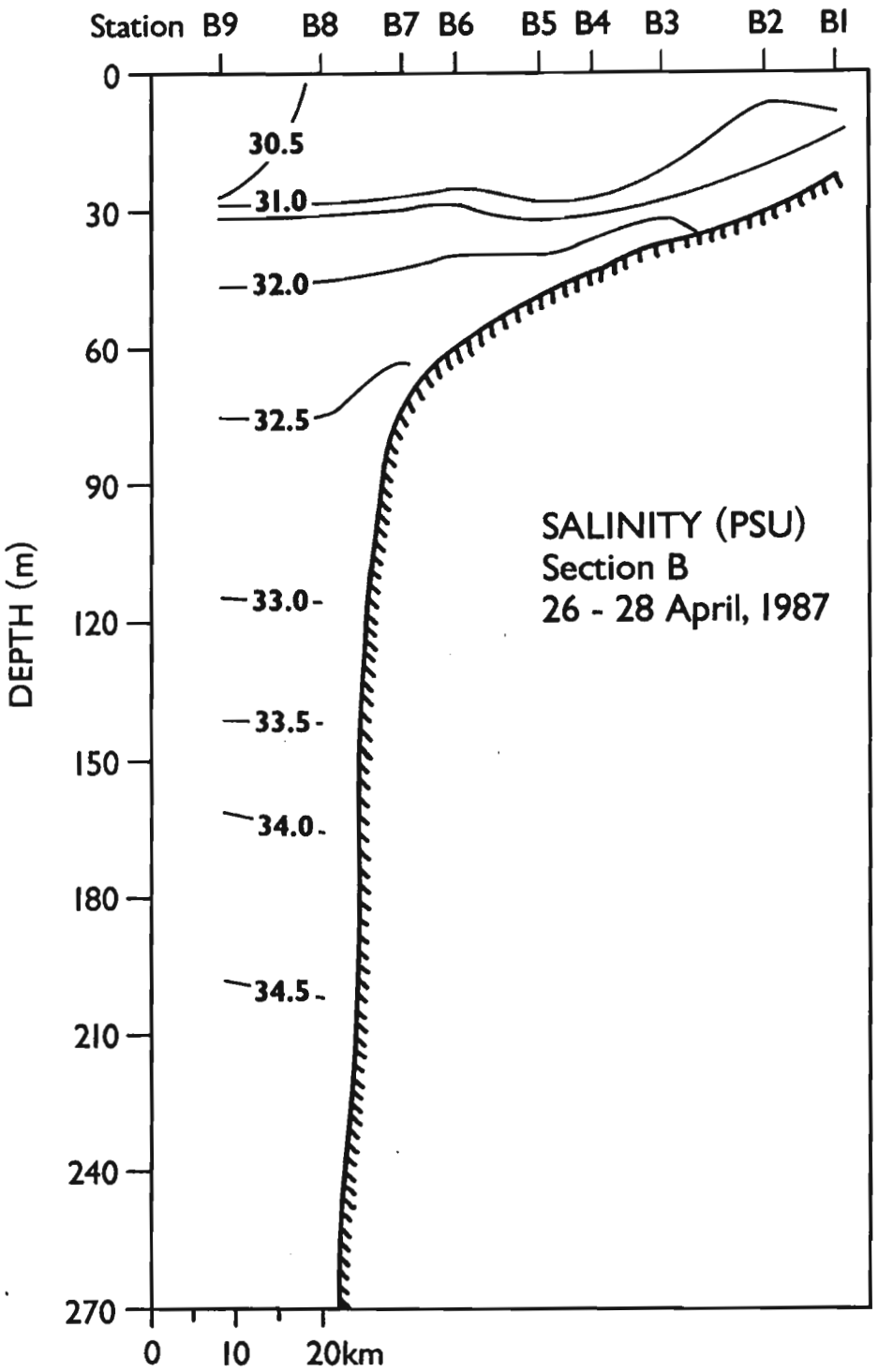

Figure 80. Salinity at section B in April 1987.

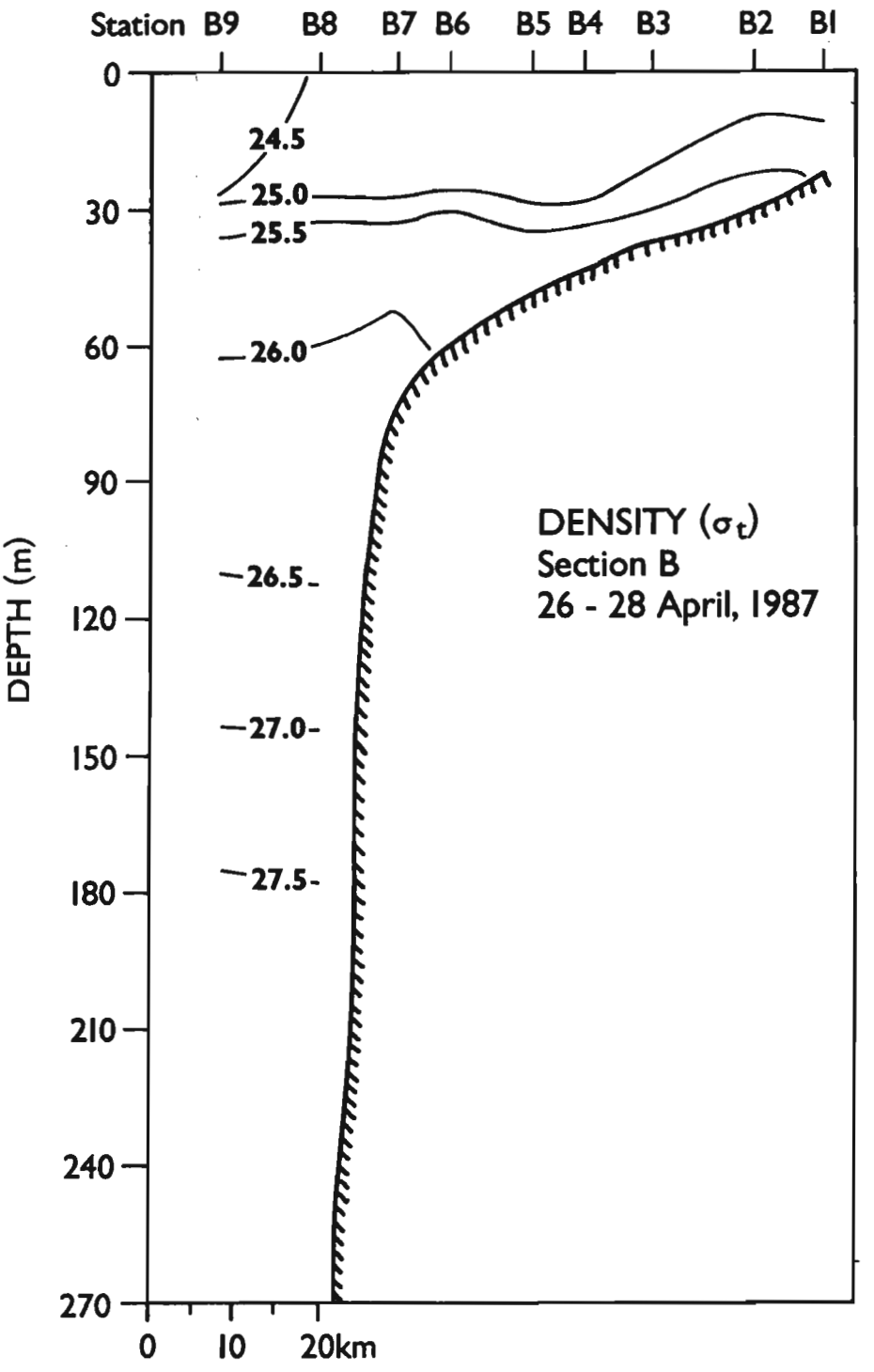

Figure 81. Density at section B in April 1987.

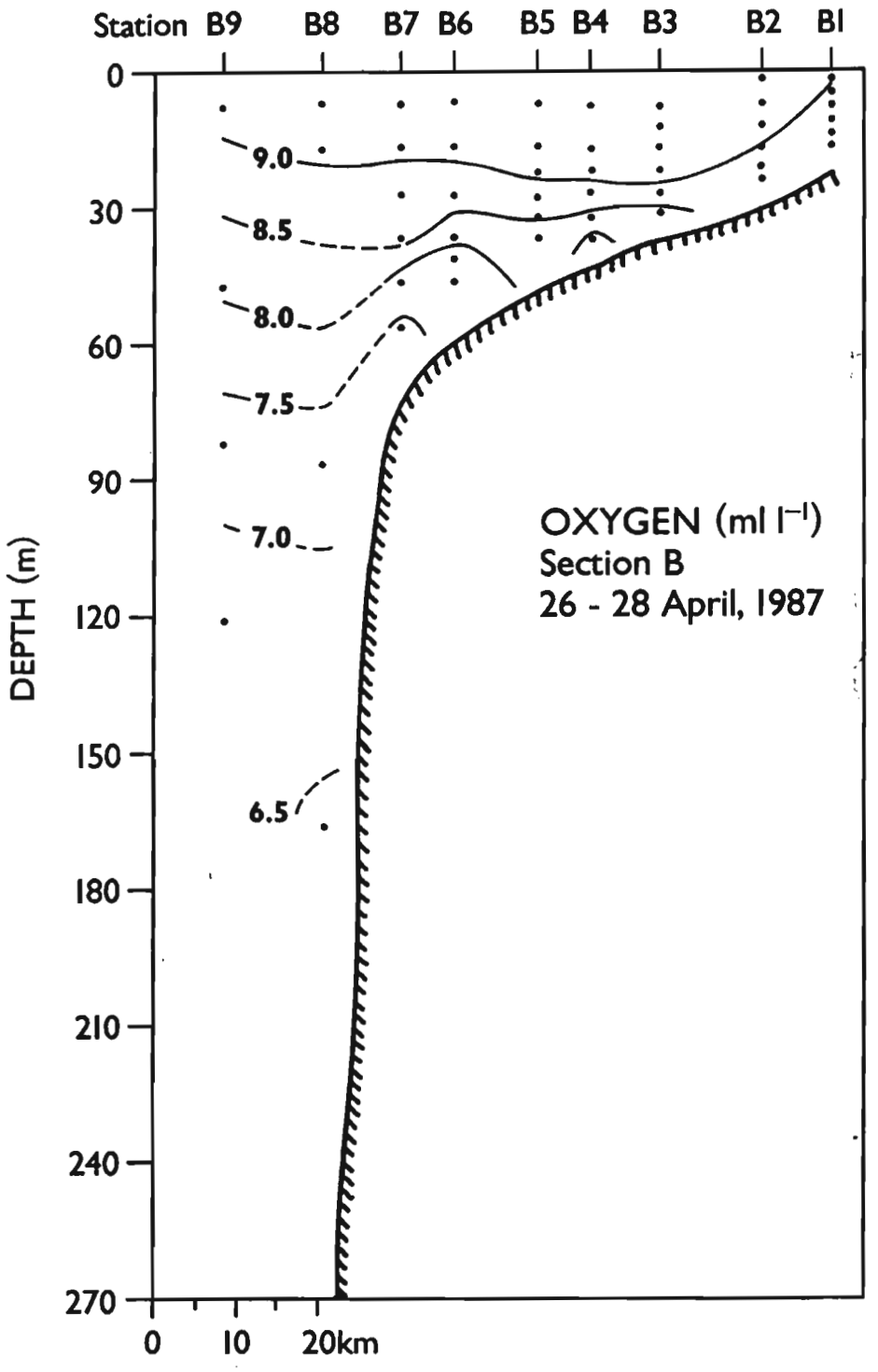

Figure 82. Dissolved oxygen at section B in April 1987.

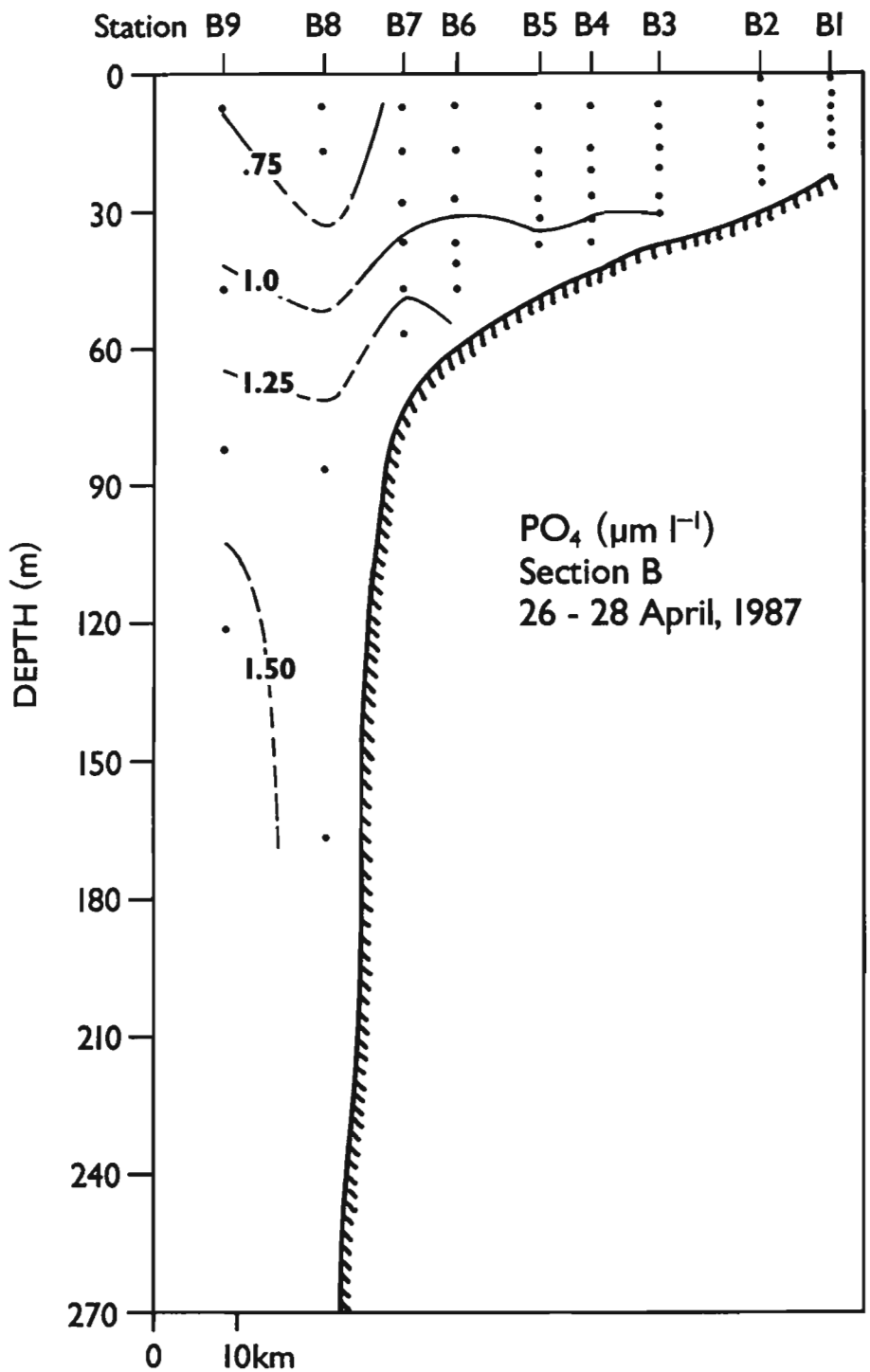

Figure 83. Phosphate at section B in April 1987.

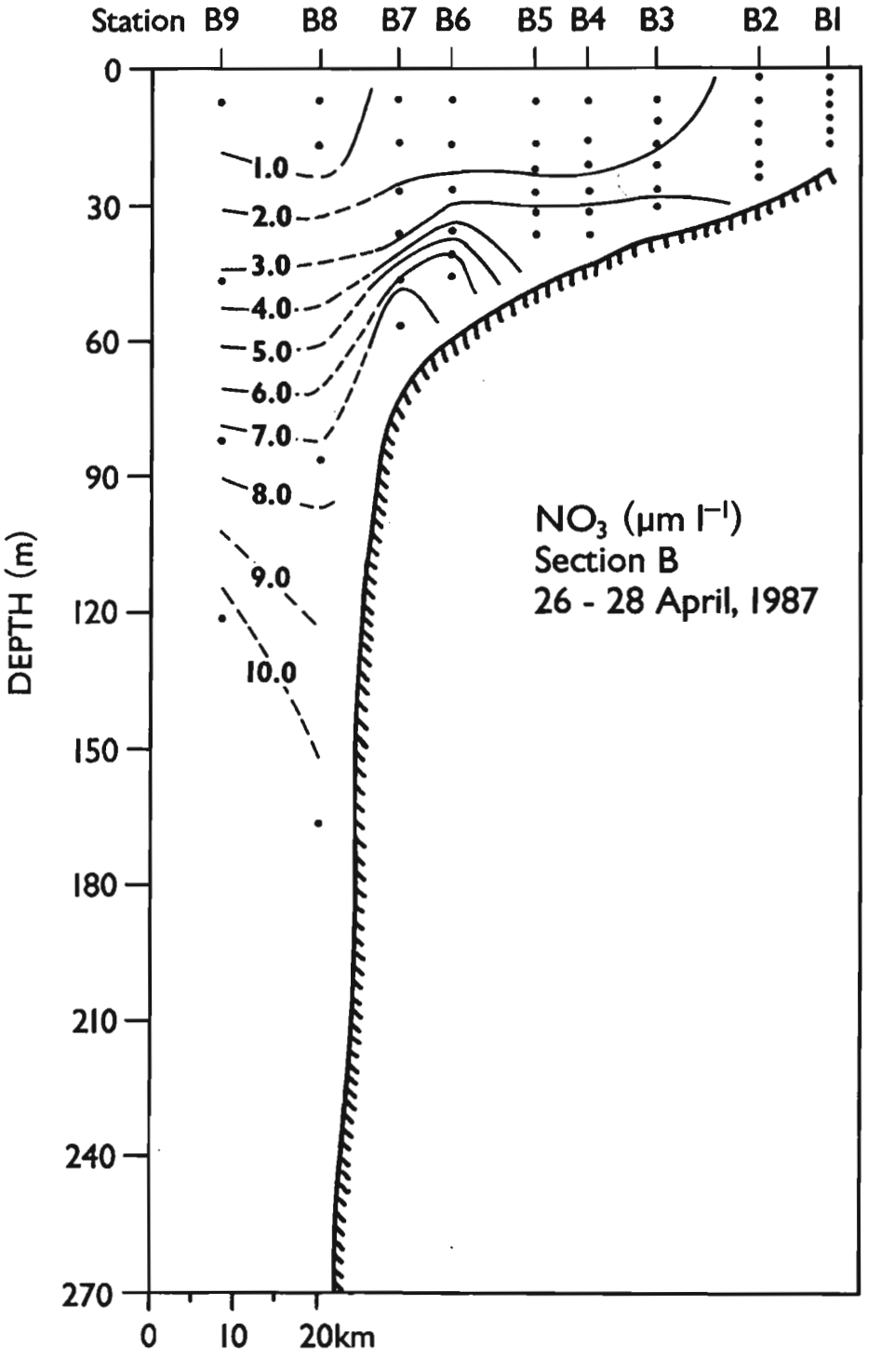

Figure 84. Nitrate at section B in April 1987.

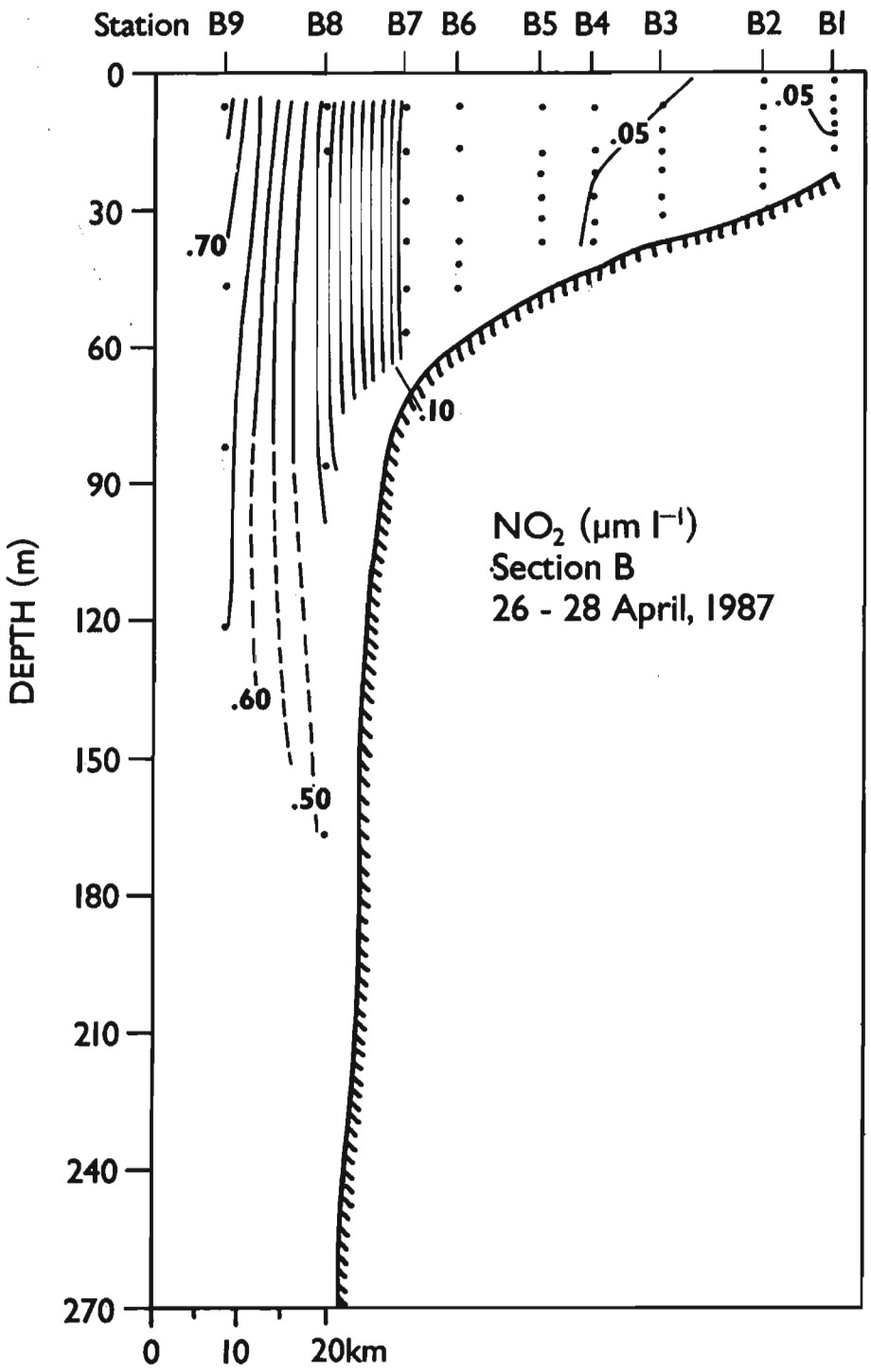

Figure 85. Nitrite at section B in April 1987.

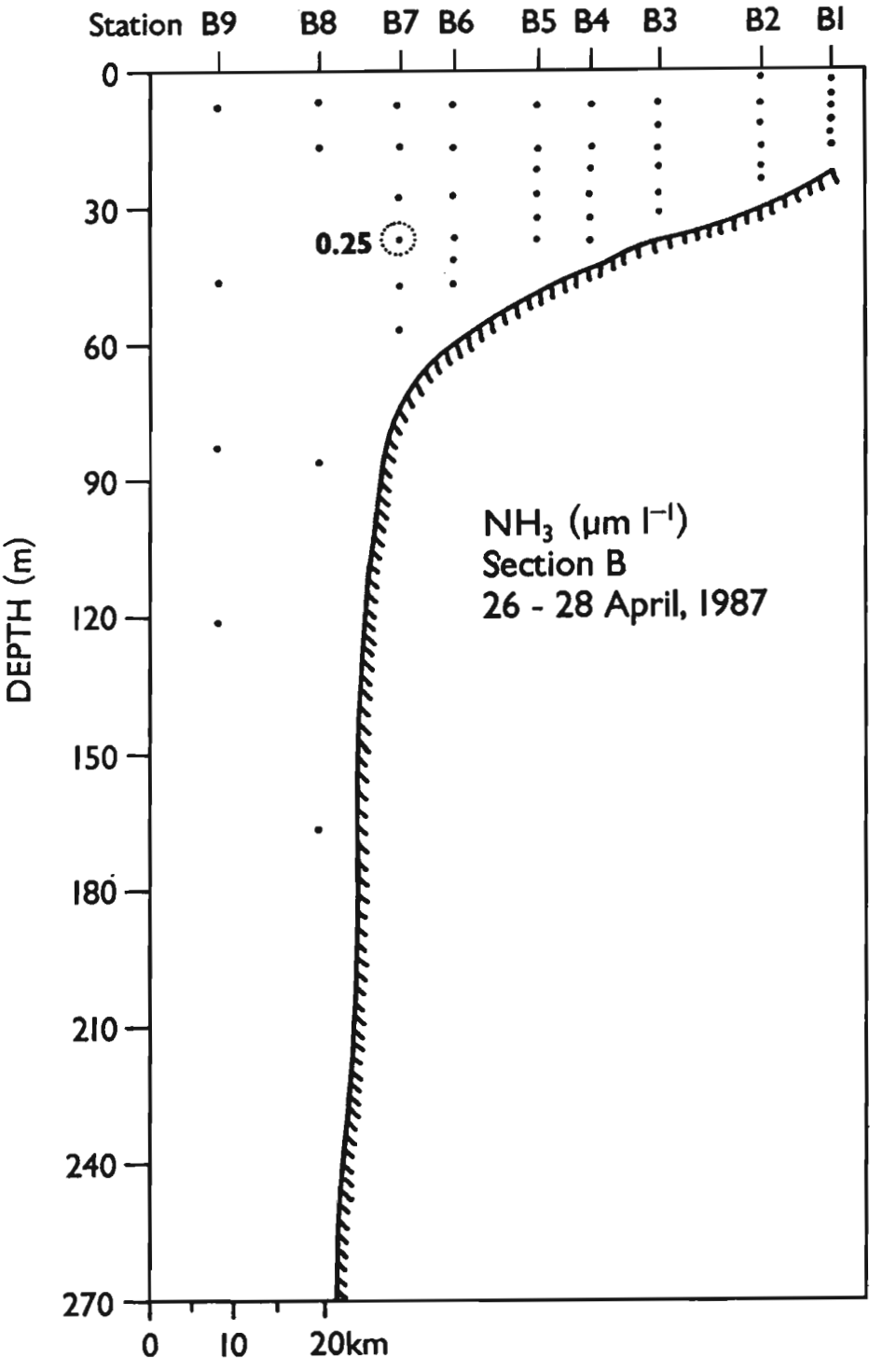

Figure 86. Ammonia at section B in April 1987.

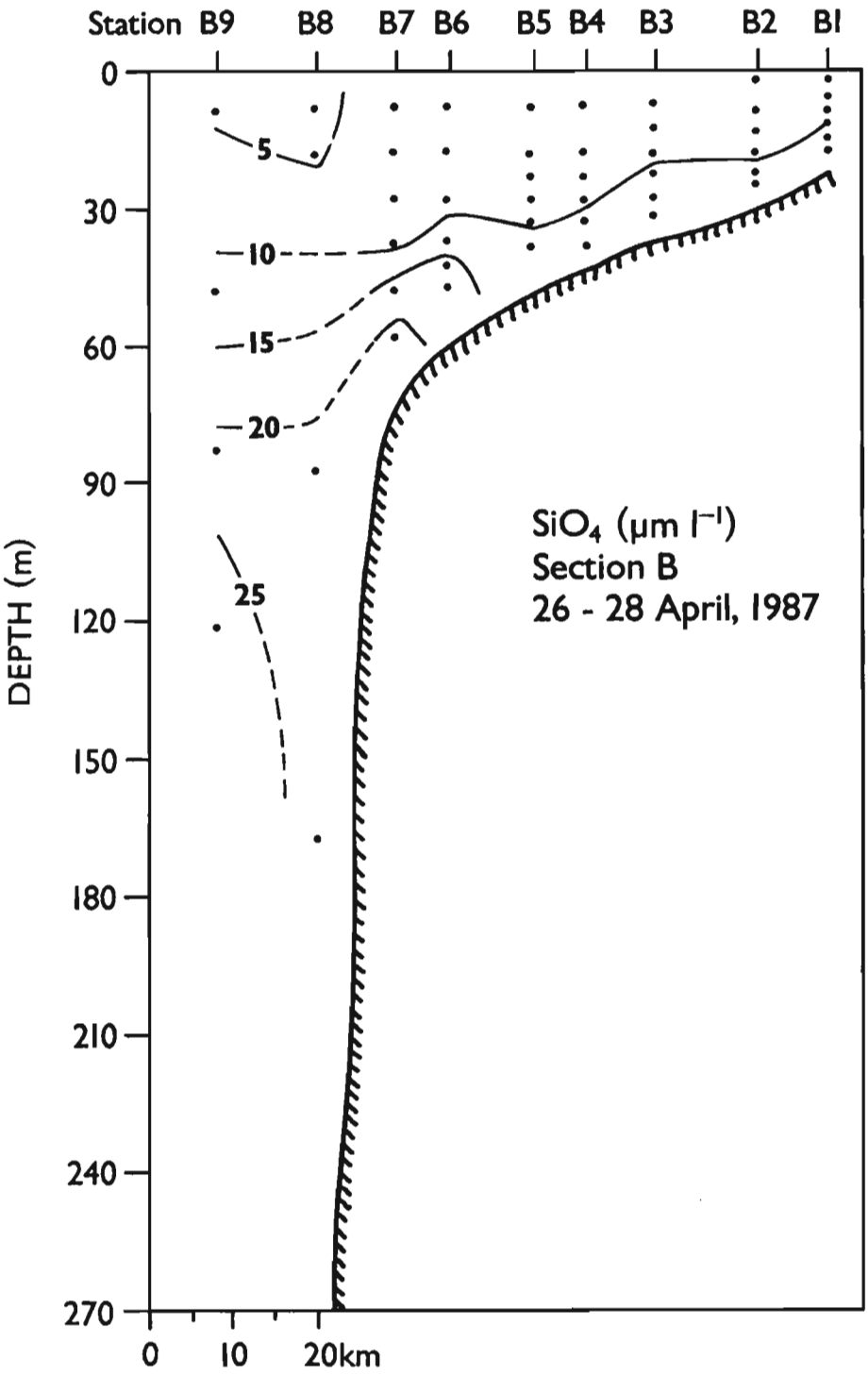

Figure 87. Silicate at section B in April 1987.

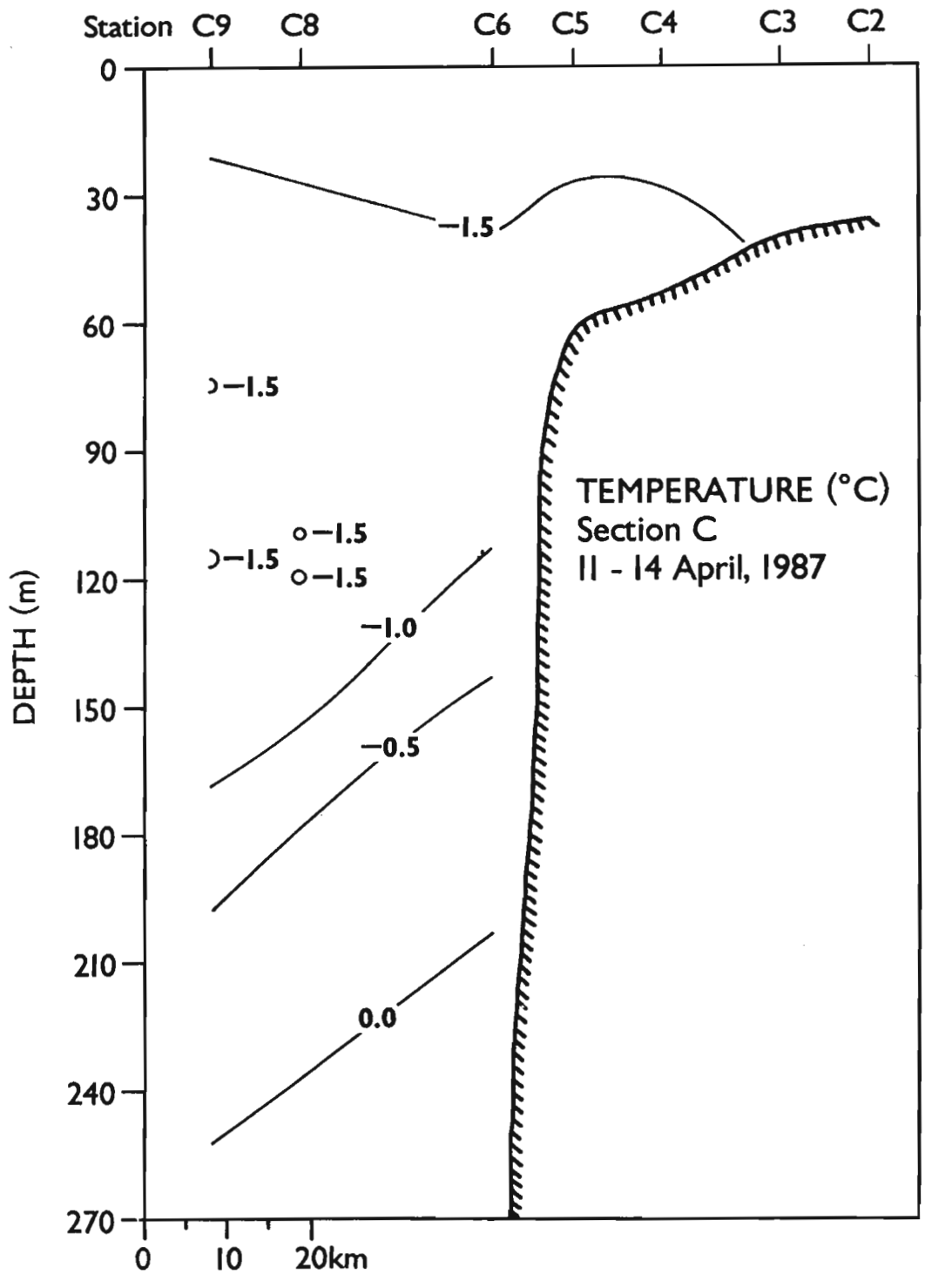

Figure 88. Temperature at section C in April 1987.

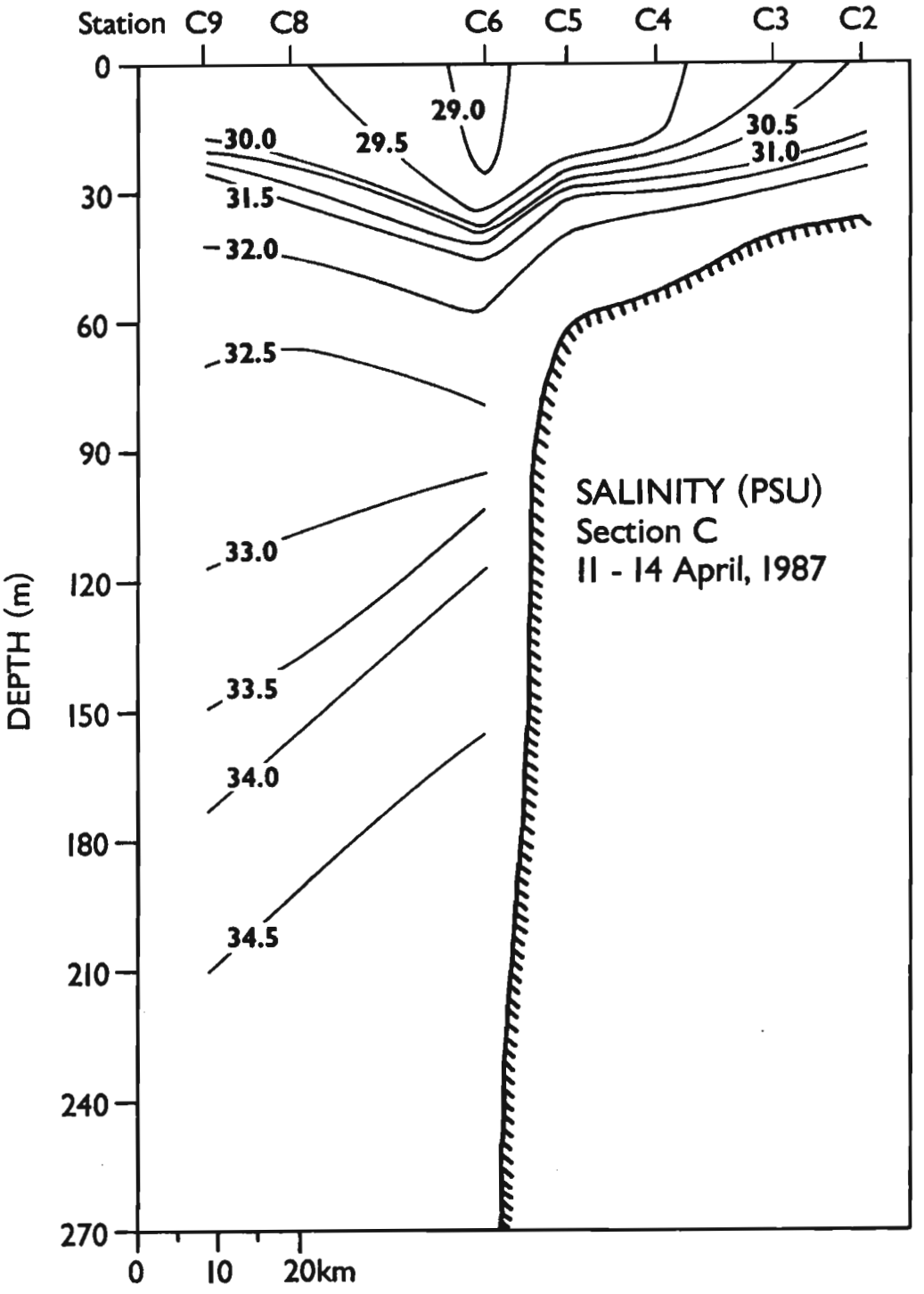

Figure 89. Salinity at section C in April 1987.

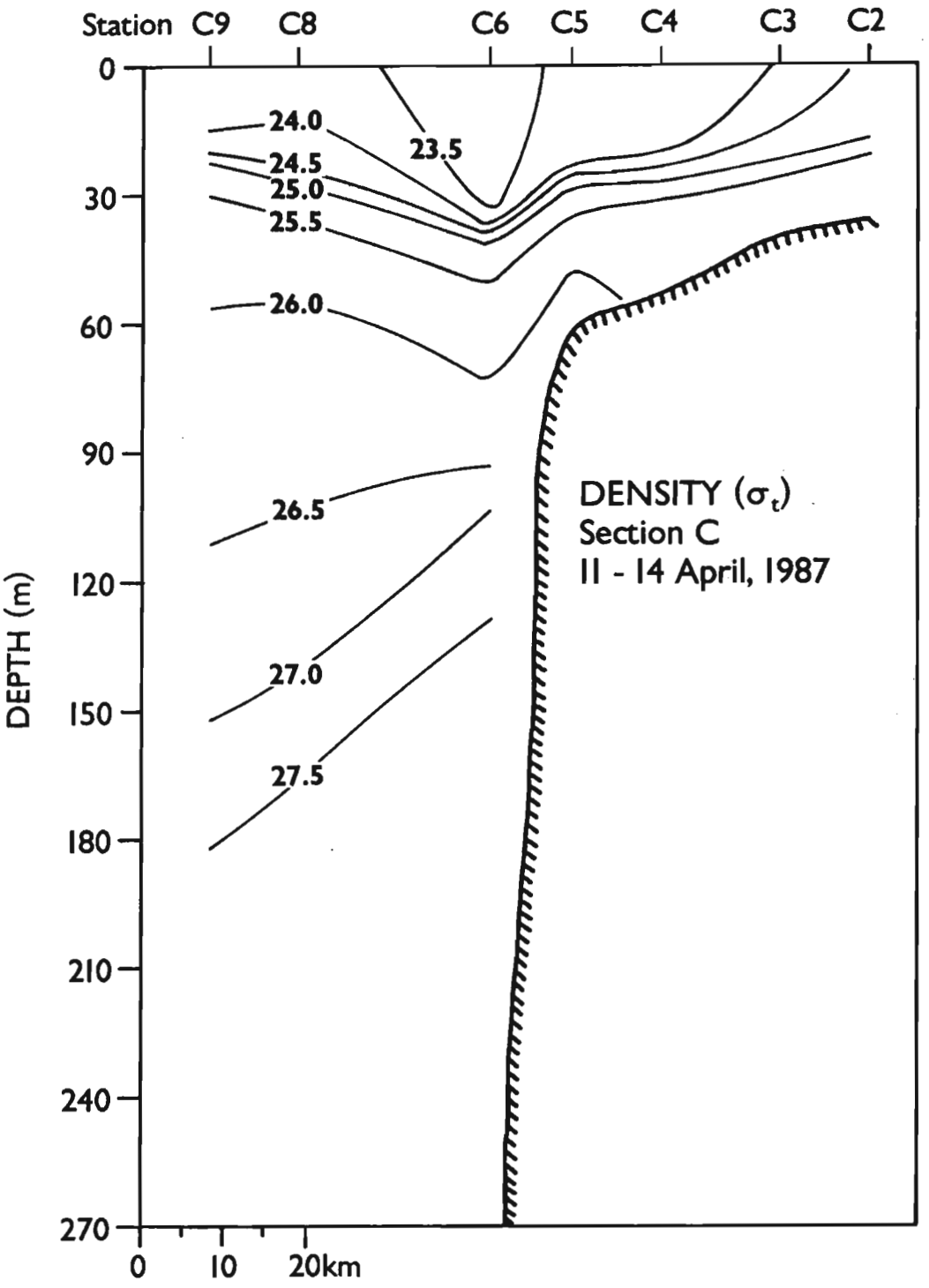

Figure 90. Density at section C in April 1987.

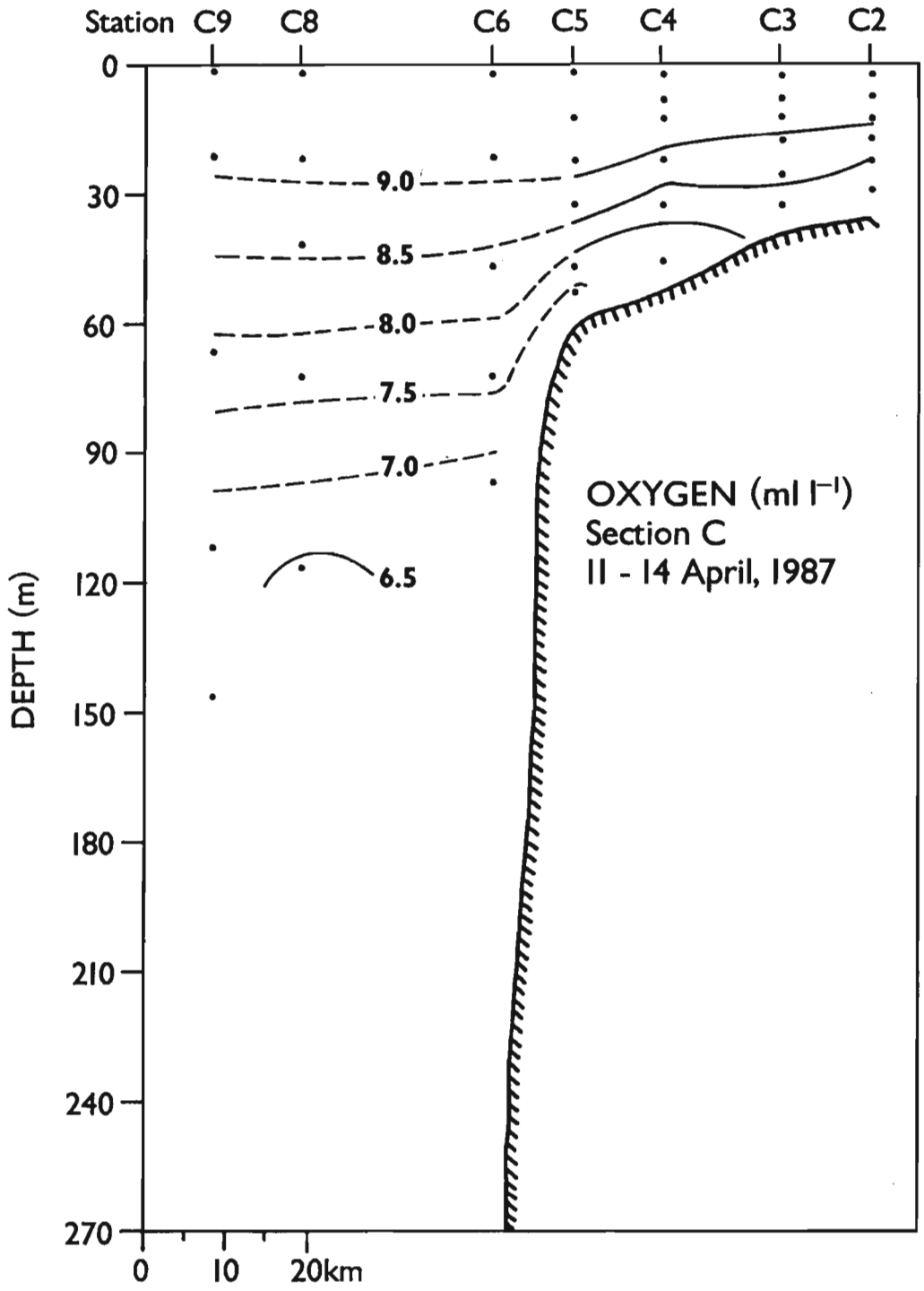

Figure 91. Dissolved oxygen at section C in April 1987.

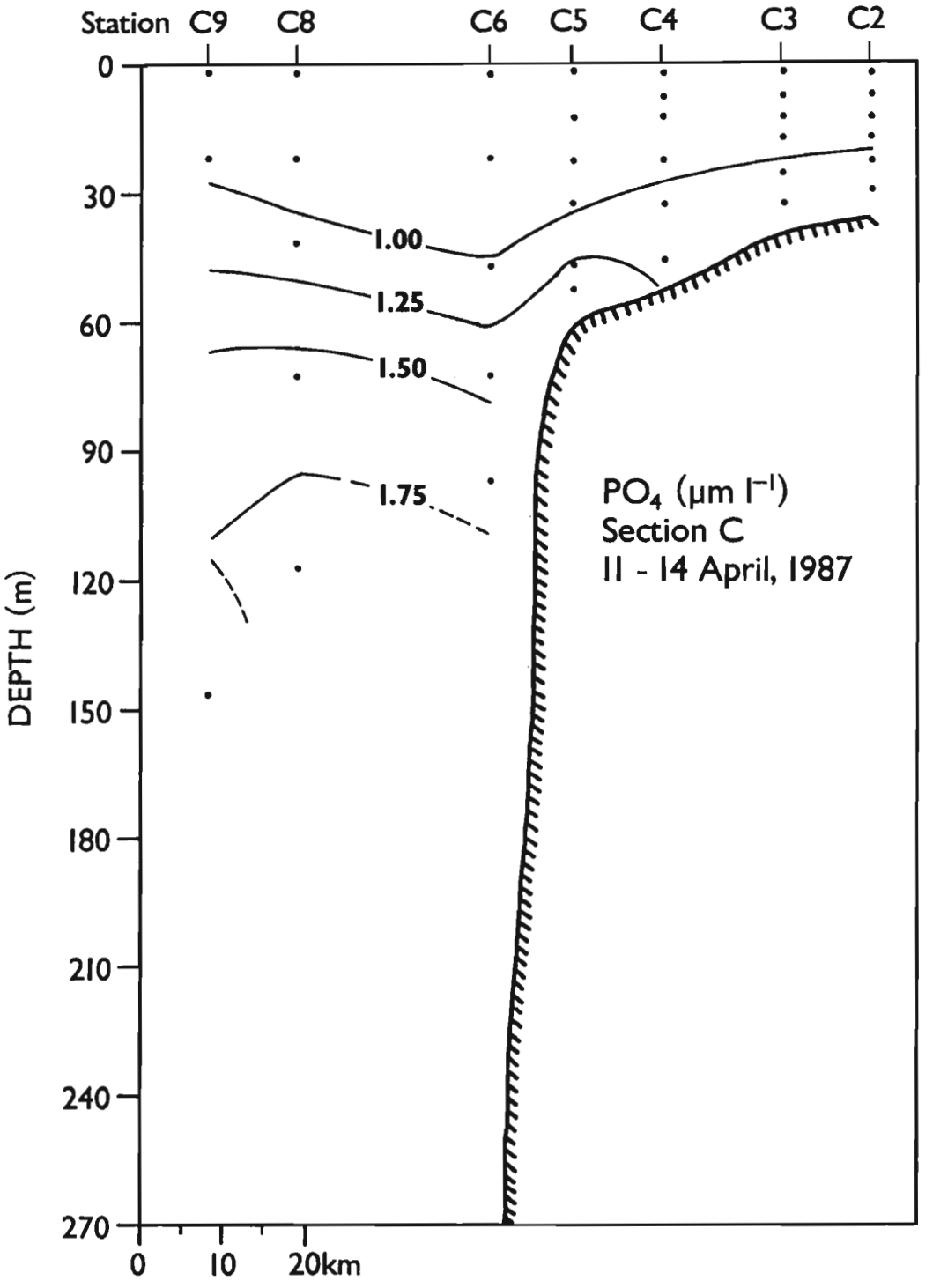

Figure 92. Phosphate at section C in April 1987.

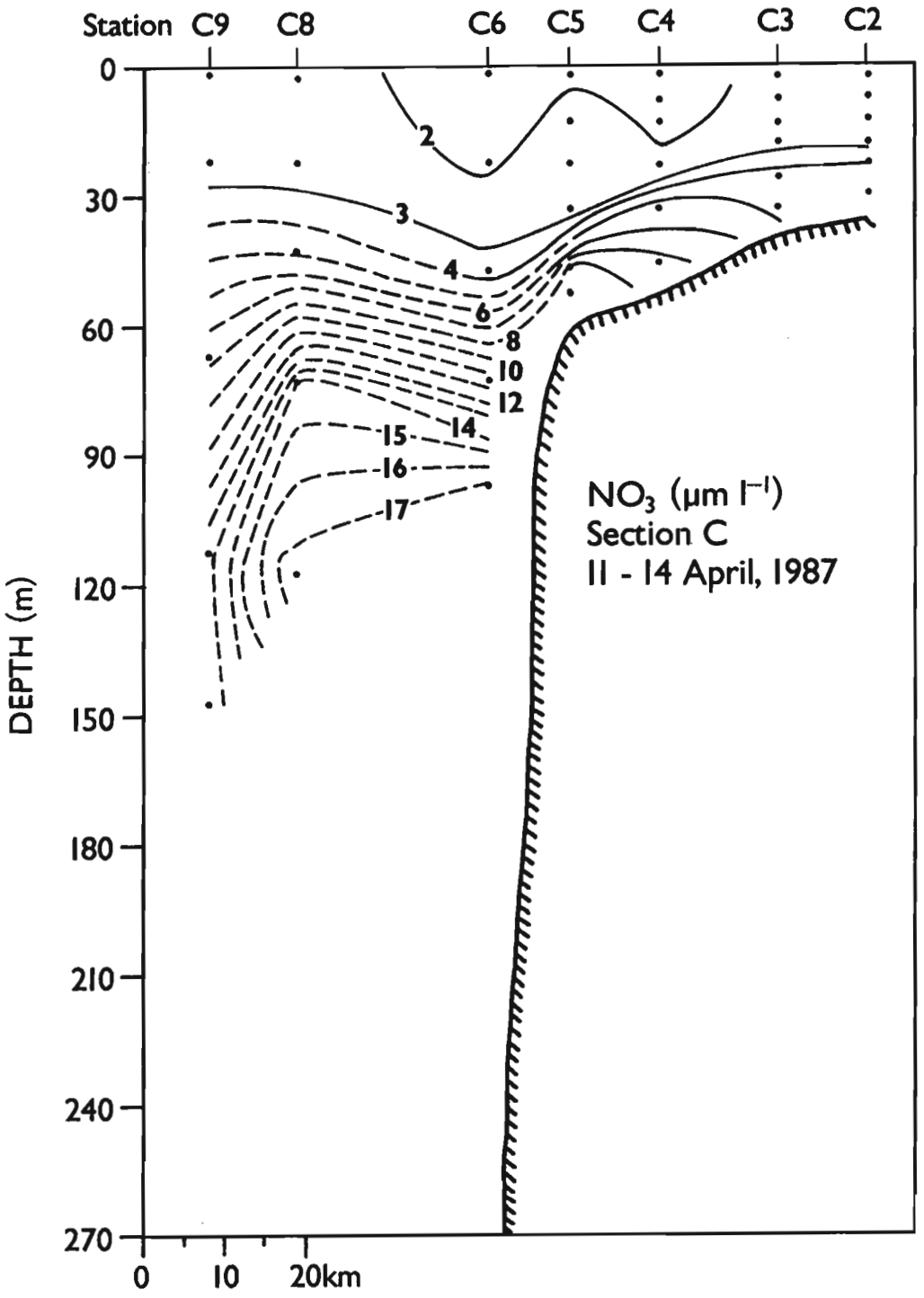

Figure 93. Nitrate at section C in April 1987.

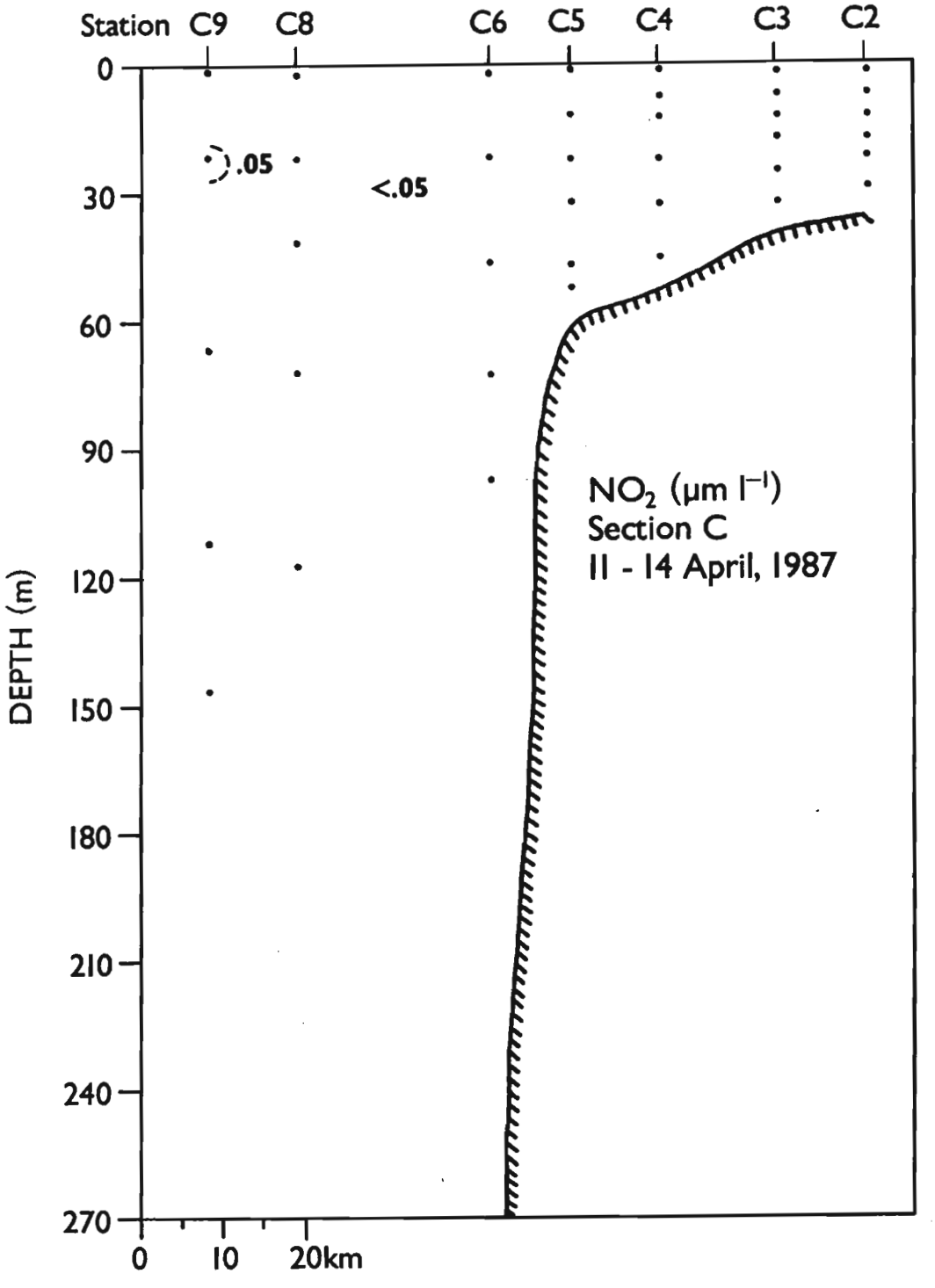

Figure 94. Nitrite at section C in April 1987.

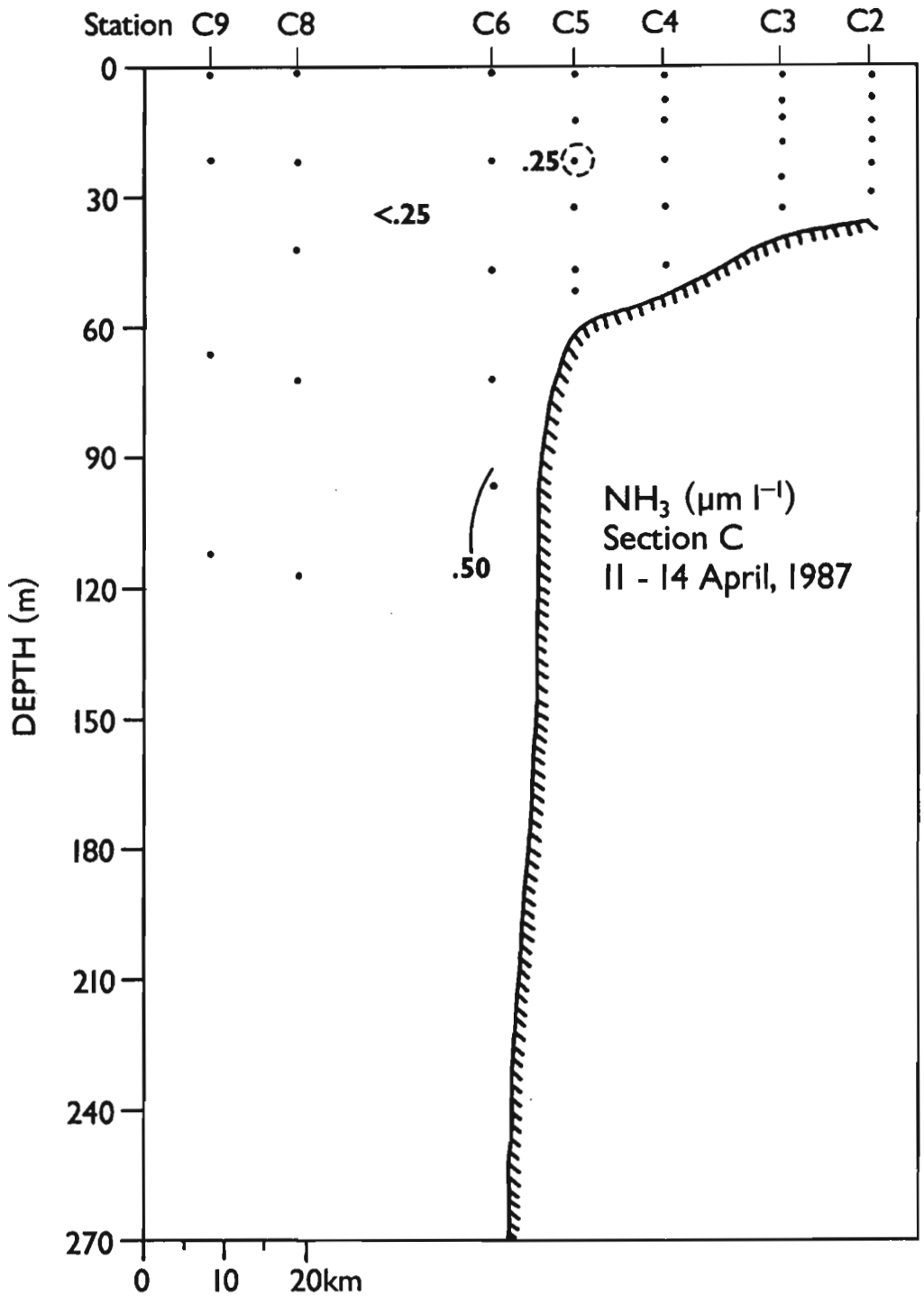

Figure 95. Ammonia at section C in April 1987.

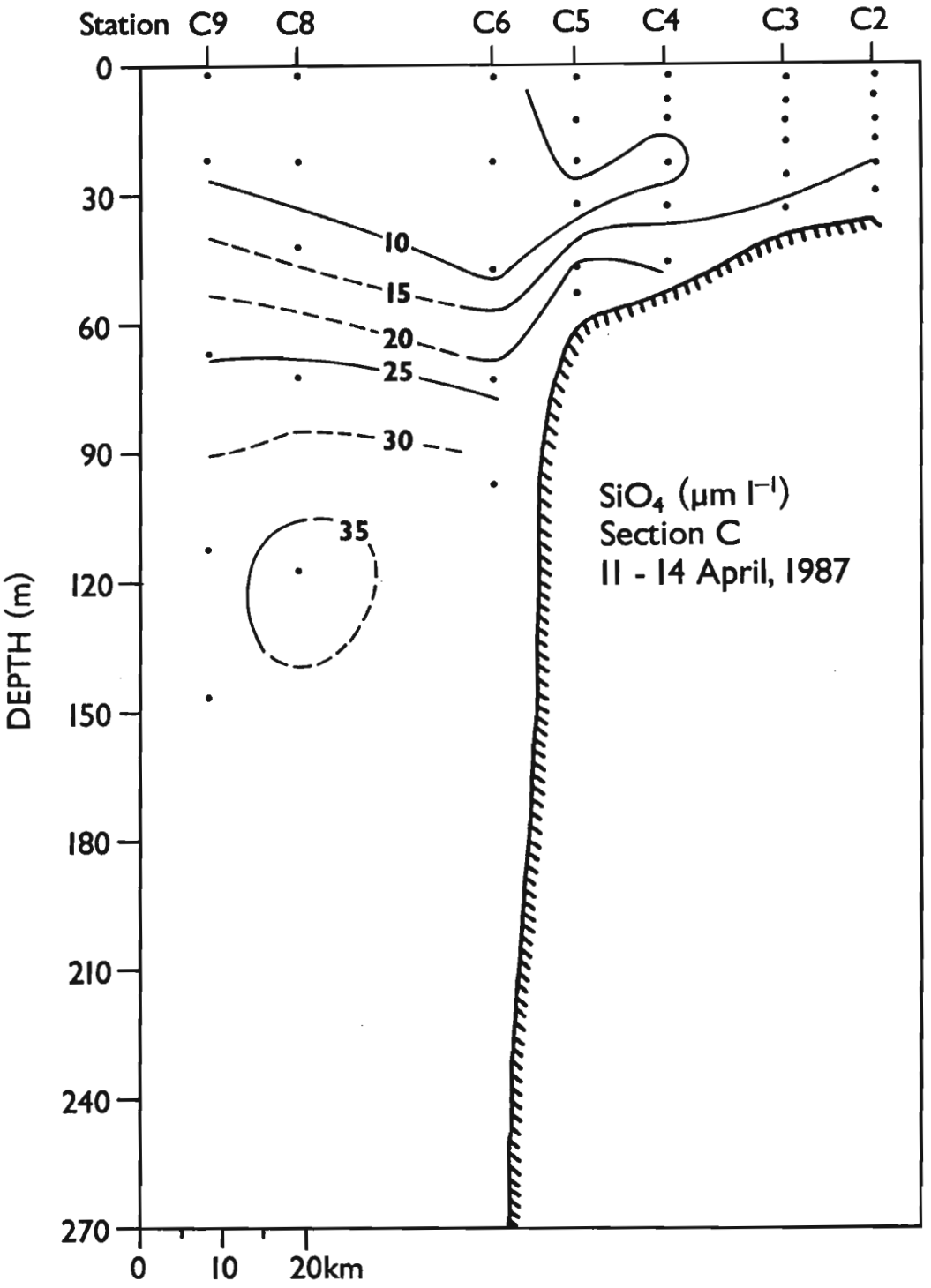

Figure 96. Silicate at section C in April 1987.

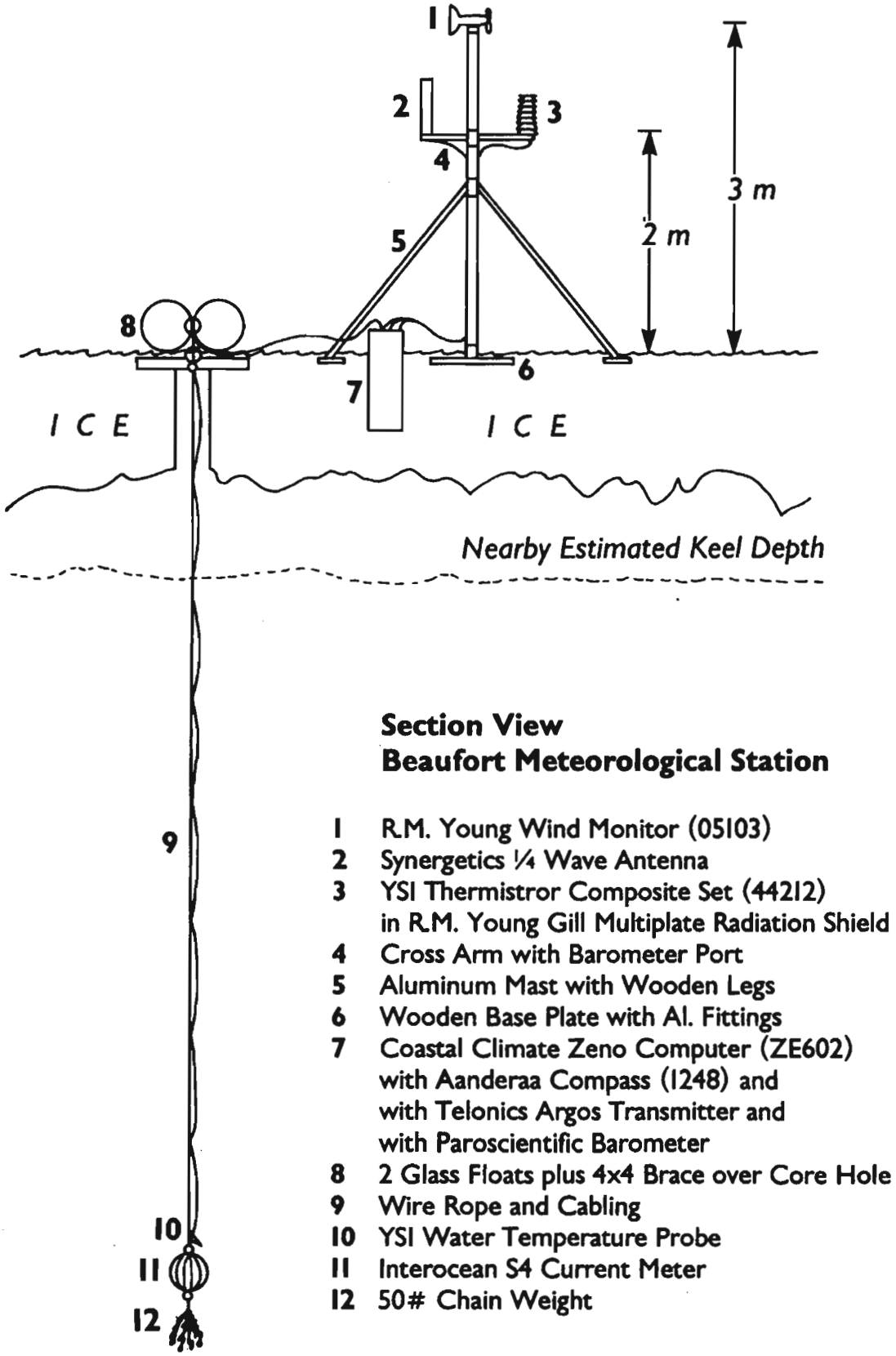

Figure 97. Section view of an ARGOS station.

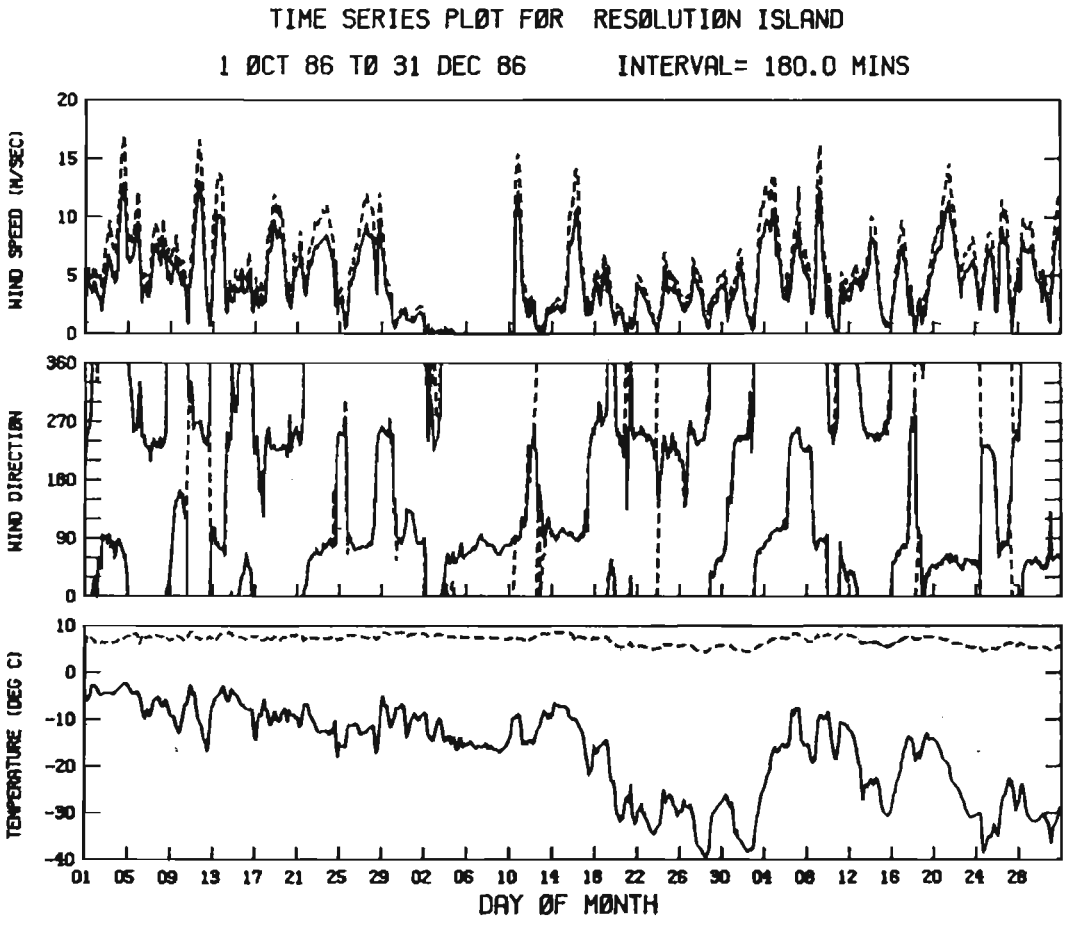

Figure 98. Air temperature and wind speed and direction from Resolution Island (Prudhoe Bay) for October-December 1986.

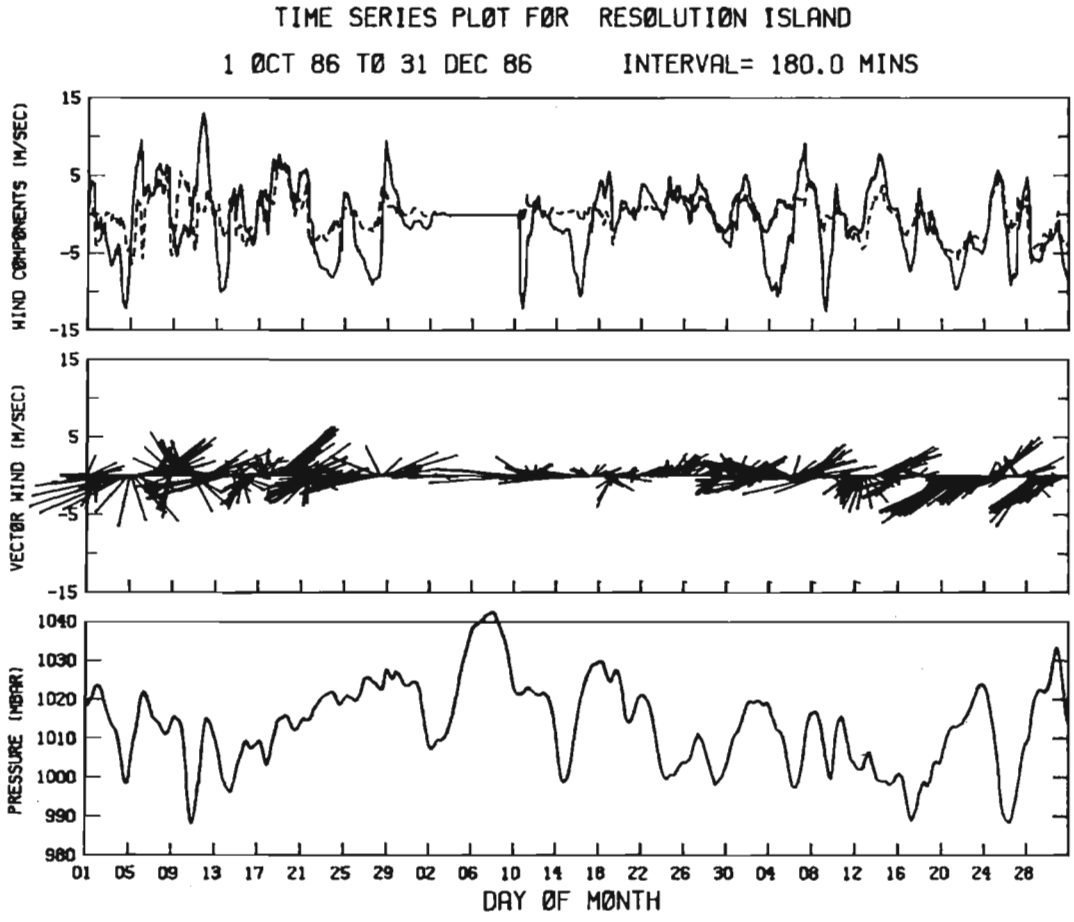

Figure 99. Sea-level pressure, wind components and vectors from Resolution Island (Prudhoe Bay) for October-December 1986.

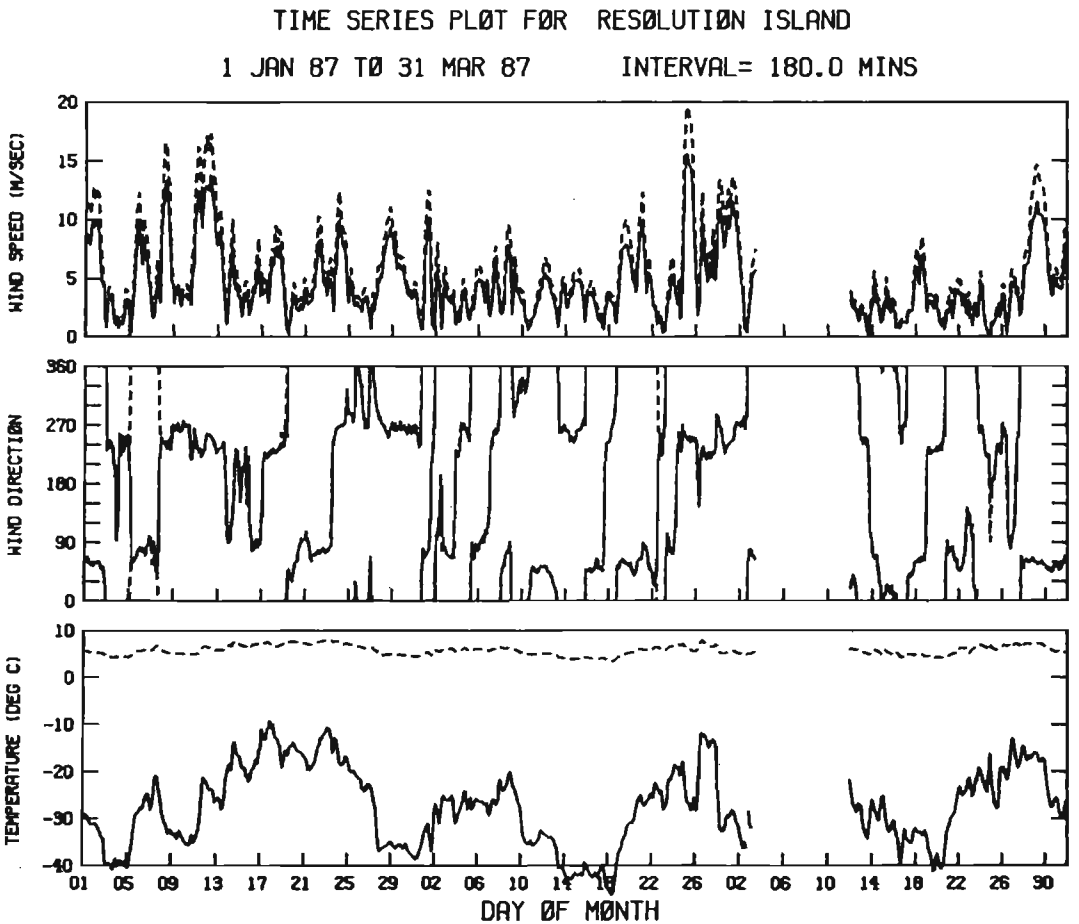

Figure 100. Air temperature and wind speed and direction from Resolution Island (Prudhoe Bay) for January-March 1987.

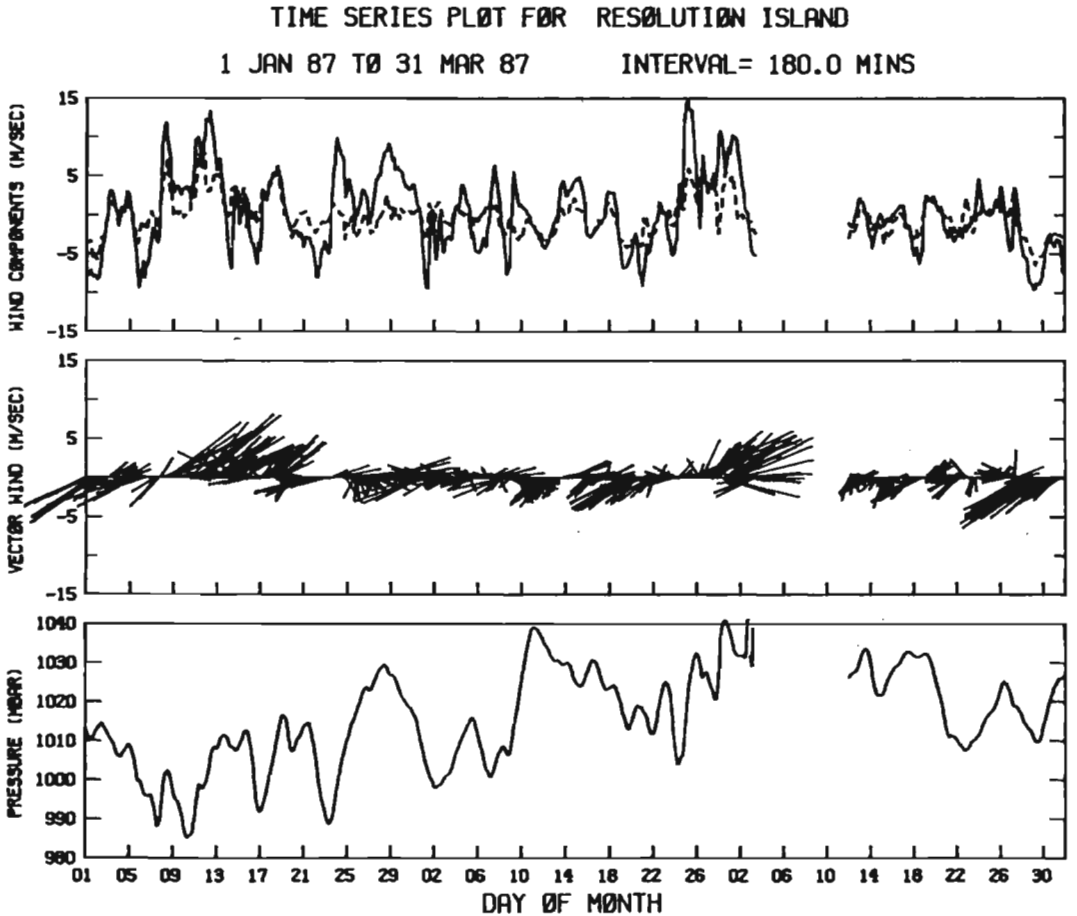

Figure 101. Sea-level pressure, wind components and vectors from Resolution Island (Prudhoe Bay) for January-March 1987.

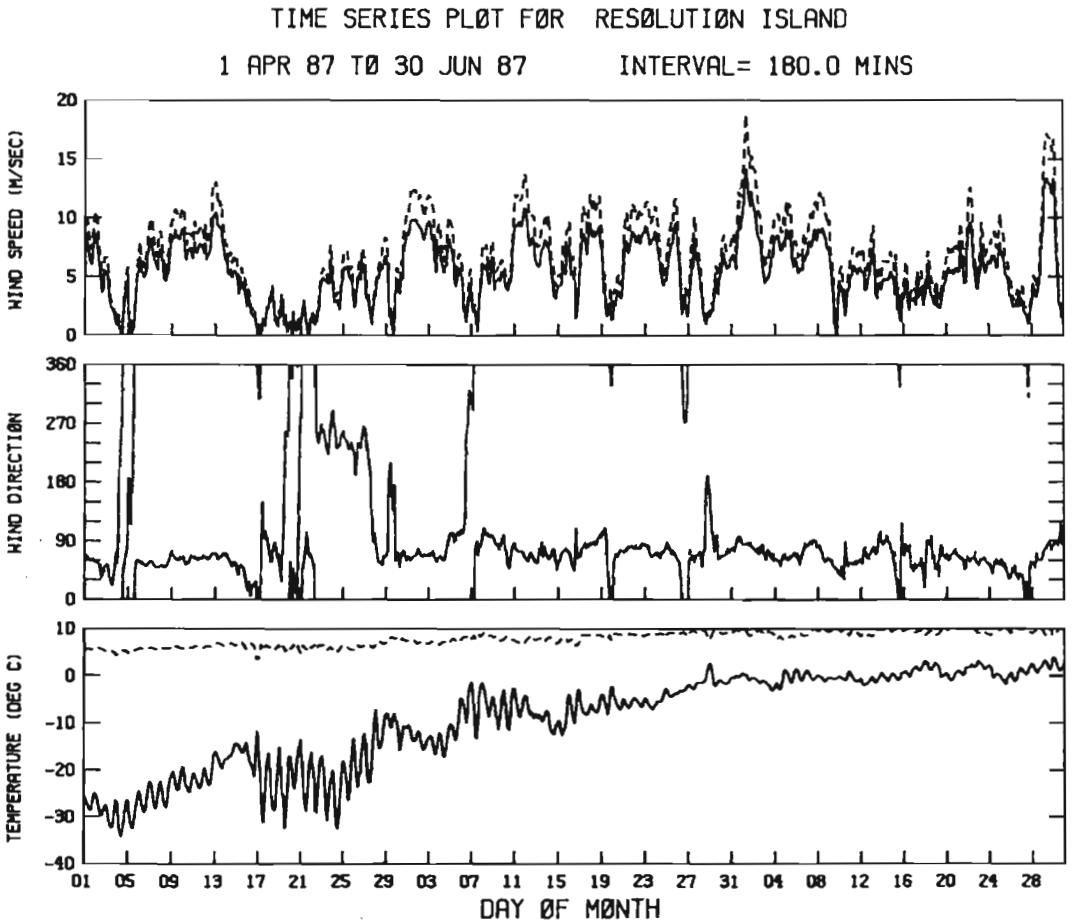

Figure 102. Air temperature and wind speed and direction from Resolution Island (Prudhoe Bay) for April-June 1987.

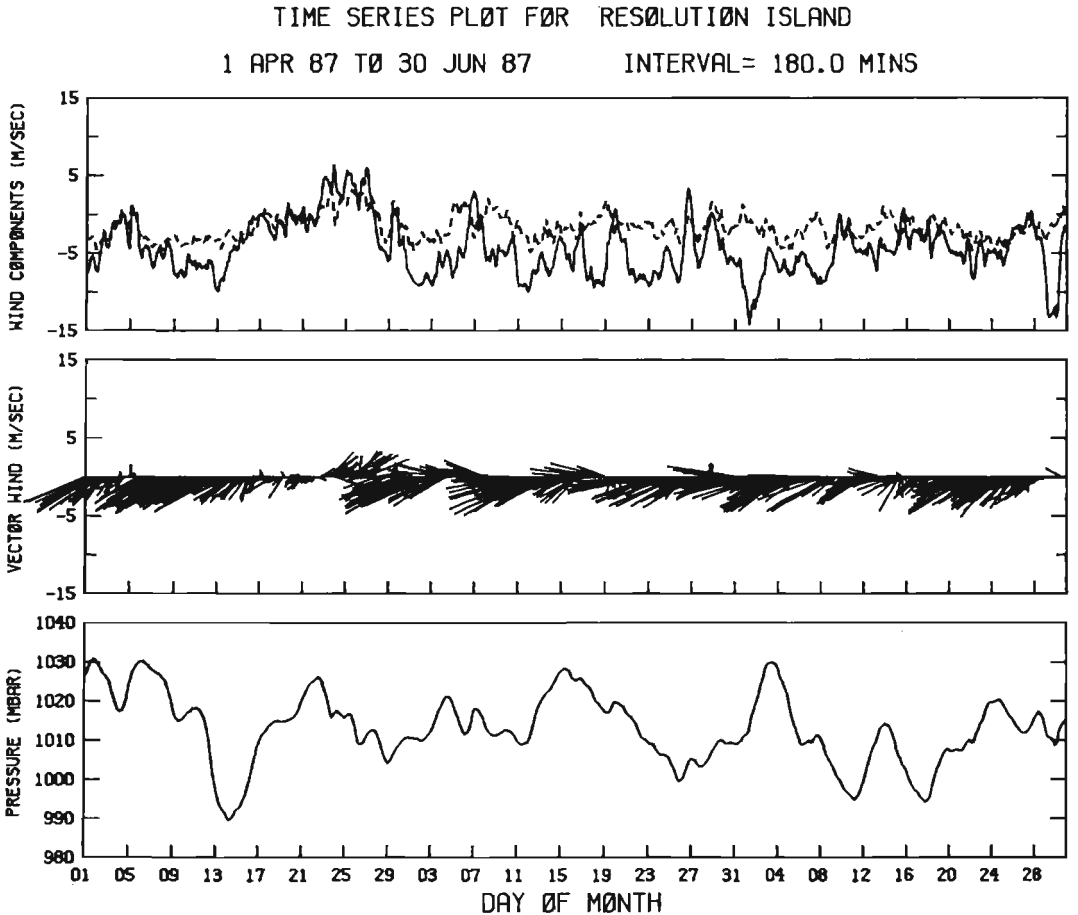

Figure 103. Sea-level pressure, wind components and vectors from Resolution Island (Prudhoe Bay) for April-June 1987.

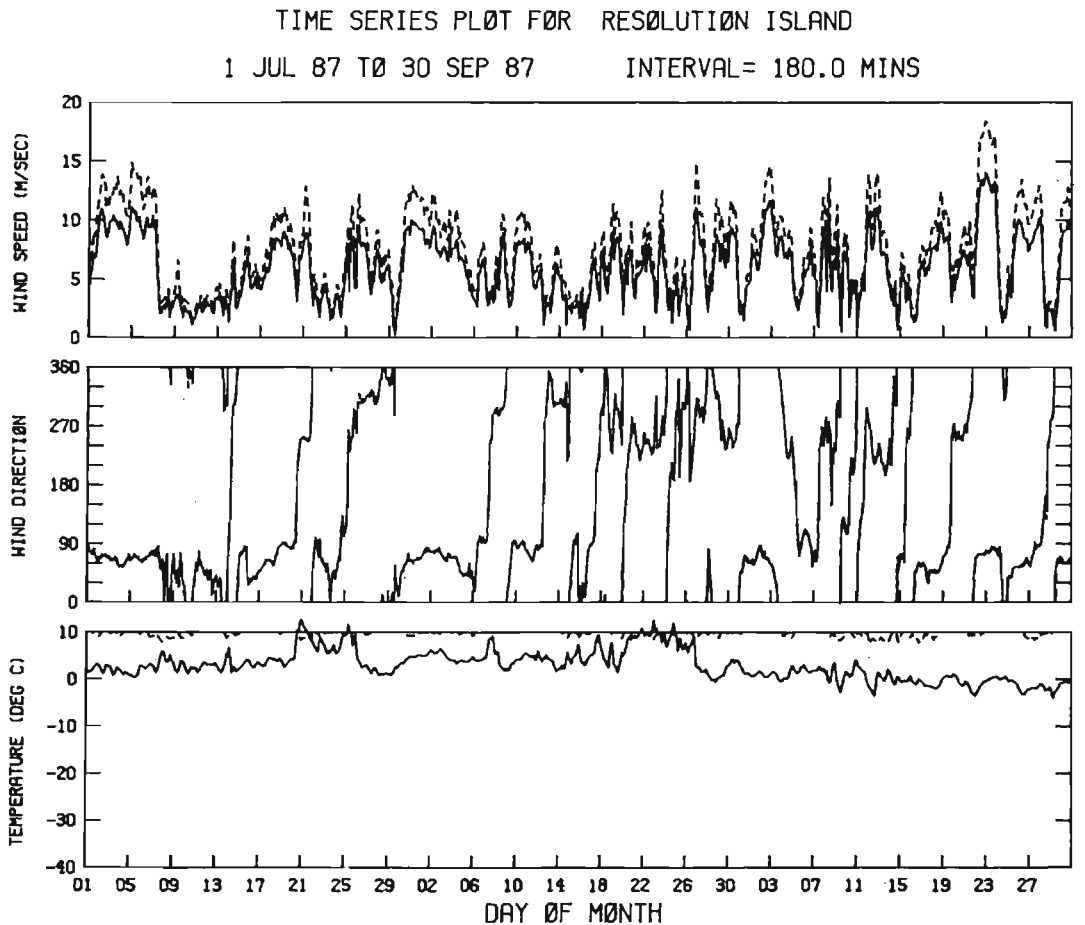

Figure 104. Air temperature and wind speed and direction from Resolution Island (Prudhoe Bay) for July-September 1987.

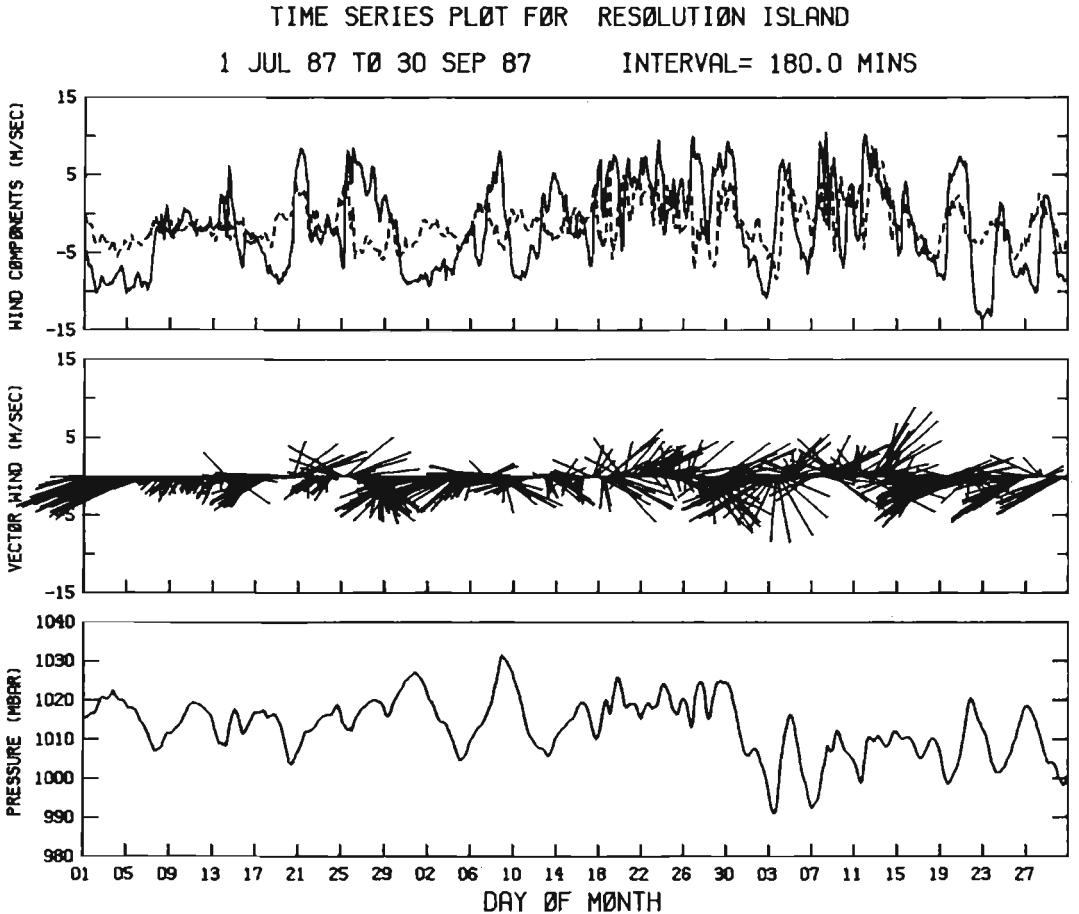

Figure 105. Sea-level pressure, wind components and vectors from Resolution Island (Prudhoe Bay) for July-September 1987.

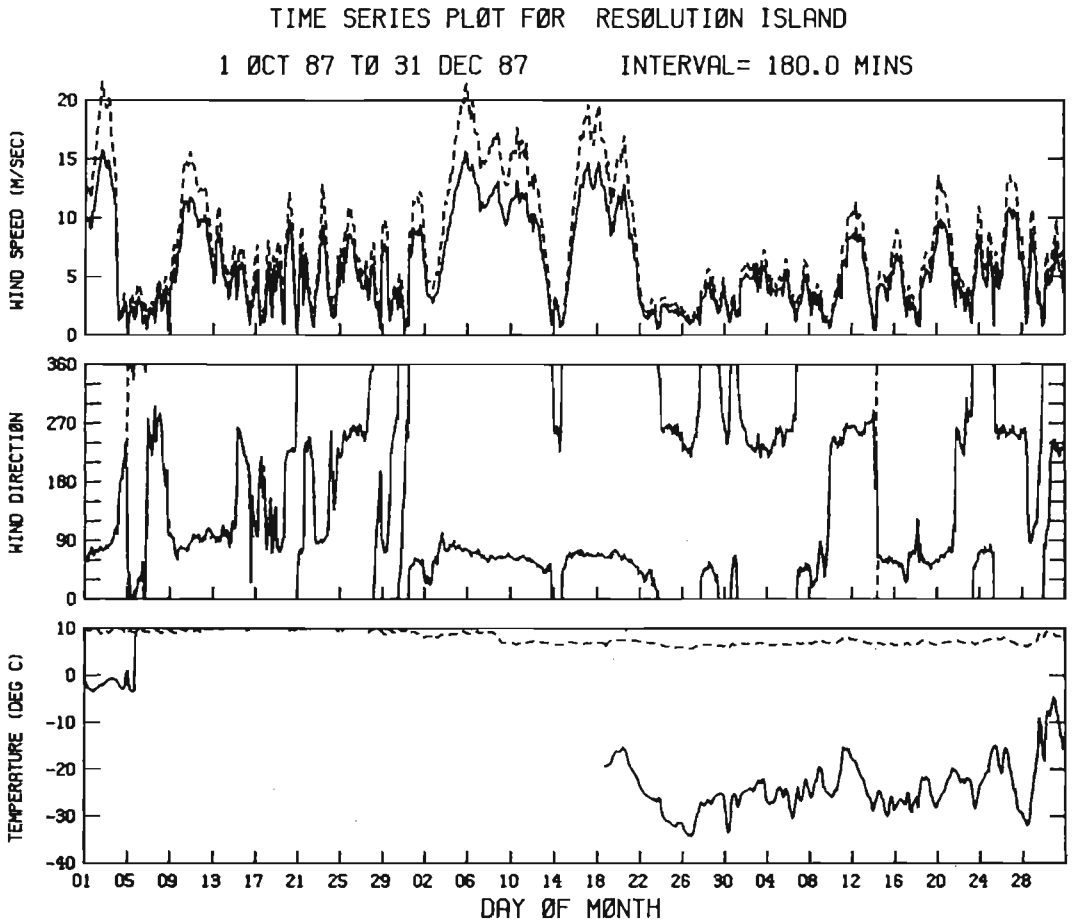

Figure 106. Air temperature and wind speed and direction from Resolution Island (Prudhoe Bay) for October-December 1987.

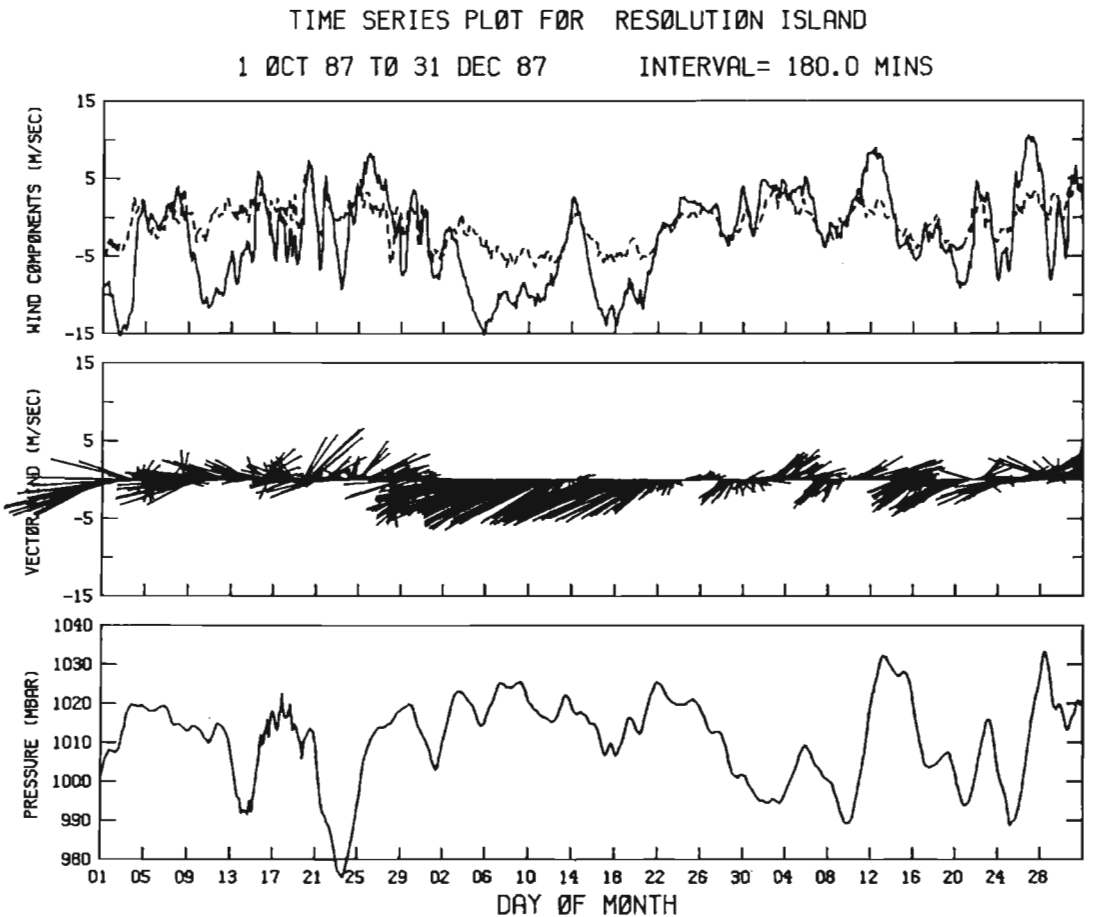

Figure 107. Sea-level pressure, wind components and vectors from Resolution Island (Prudhoe Bay) for October-December 1987.

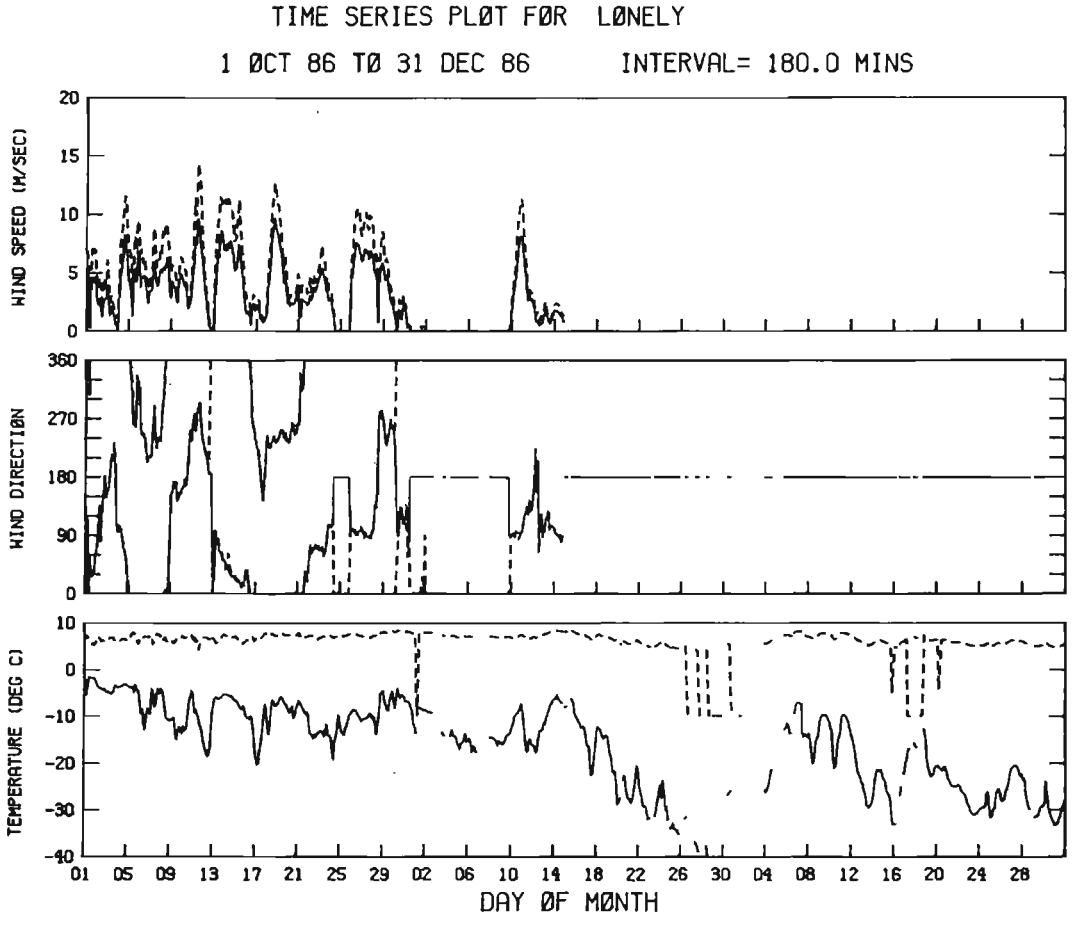

Figure 108. Air temperature and wind speed and direction from Lonely for October-December 1986.

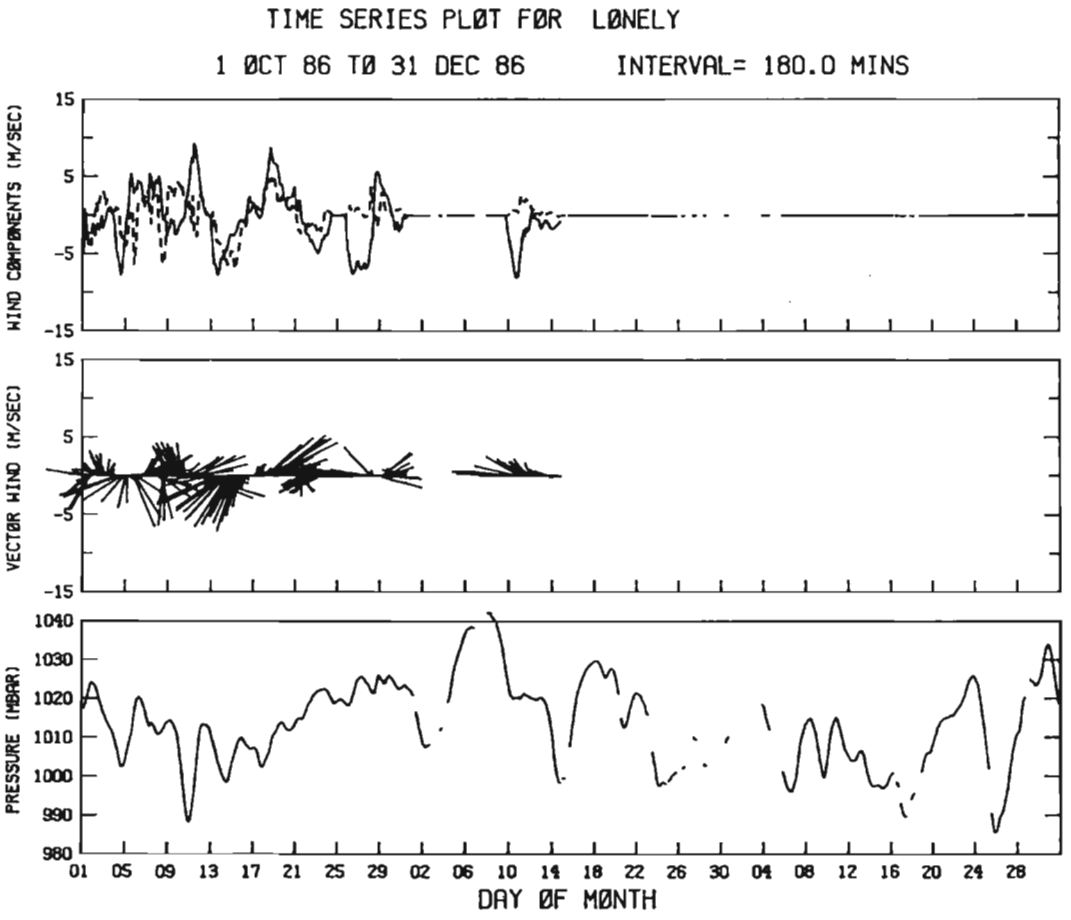

Figure 109. Sea-level pressure, wind components and vectors from Lonely for October-December 1986.

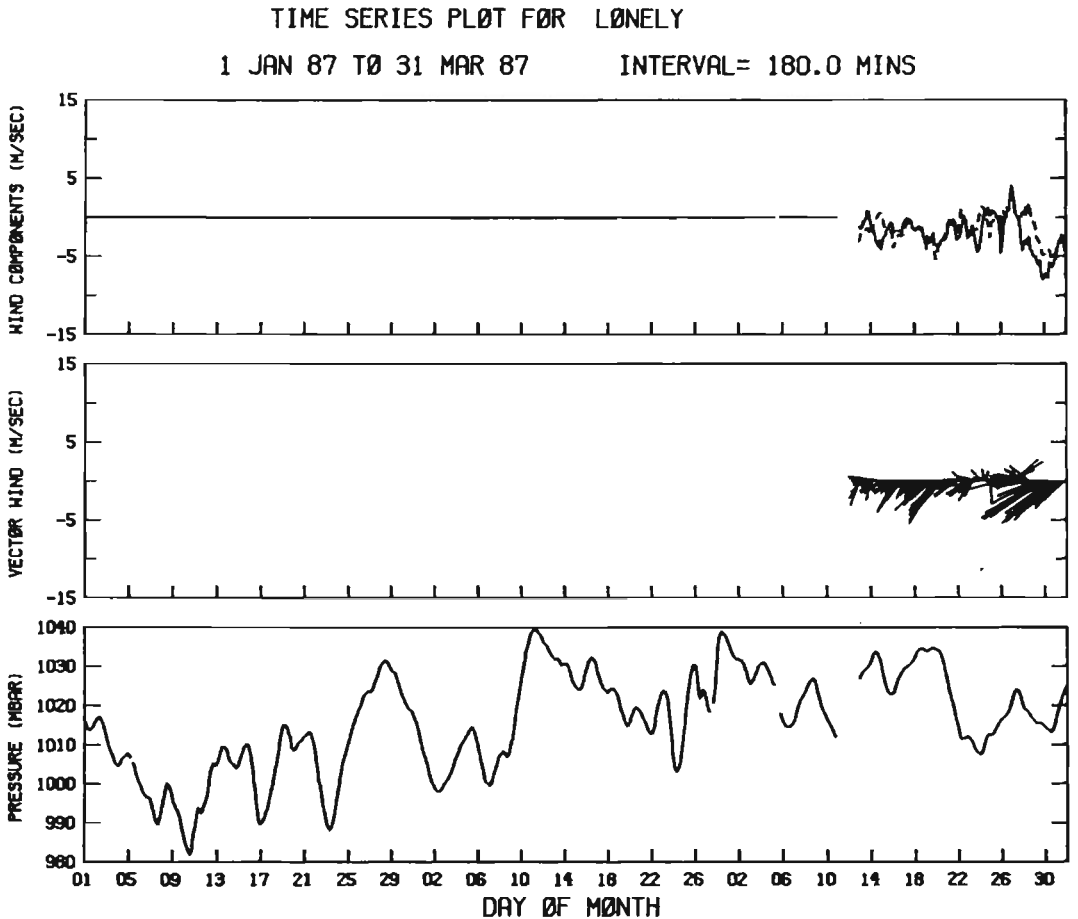

Figure 110. Air temperature and wind speed and direction from Lonely for January-March 1987.

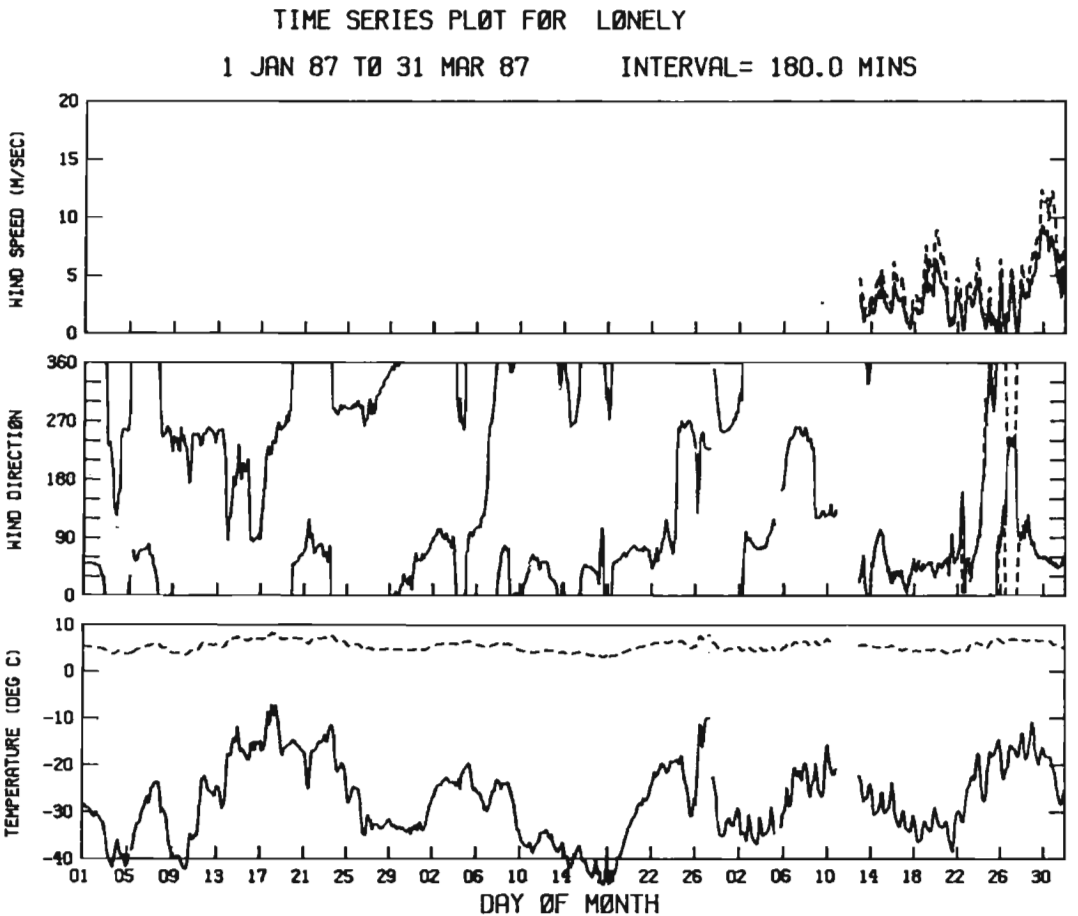

Figure 111. Sea-level pressure, wind components and vectors from Lonely for January-March 1987.

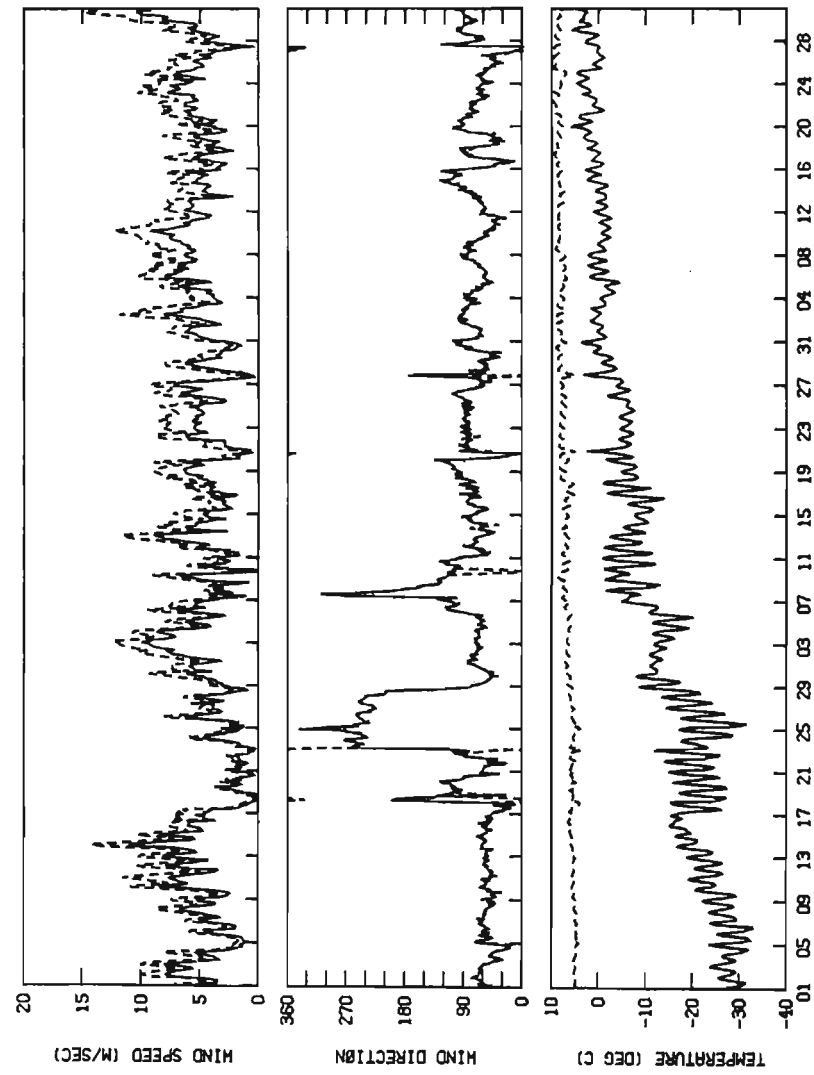

Figure 112. Air temperature and wind speed and direction from Lonely for April-June 1987.

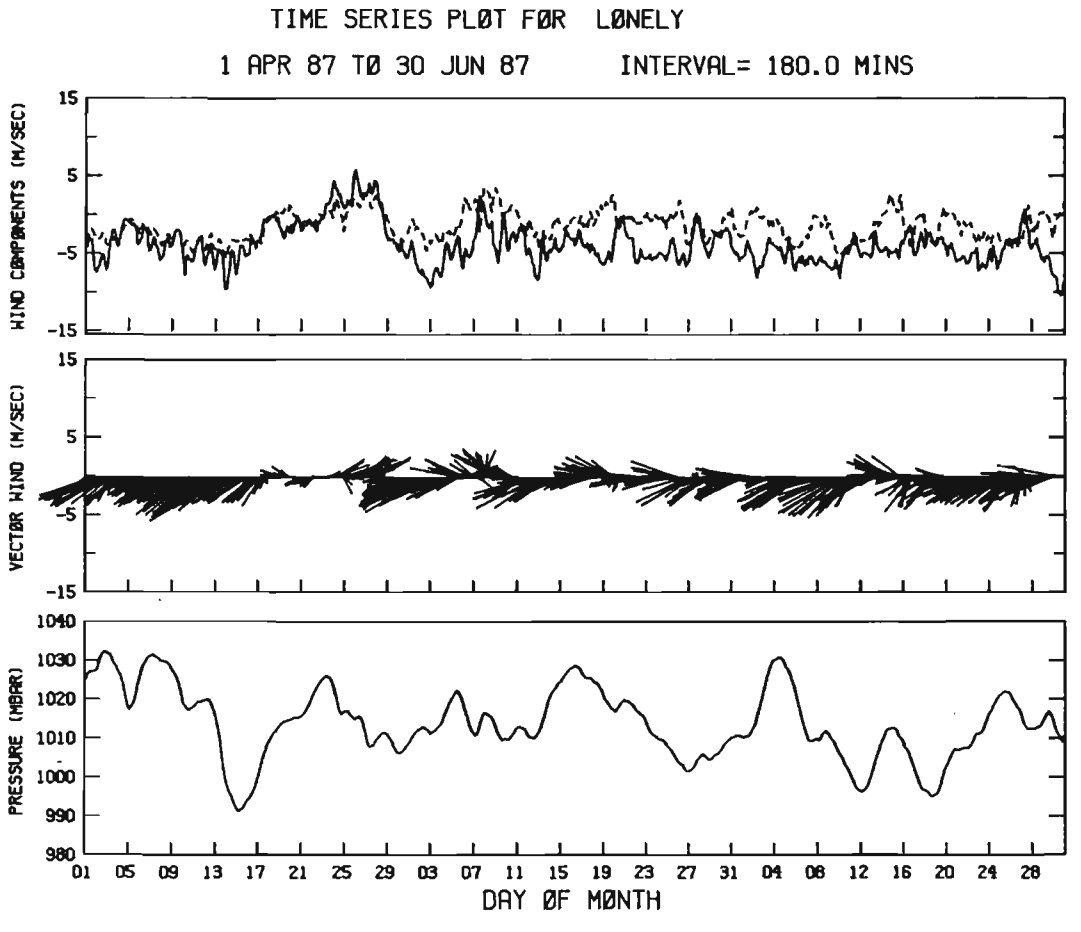

Figure 113. Sea-level pressure, wind components and vectors from Lonely for April-June 1987.

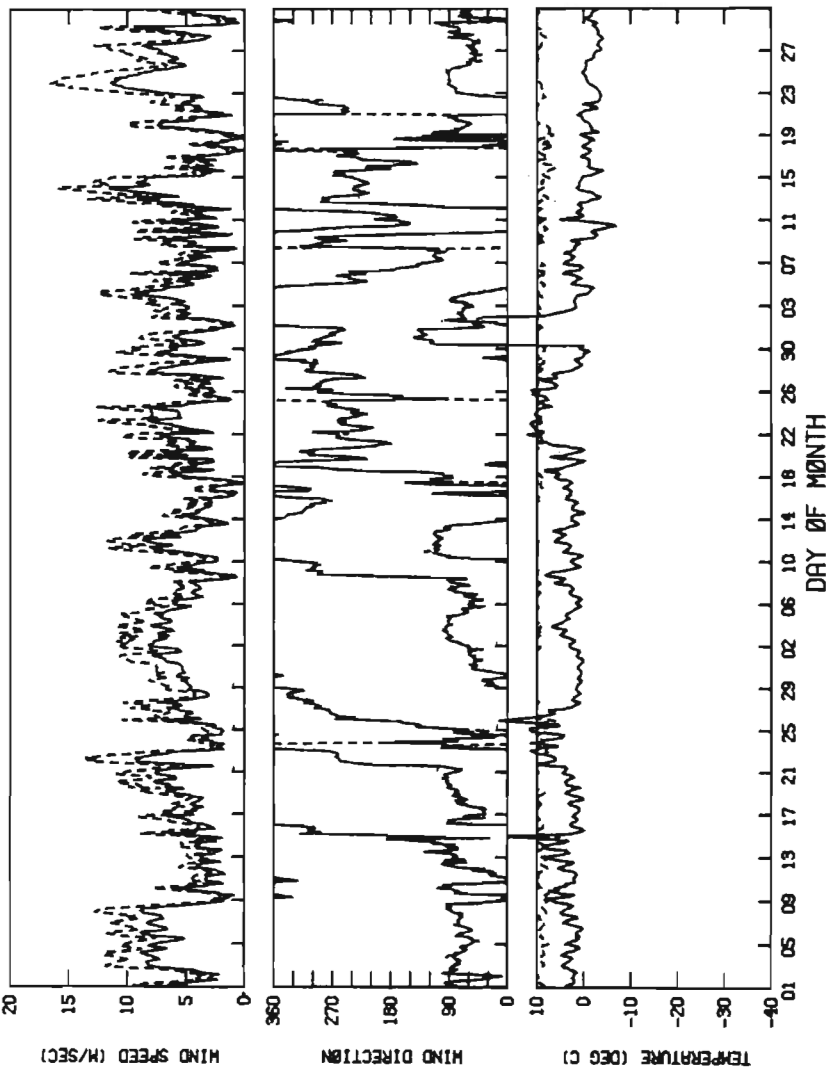

Figure 114. Air temperature and wind speed and direction from Lonely for July-September 1987.

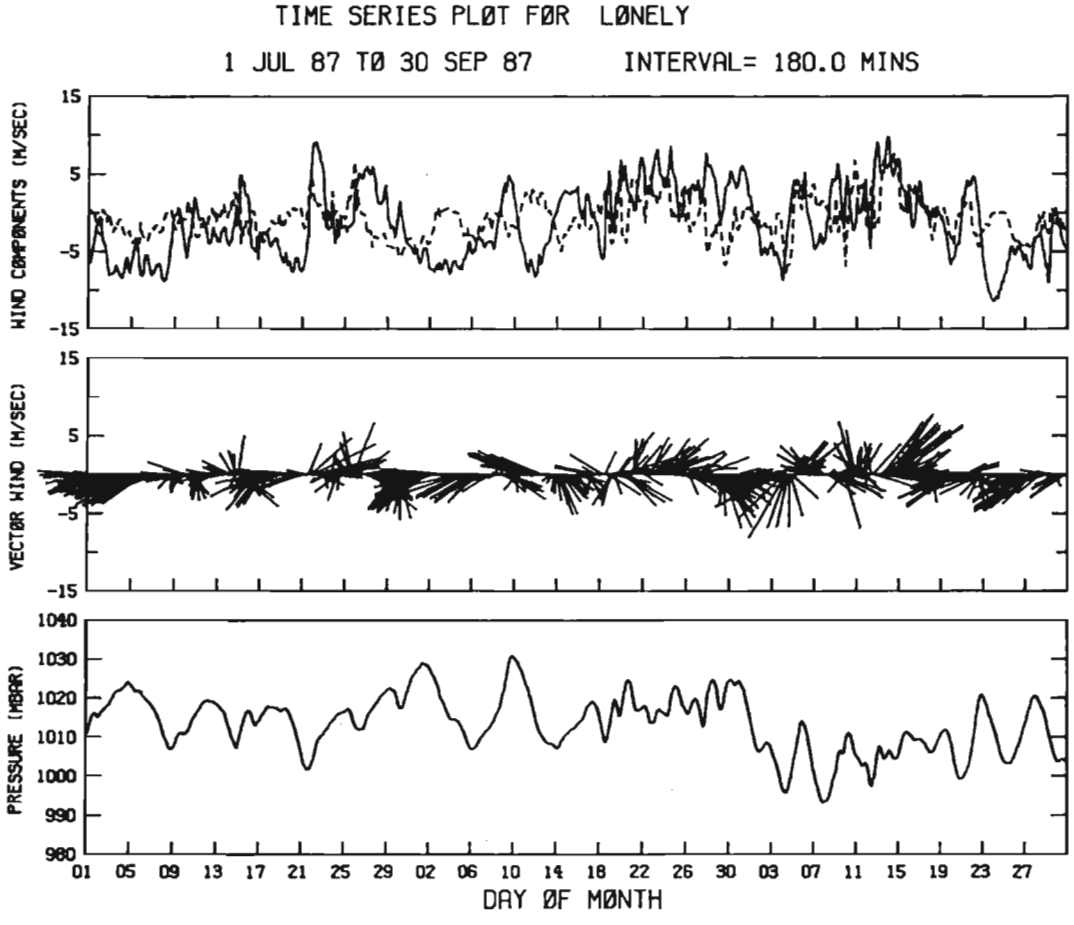

Figure 115. Sea-level pressure, wind components and vectors from Lonely for July-September 1987.

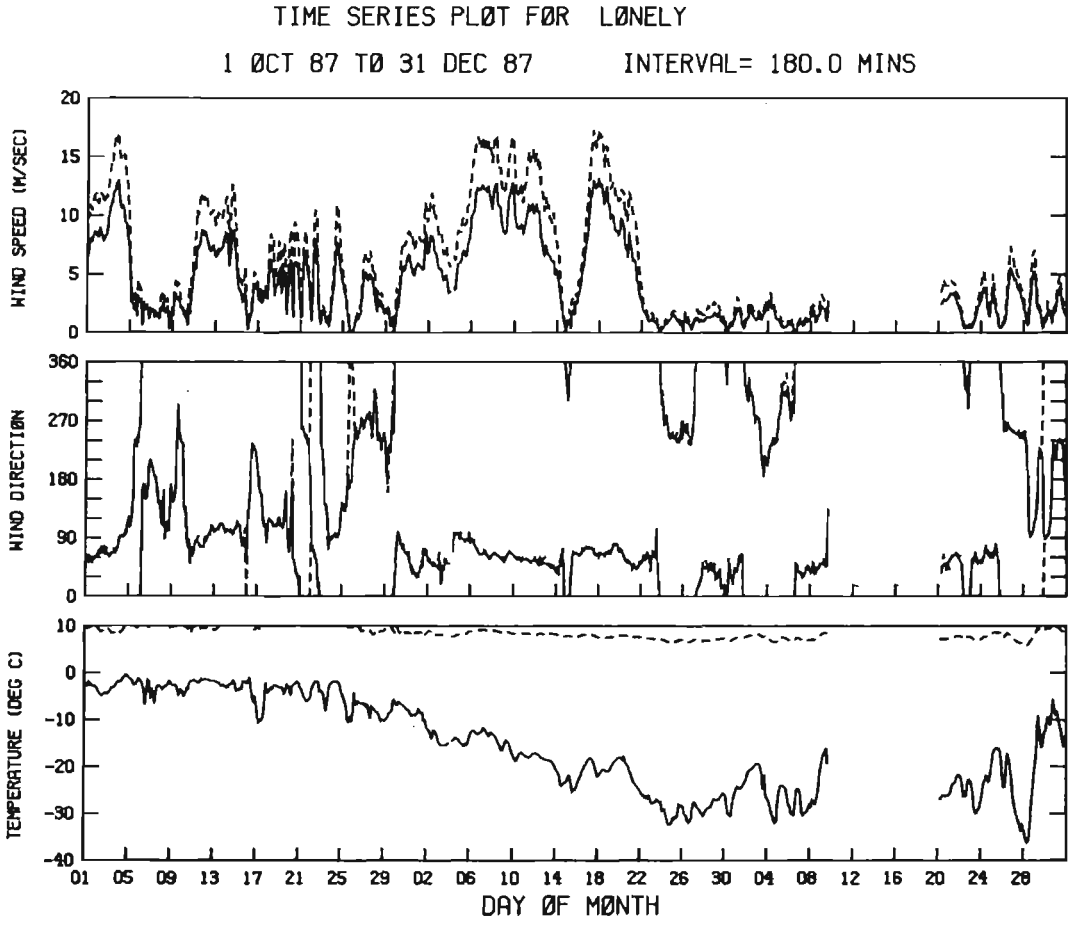

Figure 116. Air temperature and wind speed and direction from Lonely for October-December 1987.

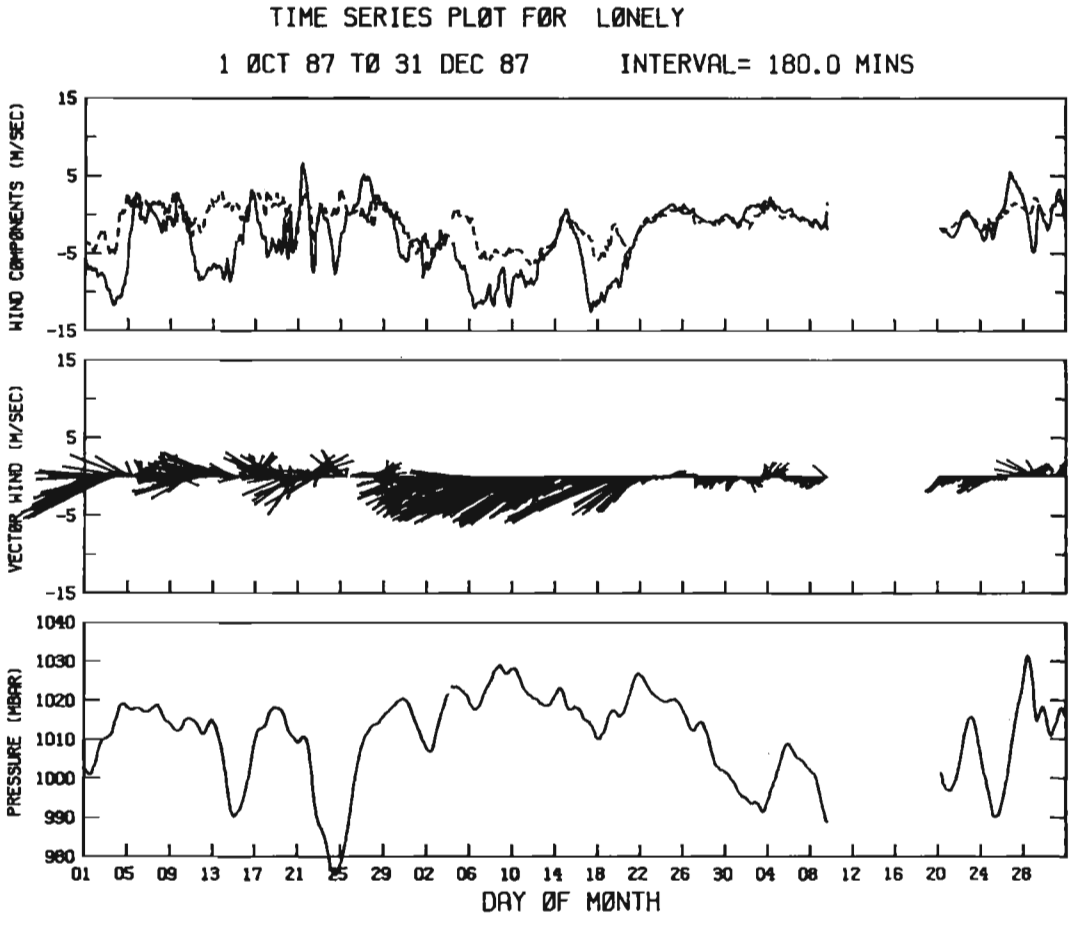

Figure 117. Sea-level pressure, wind components and vectors from Lonely for October-December 1987.

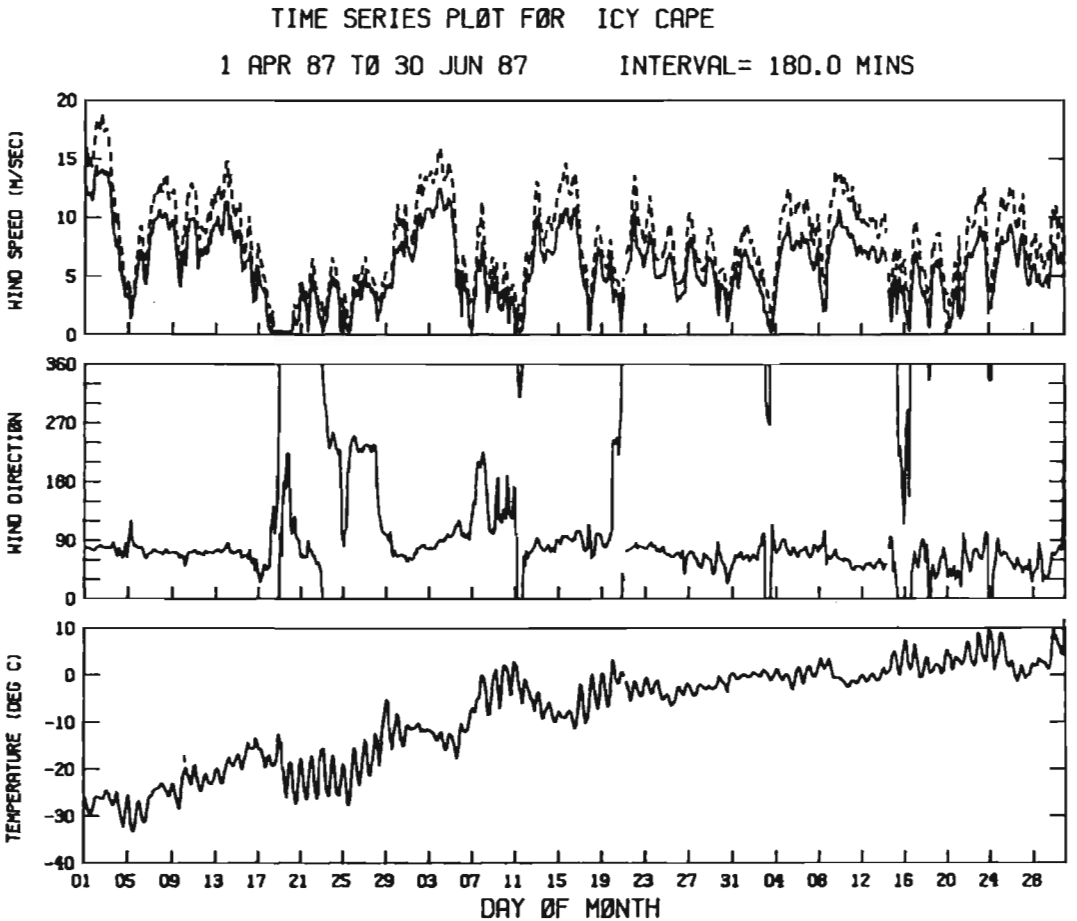

Figure 118. Air temperature and wind speed and direction from Icy Cape for April-June 1987.

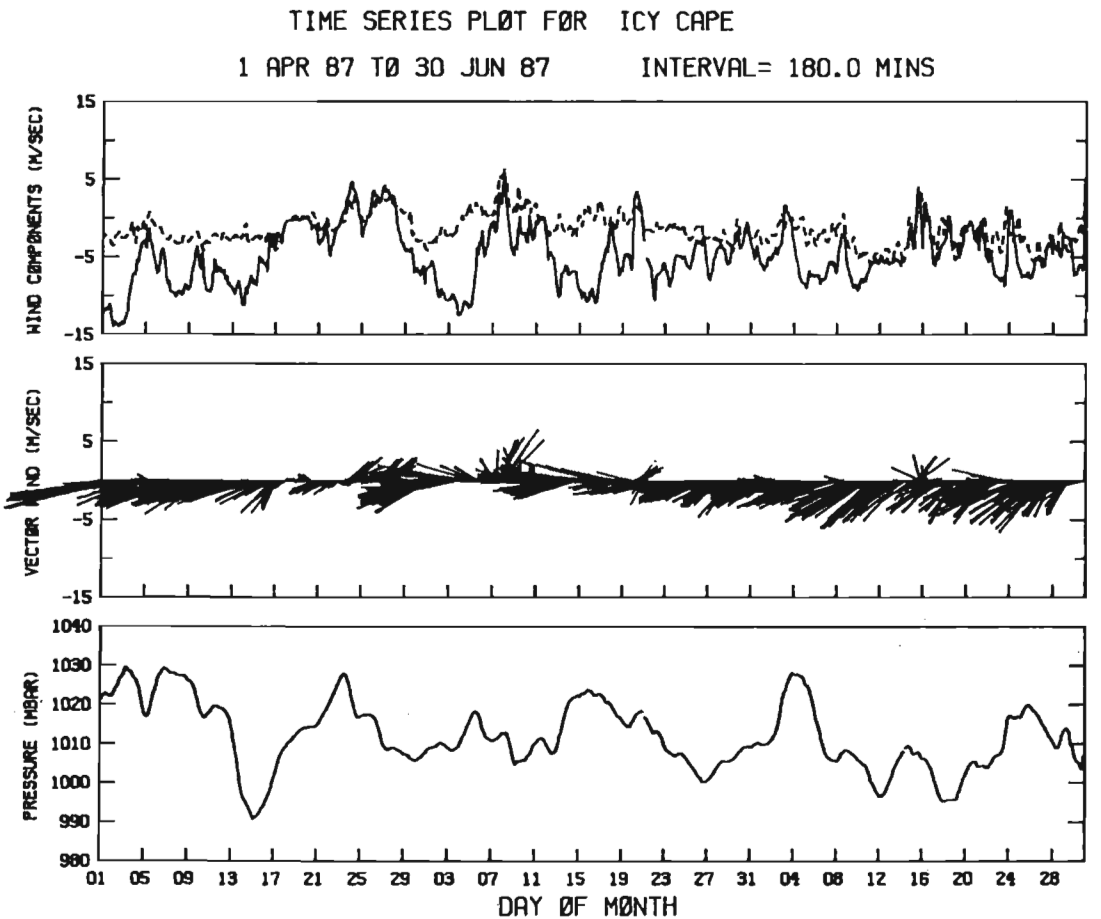

Figure 119. Sea-level pressure, wind components and vectors from Icy Cape for April-June 1987.

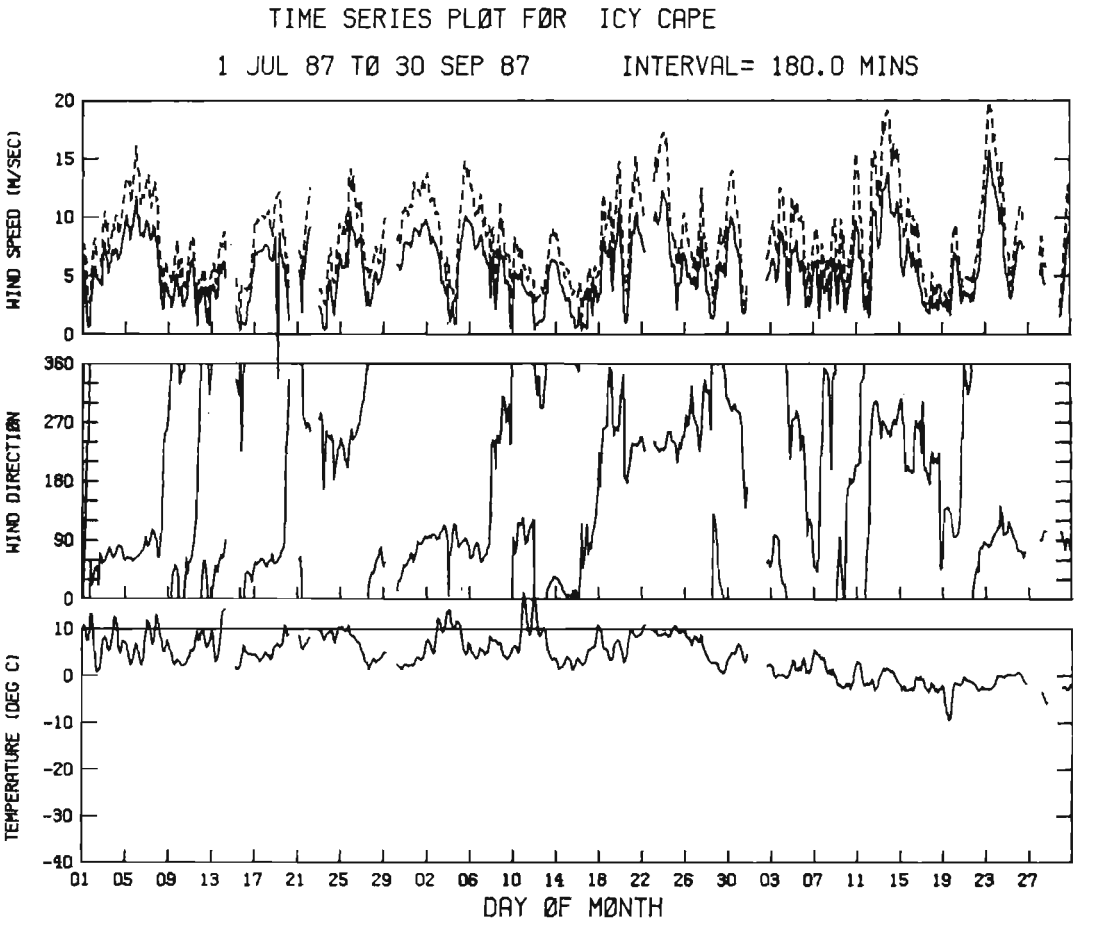

Figure 120. Air temperature and wind speed and direction from Icy Cape for July-September 1987.

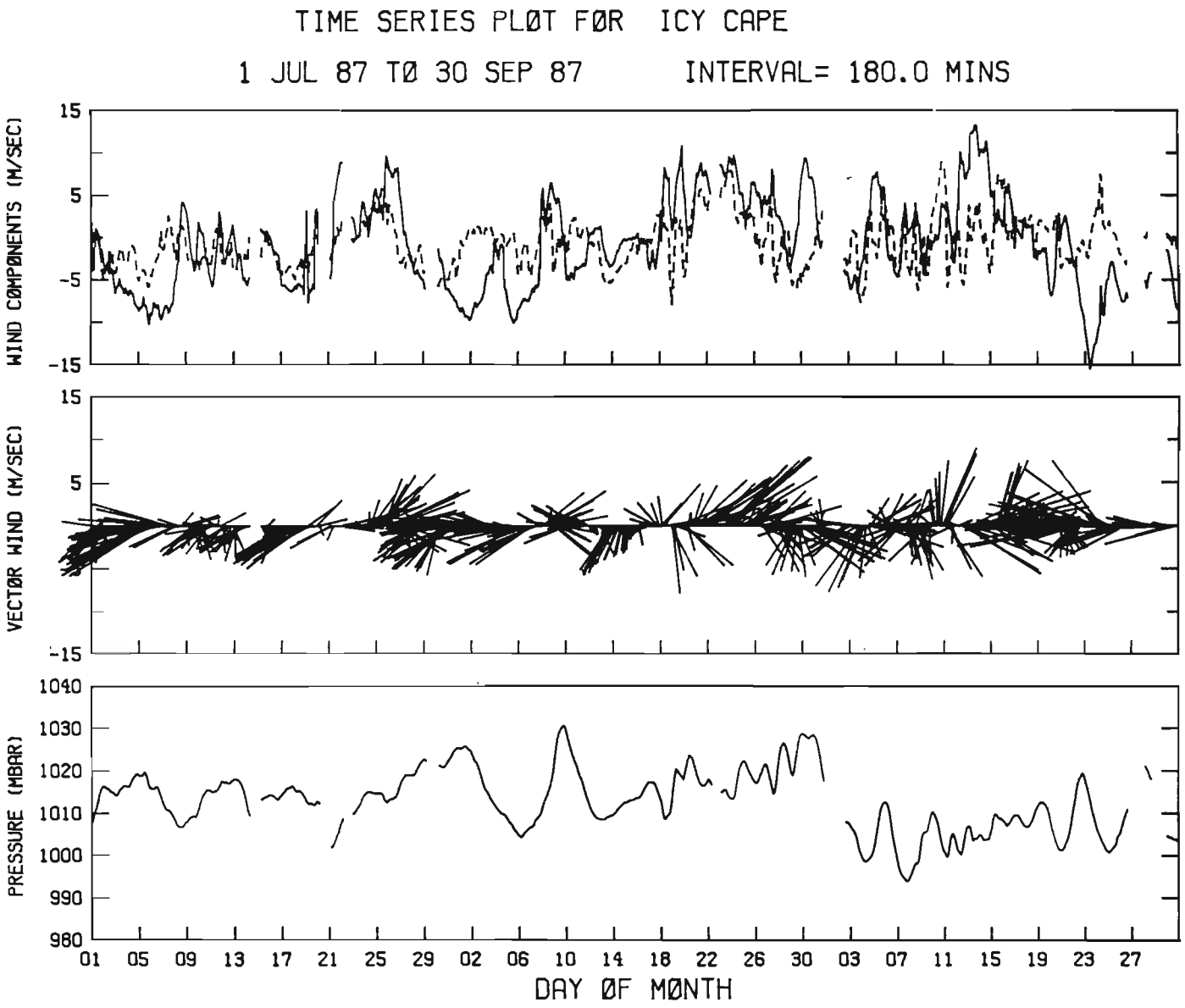

Figure 121. Sea-level pressure, wind components and vectors from Icy Cape for July-September 1987.

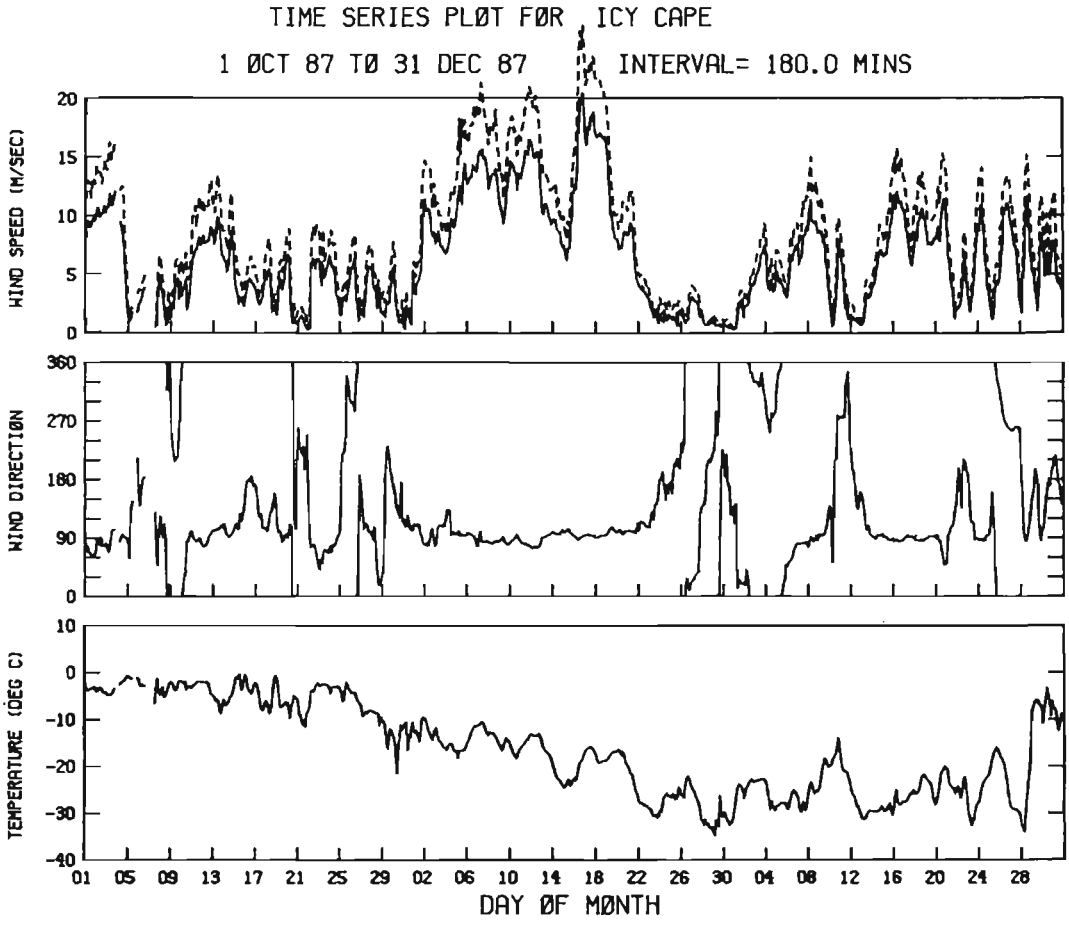

Figure 122. Air temperature and wind speed and direction from Icy Cape for October-December 1987.

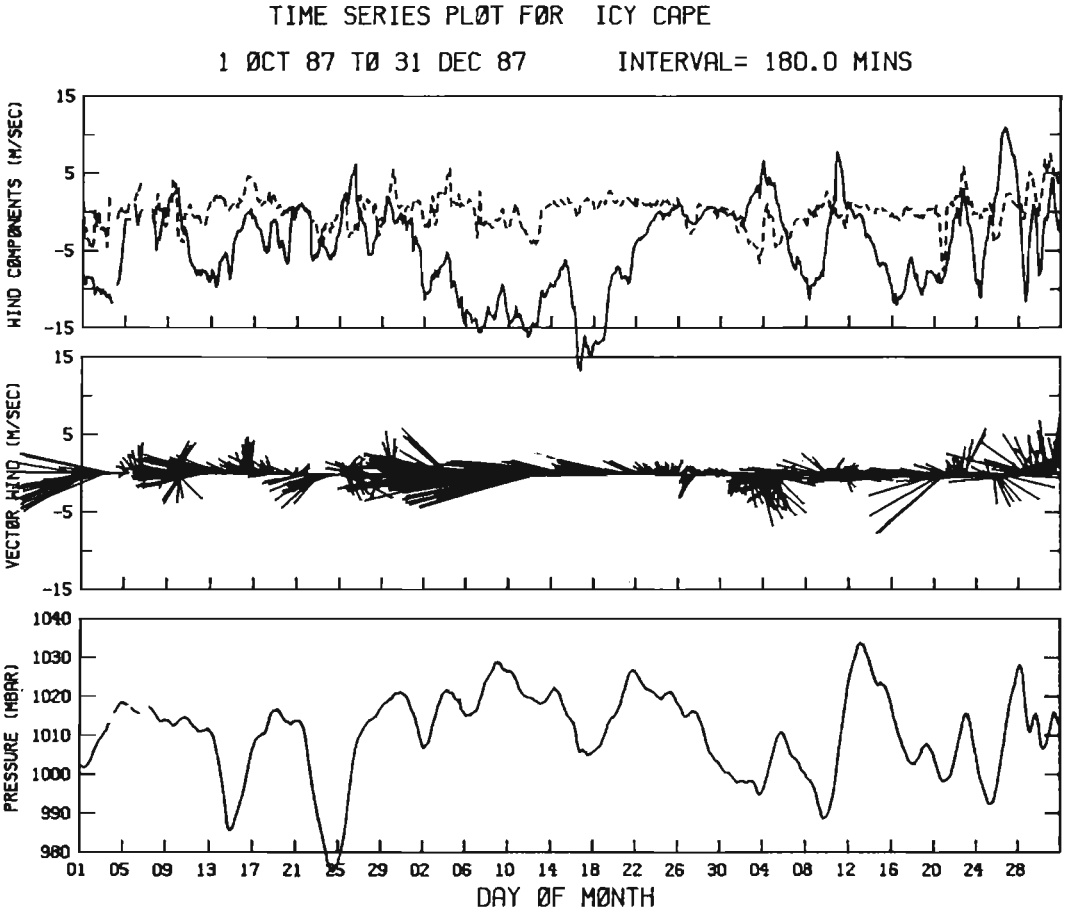

Figure 123. Sea-level pressure, wind components and vectors from Icy Cape for October-December 1987.

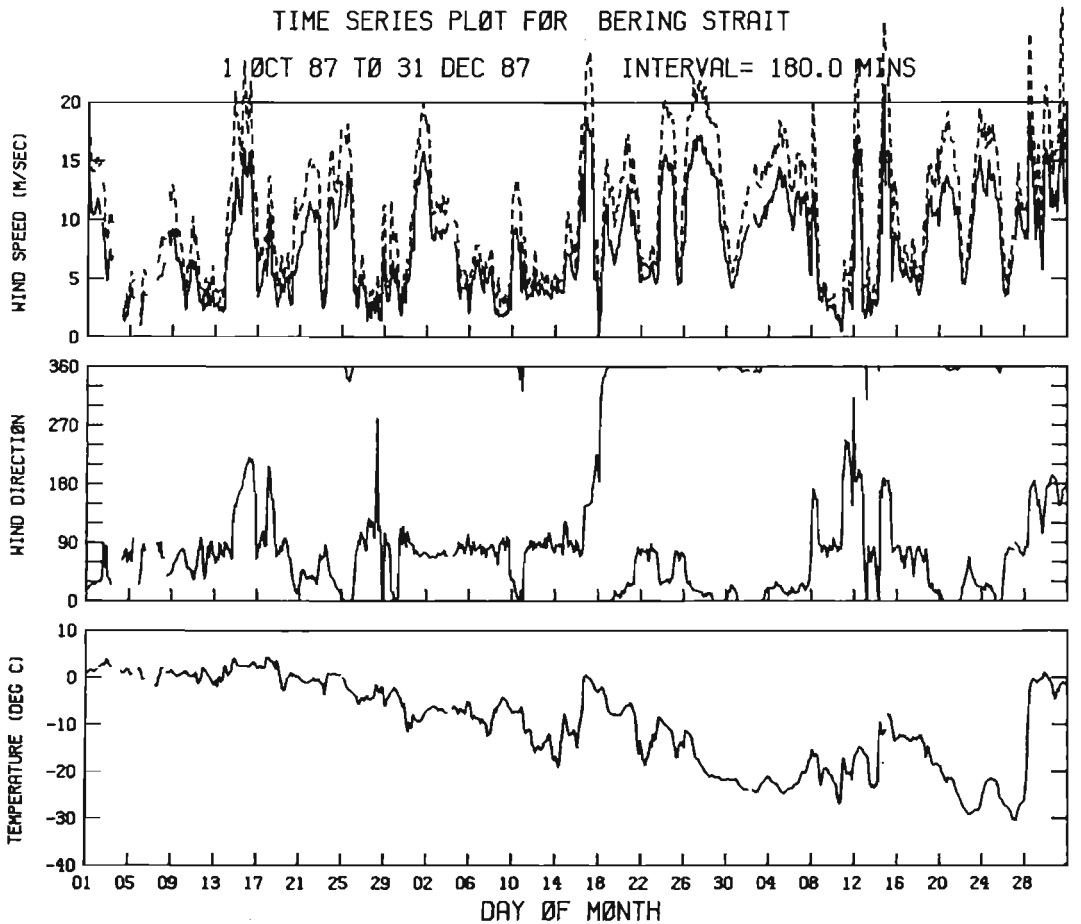

Figure 124. Air temperature and wind speed and direction from Bering Strait for October-December 1987.

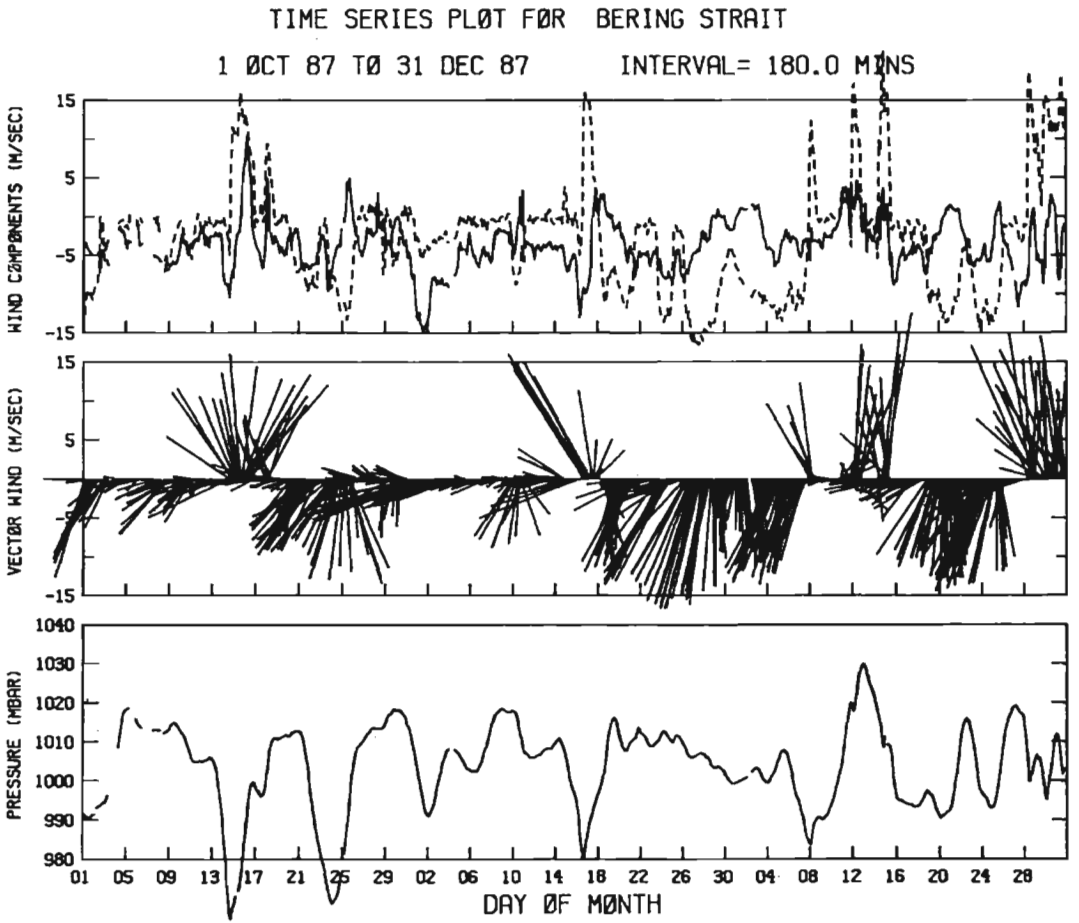

Figure 125. Sea-level pressure, wind components and vectors from Bering Strait for October-December 1987.

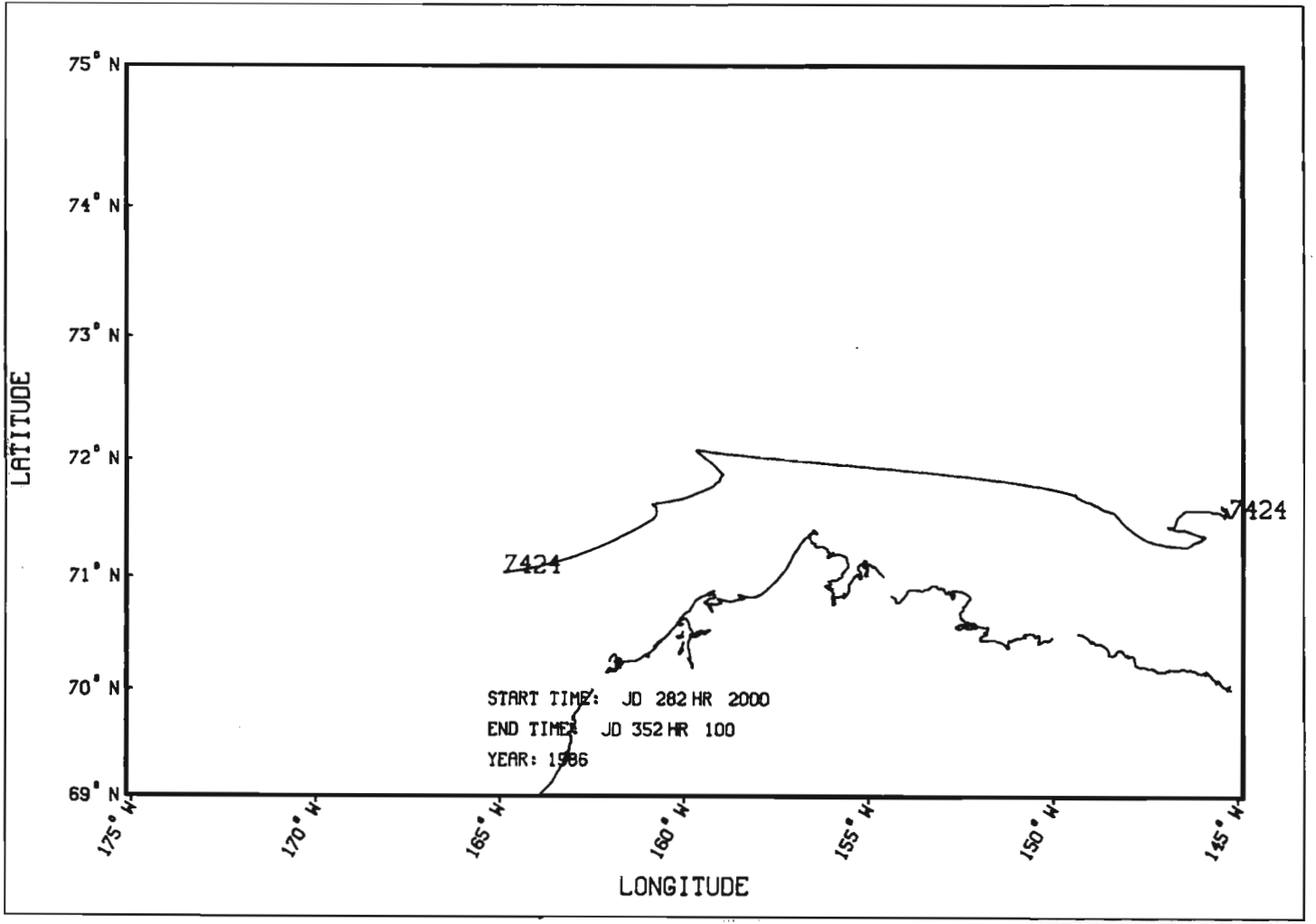

Figure 126. Drift tracks for ARGOS buoy 7424.

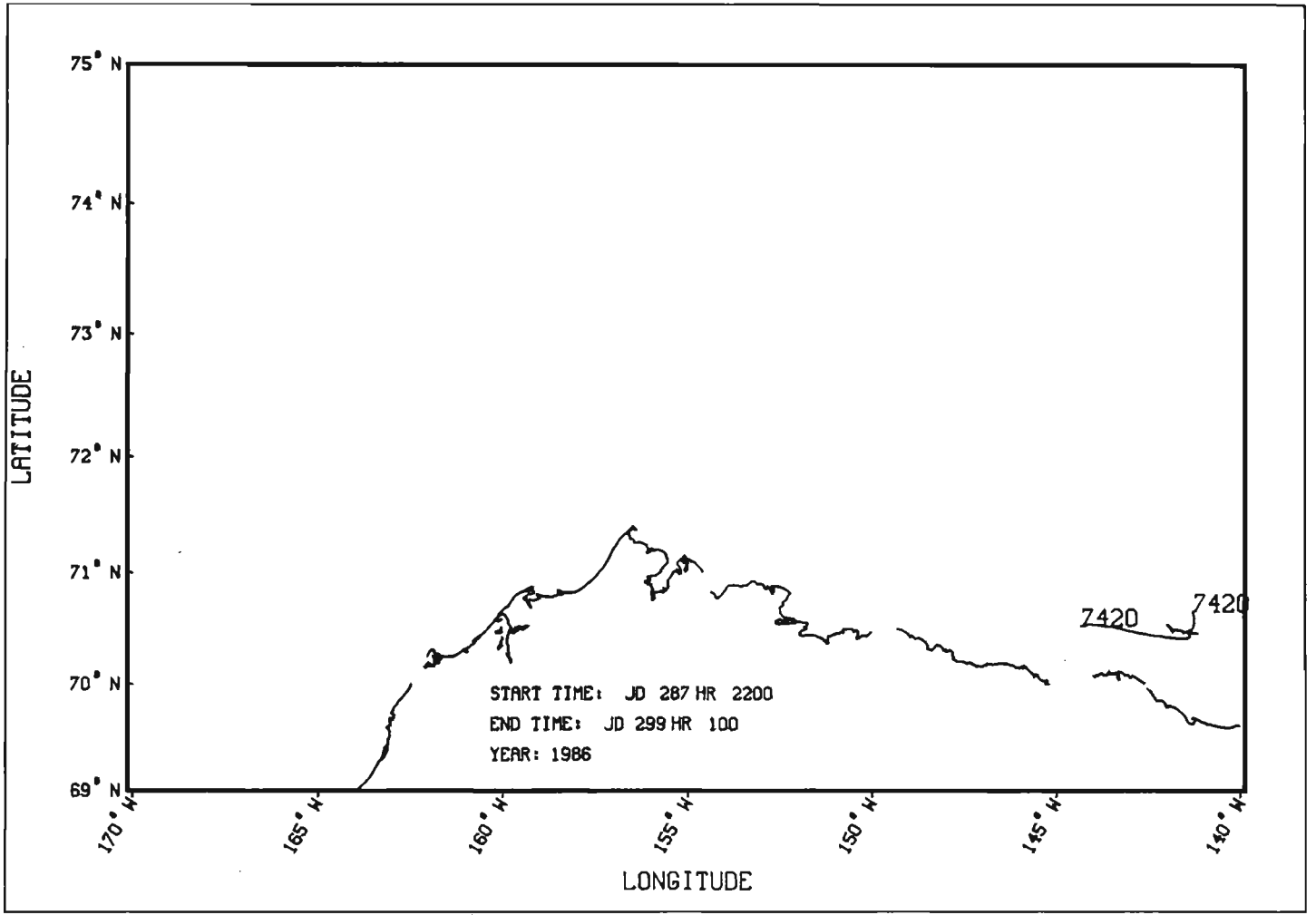

Figure 127. Drift tracks for ARGOS buoy 7420a.

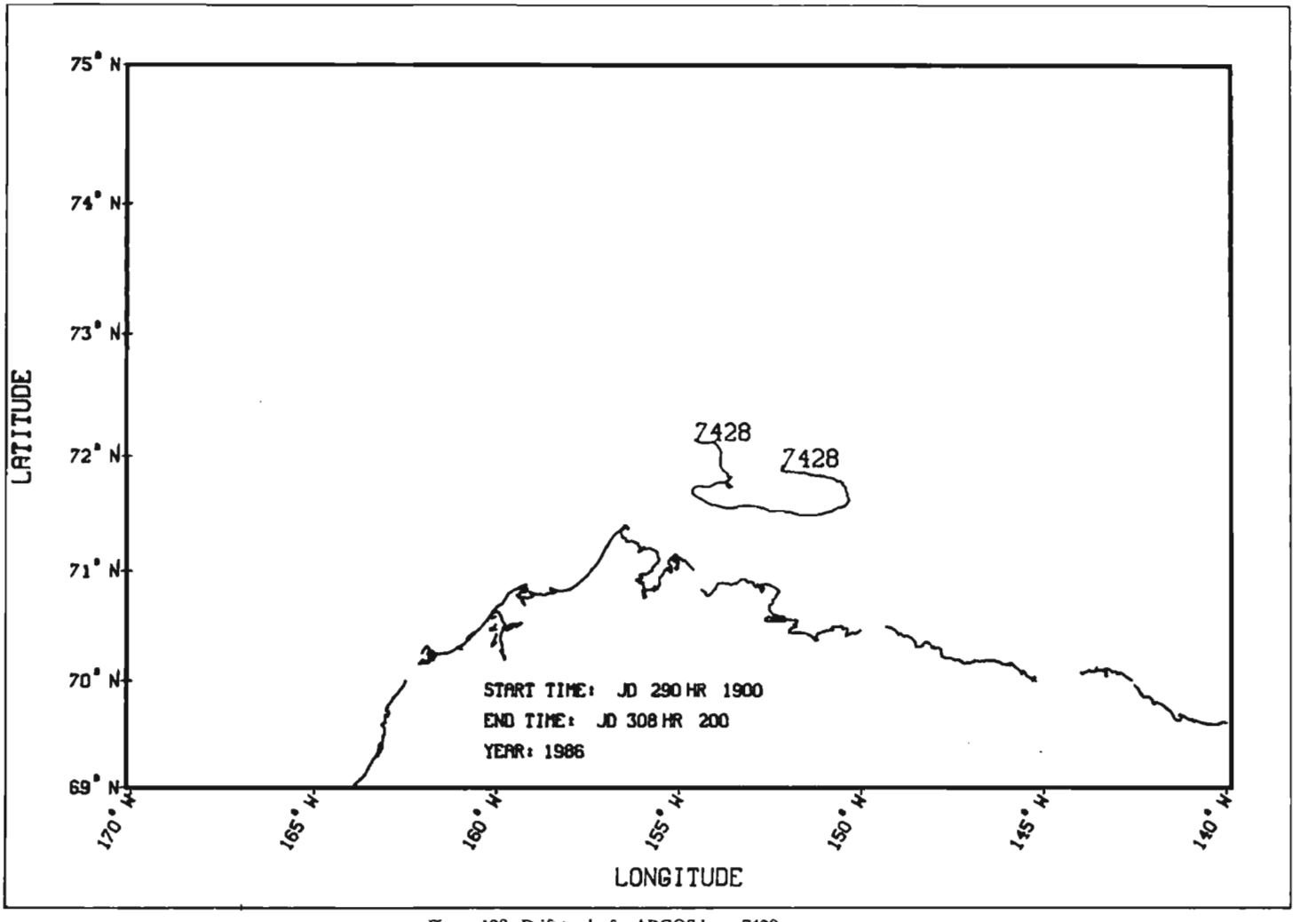

Figure 128. Drift tracks for ARGOS buoy 7428.

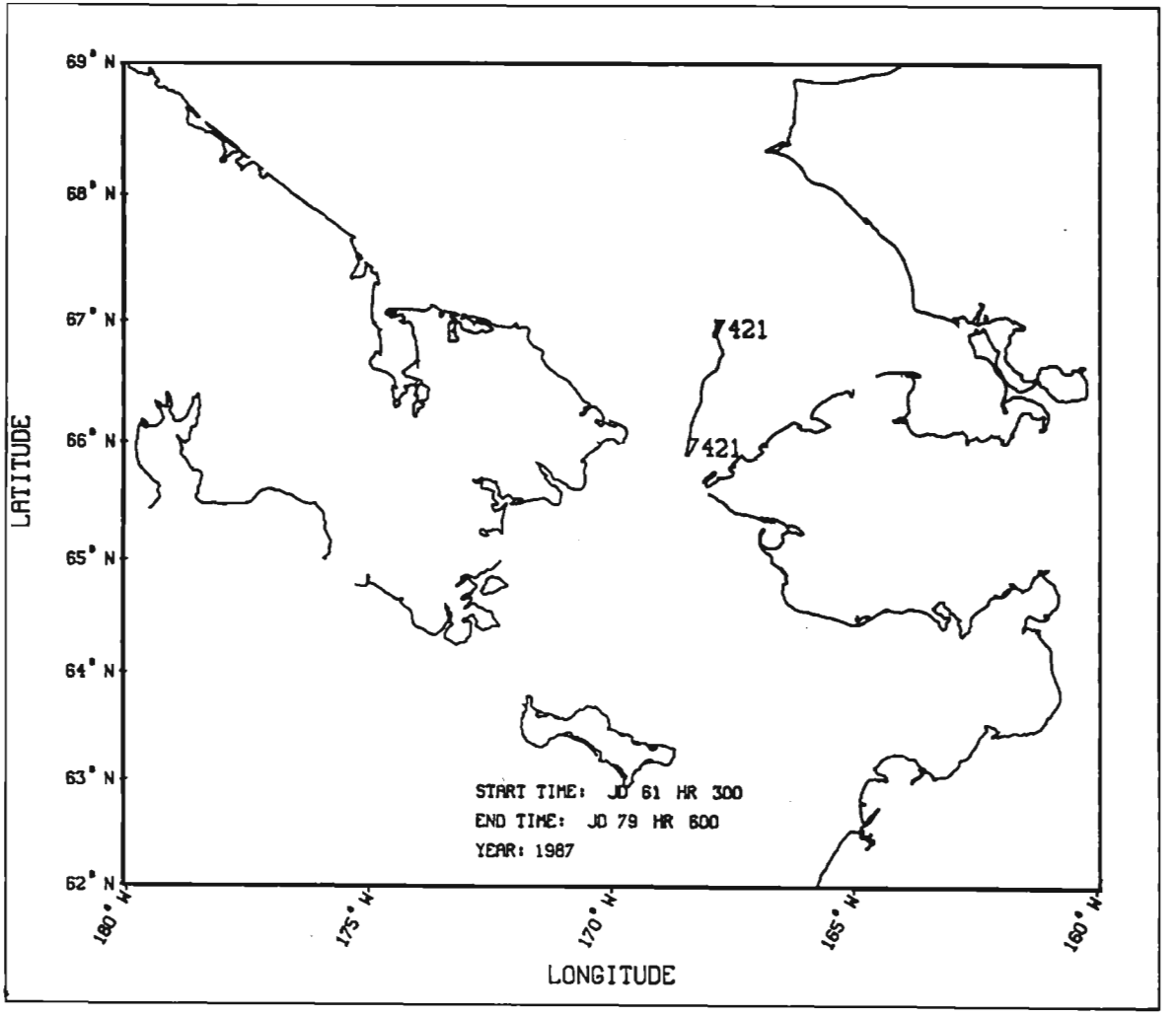

Figure 129. Drift tracks for ARGOS buoy 7421.

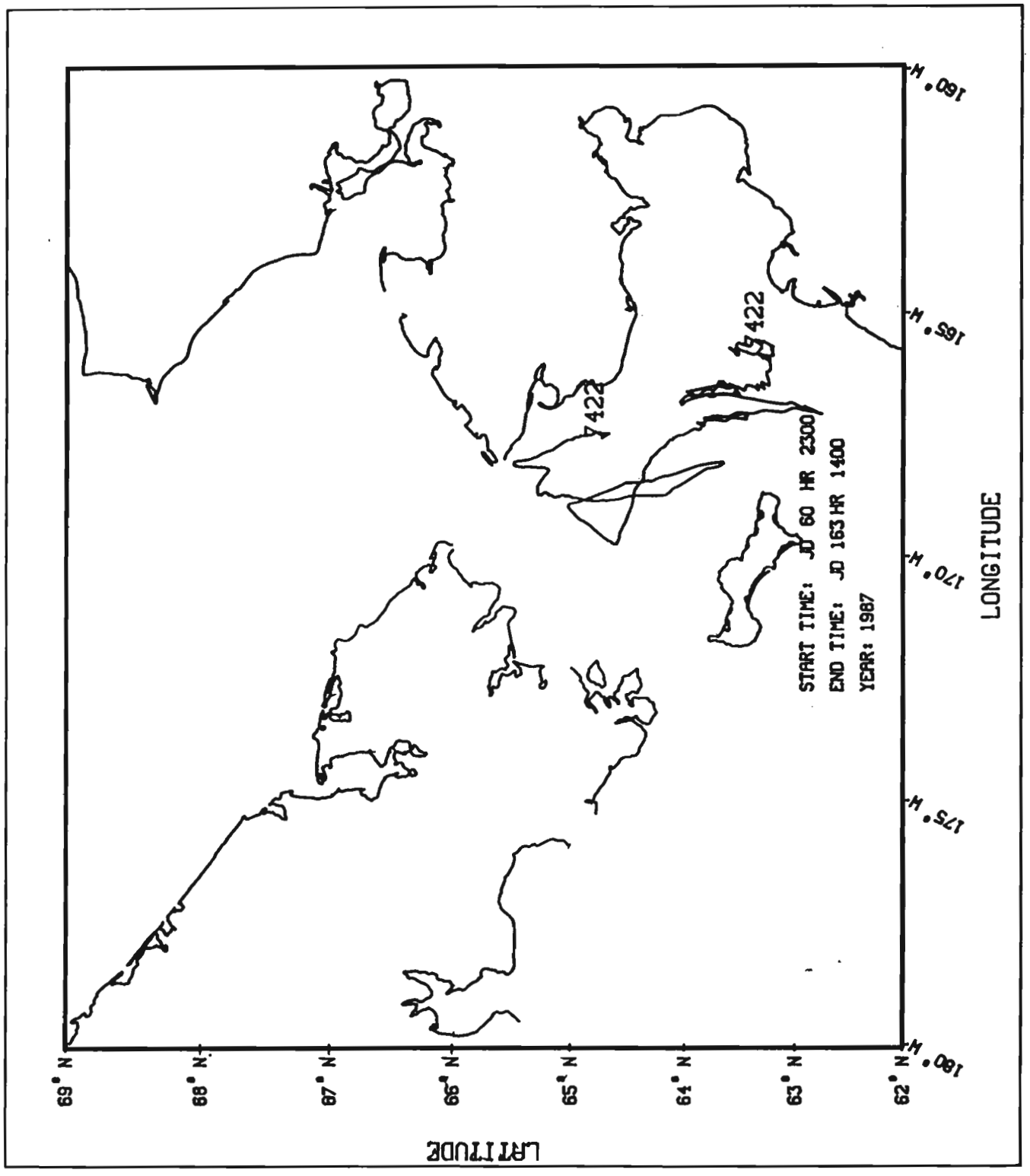

Figure 130. Drift tracks for ARGOS buoy 7422.

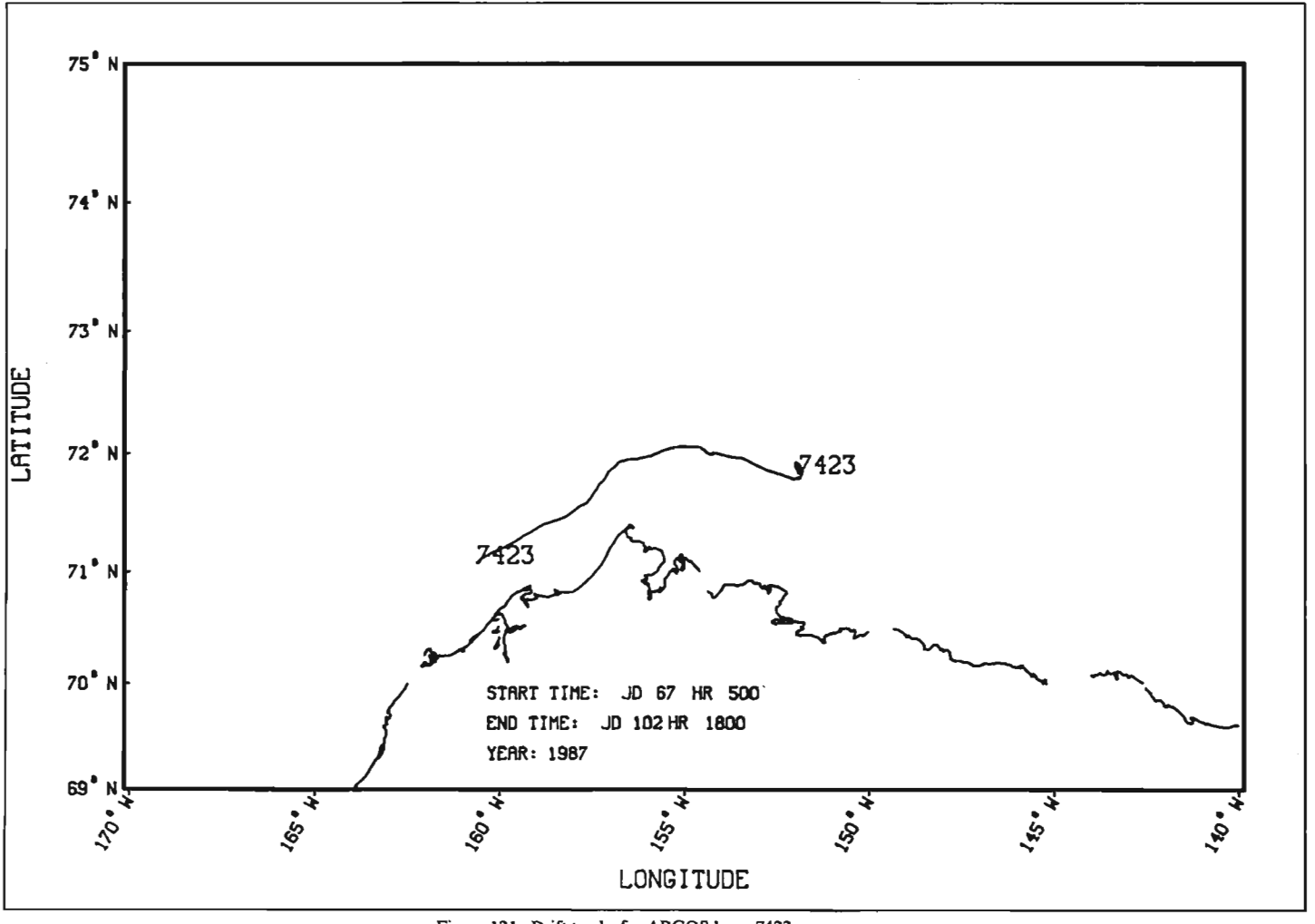

Figure 131. Drift tracks for ARGOS buoy 7423.

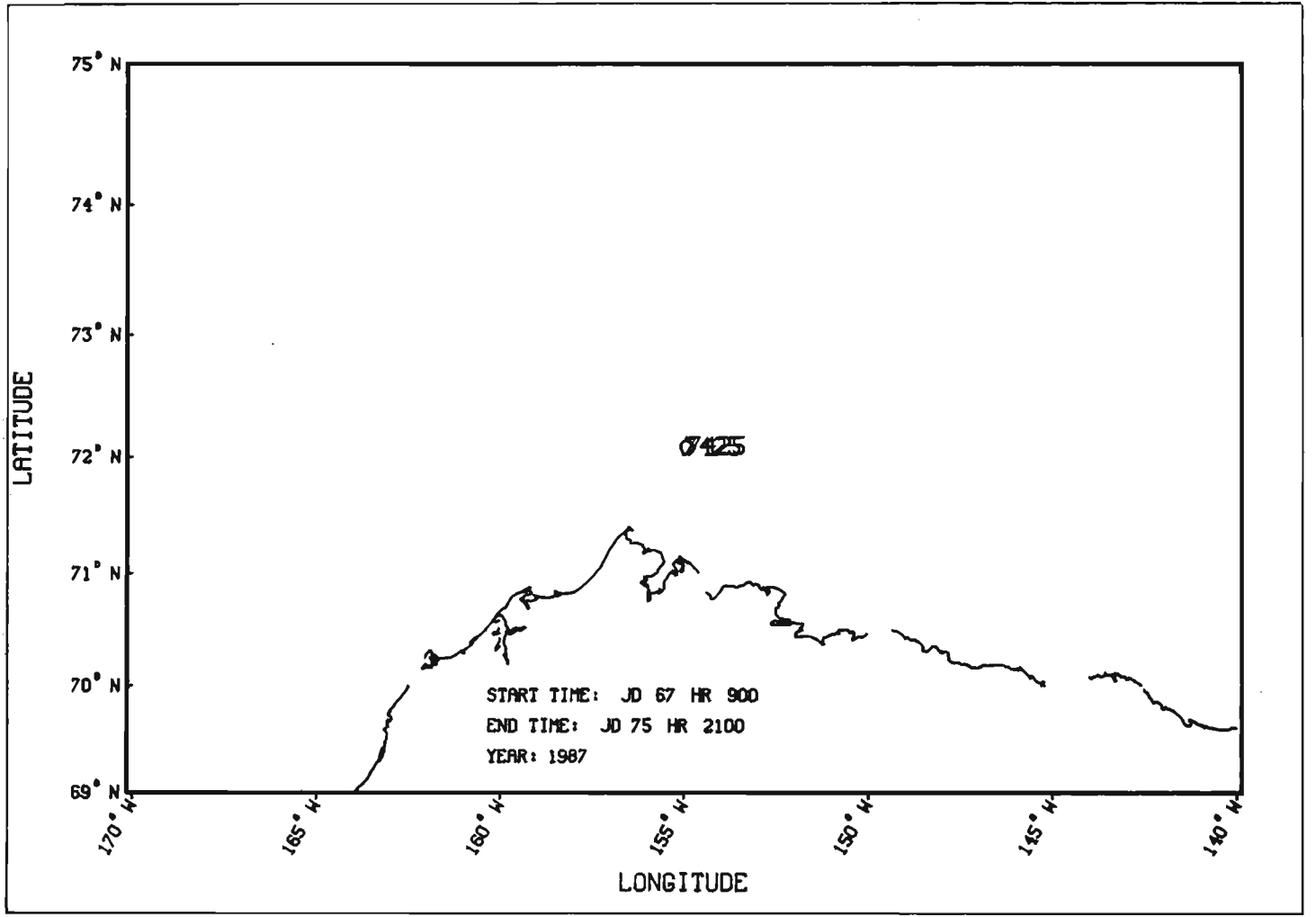

Figure 132. Drift tracks for ARGOS buoy 7425.

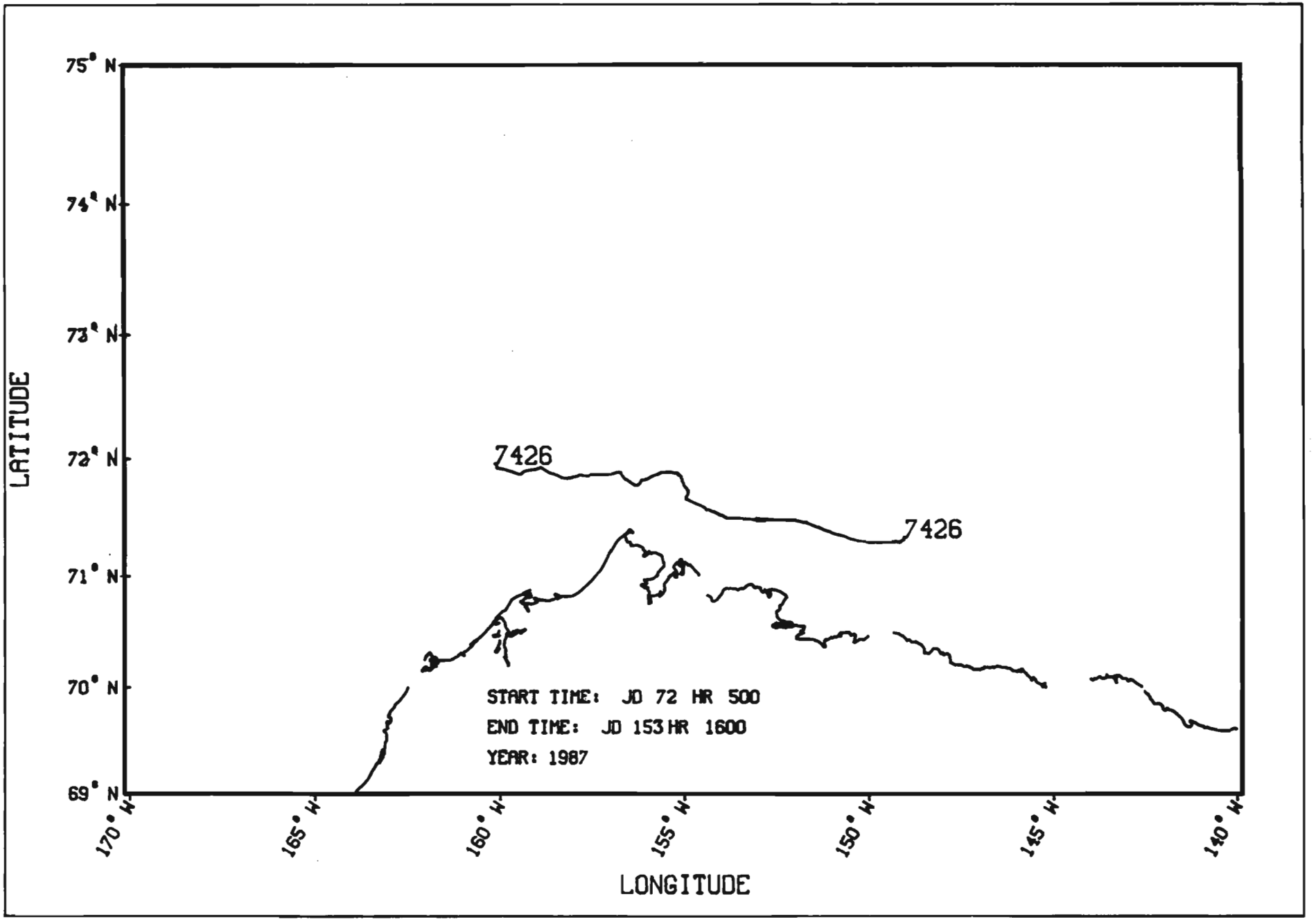

Figure 133. Drift tracks for ARGOS buoy 7426.

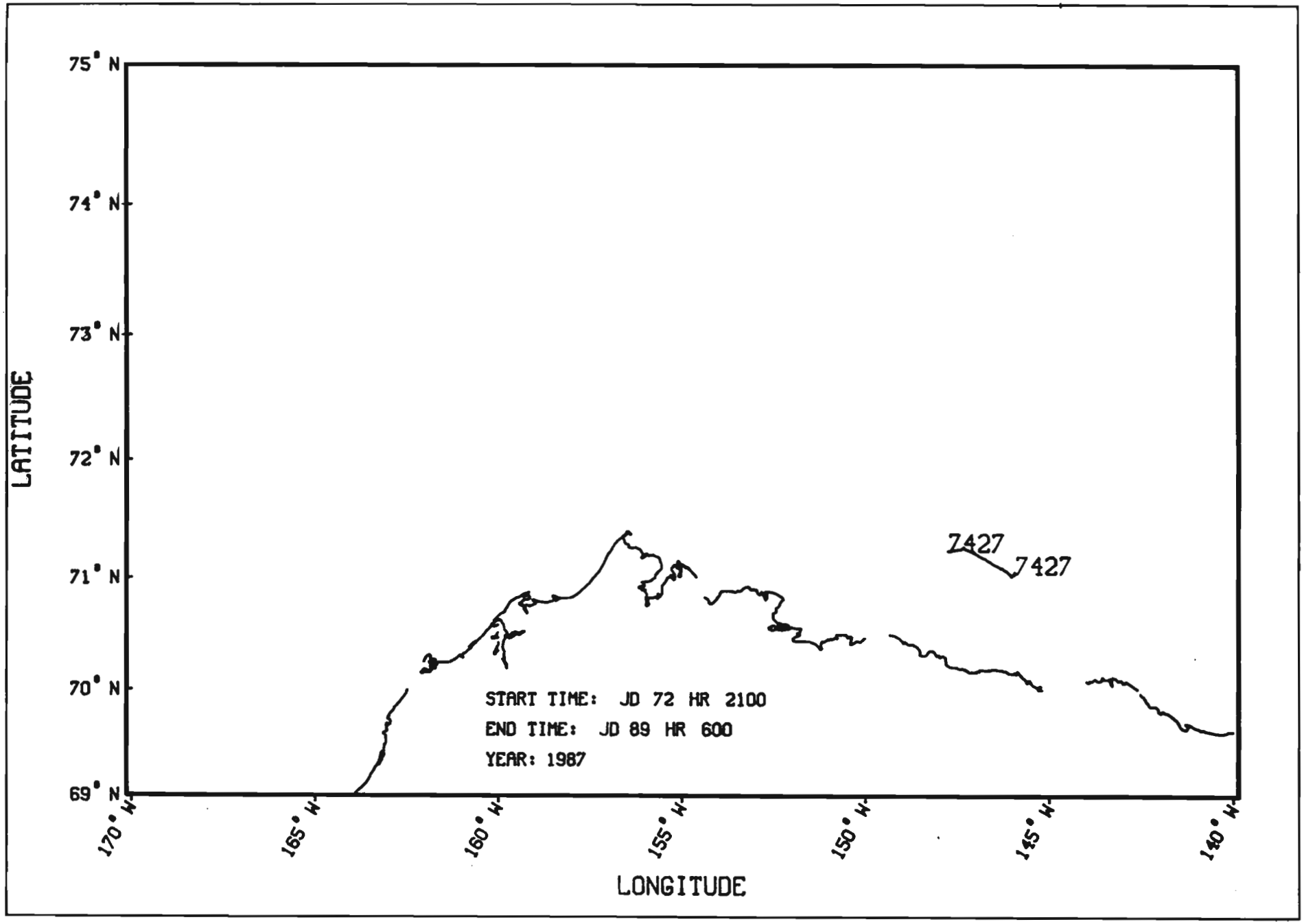

Figure 134. Drift tracks for ARGOS buoy 7427.

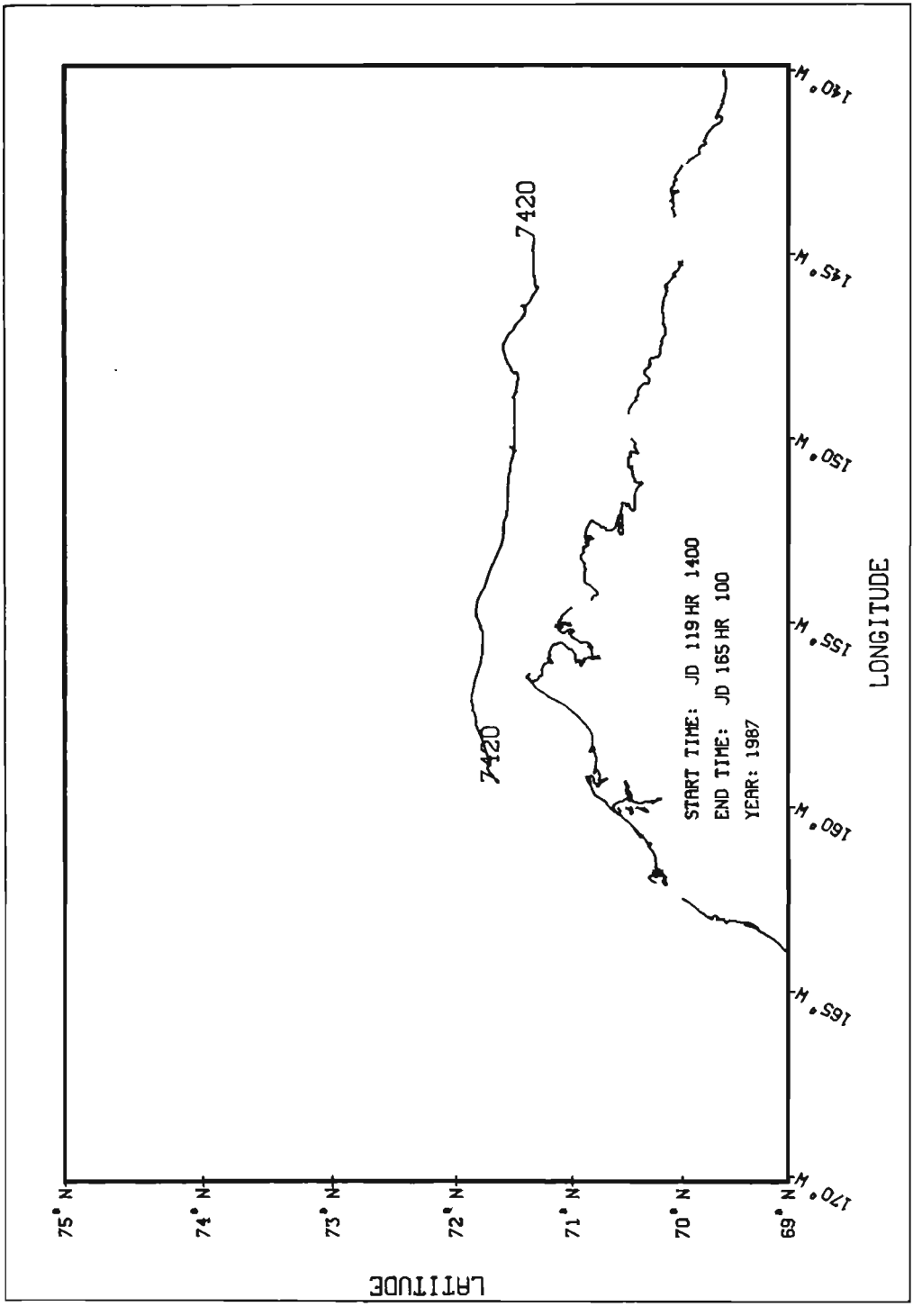

Figure 135. Drift tracks for ARGOS buoy 7420b.

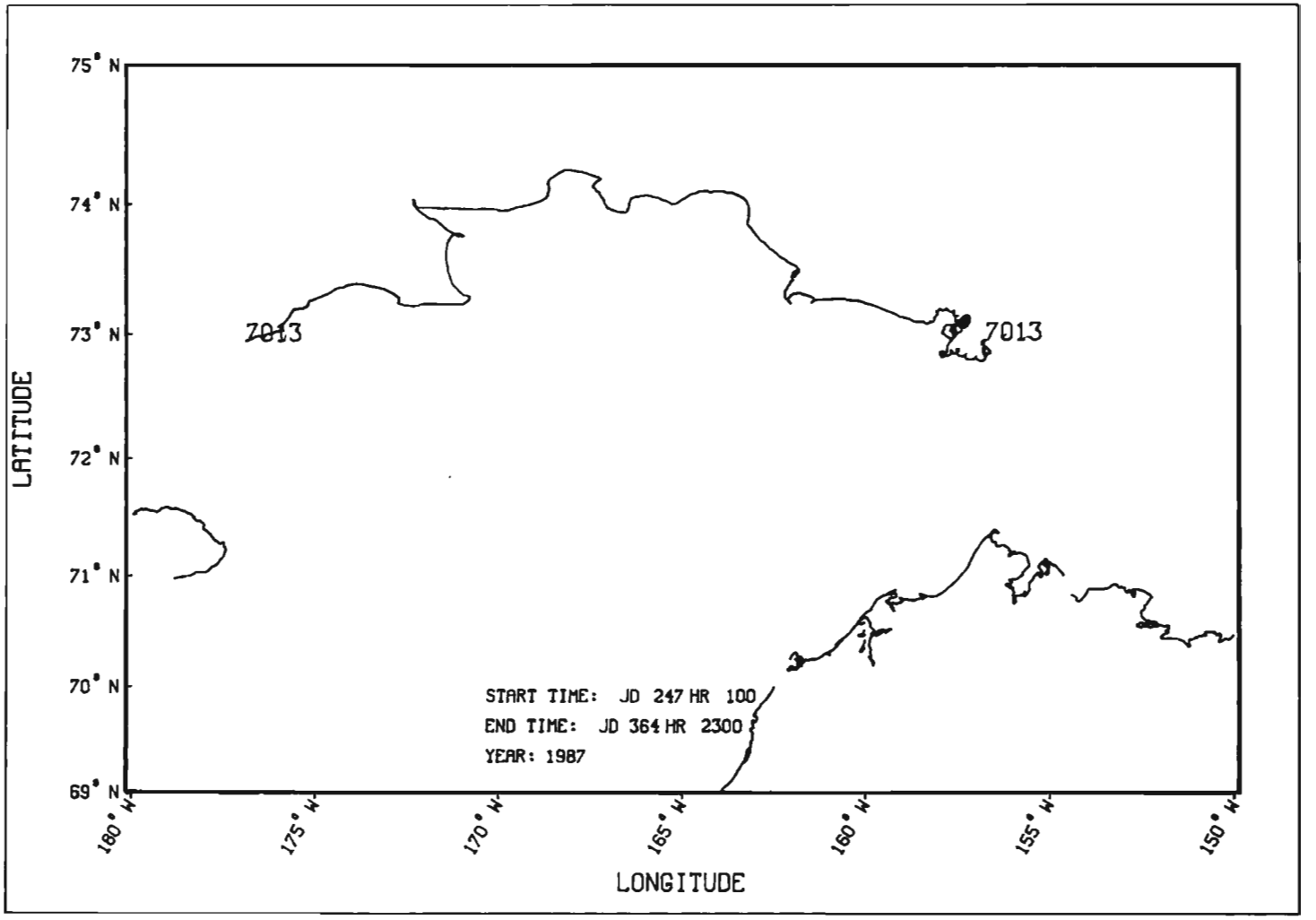

Figure 136. Drift tracks for ARGOS buoy 7013.

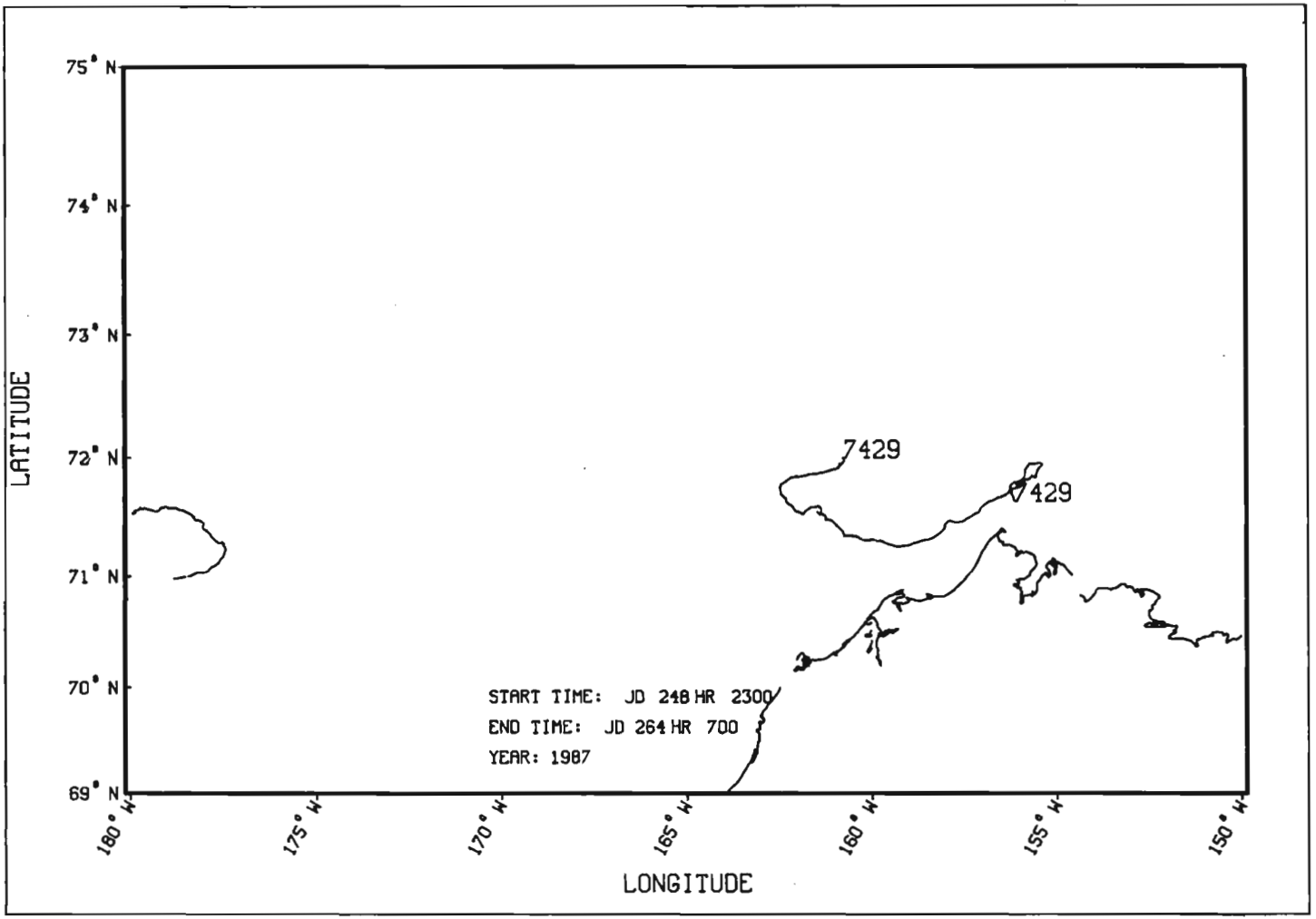

Figure 137. Drift tracks for ARGOS buoy 7429.

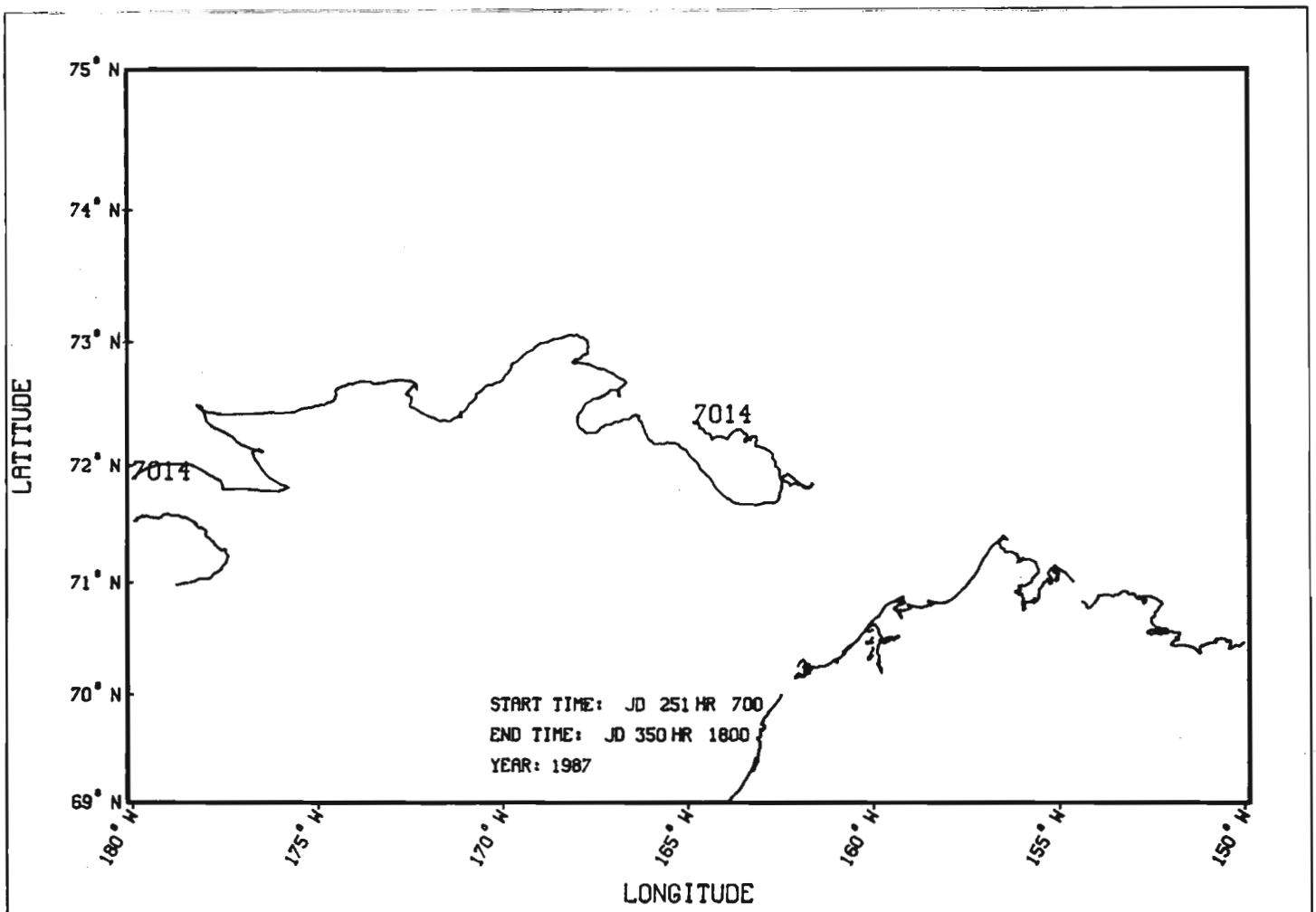

Figure 138. Drift tracks for ARGOS buoy 7014.

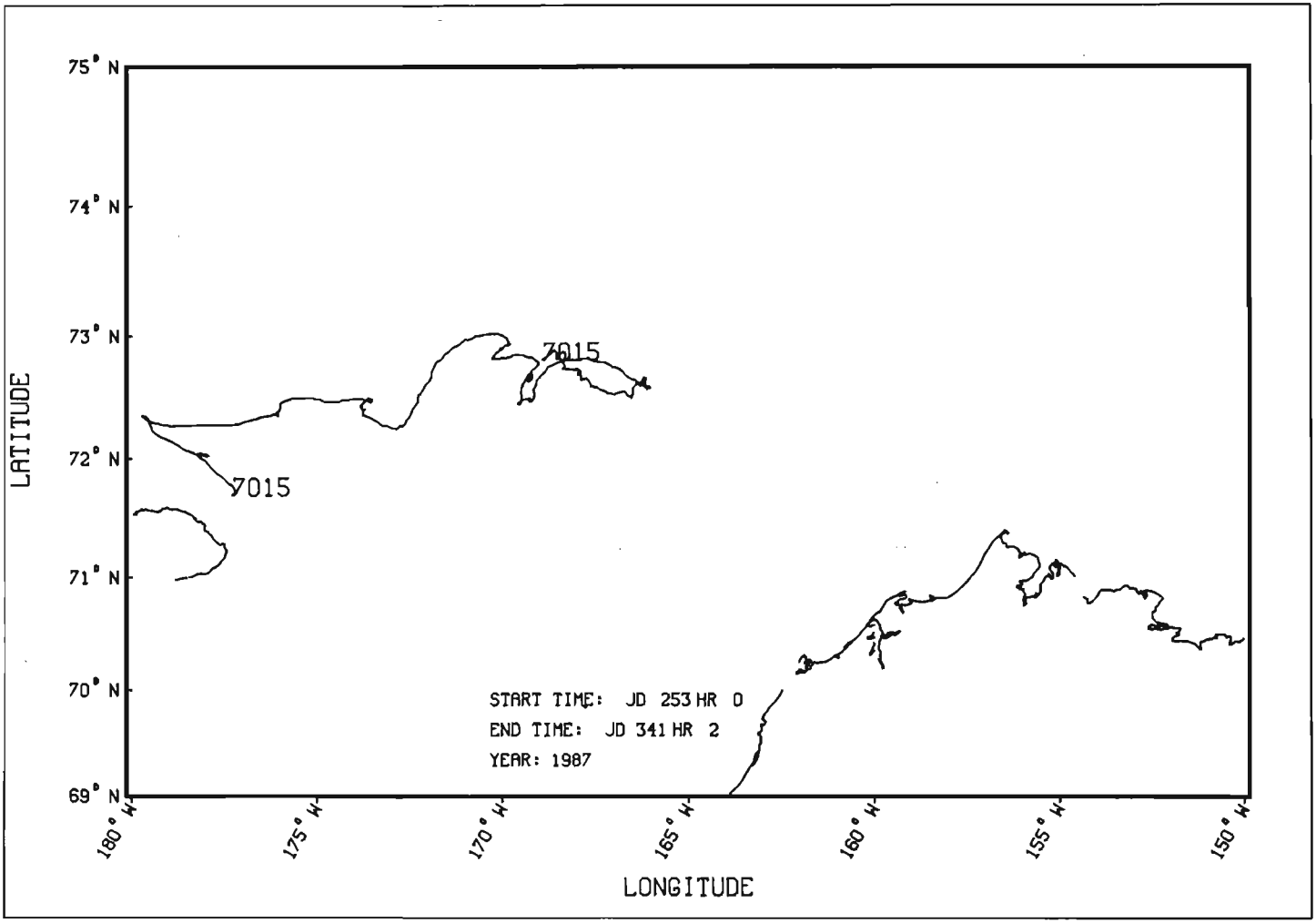

Figure 139. Drift tracks for ARGOS buoy 7015.

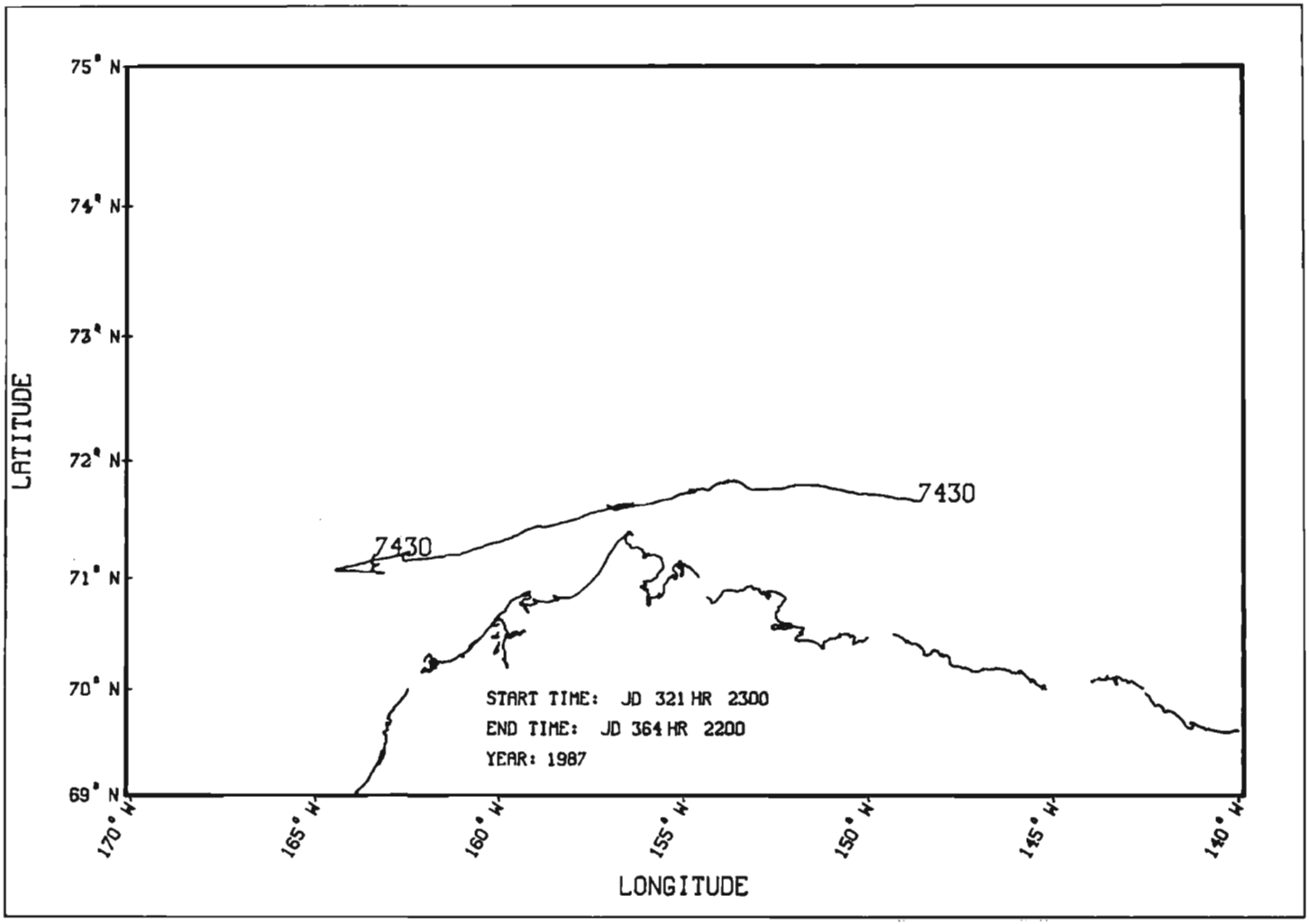

Figure 140. Drift tracks for ARGOS buoy 7430.

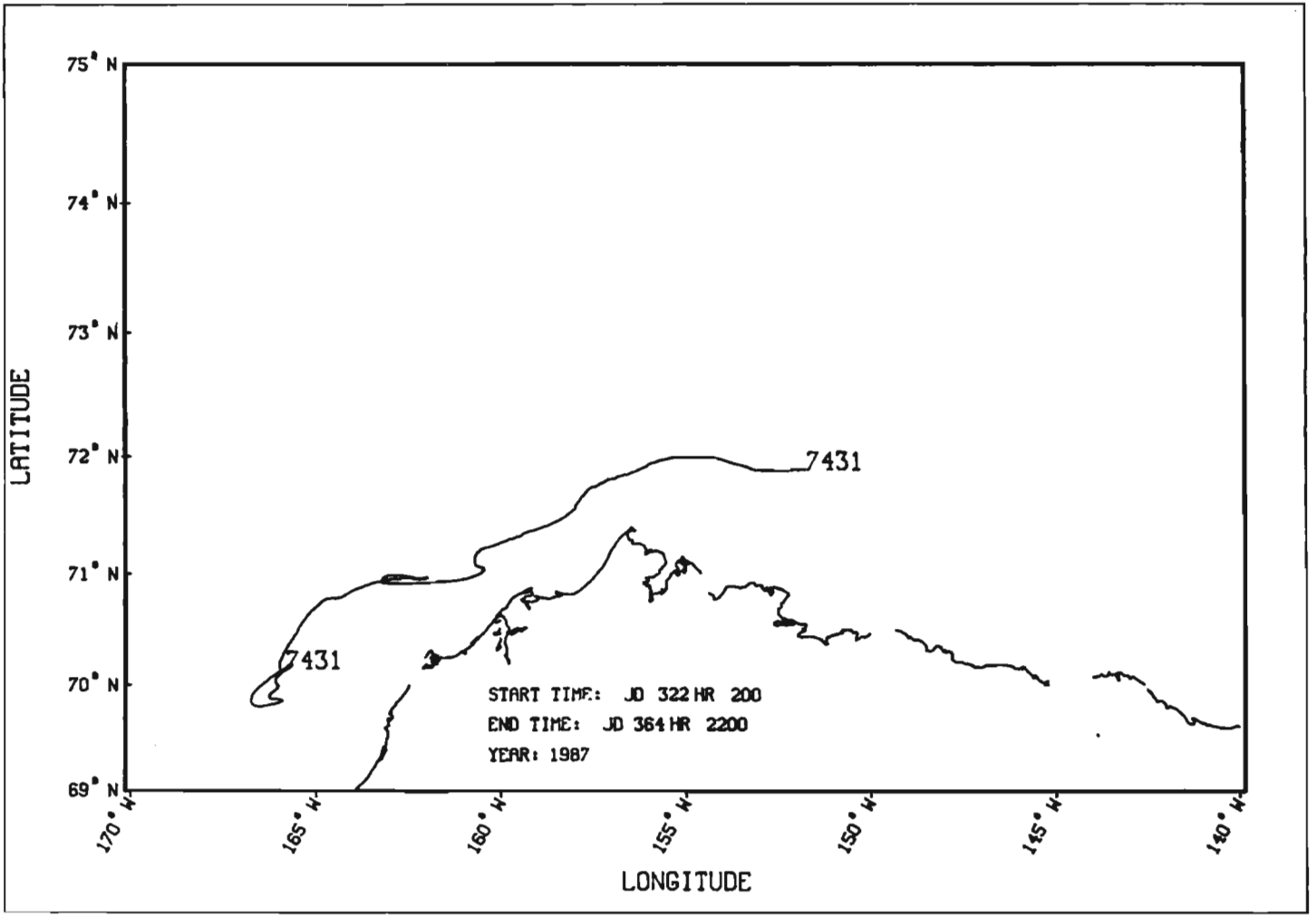

Figure 141. Drift tracks for ARGOS buoy 7431.

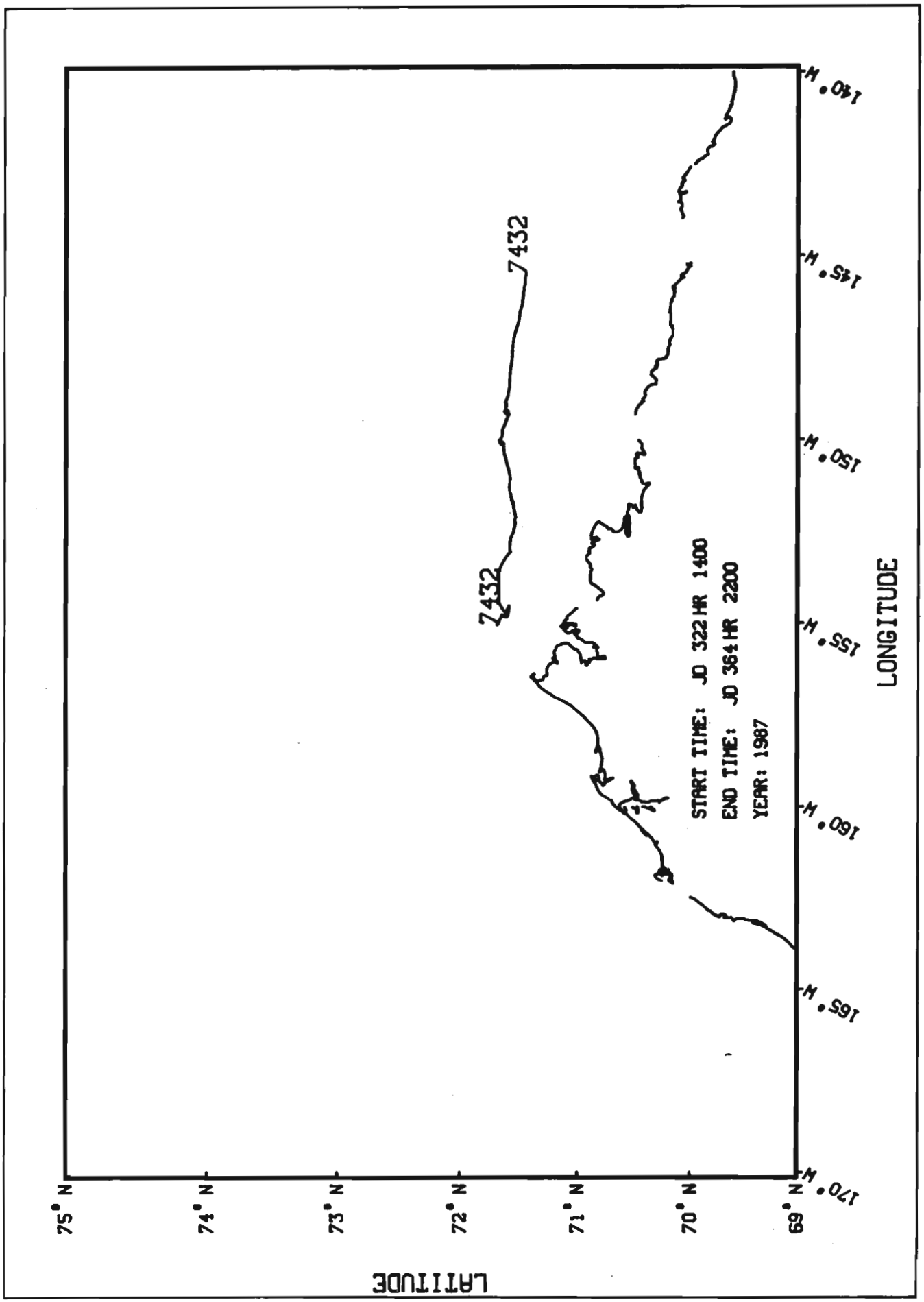

Figure 142. Drift tracks for ARGOS buoy 7432.

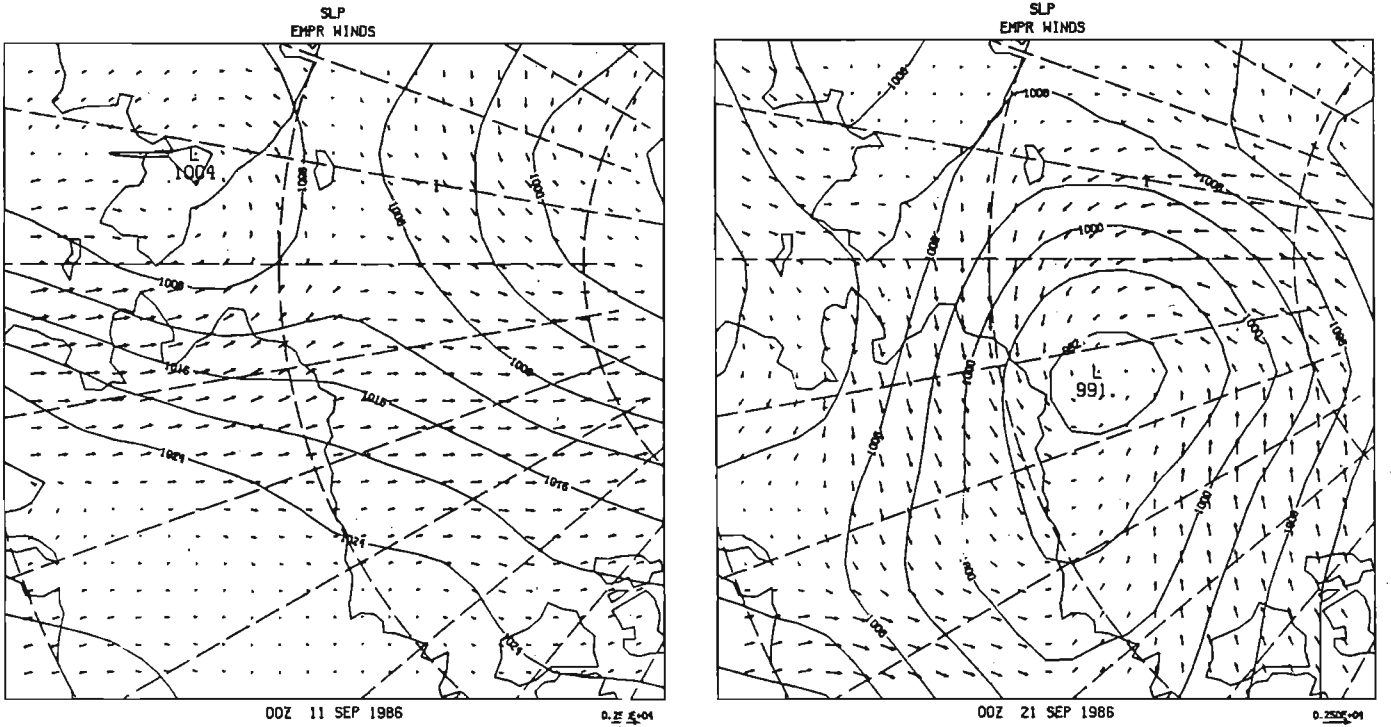

Figure 143. Sea-level pressure and gradient wind fields over the Beaufort and Chukchi Seas - 00 UTC 11 Sep 1986 and 00 UTC 21 Sep 1986.

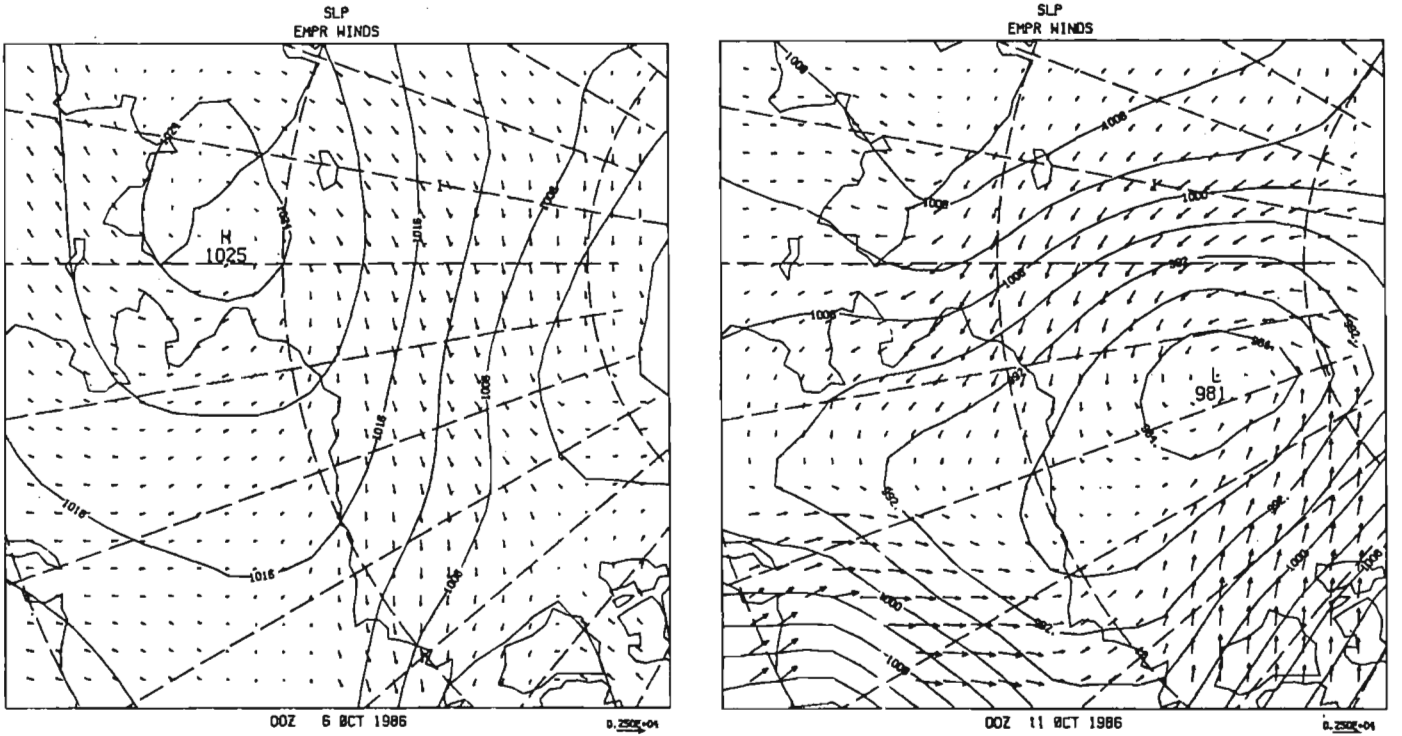

Figure 144. Sea-level pressure and gradient wind fields over the Beaufort and Chukchi Seas - 00 UTC 06 Oct 1986 and 00 UTC 11 Oct 1986.

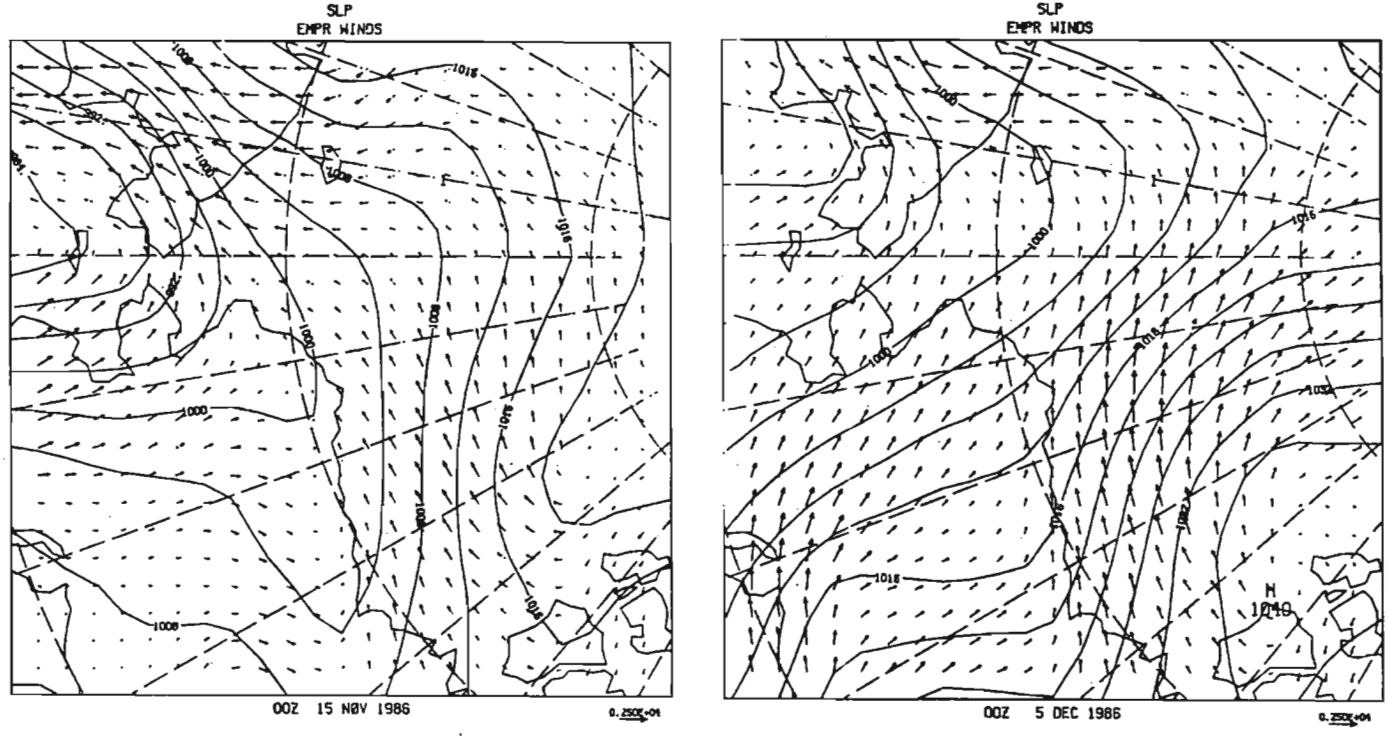

Figure 145. Sea-level pressure and gradient wind fields over the Beaufort and Chukchi Seas - 00 UTC 15 Nov 1986 and 00 UTC 05 Dec 1986.

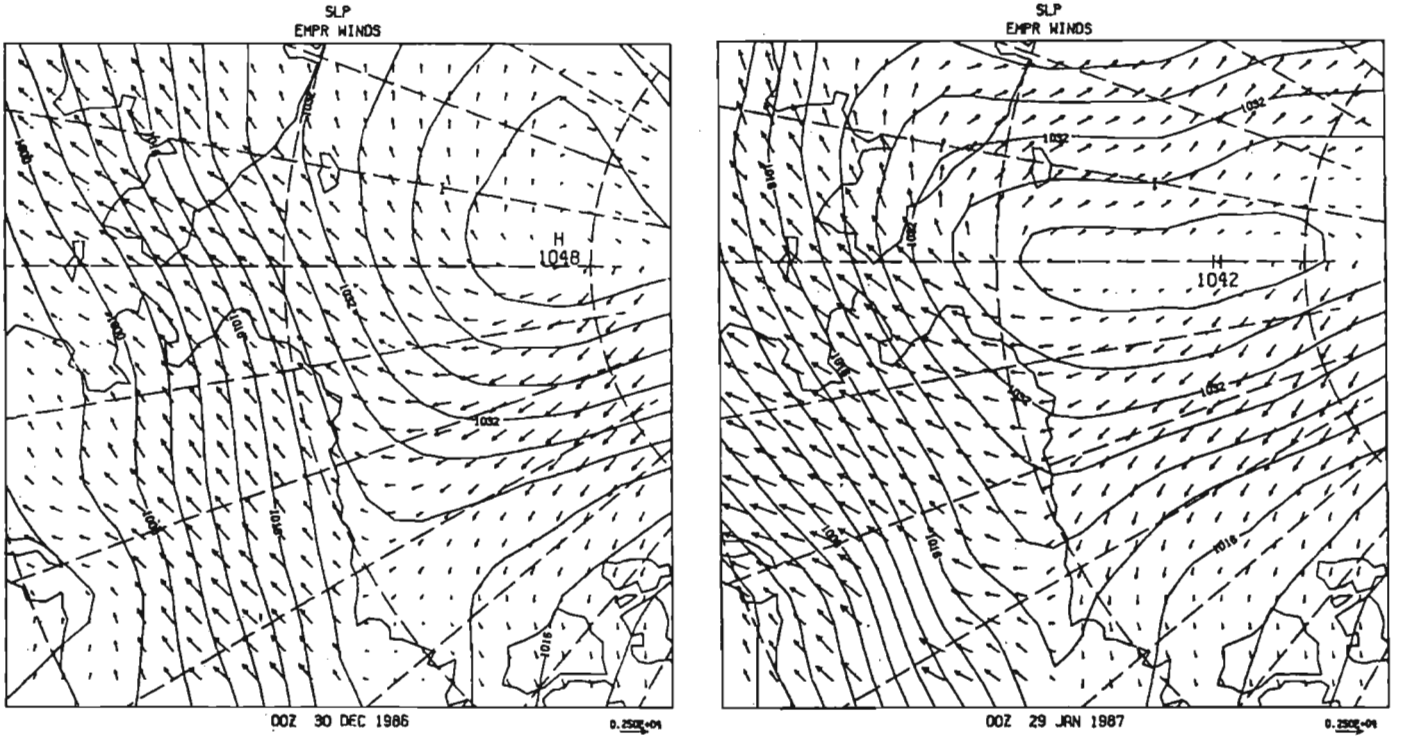

Figure 146. Sea-level pressure and gradient wind fields over the Beaufort and Chukchi Seas - 00 UTC 30 Dec 1986 and 00 UTC 29 Jan 1987.

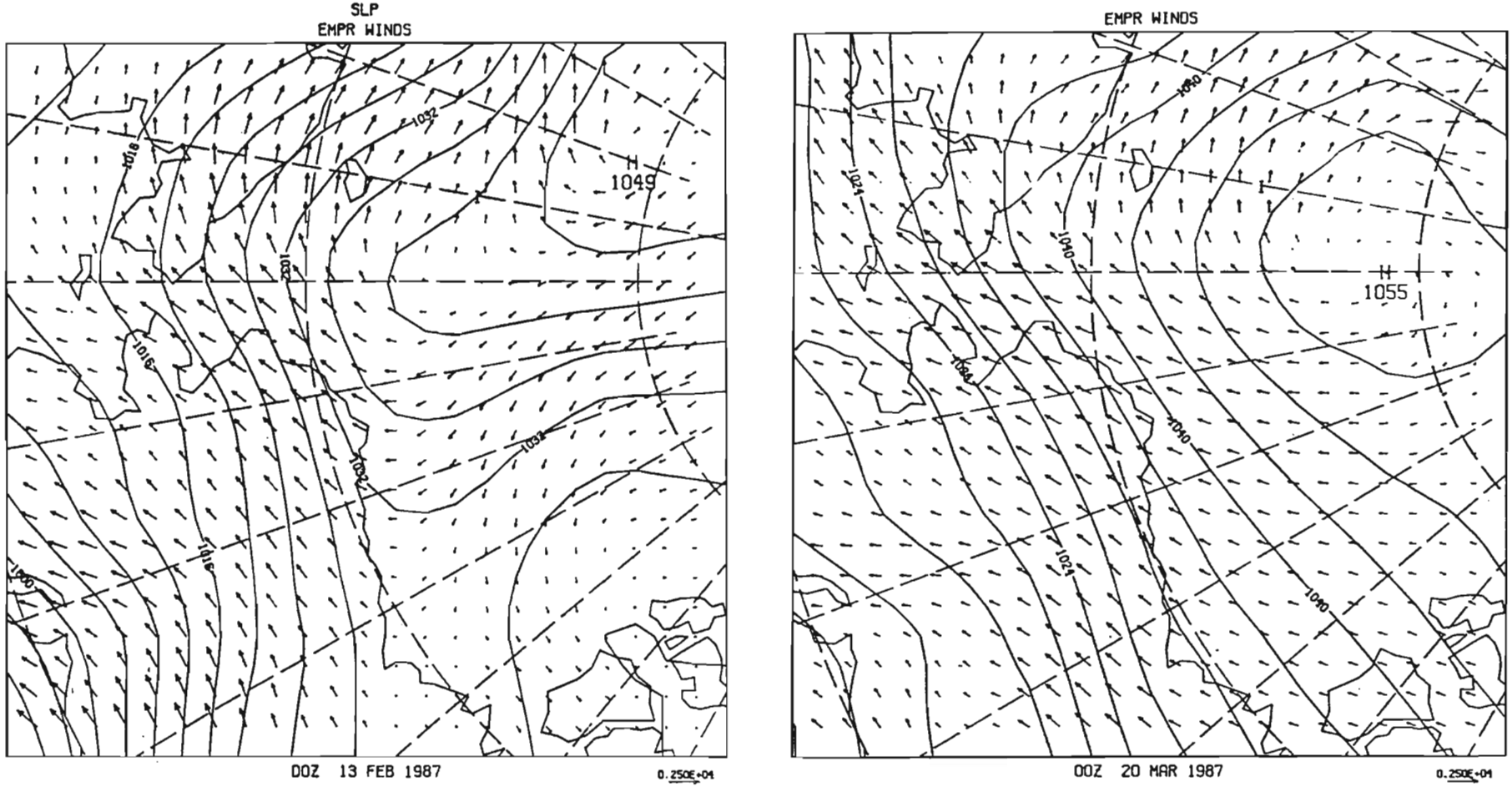

Figure 147. Sea-level pressure and gradient wind fields over the Beaufort and Chukchi Seas - 00 UTC 13 Feb 1987 and 00 UTC 20 Mar 1987.

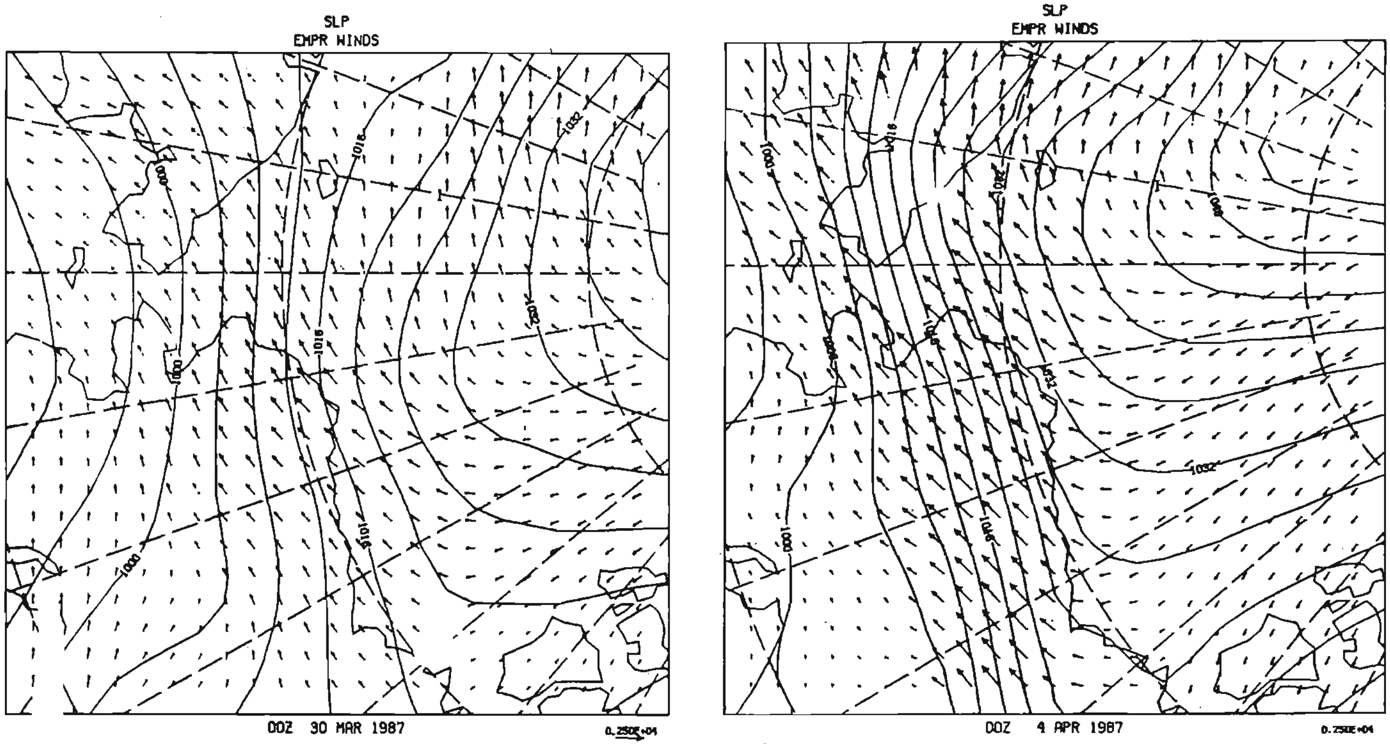

Figure 148. Sea-level pressure and gradient wind fields over the Beaufort and Chukchi Seas - 00 UTC 30 Mar 1987 and 00 UTC 04 Apr 1987.

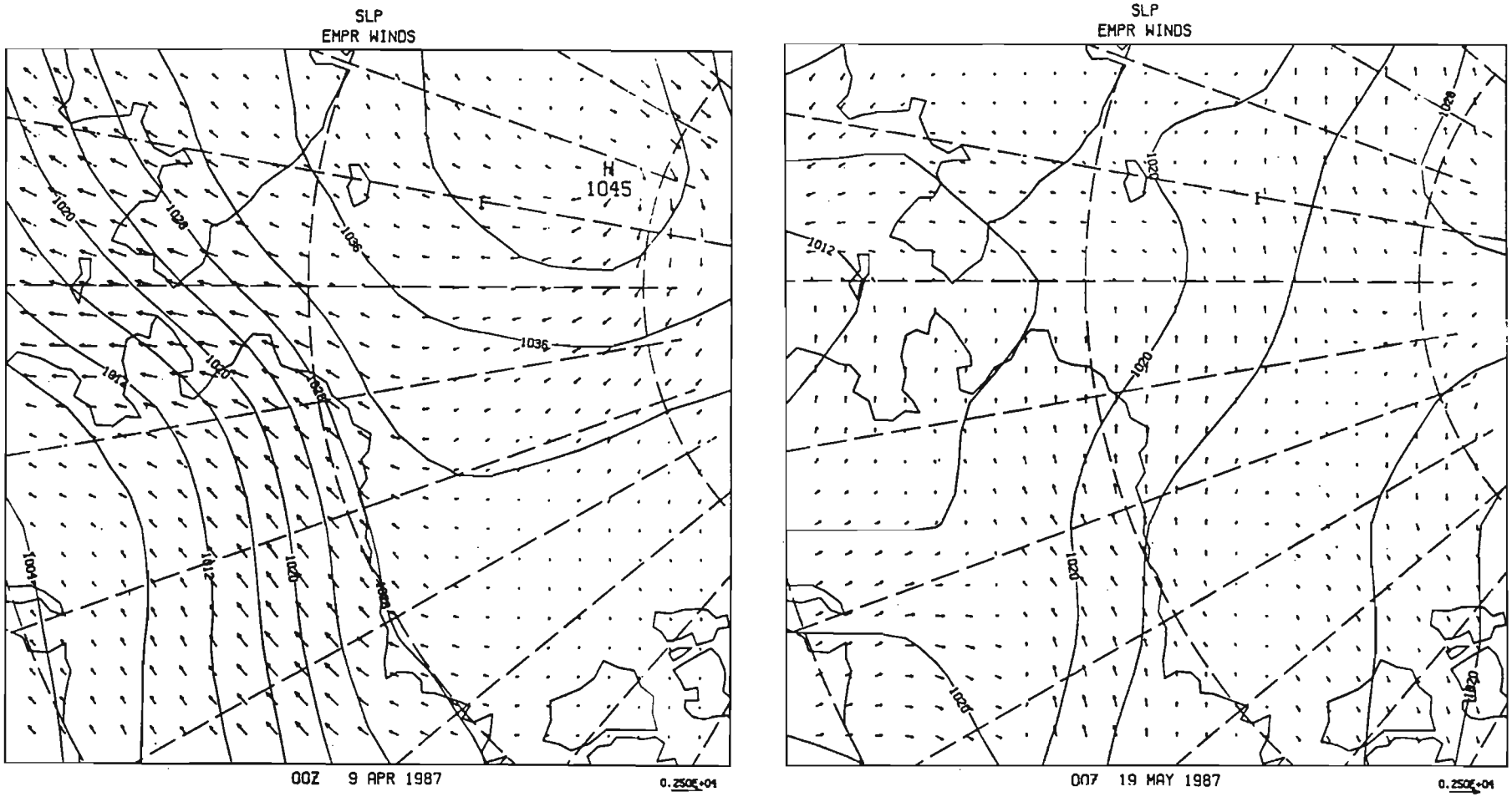

Figure 149. Sea-level pressure and gradient wind fields over the Beaufort and Chukchi Seas - 00 UTC 09 Apr 1987 and 00 UTC 19 May 1987.

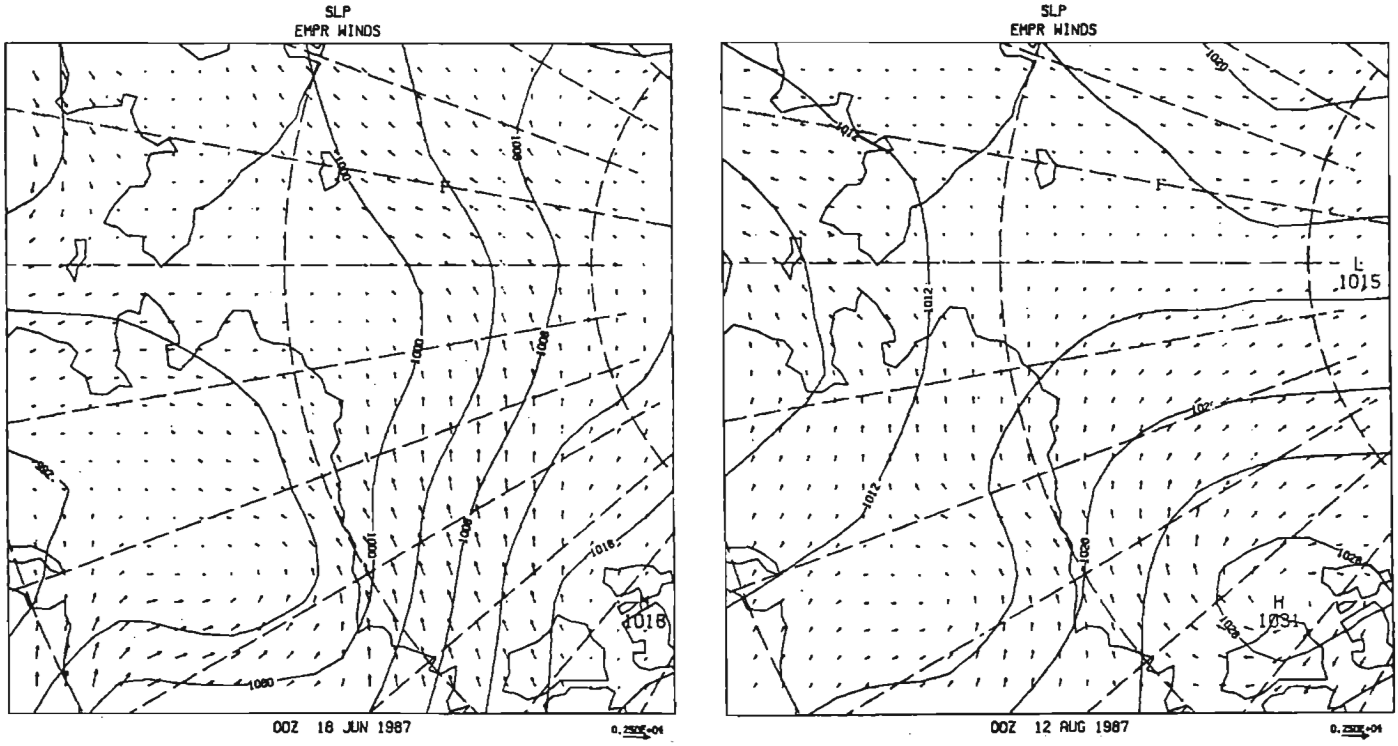

Figure 150. Sea-level pressure and gradient wind fields over the Beaufort and Chukchi Seas - 00 UTC 18 Jun 1987 and 00 UTC 12 Aug 1987.

* U. S. GOVERNMENT PRINTING OFFICE: 1988 - 0 / 92002